OPEN-FILE REPORT (GEOLOGICAL SURVEY (U.S.))

PRELIMINARY REPORT ON THE GEOLOGY AND GOLD MINERALIZATION OF THE GOLD BASIN-LOST BASIN MINING DISTRICTS, MOHAVE COUNTY, ARIZONA

by

Ted G. Theodore, Will N. Blair, and J. Thomas Nash

with a section on

K-Ar CHRONOLOGY OF MINERALIZATION AND IGNEOUS ACTIVITY

by

Edwin H. McKee

and

IMPLICATIONS OF THE COMPOSITIONS OF LODE AND PLACER GOLD

by

J. C. Antweiler and W. L. Campbell

1982

UNITED STATES DEPARTMENT OF THE INTERIOR

U.S. GEOLOGICAL SURVEY

PRELIMINARY REPORT ON THE GEOLOGY AND GOLD MINERALIZATION OF THE GOLD BASIN-LOST BASIN MINING DISTRICTS, MOHAVE COUNTY, ARIZONA

By
Ted G. Theodore, Will N. Blair, and J. Thomas Nash

with a section on

K-Ar CHRONOLOGY OF MINERALIZATION AND IGNEOUS ACTIVITY

By

Edwin H. McKee

and

IMPLICATIONS OF THE COMPOSITIONS OF LODE AND PLACER GOLD

By
J. C. Antweiler and W. L. Campbell

U.S. Geological Survey (U.S.)
Open-File Report 82-1052
1982

Frontispiece.--Placer gold nugget about 1 cm across showing gold molded partly against a rounded fragment of clear vein quartz. Collected from the King Tut placer workings, Lost Basin mining district

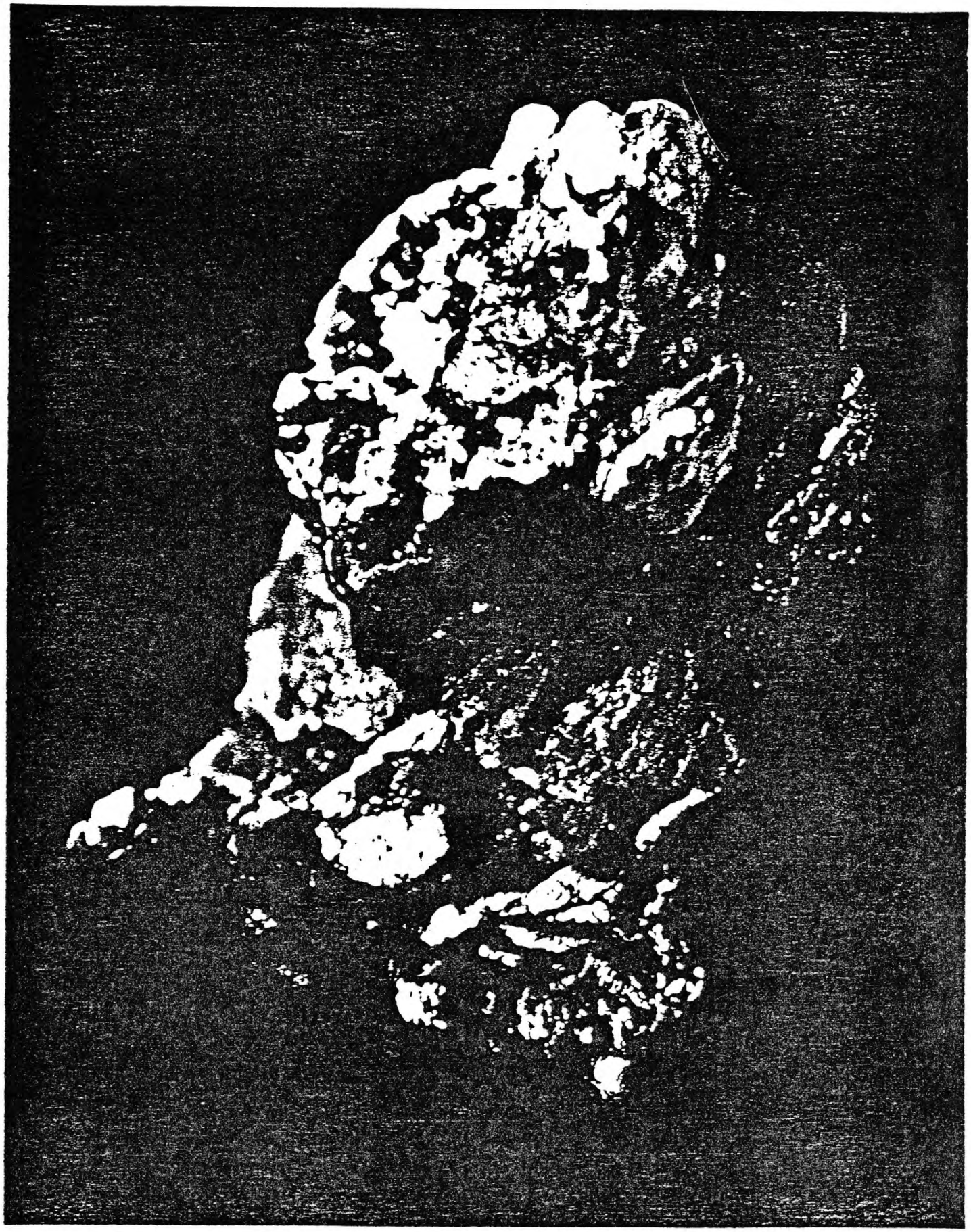

Table of Contents

List of Illustrations

List of Tables

GEOLOGY AND GOLD MINERALIZATION OF THE GOLD BASIN-LOST BASIN MINING DISTRICTS, MOHAVE COUNTY, ARIZONA

By

Ted G. Theodore, Will N. Blair, and J. Thomas Nash

ABSTRACT

The Gold Basin-Lost Basin mining districts are adjacent to each other in northwestern Arizona, south of Lake Mead, and just west of the Grand Wash Cliffs. Most recorded production from lode deposits is credited to mines in the Gold Basin district, which is in the southern White Hills, whereas the bulk of the placer production has been from placers worked along the eastern flank of the Lost Basin range, about 16 km to the northeast across Hualapai Valley. Gold in quartz veins apparently was first discovered in the 1870's. Recorded production from the districts between 1901 and 1942 includes 13,508 oz gold and 6,857 oz silver, and this recorded production has a dollar value of about $359,000 of which 98 percent is credited to gold.

Most known occurrences of lode gold in the districts are associated with widespread quartz-cored pegmatite-vein systems, presumably emplaced episodically during Proterozoic X, Proterozoic Y, and Late Cretaceous time into Proterozoic X metamorphic and igneous rocks. The bulk of the veins apparently were emplaced during the Late Cretaceous, and they were localized along both high- and low-angle structures in the Proterozoic X terrane. These veins appear to be associated genetically with presumably Late Cretaceous, two-mica magmatism. A Late Cretaceous two-mica monzogranite crops out in an approximately 4 to 5 km^2 area in the southern part of the Gold Basin district and includes some facies of episyenite. Some gold is found also in small episyenitic alteration pipes, or in veins caught up tectonically along a regionally extensive, low-angle detachment surface which crops out prominently in the southern White Hills, and has been traced for at least 30 km along the western flank of the White Hills.

Hydrothermal micas from selected veins in the districts give K-Ar ages of 822, 712, 69, 68, and 65 m.y. (million years), and from the pipes, ages of 130 and 127 m.y. The oldest ages (822 and 712 m.y.) presumably reflect resetting of veins that probably were emplaced penecontemporaneous with emplacement of the 1,400-m.y. granite of Gold Butte, which crops out just to the north of Lake Mead. The latter ages (130 and 127 m.y.) must reflect either the

presence of excess radiogenic argon in the hydrothermal environment of the evolving pipes, or contamination of the dated mineral separates by Proterozoic mica and (or) feldspar. Primary white mica from the two-mica monzogranite gives a K-Ar age of 72 m.y..

Most occurrences of gold in the veins and pipes probably reflect either remobilization of gold from gold-bearing, near-surface Proterozoic source areas, or anatectic incorporation of gold into Late Cretaceous, two-mica magmas from very deep gold-bearing Proterozoic sources. Deposition of gold occurred in a mesothermal environment during the galena-, chalcopyrite-, ferroan-carbonate-bearing stages of the veins. Homogenization studies of fluid inclusions prominent in the veins and pipes yield temperatures mostly in the range 150 to 280°C. Early-stage, trapping temperatures at the pipes probably were about 330°C and pressures in the range 500 to 700 bars can be inferred. Fluids were moderately saline, mostly 4 to 16 weight percent NaCl equivalent, nonboiling, and also contain appreciable amounts of carbon dioxide and, in places, fluorine. Such fluids associated with the deposition of gold in these districts largely bridge the fluid composition interval between many other epithermal precious-metal and porphyry coper deposits.

Approximately 350 compositional analyses obtained from native-gold samples from 20 mines in the Gold Basin district and 48 veins in the Lost Basin district show silver contents that range from 6 to approximately 50 weight percent, and copper from 0.01 to 0.5 weight percent. Metal zonation and possible relation to a porphyry copper system at depth can be inferred from some of these chemical data. The differences in the composition of placer gold from 24 occurrences in the Lost Basin district from that of nearby lode sources suggest that other sources contributed gold to the placers or that locally derived grains were enriched by oxidation and weathering of the lodes.

INTRODUCTION

The Gold Basin-Lost Basin mining districts of northwestern Arizona are located in Mohave County, 120 km southeast of Las Vegas, Nev., and about 95 km north of Kingman, Ariz. (fig. 1). These districts comprise primarily gold-bearing vein deposits containing minor byproduct lead, silver and copper and placer gold deposits. The districts lie adjacent to each other, south of Lake Mead and west of the Grand Wash Cliffs, which mark the boundary of the Colorado Plateau. The Gold Basin district is mostly in the southern White

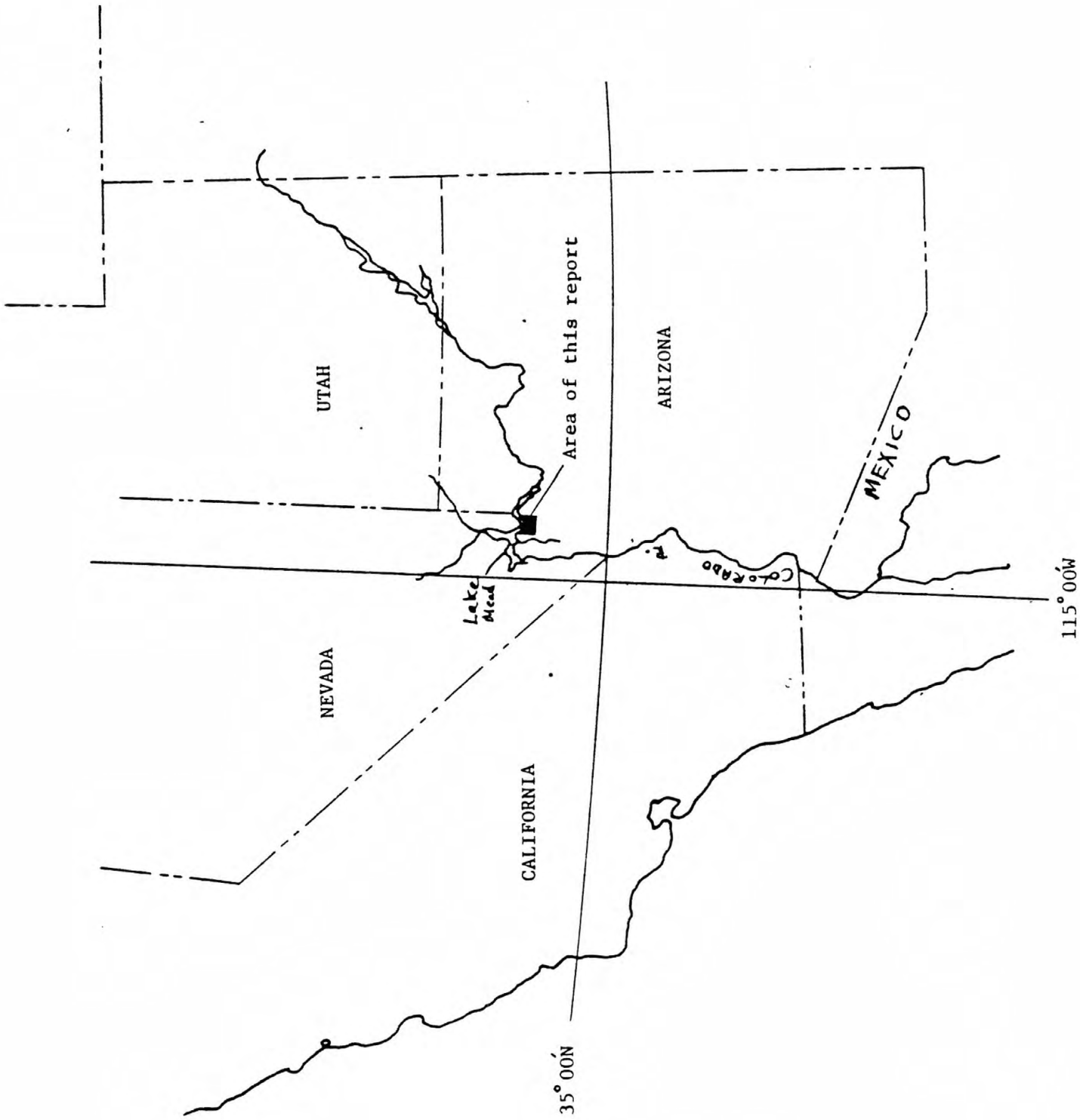

Figure 1.--Index map showing location of the Gold Basin-Lost Basin mining districts.

Hills, and the Lost Basin district occurs to its east, across Hualapai Wash; they are mostly in the Garnet Mountain 15′ quadrangle (fig. 2). This report summarizes field and laboratory investigations wherein a remarkable suite of gold-bearing samples were collected from wide-ranging localities in these districts which were first prospected in the late 19th century. Gold was first discovered there in the 1870's. Included are discussions of the environment(s) and age of gold deposition using geochemical techniques, fluid-inclusion studies, and the K-Ar method, all supplemented by observations with the scanning electron microscope (SEM). For our investigations, lode and placer samples containing visible gold were collected from more than 30 localities.

Acknowledgments

The preceding geologic investigations of P. M. Blacet of the U.S. Geological Survey in the Garnet Mountain quadrangle during the late 1960's and early 1970's (Blacet, 1975) and E. J. Kirsh (Kirsh, 1974) and A. J. Deaderick (Deaderick, 1980) provided the geologic framework upon which we built much of our studies. Further, Blacet collected many of the gold-bearing samples used in this study. R. L. Oscarson introduced us to the scanning electron microscope methods needed in the production of electron micrographs, and aided our usage of the X-ray detector (EDAX) during the qualitative chemical analysis of selected mineral grains. Fluid-inclusion studies were conducted in the laboratory of W. E. Hall, U.S. Geological Survey, at Menlo Park, California.

HISTORY OF MINING ACTIVITY

The Gold Basin district is situated mostly in the eastern part of the White Hills and is bounded on the east by Hualapai Wash (fig. 2). Gold in quartz veins apparently was discovered in the district in the early 1870's with most of the production up until 1932 from a small group of mines, including the El Dorado, Excelsior, Golden Rule, Jim Blaine, Never-Get-Left, O.K., and Cyclopic (fig. 3). About 1880 there was a minor rush into the area, and by 1881 the ores were being worked in two stamp mills (Burchard, 1882, p. 253); in 1882, The El Dorado mine included 26,000 tons of developed ore (Burchard, 1883, p. 305). Table 1 summarizes information concerning the mills previously operating in the Gold Basin-Lost Basin districts. The first stamp mill, a cooperative venture by the miners, was built about 1880 at "Grass Springs" near the present (1982) headquarters of the Diamond Bar Ranch, and in

Figure 2.--Geologic sketch map of the general area of the Gold Basin-Lost Basin mining districts. Modified from Blacet (1975), Deaderick (1980), P. M. Blacet (unpub. data, 1967-1972), and K. A. Johnson (unpub. data, 1982). (In pocket)

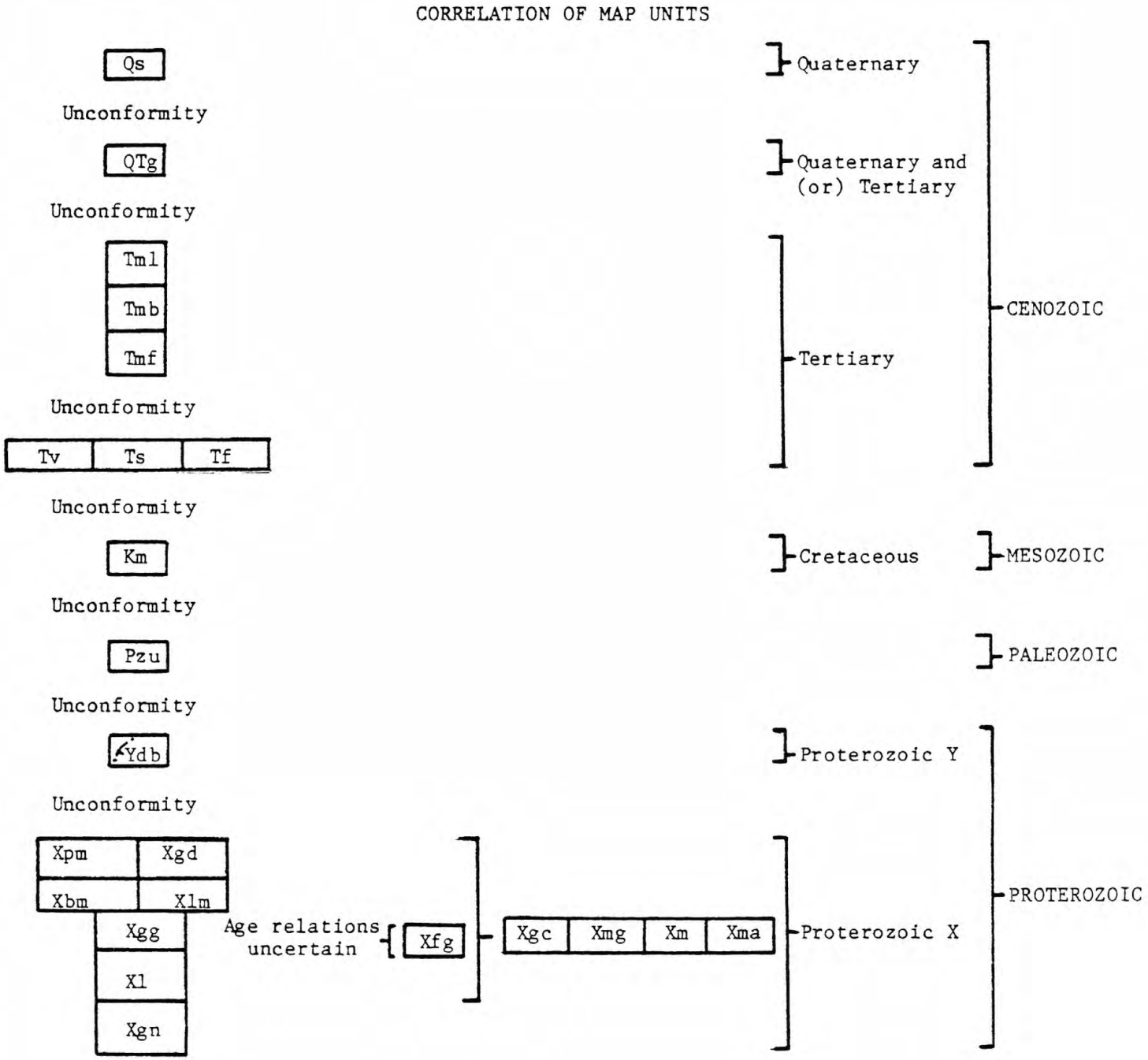

DESCRIPTION OF MAP UNITS

Qs SEDIMENTARY DEPOSITS (Quaternary)--Includes sand and gravel along active stream washes, talus, colluvium, poorly consolidated fanglomerate currently being dissected, and landslide deposits; also includes extensive high-level fanglomeratic deposits, west of the Grand Wash Cliffs in the general area of Grapevine Mesa, that may be Quaternary and (or) Tertiary in age

Qtg FANGLOMERATE (Quaternary and (or) Tertiary)--Locally derived fanglomerate deposits, south-southeast of Senator Mountain, that do not contain clasts of rapakivi granite or any interbedded tuffs

Tml HUALAPAI LIMESTONE (Tertiary)--Upper member of the Muddy Creek Formation (see Blair, 1978; Blair and Armstrong, 1979)

Tmb BASALT (Tertiary)--As shown, flows at Senator Mountain, near the western edge of the map area, and at Iron Spring Basin, near the eastern edge. Basalt in these two areas correlates probably with basalt flows, not shown, which conformably underlie the Hualapai Limestone Member and also are interbedded with fanglomerate of the Muddy Creek Formation near the northwest corner of the map area. A whole-rock K-Ar age determination of basalt from this area yields an age of 10.9 m.y. (see section by McKee, this report)

Tmf FANGLOMERATE (Tertiary)--Alluvial fanglomeratic deposits of the Muddy Creek Formation. Locally includes lenses and beds of rhyolitic tuff, and, as shown near the southwest corner of the map area, fanglomerate mapped previously by Blacet (1975) as unit Tf. The unit is also intruded by minor basalt dikes, especially in the general area of Senator Mountain. Near the northwest corner of the map area, the unit includes well-exposed flows of basalt

Tv VOLCANIC ROCKS (Tertiary)--Includes mostly andesite. Map unit near the northwest corner of the map area internally is broken highly by numerous faults, and near here, the unit includes also air-fall tuff and reddish-brown sandstone interbedded with chaotic sedimentary breccia composed of fragments of Proterozoic X gneiss. In places, unit also includes massive porphyritic hornblende andesite and basalt flows and breccias; and overall minor amounts of tightly cemented volcaniclastic rocks. Attitudes of flow layering and bedding generally dip at angles of 35° in contrast to shallow dips of about 5° in the unconformably overlying basal fanglomerate of the Muddy Creek Formation. Age ranges of 14.6 to 11.8 m.y. are reported near the type section of the Mount Davis Volcanics (Anderson and others, 1972), whereas a K-Ar age determination on sanidine from an air-fall tuff near Salt Spring Wash in the northwestern part of the area yields an age of 15.4 m.y. The volcanic rocks may be the equivalent of the Mount Davis Volcanics or the Patsy Mine Volcanics (see section by McKee, this report)

Ts RHYOLITIC TUFFACEOUS SEDIMENTARY ROCKS AND FANGLOMERATE (Tertiary)--Crops out as a steeply dipping sequence of rocks, bounded by north-striking faults, near the southern end of the Lost Basin Range. Possibly equivalent to the Mount Davis Volcanics

Tf FANGLOMERATE (Tertiary)--Coarse fanglomeratic deposits that include locally landslide or mudflow breccia. Overlain unconformably by fanglomeratic deposits of the Muddy Creek Formation, and apparently intercalated with andesite of the Mount Davis Volcanics

Km TWO-MICA MONZOGRANITE (Cretaceous)

Pzu PALEOZOIC ROCKS, UNDIVIDED (Paleozoic)--Includes Lower Cambrian Tapeats Sandstone, Lower to Middle Cambrian Bright Angel Shale, and Middle Cambrian Muav Limestone

Ydb DIABASE (Proterozoic Y)

Xpm PORPHYRITIC MONZOGRANITE (Proterozoic X)

Xgd GRANODIORITE BORDER FACIES OF PORPHYRITIC MONZOGRANITE (Proterozoic X)

Xbm BIOTITE MONZOGRANITE (Proterozoic X)

Xlm LEUCOCRATIC MONZOGRANITE (Proterozoic X)

Xgg GNEISSIC GRANODIORITE (Proterozoic X)

Xl LEUCOGRANITE (Proterozoic X)

Xfg FELDSPAR GNEISS (Proterozoic X)

Xgc MIXED GRANODIORITIC COMPLEX (Proterozoic X)

Xmg MIGMATITIC GNEISS (Proterozoic X)

Xm MIGMATITE(Proterozoic X)

Xml MIGMATITIC LEUCOGRANITE COMPLEX (Proterozoic X)

Xgn GNEISS (Proterozoic X)--Includes variably metamorphosed gneiss and some metaquartzite in the northern parts of the Lost Basin Range, and in the northern White Hills. Exposed sequence of gneiss in the southern parts of the Lost Basin Range includes abundant metabasite and amphibolite consisting partly of metagabbro, metaclinopyroxenite, metawehrlite, metadiabase, and metabasalt

—?— CONTACT--Queried where location uncertain.

FAULT--Dashed where approximately located; dotted where concealed.

DETACHMENT FAULT--Saw teeth on upper plate; dashed where approximately located; dotted where concealed.

Figure 3. Location map of major mines that are credited with the production of metal(s) and known occurrences of gold in the Gold Basin-Lost Basin mining districts. Spot indicates locality of lode gold collected for this report, or observed (see Blacet, (1975), and the section by J. C. Awtweiler in this report). Major-placer workings also indicated. F, outer limit of widespread occurrences of fluorite observed either in veins or disseminated in the upper Cretaceous two-mica monzogranite. (In pocket).

Table 1. Descriptions of gold-quartz mills in the Gold Basin-Lost Basin districts, Arizona

Name of site	Type of mill	Location	History and remarks
1. Willow Mill (Gold Spring)	Arrastre and Stamp	Red Willow Spring, NW1/4, sec. 12, T. 27 N., R. 19 W.	Possibly the location of the first arrastre in the district, built in the early 1870's. A stamp mill built here prior to 1915, perhaps as early as 1881.
2. Grass Springs (Grass Valley)	Stamp	At the headquarters of the Diamond Bar Ranch, NW1/4 sec. 27, T. 29 N., R. 16 W.	An inefficient 4- or 5-stamp mill, the first for the district was constructed at Grass Springs about 1880 as a cooperative venture by the early miners.
3. Patterson's Well	Arrastre	SE1/4 sec. 36, T. 29 N., R. 17 W.	Robert Patterson, a pioneer rancher and miner, built an arrastre near his well (water tunnels) in 1883.
4. Butcher Camp	Arrastre	NW1/4 sec. 7, T. 27 N., R. 18 W.	Two arrastres at shallow well. History unknown.
5. O.K. Mill (Gold Basin or Burnt Mill)	Arrastre and Stamp	Along Hualapai Wash, NE1/4 sec. 13, T. 28 N., R. 18 W.	This stamp mill operated intermittently at the settlement of Gold Basin from 1887 to 1890; it burned in 1893, but was rebuilt in 1896 and its 10 stamps and cyanide plant ran intermittently until it burned again in 1906 (Schrader, 1909, p. 120-121).
6. Old Senator Mill	Stamp	Near the Colorado River east of the mouth of Salt Springs Wash, SW1/4 sec. 5, T. 30 N., R. 18 W.	A 10-stamp mill was built here about 1892, operating for about 6 months on low-grade ore hauled 16 mi from the Senator mine.
7. Salt Springs Mill	Stamp	At Salt Springs near center of sec. 18, T. 30 N., R. 18 W.	History uncertain, probably built by the Salt Springs Mining Co. about 1900. This mill apparently operated as late as 1917.
8. Cyclopic Mill	Cyanide	At Cyclopic mine, SW1/4 sec. 30, T. 28 N., R. 18 W.	A 40-ton-per-day mill was built in 1905 by the Cyclopic Gold Mining Co., producing considerable bullion during the next few years. In 1923, the Gold Basin Exploration Co. acquired the property and remodeled the mill. After discovery of a new ore body in 1926, the mill was again remodeled, and its capacity increased to 100 tons per day. The mill operated intermittently during 1932-1940, and was enlarged to 125-ton daily capacity in late 1933.
9. San Juan Mill	Amalgamating and cyanide	In canyon 1 mi north of Cyclopic mine, SE1/4 sec. 19, T. 28 N., R. 18 W.	In 1929, the Kiowa Gold Mining Co. built a 60-ton-per-day amalgamating and cyanide mill to process ore from the San Juan group of claims. This plant may have provided custom milling for several small miners during the early 1930's (Mining Jour., 1929).
10. Lost Basin Mill (Scanlon)	Ball mill with flotation and cyanide	About 1 mi northeast of the Golden Gate mine, SW1/4 sec. 28, T. 30 N., R. 17 W.	In the mid-1930's, the Lost Basin Gold Mining Co. was apparently operating a diesel-powered 50-ton-per-day ball mill at the old Scanlon mine. Prior to the filling of Lake Mead, this company may have operated a mill near the Colorado River along Hualapai Wash.
11. Malco Mill (Excelsior, Eldorado)	Ball mill with flotation and cyanide(?)	At Excelsior mine, NW1/4 sec. 22, T. 28 N., R. 18 W.	A 35-ton-per-day diesel-powered ball mill was built in 1938 by the Malco Mining Co. (Mining Jour., 1938). About 1908, a stamp mill may have been built at this site by the Arizona-Minnesota Gold Mining Co.

1881 a second 5-stamp mill was constructed, probably at Red Willow Spring, 4.0 km southwest of the Cyclopic mine. By 1883 most of the important mines in the district had been located, were developed, and had produced relatively small tonnages of free-milling gold-quartz ores ranging in average tenor from 0.5-3.0 oz gold per ton.

A third stamp mill was built along Hualapai Wash about 1886, and this mill soon became the nucleus of a settlement called Gold Basin. About this time the gold-bearing veins in the Lost Basin district were discovered, and the centrally located Gold Basin mill soon became the most important in the region. Several years of relative inactivity preceded and followed the burning of the Gold Basin mill in 1893, but in 1896 it was rebuilt with 10 stamps and a cyanide plant. Water was piped about 10 km from water tunnels at Patterson's well (SW1/4 sec. 36, T. 29 N., R. 17 W.), because two wells drilled at Gold Basin had penetrated nothing but dry alluvial gravels to depths of 150 and 230 m (Lee, 1908, p. 78). Most of the mines in both districts had passed their peaks of production when the second burning of the Gold Basin mill occurred in 1906, and in June 1907 the post office at "Basin" was discontinued, and postal service was transferred entirely to a post office established in 1905 at the Cyclopic mine.

In 1904 the Cyclopic mine was purchased by the Cyclopic Gold Mining Company, and the next year a 40-ton-per-day cyanide mill was built along Cyclopic Wash just below the mine. From this time on "Cyclopic" was the main population center of the district, supporting a post office until 1917. After several years of idleness, intermittent production began again at the Cyclopic in 1919, and the old mill was remodeled in 1923 after the mine was taken over by the Gold Basin Exploration Company. In 1926 a new orebody was discovered so that the mill was again remodeled and its daily capacity increased to 100 tons.

Although the Cyclopic was one of the earliest discoveries and also was one of the largest overall producers of ore in the district, it was apparently inactive during the late 1920's. However, in 1929 the Kiowa Gold Mining Company built the San Juan mill about 1.6 km north of Cyclopic. Water for this then-new 60-ton mill evidently was obtained from the Cyclopic pumping station, previously built about 1905 to pipe water to an earlier mill at the same site. The actual source of the water was a well 5 km to the southwest (S-1/2 sec. 35, T. 28 N., R. 19 W.). About this time there was renewed

interest in the Harmonica (Climax) mine, 3.2 km north of the San Juan mill, and this mill may have processed ore from several small nearby mines until the Cyclopic mill was reactivated about 1932. The Cyclopic mine produced intermittently during 1932-34, when the shallow underground workings were abandoned in favor of a large volume opencut operation. By late 1933 a cyanide mill was operating at a daily capacity of 125 tons, and a total of about 40 men were employed at the mine and mill. Much of the ore mined in 1934 reportedly averaged approximately 0.2 oz gold per ton (Wilson, Cunningham, and Butler, 1934, p. 77). In 1936 the Cyclopic property was acquired by Manta de Oro Mines, Inc., and the mine produced more or less steadily through 1940. From 1941 to about 1967 the mine was idle, and all mine buildings are now (1982) gone. Exploration drilling in 1968 failed to locate any additional ore. However, some attempts to heap-leach at the site of the Cyclopic mine apparently were undertaken in 1981.

In addition to the Cyclopic, O.K., and Excelsior mines which were relatively steady producers over the years, the following mines had intermittent production during the depression-era mining revival from 1930 to 1942: Harmonica, Eldorado, Fry, Gold Hill, Golden Link, Golden Rule, M.O., Morning Star, and San Juan group. Most of the ore from these and several smaller mines and prospects was treated at the Cyclopic of Malco mills. In 1942, four lode mines in the Gold Basin district had a recorded production of 108 ounces gold and 24 ounces silver from 249 short tons of treated ore (Woodward and Luff, 1943). The district has been idle generally since about 1942, except for small-scale placer mining that recovered a little detrital gold.

The Lost Basin district comprises a wide-ranging group of placer and lode mines in a belt lying between Hualapai Wash on the west and the Grand Wash Cliffs on the east (fig. 3). It extends from the Colorado River at the mouth of the Grand Canyon southward through the Grand Cliffs for a total length of about 32 km. This district, although much larger in areal extent has not been as active nor as productive as the adjacent Gold Basin district. The principal gold veins were discovered in 1886 and the production of the district was reported by Schrader (1909) to be "many thousand dollars," chiefly in gold. Placers apparently were first worked in 1931 and resulted in a minor local boom. However, recorded production during 1904-32 in copper, gold, and silver was valued at less than $45,000 (Hewett and others, 1936).

The King Tut placers were discovered in 1931 and were the most important placers in the Lost Basin district. Systematic sampling of the King Tut placers by G. E. Pitts in 1932 delineated approximately 90,000 tons of indicated reserves and 250,000 tons of probable reserves before mining operations on a relatively large scale began (Mining Jour. [Arizona], 1933, p. 10). All of this was confined to more or less one section of land. In the last 4 months of 1933 the King Tut yielded 117 oz of gold (Gerry and Miller, 1935). By 1936 the gold output from the King Tut was 450 oz which represented the bulk of the entire production from the Lost Basin district. In 1939, Mr. Charles Duncan placered 13 oz of gold in 16 days, using only a sluice box and wash tub, near the King Tut placers (Eng. Mining Jour., 1939), whereas the King Tut placers themselves only were worked intermittently until 1942. Eventually placer mining of unconsolidated gravel from the upper reaches of present-day arroyos extended across approximately 25 km^2 in the general area of the King Tut placers (Blacet, 1969). Nonetheless, by 1942 there was no additional recorded production from the Lost Basin district. However, in the middle and late 1960's several small operators using dry washers were active intermittently in the general area of the King Tut placers. These washers were powered by small, portable gasoline motors. Because of the surge in the price of gold during 1978-80, small-scale placer operations and extensive exploration efforts began again, centered on an area just to the north of the King Tut placers.

A summary of the recorded metal production from the lode mines in the Gold Basin-Lost Basin districts between 1901 and 1942 reveals that 13,508 oz gold, 6,857 oz silver, 5,918 lbs (2,684 kg) copper, and 43,652 lbs (19,797 kg) lead were produced from a total of 69,189 tons of treated ore (table 2). Dollar vale of these metals was approximately $359,000, and approximately 98 percent of the dollar value is credited to gold. Recorded production from the Gold Basin district in the period 1904 to 1932 was 15,109 tons of ore yielding 6,244.91 oz Au, 5,059 oz Ag, 4,738 lbs (2,150 kg) Cu, and 1,765 lbs (801 kg) Pb, valued in all at $133,014 (Hewett and others, 1936; table 2, this report). Most of this production, excluding the 4,711 pounds copper produced during 1918, came from the Eldorado mine. The 4,711 lbs of copper is assigned questionably to an unknown mine in the Gold Basin district. Nineteen ounces of placer gold also was recovered from the Gold Basin district in 1942 (Woodward and Luff, 1943).

Table 2.--Production of gold, silver, copper and lead from lode deposits in the Gold Basin and Lost Basin mining districts, 1901-1942

[Figs. furnished by the U.S. Bureau of Mines; ----, no production recorded]

Year	Ore treated (short tons)	Gold (ounces)	Silver (ounces)	Copper (pounds)	Lead (pounds)
1901----	30	59	15	----	----
1902----	3,900	260	810	----	----
1903----	4,723	2,361	300	----	----
1904----	2,000	1,429	351	----	----
1905----	360	1,356	209	----	----
1906----	903	380	115	----	----
1907----	101	27	15	----	----
1908----	55	29	10	----	----
1910----	412	203	68	27	149
1911----	431	197	47	----	----
1913----	600	228	41	----	----
1914----	600	280	42	----	----
1915----	600	300	70	----	----
1917----	560	280	50	----	----
1918----	639	248	827	4,711	----
1919----	2,813	270	784	----	1,616
1920----	800	275	50	----	----
1922----	3	2	----	----	----
1923----	5	6	1	----	----
1929----	9	4	4	----	----
1933----	3,425	371	77	16	243
1934----	3,306	317	5	----	----
1935----	502	209	114	310	----
1936----	2,231	326	94	----	----
1937----	13,354	923	275	----	1,373
1938----	7,968	370	809	310	9,033
1939----	3,170	655	307	25	6,724
1940----	14,299	1,453	973	283	7,114
1941----	1,141	582	370	236	17,400
1942----	249	108	24	----	----
Total	69,189	13,508	6,857	5,918	43,652

GENERAL GEOLOGY OF THE DISTRICTS

The Gold Basin-Lost Basin mining districts are in the Basin and Range province, just south of Lake Mead and west of the Colorado Plateaus. Indeed, the western edge of the Colorado Plateaus reaches barely 3 km west from the east edge of the Garnet Mountain quadrangle (fig. 2), whereas the generally gently east dipping to flat lying, lower Paleozoic basal formations of the Colorado Plateau crop out along the Grand Wash Cliffs. As such, the districts occur in an uplifted region near the leading edge of the North American Platform (see Burchfiel, 1979; Dickinson, 1980), and they straddle several north-south trending ranges of mostly Proterozoic basement rocks from which the rocks of the Paleozoic stable platform have been removed by erosion. Lake Mead occupies a structurally complex area to the north marked by the junction of several regionally extensive, major geologic features (see Anderson and Laney, 1975). These features include the boundary between the Paleozoic miogeosyncline and stable platform, the Mesozoic Seveir orogenic belt, and the Las Vegas shear zone. Further, the districts occur along the southern extension of Virgin Mountains structural block of Longwell (1936) and Anderson and Laney (1975). The districts in all include two ranges of mostly Proterozoic X metamorphic and igneous rocks, the White Hills and the next range to the east herein termed the Lost Basin Range, and two intervening valleys filled by Tertiary and Quaternary deposits (Blacet, 1975). These two valleys are drained by Hualapai Wash and Grapevine Wash, and the latter valley also includes Grapevine Mesa. The Grapevine geomorphic trough includes the Grand Wash Fault zone, a N. 10°-15° E-striking system of Miocene normal faults (west block down) now covered by Tertiary fanglomerate and Quaternary gravel. The trace of the Grand Wash fault zone is inferred to pass between Lost Basin range and Garnet Mountain, southwest of which the Grand Wash fault zone is inferred to terminate against a younger northwest-striking structure (Goetz and others, 1975, fig. IV-B-2), herein named the Hualapai Valley fault. The Hualapai Valley fault is inferred then to change gradually its strike to almost north-south as it passes west of the Lost Basin range along the main drainage of Hualapai Wash (Liggett and Childs, 1977). Major offsets along the Hualapai Valley fault must predate deposition of the late Miocene Hualapai Limestone Member of the Miocene-Pliocene(?) Muddy Creek Formation, because the Hualapai Limestone apparently is not cut by the Hualapai Valley fault (see Blacet, 1975). However, initial movements along the Hualapai

Valley fault may have contributed toward local development of the embayment in which the Hualapai Limestone was deposited.

Proterozic X rocks crop out widely in both the Gold Basin and Lost Basin mining districts, and they consist mostly of presumably 1,750 m.y. (million years) gneiss, including both paragneiss and orthogneiss, the coarse-grained porphyritic monzogranite of Garnet Mountain and medium-grained, relatively small masses of leucocratic monzogranite that crop out as part of the plutonic complex of Garnet Mountain (fig. 2). In this report we use the classification of Streckeisen and others (1973). As such, the porphyritic monzogranite of Garnet Mountain and the leucocratic monzogranite correspond with the porphyritic quartz monzonite and leucocratic quartz monzonite of Blacet (1975) who followed the classification of Bateman (1961). The porphyritic monzogranite of Garnet Mountain intrudes gneiss and most likely was emplaced about 1,660 m.y. ago (Wasserburg and Lanphere, 1965). The Proterozic terrane in the quadrangle also includes small bodies of granodiorite, gneissic granodiorite, alaskite, various mappable migmatite units, feldspathic gneiss, amphibolite derived from igneous and sedimentary protoliths, and other metasedimentary rocks including some fairly widespread metaquartzite. In addition, there are some minor amounts of presumably Proterozic Y age diabase exposed mostly as thin northwest-striking dikes in the general area of Iron Spring Basin (fig. 2).

The most widespread unit of Proterozoic X age to crop out in the districts is the gneiss unit (Xgn, fig. 2). As such, it hosts most of the known quartz-gold vein deposits. These deposits are concentrated in an approximately N. 15°-20° E.-trending, 15-km-wide belt that spans the Gold Basin and Lost Basin districts, and the deposits occur mostly in the western one-half of the Garnet Mountain quadrangle (fig. 3). The remaining gold-quartz veins are concentrated mostly in the southern part of the Gold Basin district, east of the Cyclopic mine. The veins here are hosted by gneissic granodiorite and porphyritic monzogranite of Garnet Mountain.

The Proterozoic X gneiss, and here we paraphrase Blacet's descriptions for the most part, consists of an assemblage of metasedimentary rocks, mostly quartzofeldspathic gneiss, but interlayered with cordierite gneiss, biotite-garnet-sillimanite schist, and amphibolite. Locally, dark-gray to black amphibolite comprises a very significant proportion of exposed sequences of the gneiss unit, especially in the southern parts of the Lost Basin range

wherein the amphibolite sequences consist of metagabbro, metadiabase, metaclinopyroxenite, and metawehrlite. Generally, the amphibolite crops out discontinuously in variably sized lensoid masses. In addition, thin lenses of marble, calc-silicate gneiss, banded iron formation, and metachert crop out sporadically through the gneiss. All these metamorphic rocks have been deformed intensely during several episodes of deformation in Proterozoic X time (Blacet, 1975). Furthermore, the relation of a more widely exposed Proterozoic terrane in the western part of the mining districts than in the eastern part mostly reflects regional eastward- to northeastward-tilting of this block concomitant with the denudation of the once overlying Paleozoic and Mesozoic sequences. Major initial displacements to accomplish the tilting were concentrated along the Grand Wash fault zone, and they are estimated to have ranged from 1,000 to more than 5,000 m (Luchitta, 1966). This fault zone will be discussed in somewhat more detail below.

East of the Lost Basin district, well-exposed Paleozoic formations crop out at the base of the Grand Wash Cliffs, near the east boundary of the Garnet Mountain quadrangle. These formations include the conformable Lower Cambrian Tapeats Sandstone, the Lower to Middle Cambrian Bright Angel Shale, and the Middle Cambrian Muav Limestone (Blacet, 1975). The Tapeats Sandstone rests unconformably on the porphyritic monzogranite of Garnet Mountain. All of these formations are included within the Paleozoic undivided unit of figure 2.

An undeformed, leucocratic, two-mica monzogranite intrudes gneiss about 1.5 km north of the Cyclopic mine in the southern part of the Gold Basin district (fig. 2). The two mica monzogranite crops out across an area of about 4 to 5 km^2, and is upper Cretaceous in age (Blacet, 1972; see below); it includes some zones of episyenite, and minor aplite and pegmatite.

Three types of lode gold deposits are known in the Gold Basin-Lost Basin districts (Blacet, 1969; 1975). Most lode gold deposits in the districts occur as veins, presumably confined mostly during upper Cretaceous time along preexisting structures in Proterozoic X rocks. In addition, some gold-bearing quartz veins in the districts probably are Proterozoic in age. However, a minor yet geologically significant type of lode gold deposit in the Gold Basin district consists of small masses of fluorite-bearing episyenite containing macroscopically visible, disseminated gold (Blacet, 1969). Most likely, the emplacement of these episyenite bodies is related genetically to the intrusion of upper Cretaceous, two-mica monzogranite. The third type of lode gold

deposit, exemplified by the Cyclopic mine, consists of upper Cretaceous gold-quartz veins caught up along a regionally extensive Miocene low-angle fault. This fault crops out in the southern part of the Gold Basin district, and has been traced to the north along the western flank of the White Hills (fig. 2).

The oldest Tertiary rocks in the general area of the districts are volcanic rocks presumably equivalent to the Tertiary Mount Davis Volcanics or Patsy Mine Volcanics (Tv, fig. 2), rhyolitic tuffaceous sedimentary rocks and fanglomerate (Ts), and Tertiary fanglomerate (Tf). The volcanic rocks include mostly andesite and their base in the general area of the districts is not exposed but instead is marked apparently by a low-angle detachment surface. A sequence of tuffaceous mudflows and rhyolitic water-laid tuffaceous sedimentary rocks and fanglomerate crop out near the southern end of the Lost Basin Range (fig. 2) and have been mapped in detail by Deaderick (1980). This sequence is steeply dipping, is partly bounded by north-striking faults on the west, and possibly is equivalent in age to the Tertiary volcanic rocks; on the east, the sequence is overlain unconformably by conglomerates belonging to the Muddy Creek Formation. In addition, Deaderick (1980) found that the mudflows and rhyolitic tuffaceous sedimentary rocks are in depositional contact with Proterozoic X migmatic gneiss. Near the northwest corner of figure 2, Tertiary fanglomerate (Tf) apparently is intercalated with the Tertiary volcanic rocks. These coarse fanglomeratic deposits include locally landslide or mudflow breccia, and they are overlain unconformably by fanglomeratic deposits of the Muddy Creek Formation.

The Muddy Creek Formation consists of conglomerate, claystone, mudstone, and gypsum; basalt at Senator Mountain and Iron Spring Basin near the Grand Wash Cliffs probably equivalent to the Fortification Hill Basalt member of the Muddy Creek Formation at its type locality; and an upper carbonate member called the Hualapai Limestone. The conglomerate appears to have been deposited in small basins and topographic lows in an environment of interior drainage. Small patches of landslide or mudflow breccia containing Proterozoic clasts occur within the fanglomerate of the Muddy Creek Formation southeast of the Lost Basin Range. However, the Hualapai Limestone member probably was deposited in a marine environment (Blair, 1978; Blair and Armstrong, 1979). Paleonotological and chemical evidence suggest that the Hualapai Limestone may reflect deposition at the northern end of an extended embayment of the Gulf of California beginning more than 8.9 m.y. ago (Blair,

McKee, and Armstrong, 1977). The type locality for the Hualapai Limestone is along Hualapai Wash, and the thickest part of the limestone at the type locality is almost 300 m. Some beds of this limestone cover the Grand Wash fault zone near the base of the Grand Wash Cliffs where the Colorado River emerges from the Grand Canyon. Thus, there apparently has been no major movement along this fault zone since the last several hundred meters of deposition of the Miocene-Pliocene(?) Muddy Creek Formation. However in the general area of the Cyclopic mine, the Muddy Creek Formation has been faulted against Proterozoic metamorphic and igneous rocks and the upper Cretaceous two-mica monzogranite along the regionally extensive low-angle Miocene fault which crops out there (fig. 2). This detachment fault borders the White Hills along its entire western margin, and the fault probably thus establishes an eastern leading edge for low-angle detachment terranes in the Lake Mead area (see Anderson, 1971; Davis and others, 1979, fig. 1).

The overall tectonic history of this low angle structure is poorly resolved. It does not appear, however, to be similar to dislocation surfaces (decollement) immediately associated spatially with closely underlying Cordilleran metamorphic core complexes (see Crittenden and others, 1980). Furthermore, the fabric of the two-mica monzogranite is not mylonitic or cataclastic (see below). In addition, such core-complex-associated dislocation surfaces typically show an underlying microbreccia about 1 m thick which is in turn underlain by a zone of chlorite breccia. However, the detachment fault which crops out along the western margin of the White Hills and at the Cyclopic mine, may reflect the eastern, distal effect of near-surface distension associated with the emplacement of plutons penecontemporaneous with the Miocene Mount Davis Volcanics (see Anderson, 1971; Anderson and others, 1972). The overall extension associated with this structure appears to have an azimuthal bearing of approximately east-west. In the general area of the Cyclopic mine, fanglomerate of the Miocene-Pliocene(?) Muddy Creek Formation crops out in the upper plate of the detachment fault (fig. 2).

The next youngest sequence of rocks in the Gold Basin-Lost Basin districts includes some unconsolidated sediments (Blacet, 1975). Well-rounded cobbles and gravels derived from the Colorado Plateau lie scattered unconformably on the Hualapai Limestone and some ridges of the Muddy Creek Formation. Because of their patchy distribution, they are not shown as

separate map units on the geologic sketch map (fig. 2). These cobbles and gravels probably represent Pliocene high-level remnants of the ancestral Colorado River.

Some late Tertiary gravels occur as dissected alluvial fan remnants along Grapevine Wash at the base of the Grand Wash Cliffs, and are included with the Quaternary sedimentary deposits of figure 2 (unit Qs).

The Grand Wash fault zone near the base of the Grand Wash Cliffs has had a profound impact on the overall geomorphic evolution of the region. However, any viable regional interpretation must include the critical geologic relations mapped by Blacet (1975) at the Lost Basin Range, approximately 10 km west of the Grand Wash Cliffs and almost at the very center of the Garnet Mountain quadrangle. Figure 4 summarizes schematically in an east-west cross section, our hypotheses of the geologic-geomorphic history of the region during the last 15 to 18 m.y. This figure shows in cross section, inferred structural relations extending from the ancestral highland of the White Hills-southern Virgin Mountains on the west, through the rocks of the Lost Basin Range, and finally to the Grand Wash Cliffs on the east.

A sequential alternation between regional extensional tectonics and possibly very minor local compressional tectonics seems to have affected the predominantly Proterozoic X crystalline terrane, and this, in turn, apparently contributed toward the eventual distribution of the productive placer gold deposits. The development of the relatively deep, middle to late Tertiary basin along the Grand Wash fault zone appears to have been controlled primarily by regional east-west extension (fig. 4A). This extension is reflected also in the low-angle dislocation surfaces at the base of the volcanic rocks possibly equivalent in age to the Mount Davis Volcanics, and through the general area of the Cyclopic mine workings (fig. 2). Sediment was shed into the basin along the Grand Wash trough mostly from a highland at the ancestral White Hills and southern Virgin Mountains. Sometime after deposition of the lowermost sequences of the tuffaceous, gold-poor fanglomerate belonging to the Miocene-Pliocene(?) Muddy Creek Formation into the basin, local thrusting toward the east may have occurred during the late Tertiary in the general area of the Lost Basin Range to yield the steeply dipping and partly overturned sequence of mudflows and rhylotic tuffaceous sedimentary rocks (fig. 4B). Proterozoic X gneiss, migmatic gneiss, feldspathic gneiss, and amphibolite may have been thrust against this sequence

Figure 4.--Schematic east-west cross sections showing inferred geologic relations about 15-18 m.y. ago (A) , about 8 m.y. ago (B), and about 5 m.y. ago (C). Modified from P. M. Blacet (unpub. data, 1967-1972).

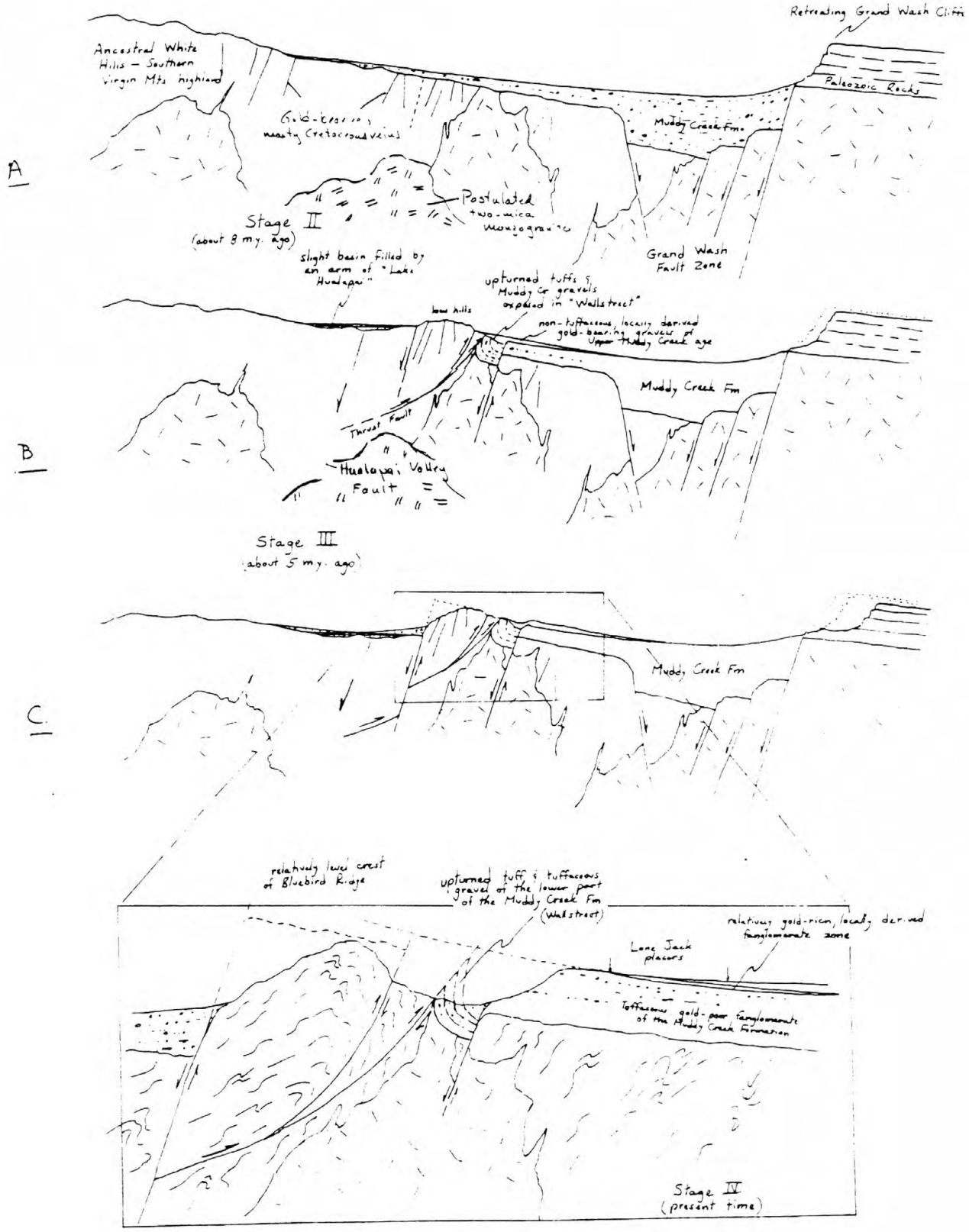
Stage I
(about 15-18 million years ago)
Middle Miocene
Retreating Grand Wash Cliffs
Ancestral White Hills – Southern Virgin Mts highland
Gold-bearing, mostly Cretaceous veins
Paleozoic Rocks
Muddy Creek Fm
A
Postulated two-mica monzogranite
Stage II
(about 8 m.y. ago)
slight basin filled by an arm of "Lake Hualapai"
Grand Wash Fault Zone
upturned tuffs & Muddy Creek gravels exposed in "Wall Street"
low hills
non-tuffaceous, locally derived gold-bearing gravels of Upper Muddy Creek age
Muddy Creek Fm
Thrust Fault
B
Hualapai Valley Fault
Stage III
(about 5 m.y. ago)
Muddy Creek Fm
C
relatively low crest of Bluebird Ridge
upturned tuffs & tuffaceous gravel of the lower part of the Muddy Creek Fm (Wall Street)
relatively gold-rich, locally derived conglomeratic zone
Long Jack placers
tuffaceous gold-poor conglomerate of the Muddy Creek Formation
Stage IV
(present time)

of steeply dipping and locally overturned mudflows and rhyolitic tuffaceous sedimentary rocks and fanglomerate (unit Ts, fig. 2). This late Tertiary shortening was a near-surface phenomenon and brought about the development of low hills at and ancestral to present-day Lost Basin Range. East-west shortening may have been followed by a rejuvenation of east-west extension as reflected by steeply west dipping normal faults (west side down) along both the east and west range fronts of the the Lost Basin range. These north-south normal faults seem to reflect a westward migration with time in extensional phenomena away from the Grand Wash fault zone. Some of the last major, normal displacements here were concentrated along the Hualapai Valley fault, and these major displacements predated deposition of the Hualapai Limestone.

The initiation of block faulting at the Lost Basin range probably occurred penecontemporaneous with the deposition of nontuffaceous, locally derived gold-bearing gravels of upper Muddy Creek age. These gravels, which contain gold in apparently noneconomic concentrations, most likely were derived in part from the now eroded, upper portions of veins exposed along Lost Basin range and uplifted possibly as a result of minor thrusting during the late Tertiary. However, continued minor movements along the normal fault inferred to bound Lost Basin range immediately on the west, together with the deep post-Muddy Creek erosion just to the west of Lost Basin range led to the relative uplifting of the gold-bearing gravels at the leading edge of Grapevine mesa and the reworking of these gravels during the Quaternary into important placer deposits (Lone Jack placers, SW1/4 sec. 15, T. 29 N., R. 17 W.). These gold-bearing placers are now perched approximately 500 m above the main drainage of Hualapai Wash, about 5 km to the west.

The relations between the apparent detachment fault, which crops out just east and southeast of Senator Mountain and along the western margin of the White Hills (fig. 2), and the Lost Basin range nonetheless are difficult to resolve. If the detachment fault, at some time prior to block faulting, approximately followed Hualapai Wash to the north, then the detachment fault would underlie the Lost Basin range, and all rocks that crop out there would be allochthonous. The faults along the eastern margin of the Lost Basin range could then be interpreted as listric normal faults. Alternatively, the detachment fault may continue to the southeast from the area of the Cyclopic mine, where it last crops out before being covered by Quaternary gravels. This latter hypothesis seems more likely (P. M. Blacet, unpub. data, 1967-

1972), and the trace of the detachment fault probably lies to the east of Table Mountain Plateau, approximately 10 km to the southeast of the Cyclopic mine area.

K-Ar CHRONOLOGY OF MINERALIZATION AND IGNEOUS ACTIVITY

By

E. H. McKee

Eleven samples in all were dated by the K-Ar method. These include nine purified mineral separates (eight white mica, one biotite, and one sanidine) and one whole-rock sample. Sample preparation and argon and potassium analyses were done in the U.S. Geological Survey laboratories, Menlo Park, Calif. Potassium analyses were performed by a lithium metaborate flux fusion-flame photometry technique and argon analyses were performed by standard isotope dilution procedures. Nine of the samples were analyzed using a 60° sector 15.2 cm radius Neir-type mass spectrometer operated in the static mode in which six manual scans of ^{40}Ar, ^{38}Ar, ^{36}Ar peaks were made during a time interval of about 10 minutes. Two samples (nos. 837 and 999, table 3) were analyzed on a five-collector first-order direction focusing, 22.9 cm radius mass spectrometer controlled by a PDP8/3 minicomputer that takes peak heights simultaneously from the three argon collectors. The constants used in age calculations are:

$\lambda\varepsilon = 0.581 \times 10^{-10} yr^{-1}$, $\lambda\beta = 4.963 \times 10^{-10} yr^{-1}$, and $^{40}K/K_{total} = 1.167 \times 10^{-4}$ mole/mole.

The precision or analytical reproducibility reported as a $\pm$ value is at σ. In a general way it reflects the relative amount of $^{40}Ar^{rad}$ to $^{40}Ar^{total}$ the higher percent of $^{40}Ar^{rad}$ the smaller the $\pm$. The $\pm$ value is determined by assessment of the various analytical procedures, including flame-photometer and spectrometer reproducibility, and standard and argon tracer calibration. The precision of the eight ages reported ranges from 0.7 to 6.5 percent of the calculated age.

Cretaceous Plutonic Rocks

Several small two-mica leucocratic quartz monzonite plutons crop out in the southwestern part of the area outlined in figure 2. Muscovite from a sample of one of these bodies about 2 km north of the Cycloptic mine was dated. The age determination is 72.0$\pm$2.1 m.y., which is Late Cretaceous (Laramide) and typical of many granitic rocks in central and western Arizona.

Biotite from a sample of Proterozoic gneiss from about 2 km east of this pluton was dated to see what effect, if any, the Cretaceous plutons have had on surrounding rocks. A number of dikes of presumed and (or) known Cretaceous age intrude the gneiss and much or most of the hydrothermal alteration and mineralization is also of Cretaceous age. It was hoped that radiogenetic ^{40}Ar in biotite in the gneiss which is easily lost at moderately low temerature would reflect the extent of pervasive regional heating during the late Cretaceous. The biotite yielded an age of 76.3±3.0 m.y., which is very near that of the pluton and substantiates the widespread character of the Late Cretaceous (Laramide) igneous event.

Cretaceous Veins

Three quartz-muscovite veins were sampled for age determination. Two of the veins cut granitic rocks, known or assumed to be late Cretaceous in age, one cuts gneissic rocks of Proterozoic age. Sample number 923 (table 3) cuts the leucocratic quartz monzonite dated at 72.0±2.1 m.y.--it yielded an age of 68.8±1.8 m.y. which is the same as the pluton (within the overlap of the ± values). The second vein in granitic rock is 4 km to the southeast of the dated pluton and vein described above. Its K-Ar age is 65.4±2.6 m.y., the same, considering the analytical precision, as the first vein.

Both veins contain fluorite and pyrite as well as white mica and quartz as major components. Gold in trace amounts also occurs in the veins, and it is the metal mostly sought in the numerous prospects and small abandoned mines throughout the area. On the basis of these age determinations, mineralization is considered to be late Cretaceous (Laramide) in age and to be a late stage of the period of Laramide plutonism prevalent throughout the Basin and Range region of Arizona.

The third dated vein cuts Proterozoic gneiss about 1 km east of the Bluebird mine in the center of the mapped area (no. 287). Hand samples of this vein contain what appears to be hydrothermal white mica along with trace amounts of gold. The white mica yields a K-Ar age of 67.8±2.0 m.y. and is within the age span of the two veins reported above and about the same as the age of primary muscovite from the leucocratic quartz monzonite. This age substantiates the thesis that Laramide igneous activity was associated with significant gold mineralization throughout the Gold Basin-Lost Basin region, roughly at the same time as the widespread Laramide porphyry copper deposits formed elsewhere in the southwest.

Table 3. K-Ar analytical data and ages

Field number and location	Unit name	Mineral dated	K_2O percent	^{40}Ar rad 10^{-11}mole/g	^{40}Arrad percent	Apparent age (m.y.) ±
733C 35°59'54" 114°17'40"	Basalt flow in Muddy Creek Formation	Whole-rock basalt	1.045 1.067	1.6619	17.1	10.9±0.6
728A 35°52'00" 114°07'00"	Air-fall tuff	Sanidine	8.48	11.9251	77.2	15.4±0.2
837 35°46'00" 114°14'00"	Quartz-muscovite-fluorite-pyrite vein	Muscovite	10.75	103.001	21.1	65.4±2.6
278A 35°53'15" 114°08'04"	Quartz vein containing hydrothermal muscovite	Muscovite	10.95	108.991	79.4	67.8±2.0
923 35°48'22" 114°15'15"	Muscovite from quartz-muscovite-fluorite-pyrite vein cutting two-mica monzogranite	Muscovite	10.73 10.75	108.465	88.5	68.8±1.8
884 35°48'22" 114°15'15"	Two-mica monzogranite	Muscovite	10.67	112.823	76.9	72.0±2.1
999 35°48'03" 114°12'44"	Gneissic granodiorite	Biotite	9.06	101.666	85.1	76.3±3.0
79GM8b 35°46'42" 114°11'07"	Episyenitic alteration pipe, gold-bearing	sericite	11.64	220.225	90.8	126.9±3.8
Do.	do.	do.	do.	226.550	87.8	130.3±3.9
735 35°58'45" 114°15'42"	Secondary mica in quartz	Muscovite	10.62	1.3342×10^{-8}	98.0	712±5.0
735-1 35°58'45" 114°15'42"	Secondary mica in quartz	Muscovite	10.67	1.6007×10^{-8}	95.0	822±6.0

Constants used in all age determinations are: $= 0.581 \times 10^{-10} yr^{-1}$

$= 4.96 \times 10^{-10} yr^{-1}$

$^{40}K/K$ total $= 1.167 \times 10^{-4}$moles/moles

Two ages were determined on fine muscovite from a gold-bearing episyenitic alteration pipe in Proterozoic biotite monzogranite about 5 km southeast of the dated Late Cretaceous two-mica leucocratic pluton. This alteration pipe is in the same general area as the dated Late Cretaceous veins and its mineral assemblage and geologic setting suggest that it is related to, and probably the same age as the other veins in the area. The ages from this pipe are 126.9±3.8 and 130.3±3.9 m.y., or twice as old as expected. If the pipe is Late Cretaceous, as field evidence indicates, some type of contamination has affected the sample. Two possibilities that seem most likely include: excess radiogenic Ar picked up by hydrothermal solutions passing through the surrounding Proterozoic rocks and incorporated in the hydrothermal vein sericite during its formation or mineral contamination caused by inclusion of some Proterozoic muscovite or feldspar from the host gneiss during collection of the vein sample. From the data available it is impossible to verify which, if either of these mechanisms accounts for the anomalously old age of the pipe's muscovite.

Proterozoic(?) Vein

Two samples of secondary, coarse-grained hydrothermal white mica from a gold-bearing quartz vein about 3 km southwest of Salt Spring Bay on Lake Mead were dated. The vein, which cuts Proterozoic gneiss, looks like the other veins in the region, some of which yielded late Cretaceous or Laramide ages (see above). It was expected that this vein also would be Laramide in age as well. The apparent ages, however, are discordant at 712±5 and 822±6 m.y. Interpretation of these values is difficult. Proterozoic gneiss of similar appearance with the host rock of the vein described here is intruded by porphyric monzogranite that was dated by Rb-Sr methods (a well-defined isochron) at 1,660 m.y. (Wasserburg and Lanphere, 1965, p. 746, and fig. 4). This age is similar to many ages of Proterozoic rocks in central and western Arizona and is considered an established age for major regional igneous events in this region (Silver, 1964, 1966, 1967; Ludwig, 1973). The discordant K-Ar ages on the vein white mica could represent partial and different amounts of argon loss from a Proterozoic vein related either to the widespread 1,660-m.y. event or a less well documented gold mineralization event at 1,440 m.y. The partial argon loss and accompanying partial resetting of the K-Ar "clock" may have been caused by slight heating during the Late Cretaceous and or early Tertiary Laramide event documented elsewhere in the area. If the area near

the vein were not heated sufficiently to release all the radiogenetically produced ^{40}Ar the age would be some indeterminable amount less than the original 1,660 m.y. age--the 822 and 711 m.y. determined here. Alternatively, it could also represent small but continuous argon diffusion from the white mica caused by general regional geothermal elevation throughout the past 1,660 m.y. The result in either case is a reset age that does not record the time of any single event. It also assumes that the vein was about the same age as the dated gneiss or approximately 1,660 m.y.

The possibility exists that the white mica mineral separate from the vein contained a small amount of Proterozoic muscovite from the enclosing host gneiss. A small and different amount of 1,660 m.y. old contaminant muscovite with a larger amount of Late Cretaceous vein white mica could produce the two aberrant ages. There is no way to evaluate the possibility of this mechanism for arriving at the 822 and 711 m.y. ages. It is assumed that the ages do not represent the time of vein emplacement. We believe, however, that the overwhelming bulk of the white mica composing these two mineral separates dated by the K-Ar method crystallized during the vein's emplacement.

Textural relations between white mica and vein quartz from the sample site at locality 735 yielding the 822 and 711 m.y. ages were studied using the SEM (fig. 5). These studies suggest strongly that the white mica there composing the dated samples is secondary. An initially unknown, 1.5 mm-long, bladed mineral (fig. 5A) chemically was verified by its SEM X-ray spectra as having the same overall proportions of aluminum, silicon, potassium, and iron as a known muscovite standard (compare fig. 5B and C). In addition, some of these very fine grained bladed crystals, which can reasonably be assumed to be white mica, appear to be growing into 3 to 5 mm, irregularly shaped cavities in vein quartz. This relation suggests the white mica is secondary; that is, it crystallized initially during vein formation. These small crystals of mica are most probably not daughter minerals but are instead trapped or captured mineral grains (see Roedder, 1972, p. JJ 24).

Tertiary Volcanic Rocks

Samples 733C basalt and 728A rhyolite ash-flow tuff were dated to aid in establishing the chronology of Tertiary rocks and tectonic events in the Gold Basin-Lost Basin area. The dates were used in conjunction with stratigraphic relations for correlation between units in the complex, lenticular sequences of Tertiary basin and subaerial deposits of the region. They also provide

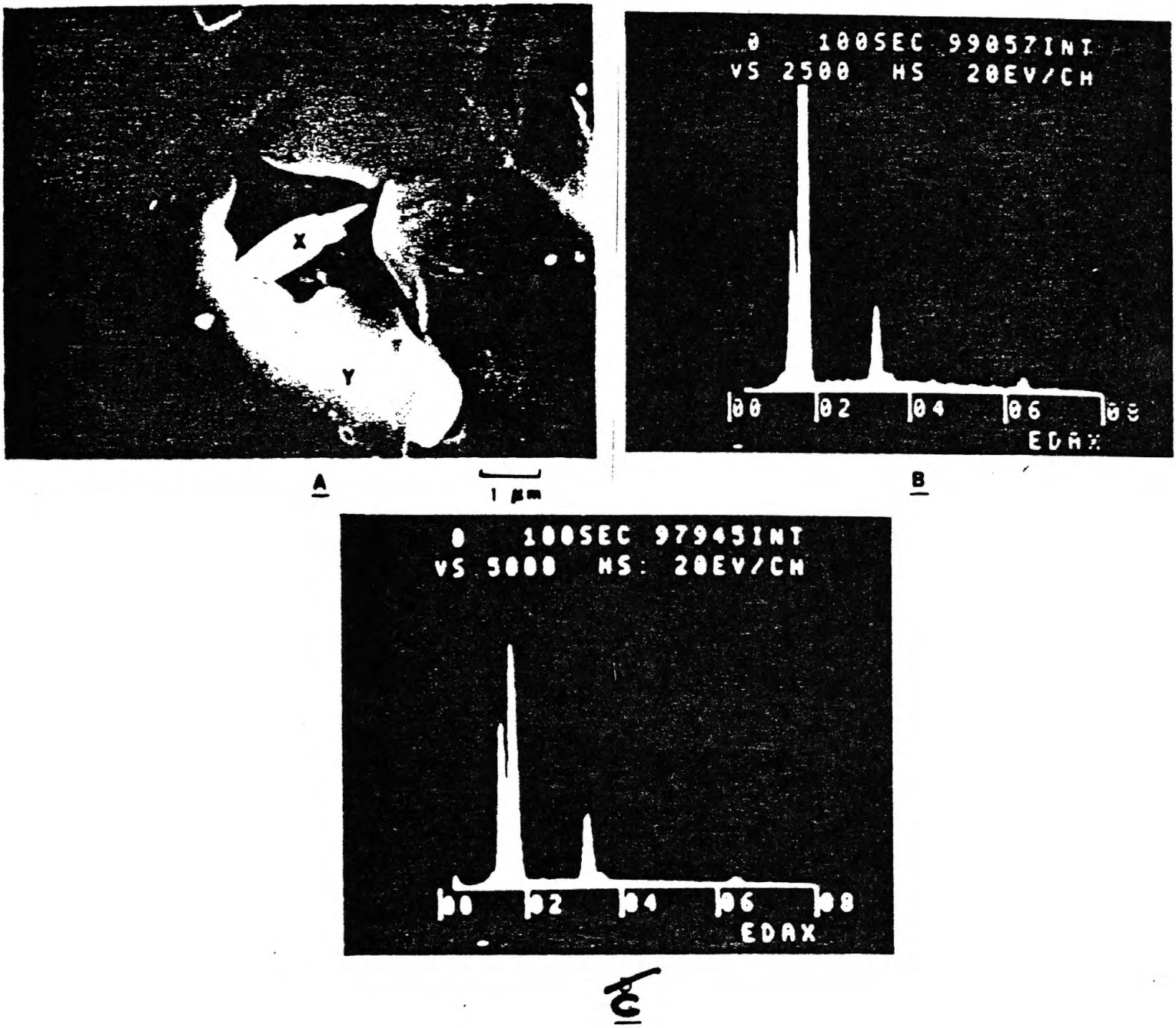

Figure 5.--Scanning electron microscope (SEM) photograph (A) showing an approximately 1.5 µm long blade of an unknown mineral (X) projecting into an open cavity in vein quartz (Y) from locality number 735 (pl. 1). SEM-produced X-ray spectra for the unknown mineral (B) compared with spectra for known muscovite (C), both spectra generated under 20 KV for 100 seconds.

limits on the age of low-angle faulting (regional sliding) that has displaced most of the Tertiary rocks in the region.

The 15.4±0.2 m.y. age on sanidine from a rhyolite welded ash-flow tuff from a large tectonic block along Salt Creek Wash suggests correlation with the middle part of the Patsy Mine Volcanics or possibly the lower part of the Mount Davis Volcanics as described by Anderson and others (1972). The Patsy Mine Volcanics are comprised of more than a thousand meters of lenticular volcanogenic rock including a variety of rhyolitic to dacitic lava flows and tuff beds. The type area for Patsy Mine Volcanics is in the Eldorado Mountains of Nevada about 70 km due west of the sample site of the tuff reported here. Unspecified Tertiary volcanic rocks of which the Patsy Mine Volcanics are a part are shown on figure 2 of Anderson and others (1972) as extending in to the Gold Basin-Lost Basin area. Because the middle part of this composite volcanic unit is rhyolite lavas and interstratified tuffaceous sedimentary rocks with K-Ar ages in the range of 14.5 to 18.6 m.y., the correlation with our 15.4±0.2 m.y. rhyolite tuff seems good. In fact, Anderson and others (1972, table 1 and appendix, nos. 36-40) record three rhyolite flows with ages that are the same within analytical uncertainty as the tuff reported here. Furthermore, sanidine mineral separates used to date the Patsy mine rocks and the Gold Basin-Lost Basin ash flow have a similar, unusually low, K_2O content suggesting a genetic relationship.

A sample of basalt collected 6.8 km south of Temple Bar from the lower of two flows beneath the Miocene-Pliocene(?) Hualapai Limestone Member of the Muddy Creek Formation yields a K-Ar age of 10.9±0.6 m.y. This is the same age (11.3±0.3, 11.1±0.5, and 10.6±1.1 m.y.) within the analytical uncertainty as the Fortification Basalt Member of the Muddy Creek as reported by Anderson and others (1972). The locality south of Temple Bar is at least 30 km from Fortification Hill and 45 km and 50 km, respectively, from the collection sites of the other basalt samples, so it is doubtful that any of the samples are from the same lava flow. The concordant ages on basalts indicate that basaltic volcanism was widespread and from a number of vents in the region about 11 m.y. ago.

All of the silicic and intermediate volcanic rocks in the Gold Basin-Lost Basin area (those correlated with the Patsy Mine Volcanics or Mount Davis Volcanics) are in fault contact with surrounding older rocks. The fault is low angle and is apparently some type of regional slide surface and not a

thrust fault. Other areas in southern Arizona, southeastern California, western Utah, and eastern Nevada in which the terrain is characterized by large slide blocks of Tertiary rocks have almost universally been related to metamorphic core complexes. Gravity tectonics caused by doming of the core complex is the driving force that causes movement of these large slide blocks. In the Gold Basin-Lost Basin area, sliding postdates the rhyolite unit dated at 15.4±0.2 m.y. A second period of sliding is recorded by low-angle fault surfaces between Tertiary conglomerate of the Muddy Creek Formation that is about 10.9 m.y. old and older rocks including Proterozoic gneiss and the late Cretaceous two-mica monzogranite (see fig. 2). This second period of sliding is probably not much younger than about 10.9 m.y. because the Hualapai Limestone Member of the Muddy Creek Formation, a thick carbonate unit in the region about 8 m.y. old (Blair, 1978), is largely undeformed and not in fault contact with older rocks.

PETROCHEMISTRY OF CRYSTALLINE ROCKS AND THEIR RELATION TO MINERALIZATION

Metamorphic rocks in the Gold Basin-Lost Basin mining districts have been derived from igneous and sedimentary protoliths that were regionally metamorphosed as high as upper amphibolite facies (Miyashiro, 1973) assemblages, and complexly deformed syntectonically and multiply, during the older Proterozoic X Mazatzal orogeny (see Wilson, 1937; 1962). This orogeny occurred 1650 to 1750 m.y. ago (Silver, 1967). The Mazatzal orogeny thus correlates temporally with the upper one-half of the Hudsonian orogeny in the Canadian Shield, final metamorphism in the Front Range, Colo., and the pre-Belt basement, Montana, (King, 1969). Proterozoic X metamorphic rocks in Arizona broadly compose three tectonic belts, of which the northwesternmost one, in the general region of the Gold Basin-Lost Basin mining districts, is mostly gneiss derived largely from an epiclastic protolith (Anderson and Guilbert, 1979); it also includes schists in the Vishnu Complex derived from shale and graywacke protoliths (Brown and others, 1979), and some relatively substantial sequences of gneiss and amphibolite derived from mafic and, very locally, ultramafic protoliths (see below). Metamorphic rocks in the districts also include metaquartzite, thin lenses of marble, calc-silicate gneiss, banded iron formation and metachert. The protolith(s) of these metamorphic rocks is difficult to correlate convincingly with specific well-studied sequences of Proterozoic rocks in central Arizona (see Donnelly and

Hahn (1981) for descriptions of these sequences). The Proterozoic X Bagdad Belt of Donnelly and Hahn (1981) includes relatively thick sequences of coarse- to fine-grained metamorphosed wackes near the top of the overall metamorphic pile there. Some of these metamorphosed wackes may be correlative with quartzofeldspathic gneiss at Gold Basin-Lost Basin.

The gneisses exposed in the Gold Basin-Lost Basin mining districts contain highly deformed and lithologically complex sequences that commonly grade or change abruptly into one another across short distances. Although a quartz-plagioclase (oligoclase or andesine) or quartzofeldspathic gneiss is probably the predominant rock type overall of the gneiss unit, quartzofeldspathic gneiss is complexly interlayered with other lithologies in many outcrops (fig. 6A). In addition, moderately thick, layered sequences of predominantly quartzofeldspathic gneiss may grade into sequences consisting mostly of amphibolite by subtle yet marked changes in the relative proportions of quartzofeldspathic gneiss and amphibolite along strike. Some of these amphibolites in the districts will be shown below to have an igneous protolith. In some sequences within the gneiss unit, rather abrupt transitions also occur across conformable contacts, perpendicular to lithologic layering between predominantly quartzofeldspathic gneiss and mixed zones of amphibolite and associated gneissic, pegmatoid leucogranite dikes and thin sills (fig. 6B). However, most of these contacts could not be laterally extended sufficiently to be shown at a scale of 1:48,000, the scale of the map published by Blacet (1975). Further, many outcrops show an overall banded aspect resulting from complex and close interlamination and interlayering of quartzofeldspathic gneiss and amphibolite. In fact, many outcrops in the gneiss unit contain abundant 0.3 to 5.0 cm, highly planar and continuous bands of amphibolite, some bands reaching thicknesses as great as 40 cm. Many such outcrops commonly show a pull apart or boudinage of the amphibolite layers. In these outcrops, the foliation in the surrounding quartzofeldspathic gneiss converges dramatically in the necked domains of the amphibolite suggesting the preferred concentration of ductile flow in the quartzofeldspathic gneiss during deformation. Additional evidence for the brittle behavior of blocks of layered amphibolite during igneous injection includes the infilling of leucogranite along fractures between separated blocks of amphibolite (fig. 7). Some further evidence for the complexity of the prolonged deformation(s) to affect the Proterozoic X gneiss terrane is reflected in highly contorted

Figure 6. Photographs showing A, Typical exposure of distinctly layered gneiss showing well-developed similar folds plunging about 35° to N. 75° W. A quartz vein cuts the gneiss near the base of the photograph. Note pocket knife near upper center for scale; B, Zone of folded, thin leucogranite layers confined to a 30-cm sequence of chloritized amphibolite within uniformly dipping paragneiss. View toward the west approximately parallel to the moderately plunging (25°) fold axes. Shearing is locally concentrated near the axial planes of the folds; C, Ribboned and spotted migmatitic gneiss containing abundant wispy and discontinuous leucogranitic segregations. Dark bands consist of an early garnet-giotite (greenish-brown, Z)--minor muscovite-quartz-opaque mineral(s) assemblage that is replaced in part by an epidote-chlorite-fine-grained muscovite-opaque mineral(s) assemblage. Some blades of chlorite are porphyroblastic and cut the schistose fabric of the earlier compatibility at high angles. Note pocket knife near upper center of photograph for scale.

A

B

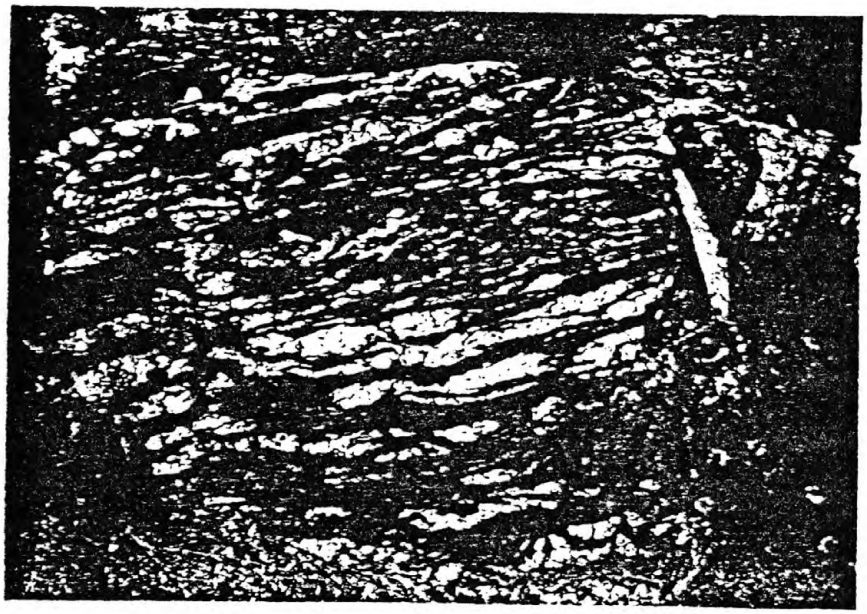

C

Figure 7.--Photograph showing coarse-grained quartz feldspar leucogranite both crosscutting the schistosity in a 40-cm-thick amphibolite layer in a quartzofeldspathic-amphibolite sequence of gneiss, and also filling a fracture opened between blocks of amphibolite. Some clots of chlorite occurring as schlieren in the leucogranite probably reflect altered amphibolite xenoliths torn from the wallrock of the leucogranite. Photo taken on the west flank of southern Lost Basin Range.

and isoclinally folded sequences of gneiss containing locally pervasive cataclasite and mylonite, and mylonitized coarse-grained leucogranite cutting amphibolite and quartz-plagioclase gneiss. The cataclastically deformed rocks must reflect a brittle-type deformation, whereas the largely recrystallized mylonite, including mylonitic schist and mylonitic gneiss, must reflect syntectonic recrystallization accompanying ductile flow.

Widespread and pervasive injection of the gneiss by Proterozoic X granitic magmas yielded migmatitic complexes now concentrated mostly along the western lower flanks of Garnet Mountain and near the southernmost extent of Lost Basin range (units Xgc, Xmg, Xm, and Xma, fig. 2). Migmatitic gneiss (Xmg) and migmatite (Xm) were mapped separately mostly on the basis of the relative proportion of granitic injecta. Migmatitic gneiss includes mostly pelitic gneiss and lesser amounts, but nonetheless relatively abundant, granitic material, whereas migmatite (unit Xm) contains mostly Proterozoic granitic rock (fig. 6C). Swarms of leucogranite, aplite, and pegmatite dikes, including varying amounts of pegmatoid quartz veins and irregular quartz masses, cut gneiss locally in the northwestern part of the Garnet Mountain quadrangle, and together comprise a migmatitic leucogranite complex.

In all, approximately 200 thin sections, prepared from metamorphic rocks showing wide-ranging overall bulk chemistries, were studied petrographically. These Proterozoic metamorphic rocks host many of the lode gold deposits known in the districts. For the most part, the metamorphic rocks show prograde mineral assemblages of upper amphibolite facies that have been retrograded partly or completely to greenschist assemblages. Approximately 70 percent of our thin-sectioned samples contain such retrograde assemblages. In addition to greenschist facies mineral assemblages locally developed syntectonically during recrystallization of a fabric showing strong crystallographic and dimensional preferred orientation of quartz and various phyllosilicate minerals, some of the metamorphic rocks also are altered deuterically to propylitic assemblages, and even phyllic and potassic (see Creasey, 1966; Beane, 1981) assemblages. The propylitic assemblages are especially well developed in the general area of the major north-striking faults in the southern Lost Basin Range (Deaderick, 1980, pl. 1), and phyllic and potassic assemblages occur in rocks very close to many of the gold-bearing quartz veins (see below). However, several areas in the districts have not been affected strongly by retrograde metamorphic effects. These areas include

the gneisses south-southeast of the Cyclopic mine, the gneisses exposed near the base of the Grand Wash Cliffs, the migmatic rocks exposed on Garnet Mountain, and an area of about 15 sq km in the northern part of the Lost Basin range, near the northern edge of the Garnet Mountain quadrangle (P. M. Blacet, unpub. data, 1967-1972).

Pelitic Metamorphic Rocks

Pelitic metamorphic rocks are widespread throughout the gneiss terrane in the Gold Basin-Lost Basin districts. We were not able from our studies, however, to establish an areal distribution of prograde mineral zones in these rocks because of the extensive and locally intense disruptions in metamorphic grade caused by superimposed dynamic retrograde event(s), and more or less passive hydrothermal phenomena associated with gold mineralization. Most of the pelitic gneisses include composite metamorphic assemblages that reflect disequilibrium or metastability generally between relict, prograde, high-metamorphic-grade assemblage(s) and a subsequent lower grade one. Incomplete metamorphic reactions are recorded in most of the rocks which now contain both product and reactant minerals. Nonetheless, we describe in the following sections petrographic details of the early assemblages in the metamorphic rocks in accordance with increasing grade of characteristic assemblages inferred from classic studies in zoned metamorphic terranes elsewhere (see Miyashiro, 1973; Winkler, 1974). The pelitic metamorphic rocks in the Gold Basin-Lost Basin districts include the following rocks, grouped by dominant characteristic mineral(s); biotite-muscovite schist, tourmaline schist, almandine-biotite±staurolite schist and gneiss, kyanite gneiss and schist, and sillimanite- and cordierite-bearing gneiss and schist. Figure 8 shows schematically the inferred mineral changes with time and the corresponding metamorphic facies in the pelitic rocks. For example, some of the pelitic metamorphic rocks record at least three superposed deformations, one prograde upper amphibolite event, and two retrograde lower amphibolite(?) events (fig. 9). As seen in figure 9, the predominant structure in the rock is a foliation (S_2) which developed penecontemporaneous with the crystallization of muscovite, biotite, and quartz sometime after the metamorphic peak was reached during crystallization of garnet, biotite, and quartz (S_1). The last deformation to affect the rock resulted in a moderately well developed strain-slip cleavage (S_3) that cuts S_2 at angles of about 30^{o}.

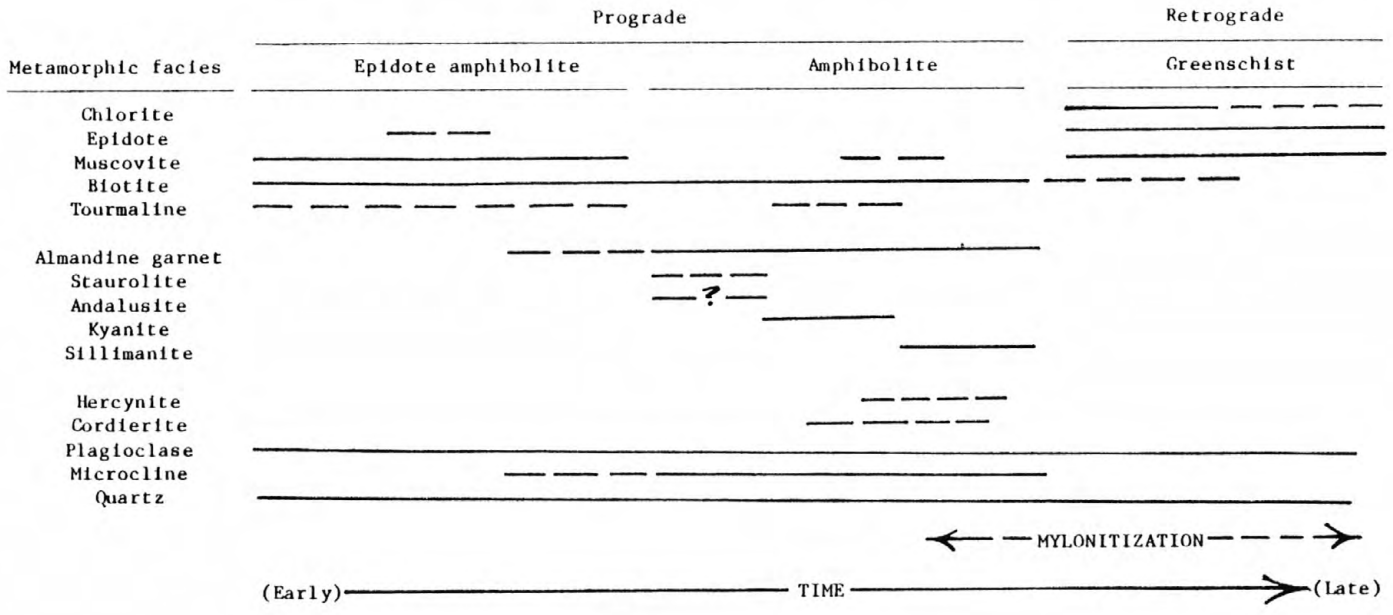

Figure 8. Inferred mineral changes and corresponding metamorphic facies in pelitic rocks from the Proterozoic X gneissic terrane of the Gold Basin-Lost Basin mining districts.

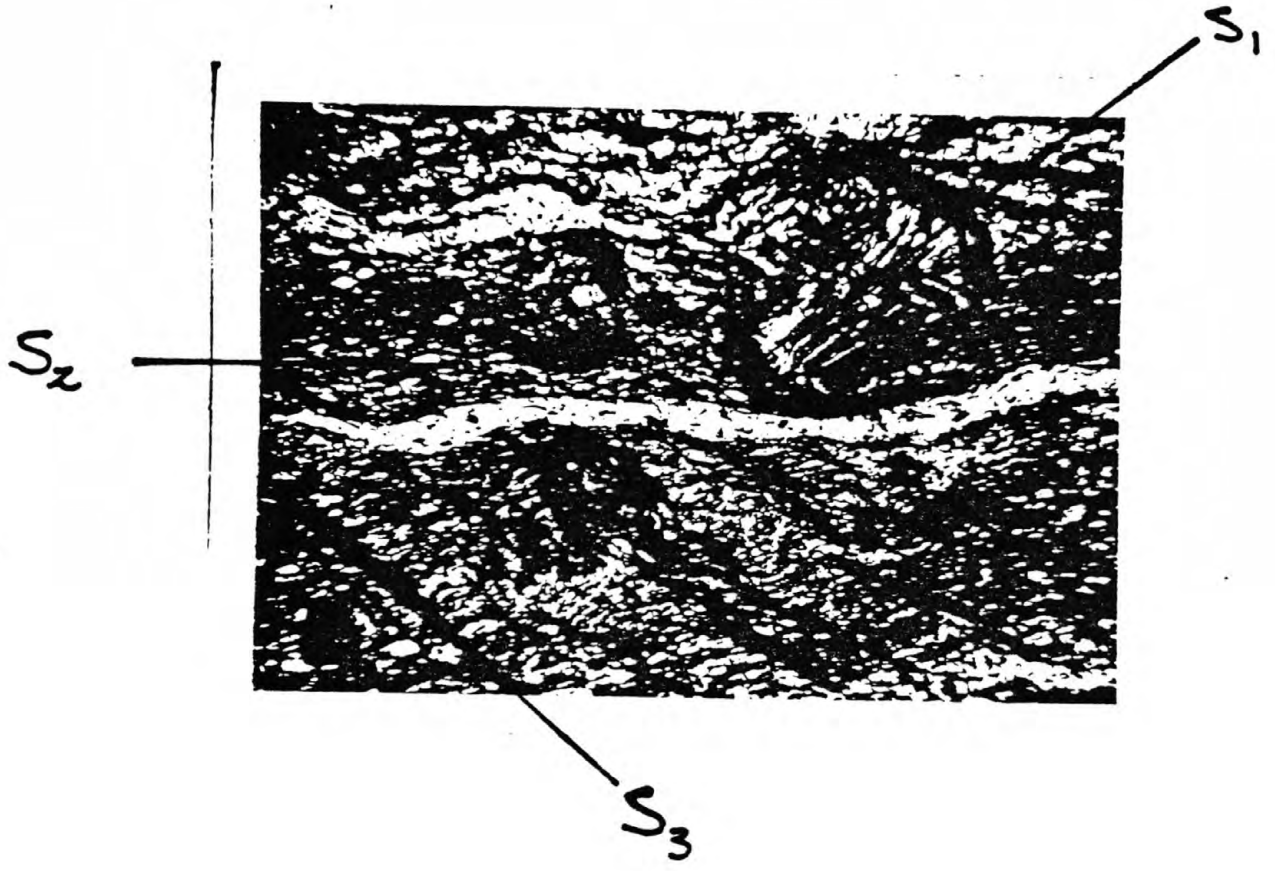

Figure 9.--Laminated muscovite-biotite-quartz schist showing a fabric composed of three distinct S-surfaces reflecting three superposed deformations. The oldest surface (S_1) has the weakest preferred orientation overall the rock and S_1 is defined by alined trains of wispy quartz (Q) inclusions in garnet (G) porphyroclasts. S_2, the dominant foliation in the rock, is defined by a strong preferred crystallographic orientation of muscovite and biotite and a dimensional orientation of quartz. S_2, a strain-slip cleavage, cuts S_2 at angles of about 30° and S_3 contains increased abundances of muscovite and biotite relative to S_2. Sample number GM-73.

Muscovite-biotite Schists

Muscovite-biotite schists that presumably date from the prograde metamorphism of the area sporadically occur interlayered with other lithologies in the gneiss. Samples of these rocks contain mostly a muscovite-biotite-quartz assemblage wherein the biotite is typically dark brown (Z) under the microscope. Potassium feldspar is notably absent from this assemblage. Muscovite and biotite in some of the more pelitic of these rocks show apparently compatible relations with minor amounts of tourmaline, oligoclase, opaque minerals, and apatite (fig. 10A). Further, where some of these schists are retrograded slightly, they show incipient neocrystallization of very fine-grained quartz and muscovite along 0.1- to 1.0-mm-wide zones of axial plane cleavage which cut the dominant foliation in the rock at high angles (fig. 10B). Such retrograded schist also contains sparse porphyroblasts of disseminated chlorite showing a strong preferred orientation of its {001} cleavage which parallels also the axial plane cleavage in the rock. We infer from the very wide ranging proportions of phyllosilicates and tourmaline in the muscovite-biotite schists that they may grade locally into very tourmaline rich rocks, described in the following section.

These white mica (presumably muscovite)-biotite assemblages are not particularly useful indicators of barometric conditions during metamorphism, but they can be used to estimate approximately the upper limit of temperatures in the rocks during the early stages of the prograde event. The absence of stilpnomelane in these rocks suggests that the metamorphic event occurred at a grade higher than the stilpnomelane isoreaction-grad (Winkler, 1974), which has been placed at temperatures slightly greater than 425° to 460°C using the experimental studies of Nitsch (1970). Nitsch studied the breakdown of stilpnomelane plus phengite to biotite plus chlorite plus quartz plus H_2O. However, these temperature estimates are based on the assumption that the partial pressure of H_2O(P_{H_2O}) equalled total pressure (P_{tot}) during the prograde event. This assumption probably is not valid, however, as will be discussed below. Therefore, the 425° to 460°C temperature range should be considered only as the highest temperatures one would infer for the onset of such biotite-white mica assemblages. Miyashiro (1973) notes that stilpnomelane may occur in high-pressure metamorphic terranes, and very rarely in low-pressure ones, a relation that may further constrain the thermal implications of the absence of stilpnomelane.

Figure 10.--Photomicrographs of schists containing relatively abundant concentrations of muscovite (M) and (or) biotite (B). Plane polarized light. Quartz (Q); Tourmaline (T). A, Unretrograded quartz-biotite-muscovite schist containing minor tourmaline, apatite (A), opaque minerals (O), and oligoclase feldspar (F). Sample number GM-233; B, Crenulated quartz-biotite-muscovite schist showing incipient neocrystallization of quartz and muscovite along zones of axial plane cleavage which cut the dominant foliation in the rock at high angles. Sparse porphyroblasts of chlorite (chl) alined with their $\{001\}$ cleavage traces parallel to the axial plane cleavage. Sample number GM-273; C, Apparently compatible, relict biotite (B) and carbonate (C) in a highly retrograded biotite-chlorite-white mica-epidote (clinozoisite) schist. Sample number GM-339.

A

B

C

Some of the mica schists also show textural relations suggesting compatibility between biotite and carbonate, probably calcite, during the prograde metamorphism of the area (fig. 10C). From the absence of talc and tremolite as the first silicate minerals to crystallize in this assemblage and the appropriate experimentally determined carbonate-silicate equilibria (Skippen, 1971; Winkler, 1974, p. 113), we infer that the molecular fraction of carbon dioxide at least locally must have been very high in the fluid(s) associated with metamorphism. Winkler (1974) further suggests that such a high molecular fraction of carbon dioxide in the fluid(s) may have been maintained by a reaction such as:

3 Fe-Mg carbonate+1 potassium feldspar+1 H_2O →
1 biotite+3 calcite+3CO_2 (1)

However, the early biotite (dark brown, Z)-carbonate- quartz assemblage in these fine-grained schists exemplified by sample no. GM-339 (fig. 10C) has been replaced significantly by a retrograde greenschist assemblage of chlorite-epidote (clinozoisite)-white mica-minor rutile. The white mica probably is mostly muscovite, but it may include some margarite. Where ductile flow was concentrated prominently in these micaceous rocks during the biotite-destructive, greenschist metamorphic event, the rocks are converted into chlorite-rich phyllonitic schists. Such changes occur usually across very sharp boundaries, and they are reflected by marked modal differences. These changes are primarily an increased abundance of chlorite and white mica, whereas there are sharply decreased amounts of biotite. Further, in these domains of chlorite-rich phyllonitic schist, calcite is a prominent relict from the earlier biotite-stable metamorphic event and it shows mostly an intensification of its dimensional orientation wherein the short axes of the calcite grains are transverse to the trace of the foliation. A chemical analysis of a sample of heavily retrograded biotite-carbonate schist shows a very low sodium content of 0.1 weight percent Na_2O, a CO_2 content of 3.1 weight percent, and a relatively high TiO_2 content of 1.9 weight percent (analysis 1, table 4).

Tourmaline Schist and Gneiss

Tourmaline, a complex boron-bearing silicate typically containing 8 to 10 weight percent B_2O_3 (Deer, Howie, and Zussman, 1962a), occurs in significant concentrations at several localities in the gneiss terrane. However, overall the gneiss, tourmaline is a relatively sparse mineral that crystallized during

Table 4. Chemical analyses of selected schists and gneisses from the Gold Basin–Lost Basin mining districts compared with analyes of slate, argillite, shale, graywacke, and arkose

[Chemical analyses by rapid-rock methods; analysts, P. L. D. Elmore and S. Botts. Methods used are those described in Shapiro (1967). Spectrographic analyses by Chris Heropoulos. Results are identified with geometric brackets whose boundaries are 1.2, 0.83, 0.56, 0.38, 0.26, 0.18, 0.12, etc., but are reported arbitrarily as midpoints of these brackets, 1., 0.7, 0.5, 0.3, 0.2, 0.15, 0.1, etc. The precision of a reported value is approximately plus or minus one bracket at 68 percent or two brackets at 95 percent confidence. Looked for but not found, Ag, As, Au, B, Be, Bi, Cd, Mo, Pd, Pt, Sb, Sn, Te, V, W, Zn, Ge, Hf, In, Li, Re, Ta, Th, Tl, Eu; ----, not detected; N.D., not determined]

	1	2	3	4	5	6	7	8	9	10	11
Field number —	GM-339	GM-555	GM-312b	GM-255	GM-295	GM-498					
					Chemical analyses (weight percent)						
SiO_2	50.9	66.8	76.3	75.4	75.0	72.3	60.6	66.9	60.2	66.7	77.1
Al_2O_3	13.6	17.	12.3	12.4	12.7	14.	17.3	15.4	16.4	13.5	8.7
Fe_2O_3	3.4	1.2	1.	1.6	1.7	2.8	2.3	2.8	4.	1.6	1.5
FeO	10.4	4.4	.68	1.9	1.7	2.2	3.7	1.9	2.9	3.5	.7
MgO	5.	1.7	.6	1.7	.4	.7	2.6	2.4	2.3	2.1	.5
CaO	5.7	.90	3.3	2.1	3.	4.3	1.5	.34	1.4	2.5	2.7
Na_2O	.1	1.4	3.	2.7	3.	3.	1.2	1.2	1.	2.9	1.5
K_2O	2.4	4.	1.3	1.3	1.	.7	3.7	6.6	3.6	2.	2.8
H_2O+	3.4	1.8	.87	.98	1.	1.1	3.5	1.4	3.8	2.4	.9
H_2O-	.05	.08	.02	.02	.05	.04	.62	.00	.89	.6	N.D.
TiO_2	1.9	.74	.08	.13	.12	.01	.73	.47	.76	.6	.3
P_2O_5	.24	.05	.00	.01	.04	.07	N.D.	.23	.15	.2	.1
MnO	.06	.12	.02	.06	.09	.06	N.D.	.05	Tr	.1	.2
CO_2	3.1	<.05	.05	.05	.15	.05	1.5	.28	1.5	1.2	3.
Total	100.	100.	100.	100.	100.	101.	99.	100.	99.	100.	100.
					Semiquantitative spectrographic analyses (weight percent)						
Ba	0.05	0.15	0.1	0.07	0.1	0.07					
Co	.005	.0015	----	.0005	.0003	.001					
Cr	.007	.007	----	.0002	.0002	.0005					
Cu	.005	.001	.0001	.001	.0005	.0005					
La	----	.007	----	----	----	----					
Mo	.001	----	----	----	----	----					
Nb	.001	.0015	----	----	----	----					
Ni	.005	.003	----	.0002	----	.0003					
Pb	----	----	.0015	.001	.0007	----					
Sc	.005	.0015	.001	.001	.001	.002					
Sr	.02	.02	.03	.015	.03	.05					
V	.05	.007	----	.0007	.002	.0005					
Y	.002	.003	.0015	.001	----	.0015					
Zr	.007	.02	.007	.007	.01	.003					
Ce	----	.02	----	----	----	----					
Ga	.003	.003	.0015	.001	.001	.0015					
Yb	.0003	.0003	.0002	.0001	.0001	.0002					

1. Highly retrograded biotite–carbonate–chlorite–white mica–epidote schist (unit Xgn, of fig. 2); NE1/4 sec. 7, T. 29 N., R. 17 W.
2. Schist showing an assemblage of biotite–chlorite–white mica–clinozoisite–quartz superposed on an earlier garnet-bearing one (unit Xgn); UTM, E753,600, N3,987,050.
3. Quartz-rich quartzofeldspathic gneiss (unit Xgn); NE1/4 sec. 19, T. 29 N., R. 17 W.
4. Quartzofeldspathic gneiss (unit Xgn); SW1/4 sec. 20, T. 29 N., R. 17 W.
5. Quartzofeldspathic gneiss (unit Xgn); SE1/4 sec. 17, T. 29 N., R. 17 W.
6. Quartzofeldspathic gneiss (unit Xgn); NE1/4 sec. 33, T. 30 N., R. 17 W.
7. Average of 16 analyses of slate (Pettijohn, 1949, p. 344).
8. Argillite, Precambrian Fern Creek Formation, Dickinson County, Mich. (Pettijohn, 1949, p. 345).
9. Composite sample of 51 Paleozoic shales (Clarke, 1924, p. 552).
10. Mean composition of 61 analyses of graywacke (Pettijohn, 1963, table 12). Also includes 0.3 weight percent SO_3, 0.15 and 0.1 C.
11. Mean composition of 32 analyses of arkose (Pettijohn, 1963, table 12).

the early metamorphism of the area. In those rocks that tourmaline occurs in relatively abundant concentrations of perhaps up to 30 volume percent, the prismatic crystals of tourmaline show a very strong preferred orientation that defines the metamorphic foliation or S-surface. Generally, the known tourmaline schists or tourmalinites comprise zones that range up to several centimeters thick, mostly in sequences of quartzofeldspathic gneiss. Many of these zones show well-developed, small-scale, composite folds which reflect a combination of shear along an axial plane cleavage and buckling due to lateral compression (fig. 11A). In such folded rocks, the leucocratic layers include mostly quartz, muscovite, tourmaline, and sparse oligoclase. These leucocratic layers show a more ductile behavior during deformation than the dark, tourmaline-rich layers. Under the microscope, the tourmaline-rich layers are composed of aggregates of fine-grained crystals that measure roughly 0.1 mm across their basal sections. The tourmaline is strongly pleochroic from very pale, light olive gray to dark greenish blue. Such a pleochroic scheme suggests that the tourmaline in these rocks is the iron-containing variety known as schorl (Deer, Howie, and Zussman, 1962a). However, the identification of the compositional variety of tourmaline primarily by color may be misleading (Jones, 1979). In addition, tourmaline in these rocks shows apparently stable compatabilities with a broad spectrum of the characteristic minerals used typically as zonal indicators in pelitic metamorphic terranes. As described above, it occurs in sparse concentrations with prograde quartz-muscovite-biotite assemblages. Tourmaline also occurs in epidote-quartz-microcline-muscovite-plagioclase-opaque mineral assemblages that comprise the wispy banded layers within quartzitic sequences of the gneiss. Tourmaline is also prominent in somewhat higher grade schists containing a muscovite-biotite-almandine(?) garnet-quartz-sparse potassium feldspar assemblage. The textural relations and crystal forms of the garnets in this assemblage suggest they are in their initial stages of crystallization (fig. 11B). Some quartz-kyanite clots in the metamorphic rocks, which will be discussed fully below in a section describing kyanite relations, also contain tourmaline. However, tourmaline was not found to be associated with sillimanite, cordierite, or staurolite. Nonetheless, it has been reported to occur with staurolite in mica schists of the Alto Aldige region, Italy (Gregnanin and Piccirillo, 1969), with garnet and staurolite in the eastern Alps, Austria (Ackermand and Morteani, 1977), with staurolite and sillimanite

Figure 11.--Photomicrographs showing structural and textural relations of tourmaline in the metamorphic rocks. Plane polarized light. T, tourmaline; Q, quartz; G, garnet; E, epidote; M, microcline. A, Composite small-scale folds in a tourmaline schist. Sample number GM-296; B, Disseminated euhedral crystals of fine-grained garnet in a biotite-muscovite-tourmaline schist. Sample number GM-297a.

A

B

in metamorphic rocks of the Kamchatka peninsula, U.S.S.R. (Lebedev, Tararin, and Lagovskaya, 1967), and with staurolite and kyanite in the Black Mountain area, New Hampshire (Rumble, 1978). A tourmaline-quartz association occurs also in some rocks of the Proterozoic X Yavapai Series of the Jerome, Ariz., area (S. C. Creasey, oral commun., 1979), and tourmaline is a common accessory in amphibolite facies, micaceous and quartzofeldspathic schists of the Proterozoic X Vishnu Complex in the Grand Canyon (Brown and others, 1979).

Experimental studies further substantiate the wide-ranging, pressure-temperature stability of tourmaline. Reynolds (1965) showed that a marked redistribution of boron occurs at metamorphic conditions of roughly the greenschist facies. He concluded that boron typically is expelled from a boron-bearing, 1 Md lattice of illite in sedimentary rocks when recrystallized during metamorphism to the 2M polymorph and that the expelled boron is fixed finally in tourmaline. However, the extremely high concentrations of boron required locally by these stratiform occurrences of tourmaline schist (fig. 11A) or tourmalinite in the usage of Nicholson (1980), indicate that boron-bearing clays could not have been the primary source of boron here (see Ethier and Campbell, 1977). Further, the tourmaline in these tourmaline schists obviously reflects recrystallization dating from the prograde metamorphism of the area. Although, detrital tourmaline grains commonly act as nucleii for any newly crystallized tourmaline, careful petrographic examination of these tourmaline-bearing rocks revealed that the tourmaline does not now show overgrowths, broken crystals, or any variably rounded crystal forms. Thus, the tourmaline-bearing, biotite stable schists in the Gold Basin-Lost Basin districts are well beyond the lower stability limit of tourmaline. At the high metamorphic end of the spectrum, the experimental studies of Robbins and Yoder (1962) in the system dravite-H_2O suggest temperatures greater than 800°C at pressures of P_{H_2O} greater than 500 bars are needed to decompose dravite, the Fe-free Mg-bearing tourmaline, into mostly cordierite bearing assemblages.

The provenance of the protolith and overall petrogenesis of these tourmaline schists remain nonetheless problematical, especially the rocks that are very quartz rich. In these rocks, tourmaline and quartz form the predominant mineral association, a common association as noted above. Elsewhere, quartz-tourmaline clasts occur in the Proterozoic Z Torridonian Group of northwest Scotland (Allen, Sutton, and Watson, 1974). These authors infer such rocks to be derived from contact aureoles of high-level granites in

the source area of the Torridonian Group. Very rarely, however, quartz has been reported also to occur as a replacement of tourmaline (McCurry, 1971). The provenance of the tourmaline-quartz schists in the Gold Basin-Lost Basin districts appears to be different, in that these schists comprise wispy layered, stratiform zones containing sparse concentrations of other minerals that also have relatively high specific gravities. The specific gravity of tourmaline is approximately 3.00 to 3.20 (Deer, Howie, and Zussman, 1962a). These relations suggest that these tourmaline schists or tourmalinites may reflect local syngenetic, exhalative emanations of boron-rich fluids onto the seafloor of the protolith of the Proterozoic metamorphic rocks. Such a syngenetic model for similar rocks elsewhere has been proposed recently (Ethier and Campbell, 1977; Nicholson, 1980; Plimer 1980; Slack, 1980). The exploration implications of these rocks will be discussed below in the section below dealing with Suggestions for Exploratory Programs.

Almandine-Biotite±Staurolite Schist and Gneiss

Pelitic schist and gneiss in the Proterozoic metamorphic terrane also include almandine-biotite-quartz-potassium feldspar-plagioclase assemblages. The potassium feldspar is mostly microcline, and the plagioclase is mostly oligoclase or andesine, although some of these rocks rarely contain albite. Minor accessory minerals include apatite, opaque mineral(s) and rutile. Some of the initial crystallization stages of almandine is recorded by rocks still containing muscovite and biotite as described above in the section dealing with tourmaline. In such a mineral association, almandine garnet occurs as euhedral, 0.1 mm across porphyroblasts in a fabric, wherein the schistosity and subsequent strain-slip clearage are defined by muscovite and biotite. Textural relations suggesting specific reactions that controlled the crystallization and growth of almandine are very difficult to ascertain. Generally, however, increased modal abundances of almandine and microcline appear to have been compensated by (1) a decrease in overall abundance and eventual disappearance of muscovite, and (2) a change in the color of biotite from dark brown (Z) to reddish brown (Z). These changes are accompanied also by an apparent increase in grain size. The first crystallization of almandine-rich garnet in these rocks is not sharply defined areally and is not marked by the disappearance of a phyllosilicate phase. Instead, we infer from our petrographic observations that the initial crystallization of garnet reflects a reaction such as:

$$\text{Biotite}_I + m\ \text{Phengitic White Mica} \rightarrow$$

$$\text{Biotite}_{II} + \text{almandine garnet} + m\ \text{potassium feldspar} + H_2O. \quad (2)$$

We suggest that early, dark-brown (Z) biotite$_I$ is an iron-rich variety, and the ensuing red-brown (Z) biotite$_{II}$ is a variety containing more magnesium than biotite$_I$. If (2) reaction is more or less correct for the onset of the biotite$_{II}$-almandine-potassium feldspar compatibility, then the magnesium-content of biotite$_{II}$ may be derived principally from the breakdown of phengitic white mica, which may have magnesium substituted for aluminum in its octahedral structural sites (Deer, Howie, and Zussman, 1962b). Further, m in reaction (2) may be greater than one thus reflecting a preferred consumption of white mica relative to biotite$_I$. In addition, reaction (2) provides a mechanism whereby biotite$_{II}$ in the rocks becomes more magnesian and thus stable to higher temperatures than biotite$_I$.

Staurolite (ideally $Fe_2Al_9Si_4O_{23}(OH)$) was found at only one locality (loc. no. GM-922), near the southern edge of the Gold Basin district, approximately 5 km south of the Cyclopic mine. Ribboned and spotted migmatitic gneisses there are retrograded partly to a chlorite-white mica greenschist assemblage. However, the melanosomes of these rocks contain a well-developed garnet-biotite-staurolite-quartz-andalusite(?) assemblage which lacks potassium feldspar and plagioclase. Andalusite is present questionably in the rock in trace amounts as crystals apparently compatible with garnet during the prograde event, but subsequently altered highly to white mica during the retrograde event. Equant to stubby-prismatic crystals of staurolite measure typically 0.5 to 1.0 mm across and they in places form 120° dihedral angles against euhedral porphyroblasts of garnet (fig. 12A). Under the microscope, the staurolite is strongly pleochroic from colorless (X) to pale golden yellow (Z); some crystals are twinned. Chlorite and white mica partly replace mostly biotite in the melanosomes of these staurolite-bearing rocks as fine-grained porphyroblasts at high angles to the trace of the foliation defined by the biotite. Many of the staurolite crystals are also rimmed by aggregates of very fine grained white mica. However, the crystals of garnet here are remarkably free of replacement phenomena related to the retrograde event.

The occurrence of staurolite in the almandine-biotite schists and gneisses allows us to make some inferences concerning the prograde metamorphism of the area during the Proterozoic X. The onset of the

Figure 12.--Photomicrographs showing textural relations among minerals in garnet-bearing gneisses. G, garnet; S, staurolite; B, biotite; C, chlorite; M, white mica; Q, quartz. Plane polarized light. A, Textural relations in a garnet-staurolite-biotite gneiss relict from a prograde event. Chlorite and white mica crystallized during the subsequent greenschist retrograde event. Sample number GM-922a; B, Rounded, and highly altered crystals of garnet in a retrograded, garnetiferous leucogneiss. Partially chloritized garnets are replaced also by aggregates of very fine grained white mica. Sample number GM-462; C, Mylonitic fabric consisting of biotite-chlorite-white mica-clinozoisite-quartz assemblage superposed during the greenschist retrograde event on an earlier garnet-bearing assemblage. Sample number GM-555.

A

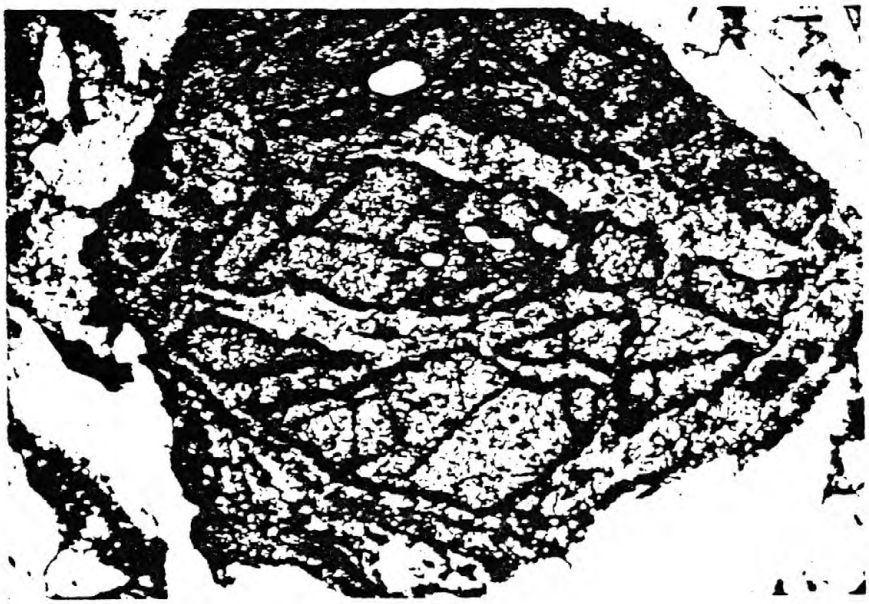

B

C

crystallization of staurolite is accepted generally to be at temperatures somewhat higher than almandine garnet (Miyashiro, 1973), and to indicate thereby that regionally metamorphosed rocks have reached at least a medium grade, or temperatures in the 500° to 550°C range (Winkler, 1974). Although staurolite can form apparently across a broad spectrum of pressure environments (Miyashiro, 1973), its maximum stability determined experimentally in the presence of quartz, muscovite, and biotite appears to be about 675°C at 5.5 kb and about about 575°C at 2 kb, $P_{H_2O} = P_{tot}$ and Mg/(Mg+Fe) = 0.4 (Hoschek, 1969). Hoschek further found that a relatively high Fe/(Mg+Fe) ratio will expand the stability field of staurolite. Thus, the very restricted occurrence of staurolite in contrast with the very wide distribution of cordierite in the Proterozoic terrane of the Gold Basin-Lost Basin districts, to be described below, may reflect such chemical controls. Although staurolite occurs here in an assemblage questionably containing andalusite, elsewhere staurolite-bearing assemblages are reported commonly to include all three alumino silicate polymorphs (Hietanen, 1973; Carmichael, 1978; Cynthia Dusel-Bacon and Helen L. Foster, unpub. data, 1982).

Almandine-biotite prograde assemblages occur also in some rocks intermediate in composition between the pelitic and quartzofeldspathic gneisses. However, many of these rocks are retrograded intensely as exemplified by some garnet-bearing leucogneisses that are interlayered with quartzofeldspathic- and amphibolite-gneisses (fig. 12B). In these garnet-bearing leucogneisses, partially chloritized crystals of garnet range up to 1 cm across in some of the layers. The cores of many of the garnets host rounded, fine-grained crystals of quartz, engulfed possibly by rapid growth of garnet during its early stages of crystallization. Further, the garnets are replaced at their margins and along fractures by pale-green chlorite and some white mica. The light-colored matrix of the rocks consists of quartz, clouded feldspar, and a few relicts of biotite now replaced largely by interlayered chlorite. Most oligoclase grains are partly replaced by white mica and clinozoisite and (or) epidote. The almandine, which occurs in some other of these gneisses that are intermediate chemically between the pelitic and quartzofeldspathic end members, shows excellent textural relations indicating the crystallization of some retrograde biotite (fig. 12C). In these rocks, fractured crystals of garnet contain alteration rims of biotite. In addition, the garnets are microveined by biotite, chlorite, and

white mica which together with clinozoisite and quartz make up the predominant minerals in the mylonitic fabric which developed penecontemporaneous with retrograde metamorphism and isoclinal folding of some sequences of gneiss. Chemical analysis of such a rock shows contents of Al_2O_3, of total alkalis ($K_2O + Na_2O$), and ratios of SiO_2/Al_2O_3 similar to fine-grained detrital rocks (compare analysis 2 with analyses 8-10, table 4).

Kyanite-bearing Gneiss

Kyanite (Al_2SiO_5) occurs in at least three localities in the Proterozoic X gneiss terrane of the Gold Basin-Lost Basin districts, and it has been reported only from about 12 localities widespread across all three Proterozoic metamorphic belts of Arizona (Espenshade, 1969; Galbraith and Brennan, 1970). However, kyanite may occur more commonly in the Proterozoic rocks of Arizona than believed previously because systematic petrographic examination of some relatively highly metamorphosed Proterozoic X Pinal Schist at Mineral Mountain southeast of Phoenix (Theodore and others, 1978) revealed its occurrence there also (T. G. Theodore, unpub. data, 1979). Indeed, the anhydrous nature of kyanite and its polymorphs, sillimanite and andalusite, make parageneses involving these minerals excellent, diagnostic pressure-temperature indicators for moderate temperature, regionally metamorphosed pelitic assemblages (Kepezhinskas and Khlestov, 1977; and many others). As described below, one can make certain barometric inferences from kyanite and sillimanite parageneses using the appropriate thermodynamically generated equilibrium curves and the appropriate experimentally determined phase relations (Helgeson and others, 1978, fig. 49). Early prograde assemblages in kyanite-bearing pelitic paragneisses in the Gold Basin-Lost Basin districts include:

Kyanite-quartz-tourmaline-opaque mineral (3)

Kyanite-biotite-quartz$\pm$magnetite(?)$\pm$graphite$\pm$apatite (4)

The kyanite-bearing assemblages (3) and (4) were found at three widely separated localities in the districts. Assemblage (3) occurs in gneissic schlieren within a mixed granodioritic complex, unit Xmg of figure 2, on the western lower flanks of Garnet Mountain (SW1/4 sec. 15, T. 28 N., R. 17 W.). Assemblage (4) occurs in samples collected from two localities: the first is in a thin layer of pelitic biotite schist within foliated and lineated hornblende amphibolite on the western flank of the Lost Basin Range (SE1/4 sec. 18, T. 29 N., R. 17 W.). The second locality is in migmatitic gneiss

that crops out in Grapevine Wash, approximately 2.5 km southwest of the Grand Wash Cliffs. This last sample locality containing kyanite assemblage (4) falls well within the projected outer limit of the suite of Proterozoic X plutonic igneous rocks exposed prominently in the general area of Garnet Mountain. Thus, two of the kyanite-bearing assemblages are related spatially with the igneous rocks of Garnet Mountain.

The kyanite-bearing assemblages known in the Garnet Mountain quadrangle now appear to be of two genetic types. The first includes locally preserved relicts initially crystallized prior to and apart from the enclosing schist, and possibly shed detritally into the metamorphic terrane's protolith or, more likely, preserved in situ from an earlier stage of the metamorphic event. The other kyanite-bearing assemblage crystallized syntectonically penecontemporaneous with development of the enclosing schistose fabric, which is strongly lineated. The former assemblage in fact shows textural relations strongly suggesting physicochemical incompatibility with its enclosing phyllosilicate dominant fabric. Kyanite in assemblage (4) thus occurs in 0.6 to 1.0 mm, sieve-textured clots containing minute, highly rounded crystals of quartz. These crystals of quartz are aligned in trains defining S-surfaces at very high angles to the schistosity in a quartz-muscovite-chlorite-albite-cordierite(?) fine-grained schist. In addition, the kyanite is altered partially along its rims to white mica, probably muscovite (fig. 13A). Kyanite in one of the two samples of assemblage (4) shows a very strong preferred orientation of its C-axes which lie in, and define partly, the foliation of sample GM- 283 (fig. 13B). Kyanite and biotite are apparently compatible in this sample, because they are juxtaposed along sharp, straight crystal contacts showing at high magnifications no indication in either mineral of replacement by the other (fig. 13B). In addition, the kyanite in this rock shows relations indicative of partial replacement by two subsequent generations of muscovite. The two generations of muscovite comprise (1) large single crystals, and (2) very fine grained crystals of muscovite aggregated into microveinlets which cut the earlier crystallized kyanite. We want to emphasize again that the important feature of sample GM-283 is its apparent hosting of syntectonically crystallized kyanite. Finally, two of the kyanite-bearing samples studied (sample nos. GM-283 and GM-1010c) contain another Al_2SiO_5 polymorph, sillimanite. However, in neither of these samples do the two minerals show textural relations of apparent mutual compatibility.

Figure 13. Photomicrographs showing textural relations of kyanite. Plane polarized light. A, Clot of kyanite (K) containing quartz (Q), tourmaline (T), and opaque mineral (O). The kyanite is partially altered along its rim to white mica (M, probably muscovite). Sample number GM-235; SW1/4 sec. 15, T. 28 N., R. 17 W.; B, Foliation defined partly by very strong preferred orientation of kyanite (K) c-axes which lie in the plane of the foliation, and by dimensionally oriented flakes of biotite (B); Q, quartz; O, opaque mineral; M, postkyanite white mica porphyroblast (probably muscovite). Sample number GM-283; SE1/4 sec. 18, T. 29 N., R. 17 W.; C, Kyanite (K) and biotite (B) in contact with each other and showing no visible signs of mutual incompatibility. Sample number GM-283; SE1/4 sec. 18, T. 29 N., R. 17 W.; D, An assemblage of kyanite (K), quartz (Q), and biotite (B) showing partial replacement of kyanite by white mica (M, probably muscovite) which is in turn partially replaced by fibrous sillimanite (S). Sample number GM-1010e; NW1/4 sec. 21, T. 29 N., R. 16 W.

A

B

C

D

Sillimanite appears to postdate crystallization of kyanite. In sample GM-1010c, fibrous sillimanite partly replaces kyanite as a direct nucleation product, but more commonly sillimanite replaces an intervening muscovite, possibly by a paired or cyclic reaction (Carmichael, 1969) to be discussed in the next section below. In sample GM-283, fibrous sillimanite partly replaces biotite in a quartz-rich domain of the rock which contains no kyanite.

Sillimanite- and cordierite-bearing gneisses and schists

Sillimanite- and cordierite-bearing gneisses and schists in the Proterozoic X metamorphic rocks show complex compatibilities, many of which are confined to very small domains (table 5). Textural and field relations documented during our petrologic studies suggest that some initially very high grade assemblages developed in these rocks and they include:

Garnet-sillimanite(?)-biotite-quartz±potassium feldspar± plagioclase±opaque mineral(s)±hercynite (5)

Biotite-sillimanite-quartz-opaque mineral (6)

Sillimanite-quartz±muscovite±rutile (7)

Cordierite-biotite-quartz±garnet±plagioclase± potassium feldspar±rutile (8)

Cordierite-sillimanite-hercynite-quartz-potassium feldspar-plagioclase (9)

Garnet, presumably rich in the almandine molecular end-member, in muscovite-free assemblage (5) contains isolated, apparently stable inclusions of biotite, quartz, opaque mineral(s), plagioclase (in trace amounts), and hercynite (in trace amounts), thereby corroborating our judgment that these minerals together certainly comprise one of the earliest stable assemblages in the gneiss. However, the paragenetic position of sillimanite in garnet-biotite assemblage (5) is problematical. Careful examination of garnet-sillimanite textural relations reveals the crystals of garnet to be corroded marginally and embayed locally by stout crystals of sillimanite (fig. 14A). Further, there is excellent textural evidence in such rocks that garnet is veined and partially replaced by the assemblage biotite-sillimanite-quartz-opaque mineral (6). Nonetheless, many garnet crystals contain swarms of very fine grained needlelike crystals of sillimanite aligned parallel to the trace of the flow lines in the enclosing matrix of gneiss. Such sillimanite elsewhere has been interpreted by others (Reinhardt, 1968) as an early, relict phase initially stable with its host garnet as a two-phase subsystem. However,

Table 5. Composite assemblages in sillimanite- and cordierite-bearing gneisses and schists in the Proterozoic X metamorphic rocks in the general area of the Gold Basin-Lost Basin mining districts

[X, mineral present; Tr, mineral present in trace amounts; ----, not observed; ?, queried where identification uncertain]

Sample number	GM-83-1	GM-125	GM-126a	GM-126b	GM-394	GM-406	GM-1010c	[1]GM-1010e	GM-1077	GM-412e	GM-51	GM-116	GM-116b	GM-126a-1	GM-135	GM-1010b	GM-1113a	GM-126c
Quartz	X	X	X	X	X	X	X	X	X	X	X	X	X	X	X	X	X	X
Biotite	X	X	X	X	----	X	X	X	X	X	X	X	X	X	X	X	X	X
Garnet	X	X	X	----	----	[2]X	----		X	X	X	X	X	X	----	X	X	X
Sillimanite	X	X	X	X	X	X	X	X	X	X	----	----	----	----	----	----	X	----
Potassium feldspar	----	X	X	X	----	X	X	X	X	X	X	Tr	X	X	X	----	X	X
Plagioclase	Tr	X	X	X	----	X	X	X	X	X	----	X	X	X	X	Tr	Tr	X
White mica	Tr	----	Tr	[3]X	X	----	X	X	X	----	[3]X	[3]X	[3]X	----	[4]X	[3]Tr	[3]X	----
Cordierite	----	X	X	X	----	----	X	----	----	----	X	X	X	X	X	Tr?	X	X
Hercynite	----	X	X	X	----	----	----	----	----	----	X	----	----	----	----	----	----	----
Opaque mineral(s)	Tr	X	X	X	Tr	X	Tr	Tr	X	X	X	Tr	X	X	Tr	X	X	X
Rutile	Tr	----	----	----	X	----	----	----	----	----	Tr	----	Tr	----	?	----	----	----
Apatite	----	----	----	----	----	----	----	----	X	Tr	----	----	Tr	----	----	Tr	----	----
Zircon	Tr	Tr	Tr	Tr	----	Tr	Tr	Tr	Tr	Tr	Tr	Tr	Tr	Tr	Tr	Tr	Tr	Tr

[1] Includes kyanite partly replaced by white mica and sillimanite.
[2] Altered partly to chlorite along grain boundaries and microfractures.
[3] Fine-grained alteration of feldspar and (or) cordierite.
[4] Almost complete replacement of cordierite.

Figure 14.--Photomicrographs showing textural relations of sillimanite. Plane polarized light. A, Embayed, and highly corroded crystal of garnet (G) showing replacement and microveining by an assemblage of biotite (B)-sillimanite (S)-quartz (Q)-opaque mineral (O). Sample number GM-406; B, Greenish-brown biotite (B) completely replacing pseudomorphically earlier crystallized sillimanite in 1-cm-across lensoid domains within an assemblage of garnet-biotite (red-brown), Z)-cordierite-plagioclase (An_{15})-quartz where in this latter assemblage, biotite is partially replaced by serpentine. Sample number GM-125; C, Sillimanite (S) partially replaced by biotite (B). Sample number GM-406; D, Rounded porphyroclasts of garnet (G) in a quartz (Q)-sillimanite (S) mylonitic schist. Sillimanite is apparently replacing both garnet and biotite (B). Sample number GM-83-1.

A

B

C

D

the overall fabric of such needles of sillimanite in garnet here suggests to us that crystallization of the needles of sillimanite occurred penecontemporeously with the crystallization of the surrounding stout sillimanite which in places embays and thus somewhat postdates the paragenetically earlier garnet. Nonetheless, because textural criteria are highly interpretive as to compatibilities and because some biotite seems to have replaced an early sillimanite (fig. 14B), we assign sillimanite tentatively as a queried phase in early assemblage (5).

Sillimanite shows additional apparently metastable relations with biotite and muscovite in the gneisses and schists. Some sillimanite appears to be in the initial stages of replacement by biotite (fig. 14C). Most of this biotite that partly or wholly replaces sillimanite is various shades of greenish brown (Z) under the microscope in contrast to the more typical reddish-brown (Z) colors of the other biotites. We have already described briefly above the growth of sillimanite in muscovite which previously had replaced kyanite (fig. 13D). Such textural relations among these three minerals may be interpreted most simply as reflecting the following cyclic or paired reactions wherein muscovite occurs as an intermediate phase (Carmichael, 1969):

$$3 \text{ kyanite} + 3 \text{ quartz} + 2K^{+} + 3H_2O \quad \text{2 muscovite} + 2H^{+} \qquad (10)$$

$$2 \text{ muscovite} + 2H^{+} \quad 3 \text{ sillimanite} + 2K^{+} \qquad (11)$$

One of the critical implications of reactions (10) and (11) is the apparent immobility of Al^{3+} (Carmichael, 1969). However, as pointed out by Glen (1979), if overall volumetric changes and half-reactions in physically separate domains of the rocks during metamorphism also are considered in such metapelites, then some elements (Al^{3+}, Si^{4+}) may indeed be relatively mobile.

The metamorphic rocks thus contain textural evidence documenting repeated and possibly prolonged periods of sillimanite crystallization sometime after the onset of crystallization of a biotite-garnet-quartz±potassium feldspar±plagioclase±opaque minerals±hercynite assemblage. These pelitic gneisses also may have included sillimanite as an early phase.

Some high metamorphic grade mylonitic rocks host an assemblage of quartz and sillimanite (7, above) which together make up the bulk of the blastomylonitic matrix of these rocks (fig. 14D). These mylonitic rocks crop out discontinuously in the metamorphic terrane, and the white mica in them occurs as poorly developed coronas that surround sillimanite. In these rocks, which also include previously crystallized porphyroclasts of garnet and

biotite, the phyllonitic structure is defined mostly by sillimanite which crystallized preferentially along the mylonitic S-surface. In addition, quartz shows a strong crystallographic and dimensional orientation wherein the orientation of its [0001]-axes coincide closely with the S-surface of the mylonite. Although quartz in the matrix of the blastomylonitic rocks shows complex and highly sutured boundaries, the bulk of the quartz is strain free and triple junctions of 120° dihedral angles are common. In some mylonitic rocks, white mica partly replaces sillimanite and may reflect continued late-stage mylonitization under hydrous conditions. Thus, local mylonitization initially occurred apparently during the metamorphic peak of the region at upper amphibolite facies conditions, and continued perhaps sporadically into the subsequent greenschist metamorphism (see fig. 8).

The cordierite-bearing rocks most commonly include a cordierite-biotite-garnet-potassium feldspar association (8, above) (table 5) which does not contain white mica that is paragenetically the same age as the cordierite. The bulk of the white mica in the cordierite-bearing assemblage of table 5 is a very late mineral which partly replaces feldspar and (or) cordierite in the rocks. Thus, the progressive and consistent decrease in the modal abundance of early white mica in these rocks suggests that the peak of the prograde metamorphism occurred at physical conditions wherein the assemblage white mica-quartz was not stable. Although cordierite isograds elsewhere commonly have been mapped fairly concisely as halos around intrusive rocks emplaced into metapelitic terranes (Loomis, 1979; and many others), we have established only a very approximate boundary for the distribution of cordierite in the Gold Basin-Lost Basin districts. Cordierite in the districts seems generally to be confined to relatively fresh, unretrograded metamorphic rocks associated spatially with the suite of Proterozoic X igneous rocks that crop out in the general area of Garnet Mountain east of the trace Grand Wash fault zone, and northeast of the intersection of the inferred traces of the Grand Wash and Hualapai Valley faults. There is some evidence in these rocks that cordierite does not reflect thermal recrystallization during a relatively dry, nondynamic contact event related primarily to final emplacement of nearby igneous rocks. Cordierite in many of these rocks forms an integral part of the gneissic fabric of the garnet-biotite assemblage(s). Many of the rocks containing cordierite are metamorphic schlieren and pendants of metapelites engulfed by more widespread igneous rocks. However, many pelitic rocks in

these schlieren and pendants do not contain cordierite very close to their contacts with adjoining plutonic igneous rocks. Some pelitic migmatitic gneisses within 3 m of very large, Proterozoic X igneous bodies show quartz+biotite+plagioclase (oligoclase to even albite, in places)+microcline±white mica±garnet composite assemblages, but also including carbonate and clinozoisite-epidote alteration of earlier plagioclase. The only contact phenomena noted are the porphyroblastic growth of white mica and feldspar (both albite and microcline), as well as the alteration of plagioclase.

Cordierite, as listed above (8) and (9), occurs in at least two parageneses in unretrograded pelitic gneiss and migmatite. The more common, and probably early, association is with biotite and garnet (table 5), and this association (8) defines partly the schistose fabric of the host pelitic gneiss. Presumably early cordierite also occurs with biotite and garnet in the melanosome (Mehnert, 1968) or dark portion of migmatites against which the light micropegmatitic portion or leucosome apparently has advanced (fig. 15A). We herein use the terms melanosome and leucosome in a purely descriptive sense. It is beyond the intended scope of our present study to attempt a full documentation of the overall genesis of these extremely complex rocks. For example, we have not established whether the melanosomes reflect simply an *in situ* residue from the parent rock (paleosome of Mehnert (1968)) or whether the melanosomes are chemically transformed even partially. However, modal analyses of adjoining layers of melanosomes and leucosomes in these rocks show roughly equivalent abundances of the felsic minerals (quartz and feldspars). The major difference between the two is the almost complete absence of biotite from the leucosome whereas the melanosome typically includes about 25 volume percent biotite. Further, in the melanosome, some cordierite is concentrated in biotite-potassium feldspar (mostly microcline)-plagioclase (An_{20-25}) domains away from garnet-quartz domains. Within these latter domains, xenoblastic garnet also commonly shows highly irregular, skeletal outlines resulting from its growth along quartz crystal outlines resulting from its growth along quartz crystal boundaries. In the melanosomes garnet appears to be associated stably with biotite. Biotite shows invariably an increased abundance within about 0.2 mm of the sharply adjoining leucosome, especially along fronts convex toward the melanosome. The leucosomes of these migmatitic rocks contain commonly a cordierite-sillimanite-hercynite assemblage (9) (fig. 15B). Contents of Al_2O_3 and K_2O, calculated from modal

Figure 15.--Photomicrographs showing textural relations of cordierite. Plane polarized light. Sample number GM-125. A, Early cordierite (C) associated with biotite (B) in the melanosome of migmatitic gneiss; B, Subsequent cordierite (C) associated with sillimanite (S), hercynite (H), and opaque minerals (O) concentrated in the feldspar- (microcline and oligoclase) and quartz-rich, 1- to 2-cm-wide leucosome.

abundances and inferred ideal compositions of constituent minerals, locally show several-fold increases in the leucosomes versus the adjoining melanosomes. The increase of Al_2O_3 is primarily a reflection of strong concentrations of sillimanite in many leucosomes and appears to document at least very local mobility of Al_2O_3. However, Al_2O_3 overall probably remained fairly constant during prograde development of the migmatites, provided these rocks behaved similar to migmatitic terranes elsewhere (Wenk, 1954; Suk, 1964; Busch, 1966; Mehnert, 1968).

The cordierite- and sillimanite-bearing assemblages correspond to assemblages in the classic Barrovian region which are indicative of medium-pressure regional metamorphism (fig. 16). Generally accepted, rough estimates of geothermal gradients during such metamorphism are about 20°C per km (Miyashiro, 1973). From what we can assemble of the prograde metamorphism of the region by "looking through" the subsequent greenschist event, the rocks appear to show transitions from garnet-biotite, staurolite, and kyanite assemblages to ones dominated by cordierite and (or) sillimanite. We infer these latter assemblages to reflect the thermal peak of the Proterozoic metamorphism in the area. The cordierite-sillimanite assemblages seem to be best preserved in the general area of the widespread, Proterozoic X plutonism at Garnet Mountain.

Petrogenetic Implications of Mineral Relations

The observed relations between kyanite- and sillimanite-bearing assemblages rank among the most critical petrogenetic ones relations established, especially taking into account their experimentally and theoretically determined stability fields (Helgeson and others, 1978). An early kyanite stable, metamorphic event (fig. 8) must have occurred at pressure-temperature (PT) conditions greater than the kyanite-andalusite-sillimanite triple point (fig. 17), because the transition recorded in the rocks is kyanite to sillimanite, and not to andalusite. Helgeson and others (1978) now place the triple point in the system Al_2O_3-SiO_2-H_2O at approximately 3.7 kilobars (kb) and 500°C, or close to the 510°C-and 4.0 kb-coordinates of the triple point proposed by Newton (1966) and Holdaway (1971). We can not ascertain how far beyond the kyanite-sillimanite transition the kyanite initially crystallized. However, it may not have been far from the transition because kyanite was found to occur only sparingly, although unknown amounts of kyanite may have been destroyed during the

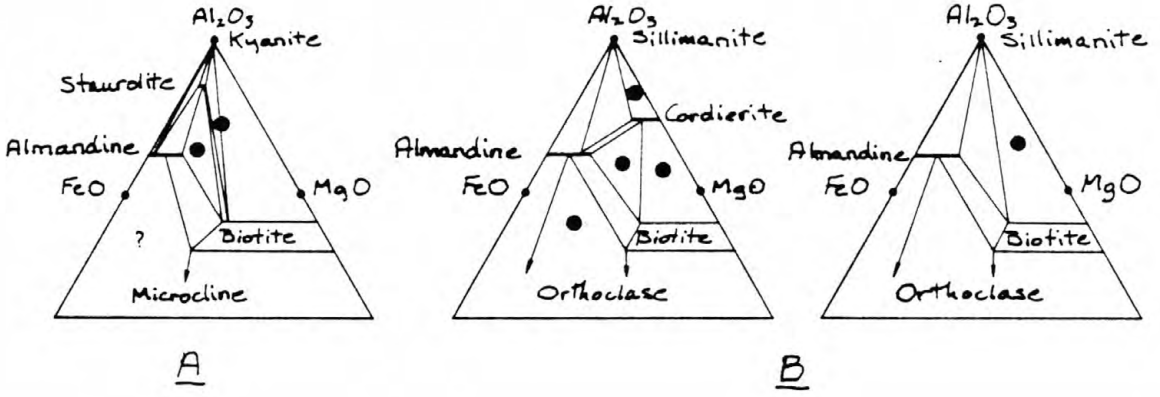

Figure 16.--Thompson (1957) AFM diagrams for medium pressure progressive metamorphism. A=Al_2O_3, F=FeO, M=MgO. Dots indicate assemblages observed in metamorphic rocks from the Gold Basin-Lost Basin districts. A, kyanite zone of Thompson; B, sillimanite zone.

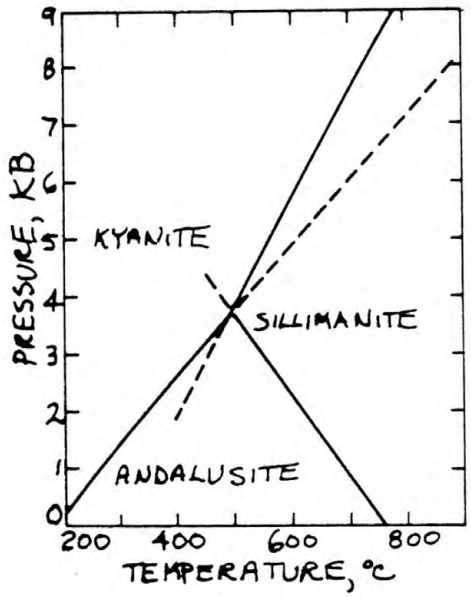

Figure 17.--Equilibrium curves generated from thermodynamic data by Helgeson and others (1978) in the system Al_2O_3-SiO_2-H_2O at high pressures and temperatures.

widespread, retrograde metamorphism of the area. Further, Kepezhinskas and Khlestov (1977) caution that the boundaries of the PT stability regions of naturally occurring aluminosilicates may in fact be not so well defined. They envision the boundaries to compose a field in PT-space rather than a line. Nonetheless, the overall transition from kyanite to sillimanite must reflect an increase in the geothermal gradient that produced the regional metamorphic maximum for the area. Assemblages of Fe-Mg cordierite, including potassium feldspar and at PT conditions of muscovite-quartz instability, comprise extremely wide-ranging stability fields that also are a function of P_{H_2O} (Holdaway and Lee, 1977). Holdaway and Lee (1977) showed that under such conditions and at $P_{H_2O} = P_{tot}$ and below the granite solidus, Mg cordierite plus potassium feldspar plus vapor is stable to a maximum pressure of about 5 kb, whereas at $P_{H_2O} = 0.4\ P_{tot}$, this assemblage is stable to about 6 kb. These pressures are probably reasonable upper pressure limits to the cordierite- and sillimanite-bearing assemblages produced during the prograde, Proterozoic X regional metamorphic event in the districts. Last, the absence of hypersthene from the cordierite-bearing assemblages suggests that the upper-temperature stability limit of cordierite here did not exceed a biotite plus quartz breakdown reaction (see Hess, 1969).

Quartzofeldspathic Gneiss

Epiclastic rocks best termed quartzofeldspathic gneiss probably comprise the most common rock type in the mapped Proterozoic X gneiss. However, quartzofeldspathic gneiss typically does not make up extensive monolithologic sequences of gneiss throughout the unit. Instead, the quartzofeldspathic gneiss is interlayered with many other lithologies including amphibolite and marble. Locally, thin layers of quartzofeldspathic gneiss occur within larger masses of amphibolite; some of these masses of amphibolite are large enough to be shown as separate map units (see Blacet, 1975) and others are included within the rocks mapped as paragneiss by him. In the amphibolite, the quartzofeldspathic gneiss ranges from sharply defined layers a few millimeters thick up to layers about 18 to 20 cm thick. However, either of these rocks, quartzofeldspathic gneiss or amphibolite, locally may grade into the other by interbedding across an interval of 2 to 3 m. In fact, quartzofeldspathic gneiss and amphibolite together impart a banded aspect to many outcrops within the gneiss unit. These outcrops may be more or less homoclinal sequences of rock or they may be isoclinally folded complexly at the outcrop scale. In

addition, some of the thicker sequences of quartzofeldspathic gneiss show sporadically occurring pegmatoid clots inferred to be "sweatouts" that formed during the peak of prograde regional metamorphism. These clots consist in decreasing abundance of feldspar, quartz, and biotite, and the clots show gradational boundaries with the surrounding more uniformly sized quartzofeldspathic gneiss. Further, layering throughout the quartzofeldspathic gneisses provided the local structural controls that determined the attitude and geometry of subsequently introduced quartz plus sulfide lenses and (or) veins that will be discussed below.

Visual estimates of representative samples of quartzofeldspathic gneiss using a microscope reveal that many samples may have consisted of mostly quartz and oligoclase prior to metamorphism. Polycrystalline quartz grains that are round to subround are fairly common in the size range 0.1 to 0.4 mm. These relations suggest that the protolith of the quartzofeldspathic gneiss consisted of fine arkosic to possibly subarkosic sandstone, using the classification of McBride (1963). We have not recognized any lithic fragments in the samples studied. The polycrystalline quartz grains show very complex, sutured, intragranular crystal boundaries for the most part, but many grains have retained their overall subrounded to well-rounded detrital outlines through the superposed metamorphic events. Although oligoclase was probably the predominant feldspar in most samples prior to metamorphism, it now has been replaced variably in most samples by a very finely crystallized, shreddy aggregate of white mica, chlorite, actinolite, sphene (trace), and opaque minerals (including some ilmenite), with or without epidote-clinozoisite, calcite, and albite. This assemblage of minerals, predominantly reflecting the retrograde metamorphic event, also occurs as a matrix which supports the quartz and feldspar framework minerals. However, the intense development of retrograde assemblages in the plagioclase feldspars and matrix generally obscures significantly the premetamorphic textural relations in the rocks between framework feldspars and matrix. In fact, the matrix may have consisted of very fine granules of plagioclase, but including variable amounts of diagenetic phyllosilicate minerals and minor amounts of calcite cement. Although relict oligoclase grains comprise the only recognizable feldspar in many samples of the quartzofeldspathic gneiss, overall plagioclase to potassium feldspar ratios are inferred to have been highly variable prior to metamorphism. Some samples contain oligoclase to potassium feldspars ratios of

approximately 10 to 1. The potassium feldspar typically has not been replaced by mineral assemblages diagnostic of the retrograde event, and the potassium feldspar includes both perthite and locally abundant microcline. Heavy minerals in the quartzofeldspathic gneiss include 0.01 to 0.05 mm across, subrounded prisms to well-rounded ellipsoids of zircon, and, less commonly, sphene and apatite.

Chemical analyses of four samples of quartzofeldspathic gneiss (analyses 3-6, table 4) reveal compositions most similar to published analyses of eugeosynclinal sandstones or graywackes. The content of SiO_2 in these analyzed samples of quartzofeldspathic gneiss ranges from 72.3 to 76.3 weight percent, only slightly higher than the 71 weight percent geometric mean determined for the eugeosynclinal graywackes by Middleton (1960). However, the mean SiO_2 content of 61 graywackes (analysis 10, table 4) compiled by Pettijohn (1963) is 66.7 weight percent. Further, the analyses of quartzofeldspathic gneiss show low K_2O to Na_2O ratios that range from 0.23 to 0.48 (table 4). Such low ratios are a feature common to graywackes (Middleton, 1960; Pettijohn, 1963, fig. 2), but they are somewhat lower than the 0.69 ratio of K_2O to Na_2O in the average graywacke (analysis 10), and significantly lower than the 1.9 ratio in the average arkose (analysis 11). The low ratios of less than one confirm our petrographic estimates for the overall low ratio of potassium feldspar to plagioclase in the detrital framework minerals. In addition, the content of Al_2O_3 in these rocks ranges from 12.3 to 14.0 weight percent, which is close to the mean value of 13.5 (Pettijohn, 1963), but is significantly higher than the 8.7 weight percent mean Al_2O_3 content of arkose (analysis 11). The contents of CaO in the four rocks range from 2.1 to 4.3 weight percent, and are thus not much different from the 2.5 and 2.7 weight percent content of CaO in the average graywacke and arkose. Such contents of CaO in the four samples of quartzofeldspathic gneiss are somewhat higher than the contents of CaO reported for the Proterozoic X Vishnu Complex by Brown and others (1979) (fig. 18). MgO in the quartzofeldspathic gneisses analyzed ranges from 0.4 to 1.7 weight percent and is thus less than the mean MgO composition of 61 graywackes (2.1 weight percent, analysis 10, table 4). Such low contents of MgO may reflect the very low content of lithic volcanic detritus shed into the protolith of the gneisses. Although these chemical analyses of quartzofeldspathic gneisses from the Gold Basin-Lost Basin mining districts show similarities generally to

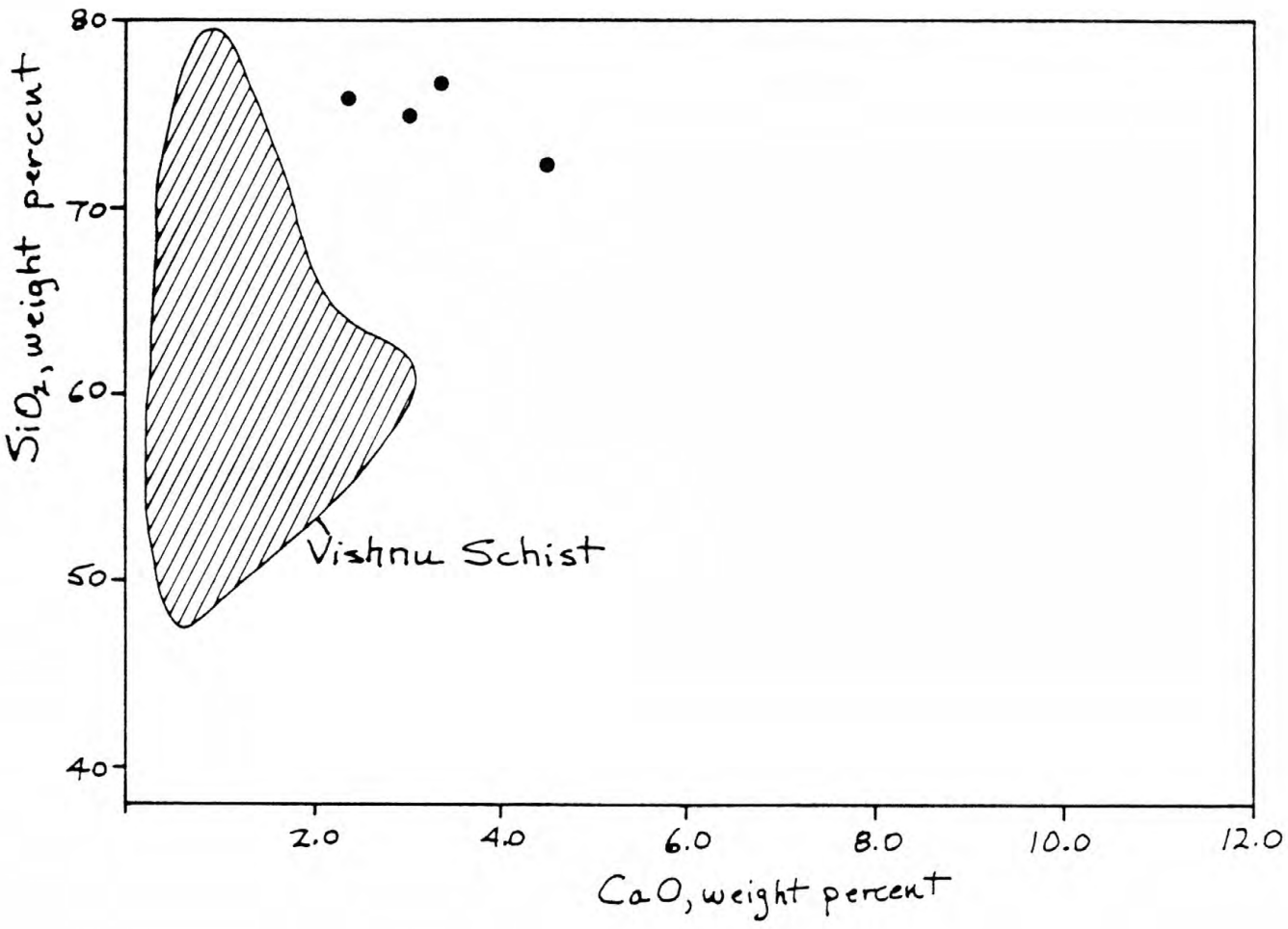

Figure 18.--Graph showing as solid dots a plot of SiO_2 versus CaO in four samples of quartzofeldspathic gneiss (analyses 3-6, table 4), and the field, shown as a lined pattern, established by Brown and others (1979) for 16 analyses of metasedimentary rocks from the Proterozoic X Vishnu Complex.

graywackes, all of these samples have been affected moderately to strongly by retrograde alteration phenomena. The rocks have been subjected to several intense and prolonged metamorphic events and weathering phenomena, all of which contributed to the final chemical composition of the gneiss. The chemical changes, if any, which accompanied each of the events cannot be ascertained.

Amphibolite

Amphibolite of varying sizes occurs throughout the Proterozoic metamorphic terrane in the Gold Basin-Lost Basin mining districts. However, only a few of these amphibolites are shown as separate map units in the district-wide geologic map by Blacet (1975), because of the of the scale of the quadrangle map, their discontinuous nature, and the overall highly irregular size-distribution of many individual outcrops. Most amphibolite occurs within the gneiss (unit Xgn, fig. 2) which includes mainly quartzofeldspathic gneiss as described above. Lesser amounts of amphibolite occur in the migmatitic units and also scattered as pendants in the various Proterozoic X igneous rocks. In the gneiss unit, some outcrops consist of 30-m-thick layers which are as much as 80 to 90 percent dark-green-gray to dark-greenish-black to black amphibolite (see fig. 6B). Such masses of amphibolite may grade across several meters into quartzofeldspathic gneiss by decreased numbers of layers of amphibolite along strike of the foliation. Layers of amphibolite also may terminate abruptly or be crosscut by coarse-grained quartz-feldspar-rich leucogranite which in turn then grades into the surrounding quartzofeldspathic gneiss. The overall abundance of amphibolite in the Proterozoic terrane here in the Gold Basin-Lost Basin mining districts is much greater than in similar metamorphic terranes just to the north around Lake Mead (P. M. Blacet, unpub. data, 1967-1972). However, even within the districts themselves there is a wide variation in the proportion of amphibolite in the Proterozoic X gneiss map unit (fig. 2). Near the south end of the Lost Basin Range, amphibolite is derived largely from igneous protoliths, an assessment based on the occurrence of widespread relict gabbroic and diabasic textures. Careful examination of outcrops there further reveals that rarely some amphibolite definitely crosscuts the lithologic layering in the enclosing paraschist and paragneiss, and clearly shows preserved chilled margins against these rocks.

Amphibolite in the Proterozoic terrane is either massive, showing no readily apparent macroscopic structure, or more commonly it contains a well-developed fabric. Generally, the fabric consists of at least one obvious foliation, and possibly a less well developed lineation. The principal foliation (S_1) is defined by millimeter-size layering of varying compositions and by differences in grain size between adjoining domains of similar mineralogy (fig. 19A). Most commonly the attitude of S_1 in the amphibolite is the same as that in the surrounding gneiss, and S_1 may be better developed near the margins of the amphibolite bodies. Lineation in the amphibolite locally is defined by a strong preferred orientation of amphibole crystals within S_1. In addition, other types of lineation in amphibolite include minor fold axes and well-developed mullion-structures consisting of aggregates of hornblende showing a strong preferred orientation of their [001]-axes parallel to the mullions. The fold axes and mullion structures commonly are coaxial. Isoclinally folded amphibolite interlayered with quartzofeldspathic gneiss is especially abundant along the west flank of the Lost Basin Range. Lineation in amphibolite may also be defined by the intersection of a subsequent fracture cleavage (S_2) with S_1. Locally, in amphibolite, ripplelike corrugations on S_1 plunge shallowly (about 10^o), and reflect the intersection of S_1 with the S_2 fracture cleavage. Typically, such S_2 fracture clevages are more widely spaced than the S_1 layering. In addition, chloritization occurred penecontemporaneously with the development of S_2, and thus the fracture cleavage most probably dates from the widespread retrograde metamorphic event described above. Nonetheless, relatively fresh amphibolite, fresh to the unaided eye anyway, occurs in small core domains between the traces of the S_2 fracture cleavage. Lastly, some amphibolitic schist is lineated locally on S_1 because of the crystallization of elongate splotches of white mica, also most probably dating from the retrograde event. These splotches of white mica parallel the hornblende lineation in the rocks.

The protolith for many individual outcrops of amphibolite or cluster of outcrops can be ascertained primarily using relict textures or geologic field relations with other lithologies of known provenance. In addition, we have supplemented and refined these observations by extensive microscopic examination of thin sections of amphibolite and chemical analyses of a few selected samples of amphibolite. However, some of the amphibolite exposed in the districts cannot be classified as to protolith because of the absence of

Figure 19.--Photomicrography of amphibolite. A, amphibole; Q, quartz; P, plagioclase or retrograde alteration products of plagioclase, including white mica, carbonate, and clay(s). A, Principal foliation (S_1) defined by lithologic layering of varying compositions. Sample number GM-290; SE1/4 sec. 18, T. 29 N., R. 17 W.; B, Fabric of hornblende-clinopyroxene-plagioclase (An_{70})-quartz-biotite (Tr) amphibolite crystallized at upper amphibolite facies conditions and, among the samples studied, judged to have been least modified by subsequent geologic events. Sample number GM-1117; C, Well-rounded grains of strained, monocrystalline quartz included within brown to olive-green-brown hornblende (Z) in a hornblende-plagioclase(?)-quartz-clinopyorxene-opaque mineral assemblage. Plagioclase has been completely replaced by a very fine grained aggregate of white mica-chlorite-epidote-tremolite and actinolite-opaque mineral(s). Sample number GM-1063; NE1/4 sec. 3, T. 28 N., R. 17 W.; D , Fabric of amphibolite showing the effects of contact metamorphism related to emplacement of the Cretaceous two-mica monzogranite of Gold Basin. Sample number GM-1103a, collected 3 m from the two-mica monzogranite; SE1/4 sec. 12, T. 28 N., R. 19 W.

A

B

C

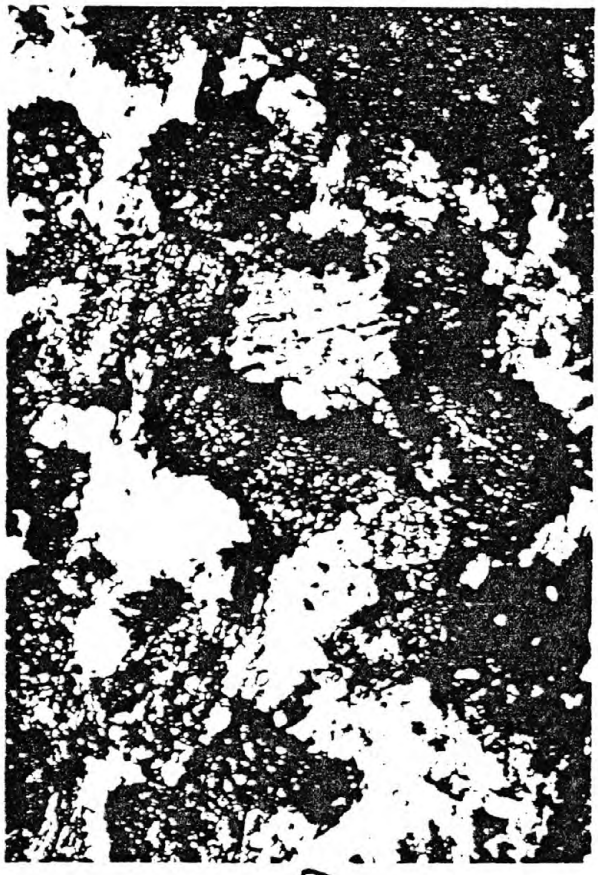

D

diagnostic macroscopic, microscopic, or chemical criteria. Locally, amphibolite in the gneiss derived from a sedimentary protolith includes relict beds which consist of calc-silicate minerals and marble, and much of this type of amphibolite is finer grained than amphibolite derived from igneous rocks. Some of these beds reach a maximum thickness of about 30 cm along a continuously exposed strike-length of about 15 m. The calc-silicate beds are conformable with the layering in the adjoining amphibolite, and in places they neck down to about 2.5 cm or less. Additional evidence for a sedimentary origin for many amphibolite layers is their delicate interlayering with quartzofeldspathic beds a few millimeters to approximately 20 cm thick. This is especially good evidence for a sedimentary protolith for some amphibolite in the gneiss when we recall from our descriptions above that the quartzofeldspathic gneisses show abundant textural and chemical evidence for a sedimentary protolith. Lastly, we will show below that many hornblende crystals in this type of amphibolite have trapped well-rounded to ovoid grains of quartz which obviously had been through a sedimentary cycle.

In all, 37 samples of amphibolite from 27 localities were studied petrographically (table 6). Almost all of these samples contain mixed mineral assemblages, which reflect crystallization during the Proterozoic X upper amphibolite facies metamorphism, and retrograde metamorphism at greenschist conditions. The amphibolites include locally some cataclastic or mylonitic fabrics, and finally some local thermal and (or) hydrothermal alteration phenomena associated with Cretaceous plutonism and vein-type gold mineralization. The latter mineralogic changes in a selected suite of amphibolite samples will be discussed in a section below describing the lode gold deposits in the districts. Nonetheless, the mineral assemblage formed during any one of the above events is relatively simple. For example, amphibolite which shows the least modification by subsequent events contains a greenish-brown to brown (Z) hornblende-plagioclase (An_{70})-quartz-clinopyroxene-biotite (Trace)-opaque mineral assemblage which includes apatite and sphene as minor accessories (fig. 19B). In outcrop, this 5- to 6-m-thick zone of amphibolite shows a "sparkling" fresh granoblastic fabric and occurs within some garnet-biotite migmatitic gneisses. Red-brown (Z) biotite in trace amounts is apparently compatible with the other minerals in the assemblage, and normally zoned, very calcic plagioclase (An_{70}) occurs as generally untwinned, stubby to equant prisms. Miyashiro (1973), Mason (1978), and many others have noted the

Table 6. Composite mineral assemblages in amphibolite and altered amphibolite from the Gold Basin-Lost Basin mining districts
[X, mineral present; Tr, present in trace amounts; 50, An content of plagioclase; ----, not found; ?, presence uncertain]

	Amphibole[1]															
	Blue green	Gray green to olive-gray green	Green-brown to brown	Quartz	Plagioclase	Clinopyroxene	Biotite[2]	Opaque minerals	Apatite	Sphene	Tremolite actinolite[3]	Epidote group[3]	Chlorite[3]	White mica[3]	Carbonate[3]
GM-92a	----	X	----	X	Tr	----	----	X	----	----	----	X	----	----	----
GM-124	----	X	----	X	X	X	X	X	Tr	----	----	----	X	Tr	----
GM-191	X	----	----	----	----	----	----	X	X	----	----	X	X	----	----
GM-191a	X	----	----	Tr	X	----	----	X	X	X	----	X	----	----	X
GM-209	----	X	----	X	----	----	----	Tr	----	Tr	----	X	X	X	----
GM-213	----	X[4]	----	----	Tr	X	----	X[5]	X	----	X	----	----	X[6]	----
GM-213a	----	X	----	----	----	----	----	X	----	X	X	----	X	----	Tr
GM-242	----	X	----	Tr	X	----	----	X	----	----	X	X	X	----	?
GM-246	----	----	X	X	40	----	----	X	X	----	X	X	X	X	----
GM-254	----	----	X	Tr	30	----	----	X	----	----	X	X	X	----	X
GM-290a	----	----	X	X	X	---	----	X	----	X	----	X	X	X	----
GM-290	----	----	X	----	Tr	----	----	X	Tr	----	----	X	X	----	X
GM-298a	----	----	X	----	Tr	----	Tr	X	X	X	X	X	X	----	X
GM-371[7]	X	----	----	X	30	----	X	X	X	X	----	X	X	X	----
GM-382a[8]	X	----	----	X	30	----	----	Tr	X	Tr	X	X	X	X	X
GM-382b[8]	X	----	----	Tr	10	----	----	Tr	X	Tr	X	X	X	Tr	X
GM-382c[8]	----	----	----	X	10	----	X	X	X	----	----	X	X	X	X
GM-392d[8]	----	----	----	X	10	----	X	X	X	----	----	----	X	Tr	X
GM-382e[8]	----	----	----	X	10	----	X	X	X	----	----	----	X	X	X
GM-412f	X	----	----	Tr	----	----	----	X	Tr	X	----	X	Tr	----	----
GM-461b	----	----	X	X	Tr	----	----	X	Tr	----	X	X	Tr	----	----
GM-468	X	----	----	X	X	----	----	X	X	X	----	X	Tr	X	----
GM-529	X	----	----	X	35	----	----	X	X	?	----	X	X	X	----
GM-529a	X	----	----	X	X	----	----	X	X	X	----	X	X	X	----
GM-539	X	----	----	Tr	----	----	Tr	X	X	X	----	Tr	X	X	X
GM-634a	X	----	----	Tr	----	----	----	X	X	X	X	X	X	----	X
GM-634a'	X	----	----	Tr	----	----	----	X	X	X	----	X	X	----	X
GM-665	----	X	----	X	X	----	----	X	X	Tr	X	X	X	X	Tr
GM-669	----	X	----	X	Tr	----	----	X	X	X	X	X	X	Tr	Tr
GM-697	X	----	----	X	X	----	X	X	X	----	X	X	X	X	Tr
GM-699	----	X	----	X	X	----	----	X	X	X	X	X	X	X	Tr
GM-855	----	X	----	X	65	----	----	X	X	X	X	X	Tr	Tr	Tr
GM-962	X	----	----	Tr	----	----	----	X	----	X	Tr	X	X	----	X
GM-1063	----	----	X	X	Tr	X	----	X	X	----	X	X	X	Tr	----
GM-1063b	----	----	X	X	55	X	----	X	X	----	----	X	Tr	Tr	----
GM-1103a	X	----	----	X	35	----	X	X	X	X	----	X	X	X	Tr
GM-1117	----	----	X	X	70	X	X	Tr	X	----	----	Tr	----	X	----

[1]Color of amphibole (Z) in microscope using plane polarized light.
[2]Both primary and secondary.
[3]Mostly part of regional greenschist retrograde assemblage and (or) local hydrothermal assemblage(s) adjacent to mineralized veins.
[4]Cummingtonite.
[5]Includes green spinel, and probable chromite.
[6]Includes serpentine.
[7]Includes potassium feldspar in hairline, microveinlets cutting metamorphic fabric of amphibolite; biotite is secondary.
[8]Sample included in alteration suite studied near a vein (see text and fig. 48).

general tendency for the calcium content of plagioclase to increase, and the color of hornblende to go from blue green to various shades of brown during an increase in the grade of metamorphism of metabasites from the lower to the upper amphibolite facies. These relations occur in amphibolites from the Gold Basin-Lost Basin districts (table 6), and they alone suggest the amphibolite reached prograde metamorphic peaks similar perhaps to zone C metabasites in the low-pressure central Abukuma Plateau, Japan (Miyashiro, 1958) or to zone B metabasites in the medium-pressure Broken Hill area, Australia (Binns, 1965a, b, c).

Quartz makes up a significant proportion of many of the samples of amphibolite, and quartz occurs in all but five of the samples studied (table 6). Quartz in these rocks is of several different parageneses. Some quartz is premetamorphic and dates from the protolith of the amphibolite, whereas the bulk of the quartz crystallized during either the prograde or retrograde events. The hornblende in some samples includes abundant, small, well-rounded monocrystalline grains of quartz and much lesser quantities of rounded grains of plagioclase. Such quartz in places is rimmed partially by an extremely fine grained unknown silicate. Many such grains of quartz were strained moderately, and they are inferred to reflect relict detrital quartz grains, engulfed by a subsequent overgrowth of hornblende during the upper amphibolite facies metamorphism of the area (fig. 19C). The fabric of much of the quartz that recrystallized during either the early amphibolite facies metamorphism or the subsequent greenschist and contact events differs markedly from these grains of quartz showing well-rounded outlines. Such metamorphic quartz typically has a blebby or shredded overall aspect and is associated very closely with blue-green (Z) hornblende and (or) tremolite-actinolite that replaces partially the early green or brown hornblende. The quartz-quartz boundaries in such associations are very complexly sutured. Further, contact effects are notable in outcrops of some amphibolite up to about 3 m from the Cretaceous two-mica monzogranite that crops out in the southern part of the Gold Basin district. Such rock under the microscope shows a well-developed granoblastic texture of tightly intergrown, fine-grained crystals of mostly blue green (Z) hornblende and quartz (fig. 19D).

There are some quartz-free metabasites in the gneisses that have been derived from clinopyroxenite. Such metabasites include black, dense, highly magnetic rocks that locally are layered and that crop out prominently along a

strike-length measuring about 100 m, as exemplified by locality number 213, (pl. 1, table 11). Here the contacts of these rocks with the enclosing gneisses are obscured by rubble. However, close examination of these rocks reveals that they are unquestionably pods of metamorphosed ultramafic rocks. These rocks are very magnesian in composition. They show marked petrologic differences from the bulk of the amphibolite in the gneisses. Under the microscope, there is no suggestion of an ophitic or subophitic texture common to many of the amphibolites derived from gabbroic protoliths, and the amphibole in the metamorphosed ultramafic rocks is colorless to very weakly pleochroic in contrast to the more common blue-green and brown hornblende in most other amphibolites (table 6). In addition, the amphibole which typically makes up about 40 to 50 volume percent of the rock, is optically positive, a relation which further suggests it is a Mg-rich cummingtonite (ideally $(Mg)_7[Si_8O_{22}](OH)_2$). Cummingtonite is the dominant mineral in the early metamorphic assemblage, and appears to be compatible with clinopyroxene, green spinel, magnetite, and only traces of plagioclase. The cummingtonite-rich assemblage is in turn replaced partially by a late tremolite-serpentine-talc composite assemblage most likely related to greenschist metamorphism of the area. The overall fabric of the rock nonetheless suggests that the protolith was a clinopyroxenite (N. J Page, oral commun., 1980).

Major- and minor-element analyses of three samples of amphibolite (analyses 1-3), a diabase, and a pyroxene banded gneiss from the districts are presented in table 7, together with calculated Niggli values. Minor-element analyses of another six samples of amphibolite and one sample of iron-oxide-rich soil along a fault cutting amphibolite are listed in table 8. The latter minor-element analyses all were obtained from samples collected from the general area of the Bluebird mine in the Lost Basin district. The composite mineral assemblages of analyses 1 to 3 (table 7) are contained in table 6, listed under the appropriate sample number, and these assemblages show that all three samples have been affected by the retrograde metamorphism. In fact, much of the plagioclase in these rocks is altered. Further, all three samples contain some modal quartz. The overall proportion of quartz in the samples ranges from trace amounts (sample no. GM-190a; 46.0 weight percent SiO_2, table 7) to approximately 20 volume percent (sample no. GM-529; 55.2 weight percent SiO_2).

Table 7. Analyses of mafic rocks from the Proterozoic X terrane in the Gold Basin-Lost Basin mining districts

[Chemical analyses by rapid-rock methods; analysts, P. L. D. Elmore and S. Botts. Methods used are those described in Shapiro and Brannock (1962), supplemented by atomic absorption, and Shapiro (1967). Spectrographic analyses by Chris Heropoulos. Results are reported to the nearest number in the series 1., 0.7, 0.5, 0.3, 0.2, 0.15, 0.1, 0.07, etc., which represent approximate midponts of interval data on a geometric scale. The precision of a reported value is approximately plus or minus one series interval at 68-percent confidence or two intervals at 95-percent confidence. Looked for but not found: Ag, As, Au, B. Bi, Cd, Mo, Ni, Pd, Pt, Sb, Sn, Te, U, W, Zn, Hf, In, Li, Re, Ta, Th, Tl, Pr, Sm, Eu]

	1	2	3	4	5
Field number ---	GM-290A	GM-242	GM-529	GM-578	GM-245
Chemical analyses (weight percent)					
SiO_2 ----------	46.0	49.6	55.2	47.5	45.0
Al_2O_3 ----------	15.	15.4	13.7	17.2	15.9
Fe_2O_3 ----------	3.2	3.2	6.5	6.7	5.8
FeO ----------	9.7	8.5	7.4	3.	9.3
MgO ----------	8.4	5.7	3.9	6.	5.7
CaO ----------	10.5	10.5	8.3	10.1	10.9
Na_2O ----------	2.1	2.	2.	2.7	1.5
K_2O ----------	.70	1.	.8	.40	.50
H_2O^+ ----------	1.3	1.1	1.5	1.2	1.9
H_2O^- ----------	.03	.08	.06	1.3	.13
TiO_2 ----------	1.3	1.	1.4	1.2	1.7
P_2O_5 ----------	.15	.12	.24	.24	.16
MnO ----------	.15	.22	.22	.12	.21
CO_2 ----------	.11	.12	<.05	1.9	.05
Total --------	99.	99.	101.	100.	99.
Semiquantitative spectrographic analyses (weight percent)					
Ba ----------	0.05	0.03	0.02	0.05	0.03
Co ----------	.007	.005	.005	.005	.007
Cr ----------	.1	.05	.001	.02	.02
Cu ----------	.007	.0015	.01	.007	.01
Ni ----------	.03	.01	.005	.01	.01
Sc ----------	.005	.005	.005	.005	.005
Sr ----------	.03	.05	.05	.07	.03
V ----------	.02	.03	.03	.015	.05
Y ----------	.003	.002	.002	.003	.002
Zr ----------	.007	.005	.007	.01	.003
Ga ----------	.0015	.0015	.002	.0015	.002
Yb ----------	.0003	.0003	.0003	.0003	.0003
Niggli values					
al ----------	19.	22.	22.	25.	21.
fm ----------	51.	44.	47.	41.	48.
c ----------	25.	27.	24.	27.	27.
alk ----------	5.	6.	7.	7.	4.
si ----------	101.	121.	151.	118.	103.
k ----------	.18	.25	.21	.09	.18
mg ----------	.41	.47	.34	.54	.41

1. Amphibolite, interlayered with quartzofeldspathic banded gneiss in feldspathic gneiss (Xfg); SW1/4 sec. 17, T. 29 N., R. 17 W.
2. Amphibolite 3 cm thick, interlayered with biotite quartzofeldspathic gneiss on contact between migmatitic gneiss unit (Xmg) and gneiss unit (Xgn); NW1/4 sec. 5, T. 28 N., R. 17 W.
3. Amphibolite in gneiss unit (Xgn); NW1/4 sec. 16, T. 30 N., R. 17 W.
4. Diabase collected from main drift, Golden Gate mine; NW1/4 sec. 32, T. 30 N., R. 17 W.
5. Pyroxene banded gneiss in migmatitic gneiss unit (Xmg); NE1/4 sec. 32, T. 29 N., R. 17 W.

Table 8. Analyses for minor metals in selected samples of amphibolite and associated soil from the general area of the Bluebird mine in the Lost Basin mining district

[Spectrographic analyses by Leon A. Bradley. Results are reported to the nearest number in the series 1., 0.7, 0.5, 0.3, 0.2, 0.15, 0.1, 0.07, etc., which represent approximate midpoints of interval data on a geometric scale. The precision of a reported value in approximately plus or minus one series interval at 68-percnet confidence or two interval at 95-percent confidence. Looked for but not found: Ag, As, Au, Bi, Cd, Mo, Pd, Pt. Sb, Sn, Te, U, W, Hf, In, Li, Re, Ta, Th, Tl, Pr, Sm, Euy; L, less than determination value; --, not detected; N.D., not determined. Chemical analyses by Joseph Haffty, A. W. Haubert and J. McDade using techniques of Haffty and Riley (1968) for Pd, Pt and Rh; and Haffty, Haubert, and Page (1980) for Ir and Ru.]

	1	2	3	4	5	6	7	8
Field number ---	79GM-1	79GM-2	79GM-3	79GM-4	79GM-5	79GM-6	79GM-7	79GM-7a
	Semiquantitative spectrographic analyses (weight percent)							
B ----------	0.002	--	--	L	--	--	--	N.d.
Ba ----------	.015	0.015	0.007	0.02	0.015	0.02	0.015	N.d.
Co ----------	.007	.005	.003	.0007	.005	.003	.003	N.d.
Cr ----------	.1	.3	.05	.007	.2	.07	.15	N.d.
Cu ----------	.00015	.0007	.015	.0015	.007	.02	.015	N.d.
Mn ----------	.15	.15	.1	.05	.07	.15	.1	N.d.
Ni ----------	.007	.02	.01	.0015	.07	.015	.03	N.d.
Pb ----------	.0015	--	--	.003	--	--	.0015	N.d.
Sc ----------	.007	.005	.003	.001	.002	.003	.003	N.d.
Sr ----------	.02	.01	.007	.015	.0015	.007	.01	N.d.
V ----------	.07	.02	.015	.005	.01	.02	.015	N.d.
Y ----------	L	.003	.0015	.0015	L	.0015	.0015	N.d.
Zr ----------	--	.003	.0015	.0015	.0015	.003	.003	N.d.
Ga ----------	.0015	.0015	.002	.0015	.001	.002	.0015	N.d.
	Chemical analyses (parts per million)							
Pd ----------	0.029	<0.001	<0.001	<0.001	0.003	0.001	0.001	0.004
Pt ----------	.027	.033	.032	.015	.024	.029	.013	.021
Rh ----------	<.001	<.001	<.001	<.001	<.001	<.001	<.001	<.001
Ir ----------	<.02	<.02	<.02	<.02	<.02	<.02	<.02	<.02
Ru ----------	<.1	<.1	<.1	<.1	<.1	<.1	<.1	<.1

1. Amphibolite, composite sample; NE1/4 sec. 20, T. 29 N., R. 17 W.
2. Amphibolite, composite sample of several centimeter-sized layers in quartzofeldspathic gneiss; NE1/4 sec. 20, T. 29 N., R. 17 W.
3. Amphibolite, composite sample assembled from several centimeter- to meter-sized discontinuous pods; NE1/4 sec. 20, T. 29 N., R. 17 W.
4. Soil along fault cutting amphibolite, iron-oxide stained; NE1/4 sec. 20, T. 29 N., R. 17 W.
5. Amphibolite, composite samples containing 1- to 2-volume percent pyrite disseminated as 1- to 2-mm blebs; NW1/4 sec. 20, T. 29 N., R. 17 W.
6. Amphibolite, composite sample; SW1/4 sec. 17, T. 29 N., R. 17 W.
7. Amphibolite, composite sample; SE1/4 sec. 18, T. 29 N., R. 17 W.
8. Do.

The average major-element composition of the three analyzed amphibolites is compared with the average concentration of these elements in various igneous rock series and other selected amphibolites (table 9). Thus, from table 9, simply by comparing the major-element compositions of these amphibolites analyzed from Gold Basin-Lost Basin to similar averages of various igneous rock series, one might suggest that these analyzed amphibolites have igneous protoliths. The average of these three analyses (1, table 9) corresponds closely with the average continental basalt of Manson (1967, p. 222) or the average tholeiite of LeMaitre (1976). Further, these analyses are not much different from an analyzed sample of diabase, collected from the main drift of the Golden Gate mine (analysis no. 4, table 7). However, the Al_2O_3 content of the diabase (17.2 percent) is somewhat higher than the 14.7 weight percent average content of Al_2O_3 in the amphibolite, probably reflecting the higher content of modal plagioclase in the diabase than in the amphibolite. However, Leake (1964) suggested that a comparison of trends of certain elements in amphibolites with similar trends in sedimentary and igneous rocks might be more useful in establishing a sedimentary or igneous protolith than a comparison of average concentrations of elements. For example, an elongation of data points along a Karroo trend at high angles to the trend for variable mixtures of calcium carbonate, magnesium carbonate, and shale would suggest an igneous parentage. Thus, from the major-element data of table 6, plots of Niggli 100mg, c and al-alk values; Niggli c versus mg; and Niggli c versus al-alk were prepared (figs. 20-22).

Plots of various Niggli values yield results that are not particularly diagnostic primarily because of the small number of analyses of amphibolite available. Niggli values in a 100 mg, c, and al-alk ternary plot for the amphibolite show that they form a cluster slightly off the trend line established for Karroo dolerites by Evans and Leake (1960), but also well within the field of values expected for various shale-carbonate mixtures (fig. 20). The analyzed diabase (analysis no. 4) also plots slightly off the trend line in this ternary diagram. A plot of the Niggli values for the pyroxene banded gneiss (analysis no. 5), however, falls within the small cluster established by the data from the amphibolite. On the other hand, the plot of Niggli mg versus c shows data from the amphibolite to plot in the field for the Karroo dolerites, and to follow a trend line roughly parallel to the differentiation trend line of the dolerites (fig. 21). On such a diagram, the

Table 9. Average major-element compositions, in weight percent, of Gold Basin-Lost Basin amphibolite and various groups of igneous rocks and other amphibolites
[--, not determined]

	1	2	3	4	5	6	7	8
SiO_2	50.3	49.9	49.58	57.94	48.87	52.8	49.3	55.5
Al_2O_3	14.7	16.2	14.79	17.02	12.26	14.7	16.3	16.1
Fe_2O_3	4.3	3.	3.38	3.27	[1]11.89	4.5	2.5	2.8
FeO	8.5	7.8	8.03	4.04	--	6.6	8.5	5.
MgO	6.	6.3	7.30	3.33	10.13	6.5	6.	5.7
CaO	9.8	9.8	10.36	6.79	9.84	8.8	10.7	6.9
Na_2O	2.	2.8	2.37	3.48	1.91	2.5	3.1	3.4
K_2O	.83	1.1	.43	1.62	1.90	.68	.59	1.7
H_2O^+	1.3	1.	.91	.83	--	1.2	1.2	1.3
H_2O^-	.06	--	.50	.34	--	.39	.10	.10
TiO_2	1.2	1.6	1.98	.87	.62	1.1	1.1	.78
P_2O_5	.17	.30	.24	.21	.09	.15	.23	.32
MnO	.19	.17	.18	.14	.34	.19	.17	.12
CO_2	.09	--	.03	.05	--	.04	.18	.04
Total	99.44	99.97	100.08	99.93	97.85	100.	99.97	99.76

[1]Total Fe calculated as Fe_2O_3.

1. Average amphibolite, analyses 1-3 (table 6), this report.
2. Average continental basalt (Manson, 1967, table III, p. 222).
3. Average tholeiite (LeMaitre, 1976, no. 28).
4. Average andesite (LeMaitre, 1976, no. 16).
5. Selected amphibolite from Proterozoic X Vishnu Schist in the Grand Canyon (Clark, 1979, table II, analysis 4).
6. Average of five amphibolites in Proterozoic X Pinal Schist from the Mineral Mountain area, Arizona (T. G. Theodore, unpub. data, 1982).
7. Average of 12 amphibolites from Condrey Mountain, Klamath Mountains, Calif. (Hotz, 1979, table 5, p. 16).
8. Average amphibolite, central Beartooth Mountains, Montana-Wyoming (Armbrustmacher and Simons, 1977).

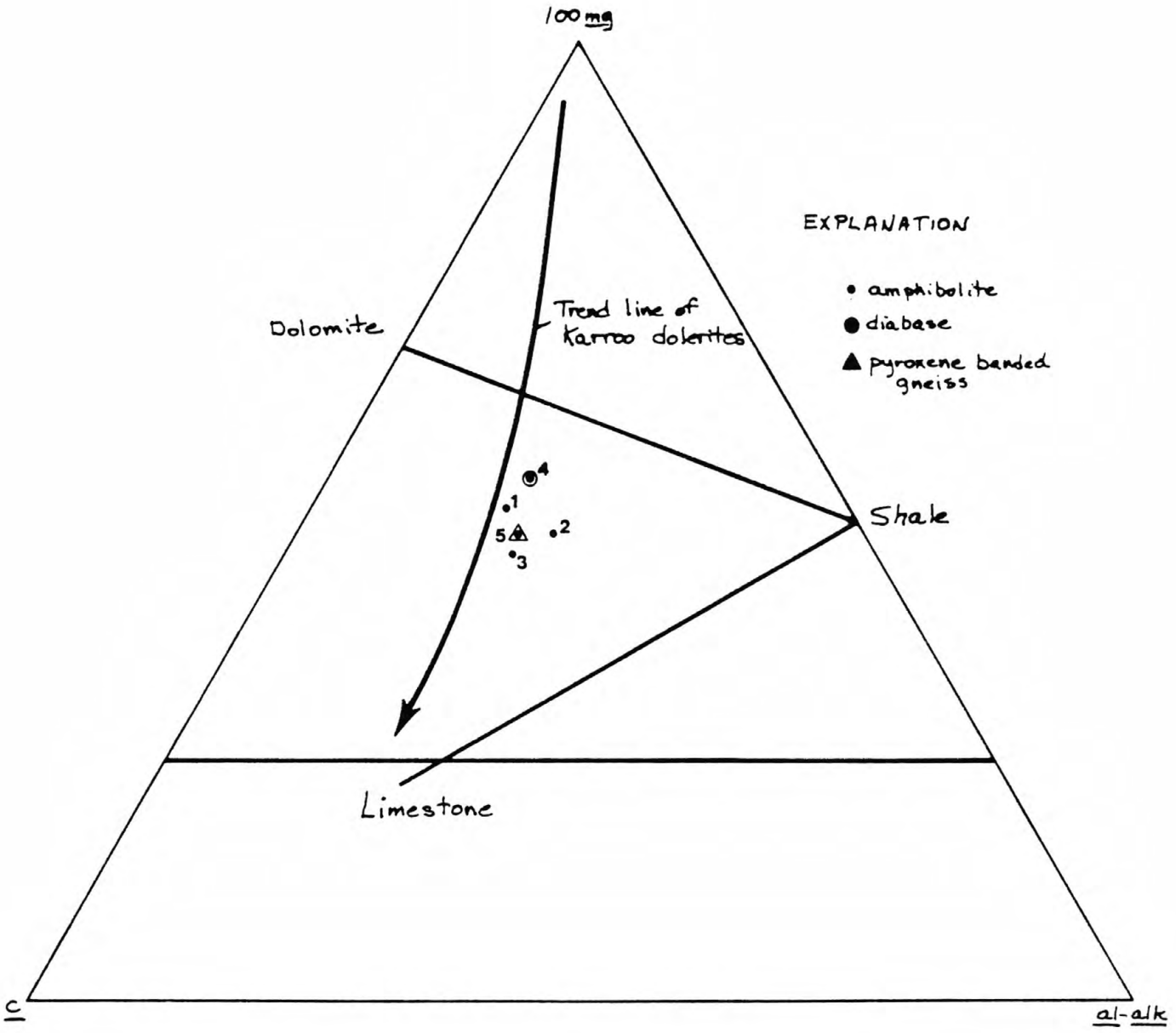

Figure 20.--Plot of Niggli 100 mg, c, and al-alk values for amphibolite, diabase, and pyroxene-banded gneiss from the Gold Basin-Lost Basin mining districts. Analysis numbers same as table 7.

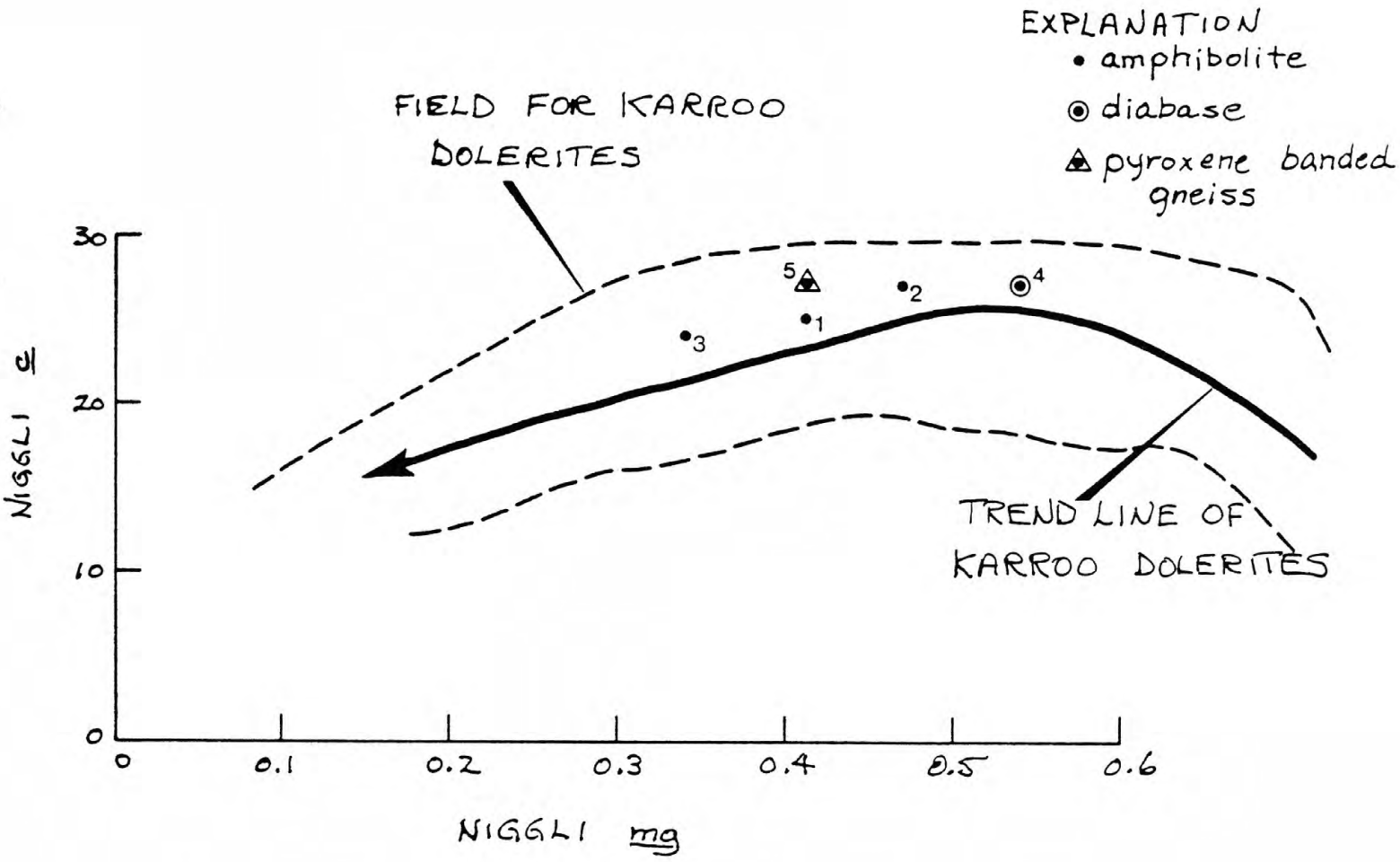

Figure 21.--Plot of Niggli c versus mg values for amphibolite, diabase, and pyroxene-banded gneiss from the Gold Basin-Lost Basin mining districts. Analysis numbers same as table 7. Also shown are the field and trend line for Karroo dolerites from Evans and Leake (1960).

analyzed diabase appears to be less differentiated than the three analyzed amphibolites. On a Niggli c versus Niggli al-alk diagram, the data for the amphibolite again cluster, and they fall just outside the most expected of such values for shale-carbonate mixtures, but still within a field of possible values for shale-carbonate mixtures (fig. 22). Again, the clustering of the small number of data points (3 amphibolite, and 1 pyroxene banded gneiss) follow clearly neither a sedimentary nor an igneous trend. Therefore, only one of the plots (fig. 21) yields a trend for the amphibolites that might be interpreted as an igneous one. The minor element data, particularly the concentration of chromium and nickel in some of the samples of amphibolite analyzed (tables 7 and 8), also suggest derivation from igneous protoliths. Further, the occurrence of detectable platinum-group metals in eight samples of amphibolite analyzed from the general area of the Bluebird mine (table 8), in the Lost Basin range, implies an igneous protolith, as does the relict igneous fabric in these samples, and in most other metabasites throughout the southern part of the Lost Basin Range. However, these observations and geologic relations together with those in the quartz-rich, sedimentary-derived amphibolites suggest very strongly that amphibolites in the districts were derived from both igneous and sedimentary protoliths.

Metachert, Banded Iron Formation, and Metarhyolite

Thin lenses of metachert, discontinuous beds of banded iron formation (see Stanton, 1972), and sparse occurrences of metarhyolite crop out in the Proterozoic metamorphic rocks of the districts. Most of the known occurrences of these three rock types are in the gneiss (unit Xgn, fig. 2), and the three rock types commonly are associated spatially with one another. They rarely occur also in the migmatitic gneiss unit. Most are quite thin and generally measure from 20 to 90 cm in lithologic thickness. Metachert tyically is well laminated, and these laminae probably reflect relict bedding. The metachert consists of irregularly banded, quartz- and feldspar-containing laminae that in places are conformable and interlayered with amphibolite. The feldspar-containing laminae have been altered mostly to various phyllosilicate and epidote group minerals. Metachert also is associated spatially with several other lithologies, including complexly scrambled calc-silicate, amphibolitic calc-silicate, and marble. Chemical analysis of a grab sample of a slightly pinkish, micaceous or argillaceous metachert shows an SiO_2 content of 79.5 weight percent (analysis 1, table 10). Examination of a thin section of this

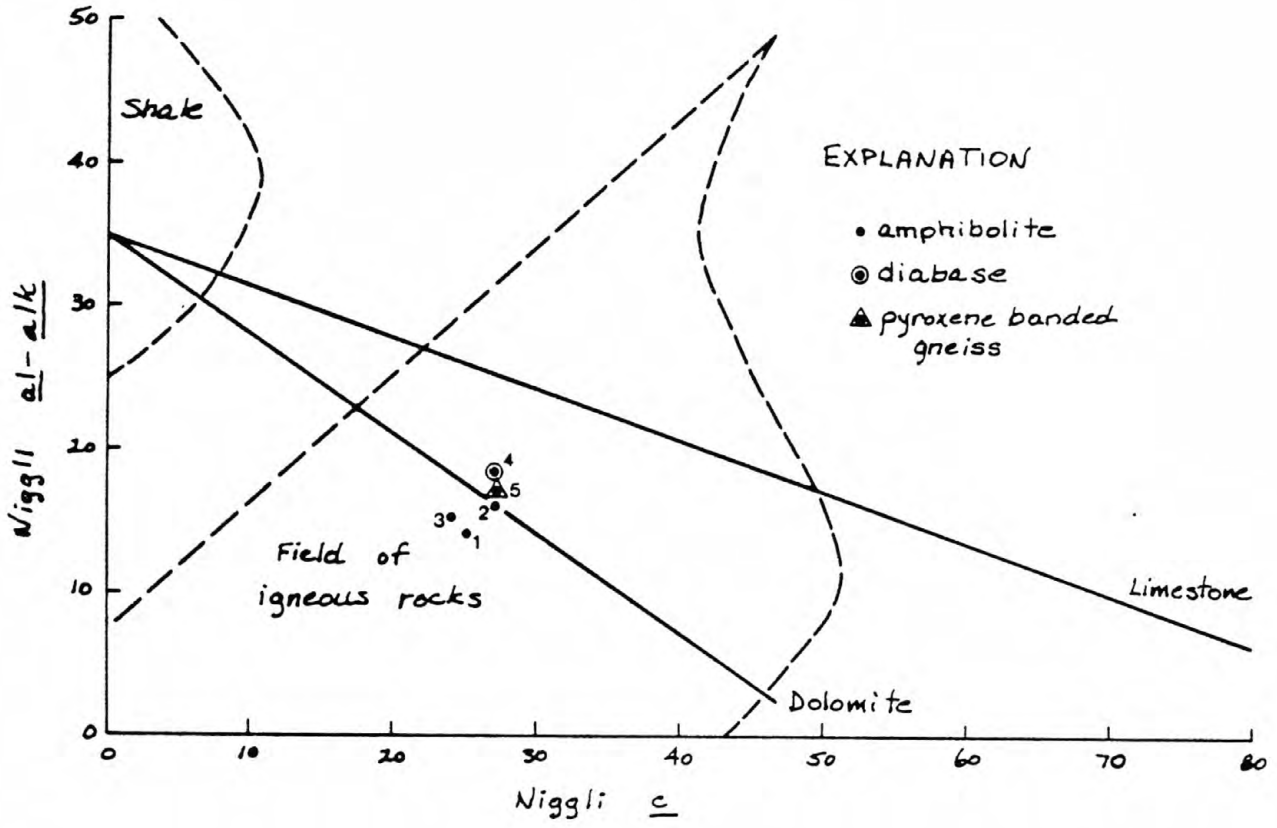

Figure 22.--Plot of Niggli c versus al-alk values for amphibolite, diabase, and pyroxene-banded gneiss from the Gold Basin-Lost Basin mining districts. Sample numbers same as table 7. Solid lines are potential trends of variation in mixtures of shale and carbonate (van de Kamp, 1969).

Table 10. Analyses of metachert, banded iron formation, metarhyolite, and calc-silicate marble in various Proterozoic X metamorphic units from the Gold Basin-Lost Basin mining districts

[Chemical analyses by rapid-rock methods; analysts P. L. D. Elmore and S. Botts. Methods used are those described in Shapiro and Brannock (1962), supplemented by atomic abospriton, and Shapiro (1967). Spectrographic analyses by Chris Heropoulos. Results are reported to the nearest number in the series 1., 0.7, 0.5, 0.3, 0.2, 0.15, 0.1, 0.07, etc., which represent approximate midpoints of interval data on a geometric scale. The precision of a reported value is approximately plus or minus one series interval at 68-percent confidence or two intervals at 95-percent confidence. Looked for but not found: Ag, As, Au, B, Bi, Cd, Mo, Pd, Pt, Sb, Sn, Te, U, W, Hf, In, Li, Re, Ta, Th, Tl, Pr, Sm, Eu; --, not detected]

	1	2	3	4	5
Field number ---	GM-216a	216	303	303a	290b
	Chemical analyses (weight percent)				
SiO_2 ----------	79.5	81.3	45.8	71.4	17.8
Al_2O_3 ----------	11.5	1.1	1.3	13.9	1.9
Fe_2O_3 ----------	1.	11.	42.4	.80	1.2
FeO ----------	1.5	4.8	4.6	3.6	3.3
MgO ----------	2.6	.50	--	2.6	2.3
CaO ----------	.2	.60	2.4	1.5	43.1
Na_2O ----------	.5	--	--	3.8	--
K_2O ----------	1.6	--	--	.90	--
H_2O^+ ----------	2.2	.58	1.1	1.8	.68
H_2O^- ----------	.05	.07	.09	.04	.11
TiO_2 ----------	.17	.08	.02	.18	.08
P_2O_5 ----------	--	.24	.43	.12	.02
MnO ----------	.06	.12	--	--	.12
CO_2 ----------	<.05	<.05	.42	<.05	30.4
Total --------	101.	100.	99.	101.	101.
	Semiquantitative spectrographic analyses (weight percent)				
Ba ----------	0.07	0.015	0.007	0.05	0.002
Co ----------	--	.0005	.0005	.0007	.0015
Cr ----------	.00015	.0002	.0005	.005	.007
Cu ----------	.0005	.01	.0007	.00015	.002
Ni ----------	.0002	.0007	.0005	.001	.002
Pb ----------	--	--	--	.001	--
Sc ----------	.001	--	--	.001	.0015
Sr ----------	.002	--	.003	.01	.02
V ----------	--	.0015	.0015	.005	.005
Y ----------	--	.001	.002	--	.0015
Zn ----------	--	.02	--	--	--
Zr ----------	.007	.001	--	.007	--
Ga ----------	.001	--	--	.0015	.0003
Yb ----------	--	.00015	.0002	--	.00015

1. Quartzite or argillaceous metachert, in migmatitic gneiss unit (Xmg) of figure 2; SE1/4 sec. 32, T. 29 N., R. 17 W.
2. Magnetite-bearing banded metachert, in migmatitic gneiss unit (Xmg) of figure 2; SE1/4 sec. 32, T. 29 N., R. 17 W.
3. Iron formation, in gneiss unit (Xgn) of figure 2; NW1/4 sec. 16, T. 29 N., R. 17 W.
4. Metarhyolite, in gneiss unit (Xgn) of figure 2; NW1/4 sec. 16, T. 29 N., R. 17 W.
5. Calc-silicate marble, in feldspathic gneiss unit (Xfg) of figure 2; SW1/4 sec. 17, T. 29 N., R. 17 W.

metachert shows that it contains a quartz-biotite-cordierite-plagioclase prograde assemblage that has been replaced very intensely during the retrograde regional metamorphic event. The retrograde assemblage includes here chlorite, white mica, albite, and rutile. These thin sequences of metachert grade locally into iron formation, which consists of alternating hematite- and magnetite-rich laminae and finely crystalline-quartz-rich laminae. Chemical analysis of a ferruginous sample which is intermediate between metachert and typical iron-formation shows a content of about 14 weight percent total iron as FeO (analysis 2, table 10). In addition, this particular sample contains 100 ppm (parts per million) copper and 200 ppm zinc. Quartz, magnetite, and hematite are the dominant minerals in the rock, and the iron oxide-rich laminae include a composite assemblage of clinopyroxene, amphibole, apatite, white mica, and abundant, paragenetically late needles of probable minnesotaite, an iron analogue of talc (see Deer, Howie, and Zussman, 1962c). These samples (analyses nos. 1, 2, table 9) are interbedded with a metaquartzite most likely derived from a pebbly, limey siltstone. The metaquartzite shows under the microscope 1.0-cm elongate clasts of monocrystalline to polycrystalline quartz set in an equigranular 0.08 to 1.0-mm-sized matrix of mostly quartz and epidote. The clots of quartz are sutured into the matrix tightly across several millimeters by intergrown quartz and epidote.

Well-developed, oxide facies banded iron formation occurs in at least five localities in the districts (locs. 303, 216, 664, 973, and 1086, table 11). All five of these occurrences of iron formation are associated closely with at least some metabasites, including amphibolite, sequences of amphibolitic gneiss, and mafic schist. The best developed iron formation probably crops out at locality 303 (table 11). Here, a 60- to 90-cm-thick sequence of laminated, hematitic but highly magnetic iron formation (fig. 23) strikes approximately N. 30° W. and dips about 50° southwest. It can be traced more than 200 m along strike primarily by using float. Further, the iron formation at locality 303 has been prospected by an approximately 20-m-deep vertical shaft. Near the shaft, the iron formation is very closely associated with laminated, fine-grained amphibolite. Approximately 100 m to the west-northwest, there is an exposed sequence of banded amphibolite and quartzofeldspathic gneiss that is very heavily stained by various iron oxides. However, these iron oxides are associated with highly manganiferous,

Table 11.--Notable occurrences of commodities in the Gold Basin-Lost Basin mining districts
[Modified from P. M. Blacet, unpub. data, 1967-1972; ?, presence of commodity queried where inferred]

Locality number (pl. 1)	Name	Approximate location (UTM 10,000-m grid, zone 11)	Commodities present	Comments
11	Golden Gate mine	NW1/4 sec. 32, T. 30 N., R. 17 W.	Au, Cu	Free gold occurs in yellowish- to red-stained quartz characterized by empty pyrite molds and cellular hematite vugs. Gold usually is in very intricate sheaves which are so fragile that they wave in the wind. Some rather solid gold pieces up to 1 mm in diameter are present also. Veins up to 1 m thick, but much of the veins consist of massive quartz containing little sulfide. Relatively abundant free gold on the dump so early miners must really have high graded the deposit. First workings probably date before 1900. Chalcopyrite, cuprite, malachite, and pyrite noted.
12	L.P.M. mine	NW1/4 sec. 4, T. 27 N., R. 18 W.	Cu, Au	Two shafts to approximately 15 m deep in pediment. Country rocks are very coarse grained, porphyritic monzogranite, including potassium feldspar phenocrysts up to 5 cm. Altered schist crops out in pit 60 m northwest of old headframe. Sparse secondary copper found. Low sulfide content and lack of coarse vein material suggests general alteration zone with many small quartzose seams. A zone of steeply north dipping to vertical quartz veins and veinlets have an average strike of N. 50° E. The veins are not persistent and the majority are stringers less than 2.5 cm, while a few reach 20 to 30 cm in length. No chalcopyrite, galena, fluorite, or carbonate was observed. A trace of gold was found in fine- to medium-grained quartz. Ore probably was hosted by silicified granite and schistose metamorphic rocks.
13	Red Norse mine	NE1/4 sec. 32, T. 28 N., R. 18 W.	Au, Cu, Pb, Mo	Vein 20 cm wide at the collar of 60° inclined shaft. Vein strikes N. 15° E., dips 60°E. Country rock is Proterozoic X porphyritic monzogranite. Free gold coarse and abundant in cellular vuggy quartz containing limonitic and hematitic cavity fills. Some secondary copper minerals and wulfenite.
14	Junction mine	SE1/4 sec. 29, T. 28 N., R. 18 W.	Au, Cu, Pb Mo	Quartz, galena, chalcopyrite (minor), pyrite (trace), and relatively abundant wulfenite in vein exposed in shallow open cut trending N. 30° E; vein strikes approximately N. 30-35° E., and dips 85° southeast. Some masses of partially oxidized pyrite show irregularly shaped blebs of free gold approximately 1 to 2 mm across. Exposed segment of the vein is approximately 1 m thick and it includes some septa of granitic rock from the surrounding Proterozoic X porphyritic monzogranite. Open cut is about 30 m southwest of two shallow shafts, each 15 to 30 m deep.
16	Cyclopic mine	SW1/4 sec. 30, T. 28 N., R. 18 W.	Au, Pb, Mo, Cu	Series of northwest open cuts and pits along Miocene detachment fault breccia which is exposed in place at several localities. Free gold in at least one hand sample picked up in southern half of series of cuts. Abundant angular fragments contain milky-white quartz with dark-reddish-gray matrix. Considerable cellular gossan, with wulfenite common. Old underground workings intersected in some of the open cuts. None accessible. Numerous prospects, pits, and trenches in the lower(?) gouge zone. Vein quartz is brecciated and widely scattered in the gouge as blocks 0.6 m long and approximately 0.3 m thick. Veins contain galena, pyrite, ferrocalcite, malachite (alteration of chalcopyrite(?)), wulfenite, gold, cerussite. Brilliant crimson mineral may be cuprite. Red, brown, and black Fe and Mn(?) oxides.

Table 11.--Continued

Locality number (pl. 1)	Name	Approximate location (UTM 10,000-m grid, zone 11)	Commodities present	Comments
17	Eldorado mine	SW1/4 sec. 21, T. 28 N., R. 18 W.	Cu, Pb, Mo, Au	The mineralized vein seems to average 1 m thick and dips east-southeast 25°-30° at west side of workings shallowing to nearly horizontal at the tunnel portals on the east side of the ridge. The workings generally dip 20° east-southeast parallel to the vein. The country rock is intensely sheared, cataclastic medium-grained Proterozoic X gneissic granodiorite. The mineralized vein(s) are occupying an intensely sheared zone that is of probable late Cretaceous-early Tertiary age. Although the vein quartz is fractured (locally intensely), it is not brecciated. Some veins crosscut highly foliated gneissic granodiorite, but generally they approximately parallel the schistosity. No red or other clay gouge and no indication of notable Tertiary movement. The main vein parallels also the pegmatite, and, inpart, the 2-m thickness of quartz probably reflects the quartz-core stage of the pegmatite. The quartz vein lies between a crumpled and kinkbanded schistose granodiorite and an overlying sill of leucogranite pegmatite. Abundant chrysocolla; moderate galena; but no chalcopyrite seen. Some wulfenite and cerrusite present also. In the irregular surface cut 10 m northwest of the opening at the northwest end of the underground stopes, altered biotite lamprophyre has consistent chilled margins against the mineralized vein quartz. This indicates the mafic dikes and sills are postmineralization. Intensely sericitized leucogranitic sills occur below the vein here, indicating a somewhat crosscutting relationship. Numerous veins 2 cm to 1 m thick are concentrated in an intensely sheared zone, which dips very gently, but is undulating overall.
19	Unnamed prospect	SE1/4 sec. 27, T. 28 N., R. 18 W.	Au, F	Fluorite-gold-pyrite-bearing episyenitic rocks, which cut fine- to medium-grained biotite monzogranite. Gold occurs in leached cavities in these episyenitic rocks (see text). In outcrop, the episyenitic rock occurs in four small pipelike masses, the largest of which measures about 8 m across (see fig. 51). Two shallow prospect pits have been dug on the pipes most likely because of the color anomaly resulting from the oxidation of pyrite.
24	Ford mine	SW1/4 sec. 33, T. 30 N., R. 17 W.	Au, Cu, Pb	Portal initially trends N. 10° W. then bends to N. 15° E. and extends 100 to 150 m intersecting raise and winze. Winze continues 10 m below level of main drift. Workings follow shear zone. Quartz vein up to 1.5 m thick, exposed in back, contains thin seams of chalcopyrite oxidizing to chalcocite, cuprite, malachite, and azurite; and a trace of galena Some fine gold seen in yellow-brown lacy quartzose gossan. Vein ends by interfingering with altered and sheared amphibolite.
25	Unnamed prospect	SE1/4 sec. 19, T. 28 N., R. 16 W.	W	Vertical shaft 30 ft deep in open cut made in garnet-epidote-quartz skarn comprising a small roof pendant or septum in Proterozoic X porphyritic monzogranite. Pendant is approximately 50 m long and trends N. 45-55° W.
26	Blue Bird mine	NE1/4 sec. 19, T. 29 N., R. 17 W.	Au	Horizontal adit 800 m along northwest-striking shear zone dipping 65° southwest. Damp clay gauge is contorted and locally contains some quartz veinlets which mushroom into quartz stringers making up to 0.5 m of the adit width.
138	Unnamed prospect	SE1/4 sec. 26, T. 28N., R. 17 W.	Mica	Two pegmatite dikes, both apparently claimed but unmined. The dikes are muscovite bearing with books up to 15 cm in diameter and 5 to 8 cm thick. One dike trends approximately N. 10° W., and is about 3 m wide. Small prospect pit at second dike.

Table 11.--Continued

Locality number (pl. 1)	Name	Approximate location (UTM 10,000-m grid, zone 11)	Commodities present	Comments
139	M. P. Mica mine	SE1/4 sec. 26, T. 28 N., R. 17 W.	Mica	A series of north-northwest-striking pegmatite lenses 3 to 5 m thick with well-defined bull quartz cores. Coarse muscovite is common, transparent in thin cleavage sheets, but inclusions of other minerals are common. The books are less than 10 to 15 cm across. This series of pegmatites possibly is continuous with a series of several muscovite-bearing pegmatites to the northwest. Proterozoic X leucocratic monzogranite makes up the country rock. The main mine workings are open cut.
205	Unnamed prospect	NE1/4 sec. 28, T. 30 N., R. 17 W.	Au?	Prospect pit just west of contact between Muddy Creek Formation and Proterozoic X gneiss. The pit exposes an alternating sequence of amphibolite and biotitic quartzite and (or) quartzofeldspathic gneiss. The rocks here also show abundant iron oxide-stained cubic molds after pyrite. No gold or secondary copper minerals observed. Locally, coarse-grained granitic dikes or sills are abundant in some of the schistose sequences.
213	Unnamed locality	SE1/4 sec. 29, T. 29N., R. 17 W.	Cr	Metaclinopyroxenite contains very sparse concentrations of chromite.
216	Valley View	NW1/4 sec. 32, T. 29 N., R. 17 W.	Fe	Banded jasper-magnetite beds associated with laminated or foliated quartzite. Foliation strikes N. 30° W. and dips 65 to 70° southwest. Quartzite includes vitreous white and micaceous pink types.
217	Malco mine	SE1/4 sec. 21, T. 28 N., R. 18 W.	Au	Inclined shaft plunging 45°-55° (30° below third main level) parallel to a prominent shear zone which strikes N. 45° E. Mineralized quartz veins are parallel to the shear zone. There are three major levels, about evenly spaced, from which irregular raises follow ore shoots. Overall workings are close to a contact between Proterozoic X gneissic granodiorite and gneiss.
259	Unnamed prospect	SE1/4 sec. 20, T. 29 N., R. 17 W.	Au?	Prospect pit exposing complexly intermixed quartz-pyrite rock and apparently genetically related and intermixed quartz-calcite-pyrite and feldspar-calcite-quartz-pyrite rock very similar to the episyenitic rocks containing visible gold in the East White Hills (loc. 19, above). Although oxidized, pyrite-rich rocks were examined carefully. No free gold was seen.
274	Unnamed prospects	NE1/4 sec. 20, T. 29 N., R. 17 W.	Au?	In one of the prospect pits, a pyrite-bearing aplitic dike strikes east-northeast and dips 40°-45° south. A large amount of weathered pyrite is associated with the dike. In addition, nearby there is a coarse-grained magnetite-rich pegmatite which may have a genetic connection with the pyrite-bearing dike. The dike is about 0.5 m wide and has rather sharp contacts with altered and silicified feldspathic gneiss.
275	Unnamed prospect	SE1/4 sec. 20, T. 29 N., R. 17 W.	Au	Prospect contained a very altered feldspar-quartz-pyrite vein several centimeters thick, judging from rock samples on the upper "ore" pile. Generally similar to rocks at location 274. The aplitic feldspar rock usually bounds the quartz vein on north sides, and the quartz-rich portions contain most of the sulfide. Gold was seen in the boxwork. No indications of copper were seen.
276	Unnamed adit and prospect pit	NW1/4 sec. 20, T. 29 N., R. 17 W.	Au?	Small adit driven straight in for about 9 m along a fault zone varying about 0.6 to 1.2 m wide. Slickensides are well developed with the wallrock altered to an ochre-orange color. The slickensides plunge westward at about 50° in the fault zone, which strikes N. 50° W., and dips about 60° west. An irregular vein zone of crushed- and carbonate-cemented (ankeritic) white milky quartz, ranging from 0 to 23 cm thick can be seen locally at the back of the adit. A small prospect also is located along the fault about 60 m to the southeast. No copper staining, sulfides, or pyrite-type boxworks present. A newspaper found inside suggests work was done in the teens or 1920's.

Table 11.--Continued

Locality number (pl. 1)	Name	Approximate location (UTM 10,000-m grid, zone 11)	Commodities present	Comments
277	Unnamed adit	NW1/4 sec. 20, T. 29 N., R. 17 W.	Au?	This adit is similar to location number 276. The adit is driven at about N. 50° W. along the same fault as in location number 276 for about 10 to 12 m. The fault dips about 60°-65° southwest, and it contains oblique mullions and slickensides plunging about 55°W. The fault zone, which is about 0.3 m to 0.9 m wide, is composed of highly sheared gouge and brecciated lenses of white milky quartz. The quartz vein observed at location 276 is not continuous through this adit. An orange-ochre color from weathering ankeritic calcite was also observed at this locality. This adit also intersects a raise to the surface about 9 m from the portal. No sulfides or copper staining was observed.
279	Unnamed prospect	NW1/4 sec. 20, T. 29 N., R. 17 W.	F, Au?	The prospect pits are along feldspathic veins which contain quartz, potassium feldspar, carbonate, and pyrite. The veins are about 0.6 m thick and strike irregularly N. 55° W. roughly paralleling the vertical layering in the surrounding banded gneiss. On the dump there are samples of fluorite and topaz. Gold was not observed but may be present in the "vuggy" (pyrite molds) quartz at the pits. There is also abundant ankeritic carbonate commonly containing large pyrite cubes to about 1.3 cm. The pyrite is generally altered. No copper stain or galena was observed.
284	Unnamed drywasher site	NW1/4 sec. 19, T. 29 N., R. 17 W.	Au	The sample was taken from above the caliche cemented fanglomerate just west of mine road leading to the adit and shaft at locality 285. A few fine-sand-size frosted colors were found. From their condition, they are probably some distance from their source.
285	No name open cut and adit	SW1/4 sec. 18, T. 29 N., R. 17 W.	Au?	The first 6 m along the adit consists of Quarternary fanglomerate which has been faulted against amphibolitic, banded gneisses. The fault strikes north-south and dips 60° west. The brecciated amphibolite and banded gneiss generally have their layering striking N. 15° E. and dipping 50°W. Well-developed striations trend N. 85° W. and plunge 43°W. The fanglomerate, gravel, and breccia generally are poorly cemented except in certain spots where they have been case hardened by caliche. About 50 m from the portal, the adit apparently was filled subsequently with waste rock from a shaft. No vein material seen in place but the dump contains vein material similar to that of the Bluebird vein.
286	Unnamed drywasher site	SW1/4 sec. 18, T. 29 N., R. 17 W.	Au	Drywasher concentrate from irregular surface consisting of amphibolite bedrock about 6 m upstream from highest Quarternary fanglomerate and fault. One small color was observed with lots of garnet.
291	Unnamed prospects	SW1/4 sec. 17, T. 29 N., R. 17 W.	Cu, Au?	This locality consists of two prospect pits approximately 3 m apart along a shear zone striking N. 30° E. and dipping 65°E. and about 1 to 1.5 m wide. Although the fault may be relatively important, and somewhat like the one at the Bluebird mine, it could not be traced because of talus- and debris-covered slopes. In the pits, the veins consist of pyrite and chalcopyrite together with milky quartz and ferruginous carbonate. Generally the veins are thin stringers, less than 3 cm wide, although one pod reached as much as 25 cm across and had a well-developed sericitic envelope.

Table 11.--Continued

Locality number (pl. 1)	Name	Approximate location (UTM 10,000-m grid, zone 11)	Commodities present	Comments
297	Unnamed prospect	NE1/4 sec. 20, T. 29 N., R. 17 W.	Cu	An approximately 8 m thick syenitic micropegmatite contains abundant quartz associated with red-brown, presumably iron rich carbonate and pyrite. This locality is approximately 30 m N. 35° E. of the two prospects known as the Jumbo (loc. no. 913, this table). The feldspar in the micropegmatite is microcline, and only traces of secondary copper minerals were noted to stain the rocks.
300	Unnamed adit	SE1/4 sec. 17, T. 29 N. R. 17 W.	Au?	An approximately 35 m long adit initially driven N. 40° E. on a black quartz-rich lens. Exposed in the workings are a series of three northeast-striking quartz veins or stringers that range up to 13 cm in width. Associated with these veins are abundant yellow or reddish-brown carbonate, and sparse amounts of weathered pyrite. Country rock consists of strongly lineated feldspathic gneiss.
303	Unnamed shaft	NE1/4 sec. 17, T. 29 N., R. 17 W.	Fe	A N. 30° W.-striking oxide facies, banded iron formation. An approximately 20 m deep vertical shaft has been sunk on the iron formation; the shaft probably follows a minor fault zone. Another shaft, approximately 100 m N. 70° W. of this locality, has been put down on dark, manganiferous gossanlike stringers in brecciated and highly altered granitoid pegmatite. See figure 23 (this report) for a photomicrograph of quartz-iron oxide relations in the banded iron formation.
305	Unnamed shaft	NE1/4 sec. 17, T. 29 N., R. 17 W.	Pb, Cu, Au	Shaft along a N. 35° W.-striking, 55°-northeast-dipping approximately 0.6 m wide quartz-carbonate vein. Downward, the vein feathers into a series of veinlets measuring from 2 to 8 cm wide. Yellow-brown carbonate fills the center of the veins, but much of the carbonate is intergrown with quartz. The primary minerals observed in the veins include galena, chalcopyrite, pyrite, and free gold. Secondary minerals include chrysocolla and malachite.
307	Ideas Lode no. 30	NE1/4 sec. 17, T. 29 N., R. 17 W.	Au?	Workings along nearly flat lying shear zone which includes irregularly distributed quartz-yellow-brown carbonate veins more or less parallel to the shallow-dipping foliation. Some evidence for the flooding of nearby rock by yellow-brown carbonate.
308	Unnamed prospect	NE1/4 sec. 17, T. 29 N., R. 17 W.	Au?	Episyenitic aplite exposed in the prospect pit. Disseminated pyrite, but relatively little carbonate and no fluorite were seen. The episyenitic aplite crops out in an approximately 9 m^2 area. The upper parts of the gulch in this general area include many small, irregular dikes of similar episyenitic aplite.
310	Vanadinite mine (Van-Wulf)	NE1/4 sec 17, T. 29 N., R. 17 W.	V, Pb, Mo, Cu	The adit is about 15 m long, driven along a fault zone striking S. 15° E. and dipping about 70° northeast. Slickensides have a variable orientation but generally they plunge moderately (50°-60°) to the north. Vanadinite and wulfenite are especially abundant in brecciated vein material and in adjacent wallrock just inside the portal. Rocks across the open cut show at least 3 m of offset. At east end of open cut is an 8-cm-thick quartz-carbonate vein, containing sporadically distributed interstitial chlorite. Minerals observed in the vein include galena, chrysocolla, wulfenite, vanadinite, red-brown carbonate, quartz, mottramite(?), chlorite, minor greenish late clear calcite, and sericite. Little or no altered pyrite, no Au seen. Minor seams of episyenitic aplite were observed also.

Table 11.--Continued

Locality number (pl. 1)	Name	Approximate location (UTM 10,000-m grid, zone 11)	Commodities present	Comments
311	Unnamed adit	SE1/4 sec. 32, T. 30 N., R. 17 W.	Pb, Au, Cu	A lower adit follows a well-defined fault zone 15cm thick striking N. 80° E; and dipping 45°-50° south. Galena is rather abundant in quartz-carbonate gangue. Upper workings consist mostly of dump material derived by strippng overburden from vein lying along a N. 75° E.; 45°-50° south-dipping fault. Vein material ranges from 0 to 30 cm thick. No vein material seen in lower workings, which follows the fault, and the quartz+minor carbonate, vein occupied a steeply plunging mullionlike opening along the fault which had no lateral extent. Some Au, but minor chrysocolla, a little unoxidized pyrite, and galena. Quartz is the major gangue together with yellow-brown carbonate. Wallrock alteration appears to be mostly introduction of carbonate. One speck of gold found in the samples.
316	Unnamed drywasher site	NW1/4 sec. 23, T. 28 N., R. 18 W.	Au	From approximately 12 hoppers processed through the drywasher, only a few colors were obtained.
319	Unnamed drywasher site	NW1/4 sec. 27, T. 28 N., R. 18 W.	Au	Only one color obtained from gravelly, reddish soil which overlies hard caliche-cemented false bedrock in the Quarternary fanglomerate.
324	Unnamed drywasher site	NE1/4 sec. 24, T. 29 N., R. 18 W.	Au	Moderate amount of fine gold.
325	Unnamed drywasher site	SW1/4 sec. 7, T. 29 N., R. 17 W.	Au	Moderate amount of gold.
327	Golden Mile mine	NW1/4 sec. 8, T. 29 N., R. 17 W.	Pb, Cu, Au?	One- to two-m-thick prominent quartz vein exposed in face west of road approximately 20 m northwest of small shack; vein strikes N. 70° W. and dips 20°-25° southwest. It is offset in a reverse sense approxiately 1 m by an intensely clay-altered shear zone striking east-west and dipping 40°N. Fe-bearing calcite occurs in coarsely crystalline irregular masses which are markedly tabular and form lenses striking N. 20° W.; and dipping 30° southwest. These lenticular and irregularly shaped calcite pods definitely are oriented obliquely to the plane of the vein, and may represent replacement of earlier quartz along opened gash fractures. The bulk of this carbonate occurs along the central zone of the vein, but it is sporadically distributed throughout the length of examined vein. A poorly developed alteration zone in the vein's walls seems to include albite and pyrite+galena and a little chalcopyrite. A second oblique slip fault offsets the vein 1 m west of the incline. Slickensides plunge N. 65° E. at 25°. Crystals of feldspar (albite?), quartz, and calcite commonly reach 10 to 15 cm across in optically continuous irregular, intergrown masses. Galena can be seen to vein or crosscut calcite, feldspar, and quartz--probably the galena, pyrite, and trace of chalcopyrite are somewhat later than the coarse crystalline material although all are probably related to transition pegmatite-vein processes. The vein exposed 15 m south of the portal is about 1 m thick and rather clearly the extension of the vein exposed in the small inclined shaft. Numerous east-northeast or easterly faults offset the vein, which strikes N. 70° W., 25° southwest. No stopes in the adit. A trace of weathered pyrite was observed along the footwall in the adit.
329	Unnamed prospect	NW1/4 sec. 8, T. 29 N., R. 17 W.	Au?	The prospect exposes approximately 2 m thick pegmatite containing well-defined crudely tabular masses of fine-grained green sericite in potassium feldspar in its 15-cm-wide alteration wall zones. A specimen found on the dump of the small cut shows a remnant of a white mica book, with cleavage faces 1 cm across. Pegmatite strikes N. 40° E., and dips 80° to 85° southeast. No sulfides except rare pyrite pseudomorphs near the walls.

Table 11.--Continued

Locality number (pl. 1)	Name	Approximate location (UTM 10,000-m grid, zone 11)	Commodities present	Comments
330	Unnamed drywasher site	SW1/4 sec. 31, T. 30 N., R. 17 W. (location uncertain)	Au	Gold up to matchhead size especially in upper reaches of small gulch.
341	Unnamed prospect	SE1/4 sec. 7, T. 29 N., R. 17 W.	Au?	A prospect cut poorly exposing small quartz-carbonate-feldspar-sulfide vein of the Golden Mile type. Vein strikes north-south, and is vertical. Maximum width about 0.6 m.
356	Glow in the Dark no. 8	SW1/4 sec. 8, T. 29 N., R. 17 W.	Pb, Cu, Au?	Prospects along wash about 0.8 km southeast of Golden Mile cabins. Open cut on south side exposes for about 8 m 15- to 25-cm-wide quartz vein striking N. 15°-20° W dipping 50° northeast in a shear zone of approximately the same attitude. Maximum depth of vein exposed in cut is about 5 m. The shear zone separates vertically dipping interlayered quartzofeldspathic gneiss from amphibolite to the east. The vein pinches and swells averaging 25 cm to 0.3 m thick. Galena and chalcopyrite appear disseminated in knots throughout quartz; sparse carbonate. No Au seen, but a trace has been reported. Another nearby prospect is on coarse magnetite-bearing highly fractured pegmatite containing galena and chalcopyrite (some altered to malachite). The sulfides in this pegmatite are scattered widely in white quartz as vug fillings. Somewhat anomalous radioactivity, approximately three times background.
372	Miss Texas no. 2	NE1/4 sec 17, T. 29 N., R. 17 W.	Au?	Pyritized zone now limonitic striking N. 60° W. and parallel to foliation in the surrounding gneiss. Several quartz veins cut this 10- to 15-m-wide altered zone which can be followed toward the southeast for at least 0.3 km. Location of zone about 100 m S. 25° E. from stone monument of the Miss Texas no. 2.
374	Bluebird no. 17-16	NW1/4 17, T. 29 N., R. 17 W.	Pb	Two veinlets generally 2 to 8 cm thick but locally as much as 15 cm thick, striking nearly east and dipping steeply south. Abundant galena, but sparse pyrite noted. Veins cut amphibolite and gneiss. Broad open fold in amphibolite, plunging approximately 35° northwest just north of prospect. Some pyrite and altered feldspar in border alteration zone, which measures about 2 to 8 cm thick.
375	Unnamed prospect	SE1/4 sec. 7, T. 29 N., R. 17 W.	Au?	A 10-m shaft along the road 300m south-southwest of Golden Mile cabins. Barren-looking veins, little carbonate, pyrite, and feldspar. No galena or copper minerals noted. The vein is about 0.6 m thick.
389	Unnamed prospects	NE1/4 sec. 6, T. 29 N., R. 17 W.	Au?	A group of prospects near the west base of Lost Basin Range, approximately 1.5 km north-northwest of the Golden Mile mine. Intensely altered mylonitic coarse-grained granite or alaskite dike striking N. 20° E dipping 55°-60° W. parallels the adjacent well-layered quartzofeldspathic gneiss which contains abundant thin, well-defined amphibolite layers. Abundant hematite with some limonite. Pyrite molds are abundant in hematitic masses along shear zone. An inclined shaft south of the wash is 10 m deep. A gneissoid very coarse grained biotite granite dike forms the footwall. There is parallel layering in quartzofeldspathic gneiss which forms the hanging wall.
405	Twin yucca gulch	SE1/4 sec. 9, T. 29 N., R. 18 W.	Au	North of Salt Springs Wash road. This general area shows evidence of old placering possibly in the 1930's and much more recent scraping using a small bulldozer. Possibly part of the early Summit Mining Company work. Good placer gold up to 2 mm obtained using a drywasher. The gold is not well concentrated on bedrock but instead is distributed throughout 20 to 35 cm of dirt above lowermost Proterozoic outcrop. Proterozoic rocks are quartz-mica schist and gneiss.

Table 11.--Continued

Locality number (pl. 1)	Name	Approximate location (UTM 10,000-m grid, zone 11)	Commodities present	Comments
409	Unnamed drywasher site	NE1/4 sec. 22, T. 30 N., R. 17 W.	Au	Some fine placer gold in heavily dug gulch. High percentage of granitoid clasts in the general area of this locality is distinctly out of proportion with the amount of granitoid rocks exposed in the Lost Basin range.
436	Unnamed prospect	NW1/4 sec. 32, T. 30 N., R. 17 W.	Cu, Au	Prospect adit about 150 m southwest of lower dump of the Golden Gate mine. The adit essentially follows a well-developed, vertical, N. 50° E. striking fault. Prominent cross faults include an east-west fault dipping 5°S. A little copper staining occurs on brecciated blocks of quartz-carbonate-minor chalcopyrite. Considerable sericitization, carbonatization of the country rock. No vein material observed. A short adit directly up the ridge to the south exposes a prominent fault striking north-south to N. 10° E. This fault occurs between the brecciated footwall of an east-dipping quartz-carbonate vein which is up to 0.6 m thick. The faulting postdates the quartz-carbonate vein whose footwall it follows. There is abundant sericitization and carbonate flooding of the quartzofeldspathic gneiss within a few meters of the vein. The brecciated vein material locally looks like that at the Cyclopic mine. A shaft at the top of the ridge is vertical and includes abundant broken-up vein quartz. Some free gold noted.
442	Unnamed prospect	NW1/4 sec. 32, T. 30 N., R. 17 W.	Pb	Small veinlets, approximately 5 to 20 cm wide, cut medium-grained quartzofeldspathic gneiss and minor amphibolite. Veins include minor galena, pyrite, carbonate, and chlorite. In addition, these veins locally develop a comb structure.
443	Unnamed prospect	NW1/4 sec. 32, T. 30 N., R. 17 W.	Cu, Au?	A small prospect pit on ridge crest at bend in ridge. A trace of copper stain occurs on an approximately 10 cm thick vein including quartz, carbonate, some chlorite, pyrite, and possibly some gold.
444	Unnamed prospect	SW1/4 sec. 29, T. 30 N., R. 17 W.	Au?	A small prospect pit along major 10-m-wide range-front fault between iron-oxide stained quartzofeldspathic gneiss and interlayered amphibolite and caliche-cemented fanglomerate or talus. Clearly quartz-carbonate vein material is broken up in the zone suggesting the fault zone may have followed locally an already emplaced vein system. The fault zone also shows evidence of having originally contained a lot of highly sericitized, chloritized, and carbonate-altered gneissic fragments. No sulfides or Au seen; little weathered pyrite noted.
445	Clipper	SE1/4 sec. 29, T. 30 N., R. 17 W.	Au?	Joins north end line of claims at Troy prospect and lies approximately 1 km southwest from the Scanlon mine. The quartz mass at this locality is bounded by two shear zones 15 cm thick dipping east approximately 75°. The shearing has been localized along the steep east-dipping northeast limb of a northwest-plunging fold. Gneissic rock inclusions are sericitized and altered by carbonate. Little indication of sulfide mineralization.

Table 11.--Continued

Locality number (pl. 1)	Name	Approximate location (UTM 10,000-m grid, zone 11)	Commodities present	Comments
446	Troy	SE1/4 sec. 29, T. 30 N., R. 17 W.	Cu, Au	Lower adit contains a splendid example of a quartz-carbonate vein disrupted and sheared out by later faulting. Lower adit driven almost due south beneath quartz vein outcrop; adit length is about 30 m, and the vein is sheared off 15 m from portal. Footwall bounded by fault, as is hanging wall. This occurrence is a brecciated quartz vein sliver in a low-angle oblique slip fault, similar to that in the vein just west of the Golden Gate. Total vein exposed in the lower adit is about 10 m long, and it has a maximum thickness of about 1 m. No sulfides seen in lower adit. In main adit or Troy vein, small amount of Cu staining (malachite) and some coarse anhedral pyrite oxidizing to cellular drusy boxworks. A few small flecks of gold seen in cellular drusy "high grade." The upper prospect pit shows four vein slivers in a nearly vertical shear zone. Overall strike of the vein is N. 5°-10° E; dip 65°-85° E. A little orange-brown carbonate occurs in the mostly quartz vein.
453	Scanlon mine	SW1/4 sec. 28, T. 30 N., R. 17 W.	Au, Pb, Cu, Mo	Very little stoping. Probably no production. Prospect probably was worked in the 1930's. Veins show sheared margins containing gouge and the veins contain milky-white quartz that is brecciated. Country rock consists complexly and tightly folded quartz-feldspar gneiss. Wulfenite and anglesite noted.
456	Unnamed prospects	SE1/4 sec. 29, T. 30 N., R. 17 W.	Au?, Cu, Pb	Vein cutting amphibolite consists of milky quartz with irregularly distributed orange-brown carbonate with some granular chlorite in distinct irregular masses. Approximately 30 to 50 m west, other prospects show flat-lying similar veins approximately 0.3 m wide, containing traces of galena and secondary copper minerals.
457	Eagle Nest	SW1/4 sec. 28, T. 30 N., R. 17 W.	Au, Cu, Pb, Mo	Workings along the same vein system as exposed at the Scanlon mine (loc. no. 453). At adit number 1, complexly layered folded quartzofeldspathic gneiss is exposed directly north of portal. In adit, quartz-cored pegmatite containing microcline crystals up to 30 cm across in its outer zones crops out. No sulfides seen in rocks on the dump, but malachite occurs as minute crystals in some boxworks showing cellular structures. No stopes in adit. Adit number 2 is a short straight N. 15° E.-striking adit. Fine gold seen at several points along vein outcrop. Here, the vein apparently cuts the pegmatite as does the fault zone. Average strike of Scanlon fault-vein in the workings is north-south to N. 3° E dipping 85°E. Some malachite, galena, and wulfenite noted in samples on dump.
464	Unnamed adit	NE1/4 sec. 32, T. 30 N., R. 17 W.	Au, Cu	Approximately 15 m long adit driven due south. A little highly cellular boxworks on dump is presume to be ore from this vein system. Gold seen in several samples. Some specular hematite may reflect on alteration of carbonate or pyrite. Another nearby short adit driven along a steep west-dipping shear zone shows sparse amounts of chalcopyrite associated with iron-bearing calcite.
466	Warren Lode no. 5 (Cumberland)	NW1/4 sec. 33, T. 30 N., R. 17 W.	Pb, Cu	Abundant galena, wulfenite, malachite in N. 15° W.-striking vein.
470	Warren Lode no. 10	SW1/4 sec. 28, T. 30 N., R. 17 W.	Pb	Poorly exposed 1-m-thick feldspar-rich dikes (albitite?) containing sparse amounts of quartz, iron-bearing carbonate, and pyrite. Quartzofeldspathic gneiss makes up the wallrock of this dike and within about 5 to 15 m of it, the wallrock shows veining by quartz and some evidence of propylitic alteration. Numerous quartz veinlet are in the range 2.5 to 10 cm wide and locally the show abundant amounts of galena, especially concentrated in the central portions.

Table 11.--Continued

Locality number (pl. 1)	Name	Approximate location (UTM 10,000-m grid, zone 11)	Commodities present	Comments
480	"BaBa" prospect ("Tungstake" on one 1955 claim notice)	SW1/4 sec. 4, T. 29 N., R. 18 W.	W?	Small 1-m-deep pit on ridge and main 6-m-across open trench to the northeast. The prospect is in layered amphibolite and biotite schist. No scheelite noted. Some tourmaline seen in quartz-feldspar-biotite pegmatitic gneiss stringer. Some quartz-carbonage-pyrite-albite(?) veinlets up to 8 cm thick. Euhedral tablets of albite(?) at extreme margins of vein. Main prospect is on southeast side of ridge 30 m northeast of small pit. The main prospect consists of an opencut 6 m long. Skarnlike amphibolite associated with quartz pods or stringers up to 18 cm thick is exposed here. Pegmatoid gneiss also occurs in crosscutting dike up to 8 cm thick which strikes N. 30° W. and dips 25° SW. Prospect across gulch to east-southeast contains more skarnlike calc-silicate rock apparently owing to the silicification of limy amphibolite or limy quartzofeldspathic gneiss. Well-layerd amphibolitic gneiss strikes north-northwest dipping 30°-35° SW.
482	Unnamed prospect	NW1/4 sec. 33, T. 30 N., R. 17 W.	Au, Cu, Pb, Mo	An exposed feldspathic vein here is 45 to 60 cm thick and shows a well-developed quartz core. The vein strikes N. 55° W and has an almost vertical dip. Stringers of quartz-carbonate-pyrite-chalcopyrite cut the south end of the vein. They are up to 5 cm thick and strike north-south dipping 70°-75° E. The northeast wall of the vein is a 5-cm-thick crumbly fault gouge; whereas the southwest wall of the vein is healed to country rock. A second vein of quartz-carbonate strikes N. 10°-15° E approximately one-half of the way to the top of the hill from this locality and approximately 60 m S. 10° E. of the termination of the first vein described above. The second vein is 10 to 20 cm thick, locally brecciated, and shows no apparent copper staining or sulfides. No prospects on this second vein. Rock fragments included in the second vein are intensely sericitized. There are several pegmatites of the quartz cored and related types which strike N. 50°-60° W. and are also cut by quartz-carbonate veins. A partial list of minerals identified in the veins include: galena, wulfenite, malachite, chalcoyrite, gold (fine, fernlike in quartz and oxidized chalcopyrite), ferruginous carbonate, tenorite-cuprite(?), chrysocolla, opal, specular hematite, goethite.
483	Unnamed drywasher site	SE1/4 sec. 30, T. 30 N., R. 17 W.	Au	One moderate-sized color obtained from approximately 10 to 12 hoppers of gravel taken from two localities about 8 m apart.
498	Climax mine	SE1/4 sec. 33, T. 30 N., R. 17 W.	Pb	Vein strikes N. 18° E., dips WNW. 80°, and swells to at least 2 m thick about 15 m south of the headframe. Massive milky quartz is present with some brecciated and recemented zones. A little carbonate, galena, pyrite molds, and honeycombed quartz showing cubic molds and elongate molds were noted. The host rocks are a sequence of granitoid gneiss within the mapped paragneiss unit.
505	Unnamed drywasher site	NE1/4 sec. 9, T. 29 N., R. 17 W.	Au	Sample of relatively small volume, approximately three hoppers, of red soil. Sample was not obtained from a good caliche horizon. One pinhead-sized color obtained.
509	Unnamed prospect	SE1/4 sec. 32, T. 30 N., R. 17 W.	Au, Cu	Prospect pit 3 m deep on lenticular, discontinuous quartz-carbonate-chalcopyrite-pyrite-gold vein. Lenticular masses of chalcopyrite and pyrite are largely altered to limonitic boxwork. No galena was noted. Gneissic inclusions are sericitized. Gold occurs along boundaries of chalcopyrite boxwork and quartz.

Table 11.--Continued

Locality number (pl. 1)	Name	Approximate location (UTM 10,000-m grid, zone 11)	Commodities present	Comments
513	Unnamed prospect	SE1/4 sec. 32, T. 30 N., R. 17 W.	Au	Prospect in 3-cm-thick vein, showing mullionlike striae plunging 20° north-northeast along footwall. Gold seen as fine dendritic foil in quartz. Webbed boxwork similar to that at the Golden Gate. Massive, granular chlorite and sericitized quartzofeldspathic gneiss inclusions occur in the vein. Some are lined by quartz crystals and calcite. Pyrite is rather abundant but no chalcopyrite, galena, or copper stain observed. A second nearby prospect contains a 45-60-cm-thick vein including intense sericitization of the wallrock. Small crosscut adit. Massive anhedral pyrite is the only sulfide observed. There was no galena, chalcopyrite, or malachite seen at any of these largely en echelon quartz veins. Numerous small quartz-carbonate stringers cut quartzofeldspathic host.
546	Unnamed prospect	SE1/4 sec. 35, T. 30 N., R. 18 W.	Cu	Small prospect pit in chalcopyrite-quartz bodies in coarse-grained granite pegmatite. The chalcopyrite occurs locally in the feldspathic portion of the pegmatite, and mineralization is probably cogenetic with the late hydrothermal stages of the pegmatite.
552	Unnamed prospect	(In Iceberg Canyon quadrangle) UTM: 752,500 m E., 3,987,670 m N.	Mn	Breccia cemented with manganese oxide and calcite. Maximum amount of vein exposed is 20 cm. The vein cuts Proterozoic gneiss. Prospect is approximately 3 m long.
604	Gold Barr	NE1/4 sec. 16, T. 29 N., R. 18 W.	Au, Pb, Cu	Gold-bearing quartz stringers up to about 15 cm thick, poorly exposed in prospect pit, where they are seen to occupy a shear zone in biotite gneiss. Quartz, galena, iron-bearing calcite, albite, chlorite, pyrite pseudomorphs; trace Cu stain. Free gold associated with pyrite and red chalcopyrite boxwork observed in three samples.
608	Unnamed drywasher site	UTM: 749,800 m E., 3,978,540 m N.	Au	Sample collected from alluvial gravels along a present-day arroyo bottom. Collected to a depth of about 20 cm, and approximately 1 cu ft of material put through drywasher. Few colors were obtained.
609	Unnamed site	UTM: 749,800 m E., 3,978,540 m N.	Pb, Cu, Au?	Thin east-west striking quartz vein containing fine-grained albite along its walls, orange-brown-weathering iron-bearing calcite in knots, a moderate amount of pyrite, and some galena and secondary copper minerals. Not prospected.
611	Mead Tungsten	UTM: 749,770 m E., 3,979,070 m N.	W	Abundant scheelite in crystalline masses up to about 3 cm across. Scheelite occurs in narrow west-dipping skarn zones, developed as small pods less than 0.3 m thick adjacent to a 10-cm-thick granitic pegmatite stringer.

Table 11.--Continued

Locality number (pl. 1)	Name	Approximate location (UTM 10,000-m grid, zone 11)	Commodities present	Comments
623	Marihauna	NE1/4 sec. 16, T. 29 N., R. 18 W.	Au, Cu, Pb	Trace of gold associated with oxidized blebs of chalcopyrite in quartz stringers. Stringers cut a fine-grained porphyritic granite dike exposed at southeast end of small open cut. Microcline(?)-bearing alteration assemblages are apparently similar to that noted previously at locality 19 (this table), but no fluorite was found here. Ferrocalcite and galena in quartz occur in surficial rubble. Over the hill from the highest cut, galena found in place as sparsely scattered blebs and irregular grains up to 0.6 cm in diameter together with minor chalcopyrite. An open trench exposes vein apparently striking N. 10° W. that cuts gently east dipping gneiss. Approximately 9 m west of north end of northern prospect cut, a quartz vein is at least 12 to 15 cm thick, and contains abundant galena and chalcopyrite. Narrow alteration zones and quartz seams cut a granite dike here striking most likely N. 10° W. and dipping 55° E.
626	Unnamed drywasher site	SW1/4 sec. 21, T. 29 N., R. 18 W.	Au	There is a moderate amount of surface scraping by bulldozer in this general area. Bedrock in this placer area consists of weathered and caliche-encrusted gently dipping gneiss. The gold and some rounded pebbles of magnetite appear to be coming off the low ridge to the northwest. Swept bedrock at head of the gulch at this site yielded not one single color, suggesting that the placer gold that was found is not local.
627	Unnamed drywasher site	SW1/4 sec. 21, T. 29 N., R. 18 W.	Au	Rather fair showing of placer gold in concentrates from drywasher. Some gold is approximately 1 mm across in longest dimension.
629	Unnamed drywasher site	SW1/4 sec. 20, T. 29 N., R. 18 W.	Au	Gold concentrated in coarse quartz gravel at scoured and winnowed head of delta in previously worked placer gravels.
635	Unnamed drywasher site	UTM: 749,230 m E., 3,977,500 m N.	Au	Only a trace of gold, one color, obtained in concentrate from gravels excavated from deep cracks in outcrops along main gulch. Concentrate included abundant lavender zircon and some fresh garnet.
636	Unnamed prospects	UTM: 750,310 m E., 3,977,500 m N.	Pb, Cu	Two veins, approximately 6 m apart, follow shear zones developed along the schistosity in the surrounding gneiss. Quartz is the predominant mineral in the veins and only trace amounts of secondary copper minerals and galena were noted in one of the veins. In an incline, one of the veins pinches and swells along the shear zone. Adjacent to the veins where they cut amphibolite, there is a marked development of chlorite and carbonate for about 1 m.
637	Red Rattler or Richman	UTM: 749,150 m E., 3,977,170 m N.	Au	Vein is approximately 0 to 0.6 m thick, and it has been explored by a shaft approximately 15 m deep. Gold occurs in fine honeycomb and pyrite(?) boxwork. Minerals in the vein also include quartz, ferrocalcite, and chlorite. Chlorite most likely reflects altered fragments of country rock picked up by the vein.
639	Unnamed adit	UTM: 748,950 m E., 3,977,060 m N.	Cu	Abundant staining by secondary copper minerals occurs at this adit driven approximately N. 20° E. Another prospect approximately 20 m north-northeast of this locality shows gneissic biotite granite cut by a 0.6-m-wide vein which is in turn cut off by a N. 10° E.- striking fault.
640	Unnamed prospect	UTM: 748,670 m E., 3,977,530 m N.	Cu	Prospect in gently north dipping granite gneiss. Honeycomb quartz; trace of Cu stain in quartz-pyrite-chalcopyrite(?) vein. No gold observed.
641	Songbird	UTM: 749,850 m E., 3,976,890 m N.	Au, Cu, Pb	Late irregular patches of chalcopyrite, galena, pyrite pseudomorphs in irregular quartz vein; thickness approximately 0.3 to 0.6 m. Very minute gold specks associated with chrysocolla in a late fractures.

Table 10.--Continued

Locality number (pl. 1)	Name	Approximate location (UTM 10,000-m grid, zone 11)	Commodities present	Comments
642	Summit	NE1/4 sec. 16, T. 29 N., R. 18 W.	Cu	Mullion structure on footwall. Quartz vein approximately 30 to 45 cm thick, traced laterally about 1 m using float. Trace of malachite, chrysocolla, and dark-red cuprite(?). Generally poor in sulfides.
643	Pick 'N' Pan Originally named: Intention to Gold	NW1/4 sec. 16, T. 29 N., R. 18 W.	Au, Cu	Two parallel veins dip approximately 45° to 50° E., parallel to layering in surrounding gneiss. Lower vein explored by an incline sunk along the vein which is 0.3 to 0.45 m thick. Trace of gold occurs as minute inclusions in oxidized chalcopyrite. A sheared alteration zone above and below lower vein consists of orange carbonate. A third vein is poorly exposed in upper portion of the prospect and includes very minor amounts of chalcopyrite.
644	Unnamed drywasher site	NW1/4 sec. 15, T. 29 N., R. 18 W.	Au	Very fine gold, some quite flakey, collected at this locality.
645	Unnamed prospect pit	SW1/4 sec. 15, T. 29 N., R. 18 W.	Cu	Prospect pit on 20- to 50-cm-thick quartz vein, containing minor pyrite, chalcopyrite, and carbonate. Considerable chlorite and carbonate alteration of the gneissic diorite country rock.
646	Merrieta	SW1/4 sec. 15, T. 29 N., R. 18 W.	Au, Cu	Sparsely scattered patches of altered chalcopyrite and pyrite are included in milky-quartz vein. Trace amounts of gold occur as minute platelike inclusions in pyrite and possibly in chalcopyrite. Open stope along vein and inclined shaft suggest that gold was once much more plentiful than may be inferred from samples now available. Very little sulfides overall, however.
647	Unnamed prospect (part of Gold Hill workings)	NE1/4 sec. 16, T. 29 N., R. 18 W.	Cu, Au?	Swarm of veins and associated altered country rock exposed in prospect cut. Overall shear zone strikes about N. 35° W., and dips approximately 40° NE. Irregular main vein contains pyrite and patches of chalcopyrite generally less than 2 cm across almost completely altered to dark-red mineral and chrysocolla. No gold observed. Country rock is altered diorite gneiss. In uppermost portion of prospect, a vein approximately 10 to 15 cm thick cuts a gently dipping leucogranite pegmatite dike. Minor amounts of carbonate, pyrite, and oxidized chalcopyrite are included within this vein.
648	Gold Hill mine	NE1/4 sec. 16, T. 29 N., R. 18 W.	Au	Intermittent production of gold from 1930 to 1942 (see text, this report).
651	Smokey (or Highline)	NW1/4 sec. 16, T. 29 N., R. 18 W.	Cu, Au, Pb	Irregular and brecciated vein approximately 10 to 15 cm thick, dips gently to the northeast. Six adits are driven to intersect the vein, in total, they aggregate approximately 90 m of workings. Minor oxidized chalcopyrite occurs as late fracture fillings and irregular patches. Minor galena, mostly altered to cerussite, occurs as blebs filling quartz-lined vugs. Gold occurs as minute grains in oxidized pyrite and quartz.
653	Unnamed prospects	UTM: 749,440 m E., 3,977,060 m N.	Au, P, Cu, Ba	A series of pods and stringers of quartz veins emplaced along what appears to be a N. 80° W-striking and 35° to 50° N.-dipping shear zone. An early quartz-carbonate-pyrite-galena-chalcopyrite-gold assemblage in the veins has been brecciated and cut by subsequent seams of white calcite, limonite, and barite. Bladed groups of thin barite crystals fill vugs from which the early carbonate has been leached. Considerable free gold found along pyritic seams in large quartz blocks on the easternmost dump along these workings. Galena and chalcopyrite are also abundant. Country rock consists of an altered granitic gneiss sequence within the gneiss unit.

Table 11.--Continued

Locality number (pl. 1)	Name	Approximate location (UTM 10,000-m grid, zone 11)	Commodities present	Comments
654	Unnamed adit	UTM: 748,710 m E., 3,978,170 m N.	Au?	An approximately 1.5 m long adit underlies a 40-cm-thick milky quartz vein. The close association of an altered pegmatite beneath the vein may indicate that the vein itself may be the quartz-core portion of a small "pegmatite"-vein system here. No sulfides or secondary copper minerals were observed. A quartz pod approximately 1.2 m thick is exposed 30.5 m northest of the prospect; and it also may be related to the pegmatite.
657	Gold Bond	UTM: 748,650 m E., 3,977,450 m N.	Au, Pb, Cu	Massive milky quartz veins are cut by many low-angle faults. Along the Gold Bond incline, several quartz veins approximately 1.7 m thick do not show significant alteration of the adjoining country rock. However, seams of pyrite voids and boxworks honeycombed by quartz are distributed throughout the vein parallel to its surface. Unaltered pyrite, chalcopyrite, and galena found in trace amounts. No gold was observed in place within the workings, although chalcopyrite and associated gold were found in an ore sample at the miners' camp. Mine predominantly worked during 1910-1920. A second period of occupation of the workings occurred during the following depression.
659	Solomon	UTM: 748,590 m E., 3,976,540 m N.	Au?	A simple, massive, milky quartz vein about 0.6 m thick. An approximately 3 m deep prospect shaft penetrates the vein at approximately 1.5 m below the surface. Cubic pyrite boxwork, partially filled by jarosite(?), is present in outcrop. No sulfides were observed.
664	Unnamed site	SW1/4 sec. 4, T. 29 N., R. 18 W.	Fe	An approximately 20 cm thick sequence of highly magnetic iron-formation crops out at this locality. The iron-formation is conformable with the surrounding amphibolite and mafic schist. In this general area, there are also some centimeter-sized tourmaline-bearing pegmatitic dikes which crosscut sharply the layering in the amphibolite and quartzofeldspathic gneiss.
668	Unnamed prospect	UTM: 749,660 m E., 3,978,160 m N.	Cu	A 20-cm quartz-ankerite-pyrite vein contains trace amounts of secondary copper, and honeycomb partings. No gold was observed.
675	Unnamed site	UTM: 749,650 m E., 3,981,510 m N.	W	Calc-silicate rock and stringers of marble occur in a zone up to 0.6 m thick, largely adjacent to 2- to 15-cm-thick sills and pods of quartz-rich leucogranitic pegmatite. Generally, the overall zone of calc-silicate rock and marble is enclosed within laminated amphibolite. The presence of scheelite in the calc-silicate rocks was verified using a black light. In addition, approximately 30 m north of the locality there is a post regional-metamorphic granite dike striking approximately N. 10° W.
676	Unnamed site	UTM: 749,560 m E., 3,981,030 m N.	Cu	A 20-cm quartz-ankerite (or siderite)-chalcopyrite vein, about 12 to 25 cm thick crops out here. No gold or galena found.
678	Unnamed prospects	NW1/4 sec. 34, T. 30 N., R. 18 W.	Cu, Au?	Prospects at top of peak show quartz-ankerite-sericite-pyrite veins. Trace secondary copper present, and some gold was observed. The remoteness and amount of past work done at the site suggest that some gold must have been found here previously.
687	Unnamed site	SE1/4 sec. 28, T. 30 N., R. 18 W.	Ba	Group of approximately N. 10° W.-striking veins which dip 30° to 35° NE crop out here. Irregular stringers and elongate masses of coarsely crystalline barite are somewhat abundant in this general area as late fillings of en echelon gashes. Ankerite is associated with the barite, and an albite-pyrite-ankerite assemblage is common along the walls of individual veins.

Table 11.--Continued

Locality number (pl. 1)	Name	Approximate location (UTM 10,000-m grid, zone 11)	Commodities present	Comments
689	Unnamed site	NE1/4 sec. 28, T. 30 N., R. 18 W.	Ba	Veins showing an assemblage of quartz-carbonate-barite-albite-pyrite crop out here. There is considerable albite along the wall zone of the veins. The main vein here measures about 20 cm thick, but several others are in the 2- to 5-cm range in thickness.
690	Unnamed site	NE1/4 sec. 29, T. 30 N., R. 18 W.	Ba, Cu	A 0.6-m-thick vein here includes chalcopyrite in its quartz-carbonate-barite-albite-pyrite assemblage.
735	Unnamed prospects	UTM: 747,180 m E., 3,984,640 m N.	Au	Gold was observed at five different prospects in this general area. A deep vertical shaft approximately 30 m deep had the largest amount of secondary(?) gold (see fig. 42). The veins generally pinch and swell irregularly, and are composed essentially of quartz, carbonate, pyrite, and gold. They may be Proterozoic in age (see text).
754	Unnamed prospect	UTM: 746,850 m E., 3,984,420 m N.	Hg?	An adit approximately 9 m long intersects a gently south dipping shear zone. Apparently, the prospect was for mercury, as the remains of an old hearth and a stockpile of hematitic schist suggests that the early prospectors mistook this for cinnabar.
800	Unnamed site	SW1/4 sec. 35, T. 28 N., R. 18 W.	Au?	Leucosyenitic pipe, elongated in a northeasterly direction crops out at this locality. Its overall dimensions at the surface are about 20 by 60 m. The pipe contains a quartz-free central zone which also shows fairly abundant concentrations of fluffy orange iron oxide(s) replacing iron carbonate. The outer portion of the pipe shows increasing concentrations of quartz in irregularly distributed stringers and veinlets. Although this locality shows no fluorite or obvious pyrite, the pipe here is nonetheless similar to that at locality 19 which contains visible disseminated gold.
802	Unnamed site	SE1/4 sec. 34, T. 28 N., R. 18 W.	F	Quartz-fluorite vein crops out here, and shows an average thickness of about 20 cm. The quartz is intergrown with the variably colored fluorite, which ranges from colorless to deep purple.
803	Unnamed site	SE1/4 sec. 34, T. 28 N., R. 18 W.	F, Au?	An approximately 2 cm wide quartz-fluorite-specularite-pyrite vein crops out here. One possible speck of free gold observed in limonitic boxworks after pyrite. Bleaching and the possible introduction of feldspar extends into the country rock for about 2 cm adjacent to the vein.
804	Unnamed site	SE1/4 sec. 34, T. 28 N., R. 18 W.	F	Fluorite occurs as coarsely crystalline knots in a quartz-fluorite-chlorite-iron carbonate-hematite-pyrite vein. The vein has a maximum observed thickness of about 20 cm.
810	Unnamed site	SW1/4 sec. 34, T. 28 N., R. 18 W.	F, Pb	A quartz-carbonate-fluorite-chlorite-galena vein system cuts a mixed zone of Proterozoic X biotite monzogranite and porphyritic monzogranite. Most of the veinlets in the system measure about 0.6 cm thick, and they contain colorless fluorite.
811	Unnamed site	SW1/4 sec. 34, T. 28 N., R. 18 W.	F	A quartz-purple fluorite veinlet parallels the local northwest-striking joint set in the porphyritic monzogranite.
812	Unnamed site	NW1/4 sec. 34, T. 28 N., R. 18 W.	F	Quartz-fluorite-iron carbonate-pyrite-chlorite veinlets fill northeast-striking joints.
815	Unnamed site	NW1/4 sec. 34, T. 28 N., R. 18 W.	F	Quartz-fluorite-pyrite and quartz-pyrite veinlets up to 15 cm thick fill northeast-striking steeply dipping joints.
817	Unnamed site	NW1/4 sec. 34, T. 28 N., R. 18 W.	Cu	An approximately N. 15° E.-striking and 75° NW.-dipping vein includes quartz, pyrite, chlorite, and secondary copper mineral(s).

Table 11.--Continued

Locality number (pl. 1)	Name	Approximate location (UTM 10,000-m grid, zone 11)	Commodities present	Comments
820	Lady Mary	SW1/4 sec. 27, T. 28 N., R. 18 W.	F, Pb, Cu, Au	Numerous parallel veins and veinlets,less than or equal to 15 cm thick parallel the jointing in coarse-grained porphyritic monzogranite. Pale-lavender fluorite is in association with brown carbonate in quartz-lined cavities. There are abundant indications of galena and alteration products of chalcopyrite; numerous zones of small (less than 2 mm) pyrite molds and pseudomorphs; and minor unaltered pyrite. These veins were explored by three small inclines, but apparently the veins pinch out with depth as they are exposed only in the open cuts.
821	Unnamed prospect	SW1/4 sec. 27, T. 28 N., R. 18 W.	F	Vein cuts coarse-grained porhyritic monzogranite. Purple fluorite occurs with pyrite along late hypogene fractures; as well as in masses up to about 1.0 cm across in milky quartz. No galena, gold, or copper stain was observed. The vein probably was emplaced along a northeast-striking fault as suggested by an intensely altered and friable zone at least 0.6 m in thickness along the footwall of the vein.
823	Unnamed site	SE1/4 sec. 28, T. 28 N., R. 18 W.	F	A quartz-fluorite-pyrite-chlorite-bearing vein strikes approximately N. 50° E., and dips 35° to 40° NW. The vein ranges up to 0.3 m thick and can be traced at the surface for a distance of about 30 m along strike. The fluorite in the vein consists of coarsely crystalline masses up to 6 cm across.
824	Unnamed drywasher site	SW1/4 sec. 4, T. 27 N., R. 18 W.	Au	Fine particles of detrital gold are moderately abundant in gravel on a somethat consolidated, reddish-brown clay soil. This soil fills irregularities developed in the true bedrock here. However, the reddish-brown soil does not itself contain placer gold particles.
828	Unnamed prospect	NW1/4 sec. 4, T. 27 N., R. 18 W.	Cu	Relatively abundant iron oxides replacing chalcopyrite in wispy quartz stringers following a N. 70° E.-striking and north-dipping shear zone. Considerable silicification along the zone.
831	Unnamed site	SE1/4 sec. 32, T. 28 N., R. 18 W.	F	An approximately 3 cm thick quartz-pyrite-fluorite-carbonate vein cuts porphyritic monzogranite at this locality. The vein strikes N. 65° E, and dips 70° SE.
832	Unnamed site	SE1/4 sec. 32, T. 28 N., R. 18 W.	F	At this locality, two veins crop out about 1 m apart. The mineralogy of the veins includes quartz, pyrite, pale-lavender fluorite, carbonate, white mica, and possibly potassium feldspar.
834	Unnamed shaft	SW1/4 sec. 33, T. 28 N., R. 18 W.	Pb, Cu, Au	Quartz veins, up to 20 cm wide, appear to parallel a strongly developed foliation in a N. 35° E.-striking shear zone in cataclastically deformed porphyritic monzogranite. The porhyritic monzogranite contains some scattered patches of galena, and secondary copper minerals. One small grain of gold was noted.
835	Unnamed site	NW1/4 sec. 33, T. 28 N., R. 18 W.	Cu, Pb, Au	Several quartz-pyrite-carbonate±chalcopyrite±galena± gold (trace) veins cut coarse-grained porphyritic monzogranite. Gold occurs as minute grains in iron-oxide-stained cavities possibly reflecting the former presence of chalcopyrite. In addition, a hornblende porhyry dike crops out at this locality, and strikes northeasterly.
836	Unnamed prospect	SE1/4 sec. 33, T. 28N., R. 18 W.	F, Pb	A quartz, fluorite, pyrite, and galena (trace) vein strikes N. 25° E., and dips 80° NW. Fluorite in the vein ranges up to 4-cm-across, and varies from colorless to dark purple.
837	Unnamed site	SW1/4 sec. 32, T. 28 N., R. 18 W.	F	Two quartz-fluorite-white mica veins crop out here approximately 3 m apart. The veins strike approximately N. 65° E. Greisen occur in the surrounding coarse-grained porphyritic monzogranite, and the greisen includes some pyrite and feldspar. A potassium-argon age determination of white mica from these veins yielded an age of 65.4 m.y. (see table 3).

Table 11.--Continued

Locality number (pl. 1)	Name	Approximate location (UTM 10,000-m grid, zone 11)	Commodities present	Comments
838	Unnamed site	NE1/4 sec. 32, T. 29 N., R. 18 W.	F	Quartz-pyrite-fluorite veinlets in porphyritic monzogranite strike N. 20-25° E., and dip 70° NW. In addition, several mafic dikes at this locality parallel the trend of the veins, but no veins were observed to cut the mafic dikes.
856	Unnamed prospect	SE1/4 sec. 30, T. 28 N., R. 18 W.	Au?	Prospect sunk on a 15- to 20-cm-thick, brecciated, quartz-carbonate-pyrite vein. Further, a nearly flat lying shear zone is exposed throughout the prospect pit. The shear zone includes abundant sericitized and broken up schist.
858	Red Cloud	NW1/4 sec. 31, T. 28 N., R. 18 W.	Cu	Approximately 30 m long adit and 5 m raise to surface along quartz-pyrite-carbonate-chalcopyrite (trace) veins cutting porphyritic monzogranite. Numerous minor faults in the workings show shallow dips.
868	Cyclopic no. 6 prospects	NE1/4 sec. 25, T. 28 N., R. 19 W.	Au?	Major splay of detachment fault zone containing red-brown gouge and comminuted monzogranite cuts through the prospects. A minor faults strikes N. 10°-15° E., dips approximately 40° W.; and is possibly parallel to the main fault system. Quartz-carbonate-pyrite veins and recemented quartz breccia of the Cyclopic type occur in the gouge zone.
			Pb, Cu, Au, Mo	Approximately 150 to 300 m southeast of this locality, there are numerous prospects, pits, and trenches in the lower gouge zone. Vein quartz is brecciated and widely scattered in the gouge as blocks 0.6 m long and approximately 0.3 m thick. Veins contain galena, pyrite, iron carbonate, malachite (alteration of chalcopyrite(?)), wulfenite, gold, and cerussite. Brilliant crimson mineral may be cuprite. Red, brown, and black iron and manganese(?) oxides are relatively abundant.
869	Unnamed prospect	NE1/4 sec. 25, T. 28 N., R. 19 W.	Au?	Two prospect pits expose approximately 2 m of friable, coarse-grained, porphyritic monzogranite. The entire ridge to the east has similar lithology. Several thin seams of gouge dip gently to the southwest.
871	Fry mine	NE1/4 sec. 25, T. 28 N., R. 19 W.	Au?	A shaft is sunk on a late Tertiary fault zone and sheared Proterozoic rocks and Miocene and (or) Pliocene fanglomerate.
872	Beppo	SE1/4 sec. 32, T. 28 N., R. 18 W.	Au?	Fine-grained granular quartz veins containing numerous thin seams of pyrite in cubes. Several minor shear zones are present, yet there is no brecciation of the veins themselves. Country rock is foliated and sericitized, coarse-grained porphyritic monzogranite.
876	Unnamed site	NE1/4 sec. 24, T. 28 N., R. 19 W.	F	Quartz-carbonate (minor)-pyrite-fluorite-white mica veins cut the upper Cretaceous two mica monzogranite.
877	Unnamed site	NE1/4 sec. 24, T. 28 N., R. 19 W.	F	Abundant quartz-white mica-fluorite veins and veinlets cut the upper Cretaceous two mica monzogranite. The fluorite in these veins is colorless, and the veins range up to 8 cm thick.
878	Unnamed site	NE1/4 sec. 24, T. 28 N., R. 19 W.	F	A local swarm of nearly vertical, quartz-pyrite-white mica veinlets shows white mica-fluorite-quartz-potassium feldspar alteration assemblages in the adjacent two mica monzogranite. In addition, small cubes of pyrite are oxidizing to red and yellow iron oxide(s) in some of the fluorite-bearing assemblages.
885	Unnamed adit	NE1/4 sec. 25, T. 28 N., R. 19 W.	Pb	Prospect adit driven into a major splay of the detachment fault zone which crops out at the Cyclopic mine area. In the adit, friable and cemented Cyclopic-type quartz is exposed. The quartz vein is oxidized, and contains abundant cerussite.

Table 11.--Continued

Locality number (pl. 1)	Name	Approximate location (UTM 10,000-m grid, zone 11)	Commodities present	Comments
887	Unnamed prospect	SW1/4 sec. 19, T. 28 N., R. 18 W.	Cu	Quartz-pyrite-chalcopyrite-white mica-potassium feldspar-specular hematite vein, approximately 5 to 45 cm thick. Immediate country rock consists of a septum of metamorphic rocks that have been engulfed by the two mica monzogranite.
889	Unnamed shaft	SW1/4 sec. 29, T. 28 N., R. 18 W.	Au?	Shallow, 8-m-deep shaft is sunk in gneiss intruded by numerous biotite minette(?) and fine-grained andesite dikes. No obvious signs of mineralization present.
891	Unnamed prospects	NE1/4 sec. 30, T. 28 N., R. 18 W.	Pb	Series of prospects along generally east-west striking structures crop out in the vicinity of this locality. One quartz vein (probably 15- to 30-cm thick) lies along a N. 85° E.-striking fault. Movement along the fault probably is premineralization. Abundant cerussite, minor galena, and some pyrite molds were noted locally. Numerous quartz veins and pods occur along a sericitized and deformed contact zone between medium-grained gneissic biotite granodiorite and leucocratic granite-bearing metamorphic complex. The easternmost prospect pits were sunk on two quartz-pyrite-galena-cerussite veins, 15 to 30 cm in thicknesses.
897	Golden Rule mine (Gold Day mine)	NW1/4 sec. 29, T. 28 N., R. 18 W	Au, Pb	At top of hill, a shaft 6-m deep is sunk on a quaftz vein, 0.9 to 1.2 m thick, striking N. 20° E. and dipping 45° SE. Pyrite and other sulfides are concentrated along late hypogene fractures parallel to the overall strike of the vein. Only a small percentage of the vein is mineralized.
			Zn?, Cu, Au, Pb	Downhill to the east, the vein strikes N. 35° E., dips 20° SE, and varies from 15 cm to 1.2 m in thickness. Here, the vein pinches and swells, cutting strongly sheared gneiss or medium-grained granodiorite, and it includes a quartz-iron carbonate-chlorite-pyrite-galena-sphalerite(?)-chalcopyrite(?) assemblage. Chrysocolla is abundant; no chalcpyrite was observed, although it may be present. Mineralogy of the north-northeast-striking, gently to moderately southeast dipping vein includes quartz, pyrite, galena, and cerussite. Trace amounts of secondary copper minerals were noted. Gold was found in the dump of the main shaft, approximately 30 m north-northeast of the hilltop. Veinlets locally cut hydrothermally altered alaskite.
900	Mountain View no. 2	SE1/4 sec. 20, T. 28 N., R. 18 W.	Cu, Pb	A fine-grained granular quartz-galena vein includes a trace of copper stain.
902	Unnamed shaft	SE1/4 sec. 20, T. 28 N., R. 18 W.	Cu, Pb	Incline workings have a maximum depth of about 12 m, and they include a short, approximately 7 m long, drift along a minor fault. Traces of galena and secondary copper minerals were noted.
903	Ridgetop prospect (Never-get-left)	SE1/4 sec. 20, T. 28 N., R. 18 W.	Cu, Pb	Uppermost working is a 9-m-long, 0.6- to 3.1-m-deep opencut; along a N. 50° E. striking, 75° SE.-dipping fault vein. The vein contains minor chalcopyrite, galena, and pyrite.
904	Unnamed prospect	SW1/4 sec. 28, T. 28 N., R. 18 W.	Zn?, Pb, Cu, Mo	The prospect pit is approximately 1.5 m deep, and cuts an irregular quartz-galena-sphalerite(?)-chalcopyrite-pyrite vein. Wulfenite is abundant; chalcopyrite and pyrite are rare. No free gold was found after an extensive search.
909	Unnamed prospect	SW1/4 sec. 20, T. 28 N., R. 18 W.	Cu, Pb	A 0.6-m-thick quartz-galena-chalcopyrite vein here dips about 45° S. and strikes N. 85° E.
911	Unnamed adit	Location uncertain	Pb, Cu, Au, Mo	Irregular sulfide-bearing quartz pods and stringers, parallel to foliation in sheared mafic gneiss. The veins have been deformed by the regional metamorphic events (see text). Sulfides include galena, chalcopyrite, pyrite, minor secondary cerussite, wulfenite, and green-blue copper stains.

Table 11.--Continued

Locality number (pl. 1)	Name	Approximate location (UTM 10,000-m grid, zone 11)	Commodities present	Comments
913	Jumbo prospect	SW1/4 sec. 19, T. 28 N., R. 18W.	Au?	Main vein is 2.4 to 3 m thick, strikes N. 10° W., and has a vertical dip. The vein crops out continuously for approximately 140 m, and appears to branch out into several veins at its north end. In the main prospect pit, which is about 3 m deep, the vein is 3.1 m thick and dips 80° E., cutting the gently northeast diping gneisses. A second vein, 2 to 3 m thick, lies 30 m to the west and crops out for 30 m. The strike is N. 10° W, dip vertical. Veins consist of quartz, minor pyrite, trace sericite, and trace ferrocarbonate. No copper, lead ore, fluorite, or gold was observed, however.
913a	Unnamed prospect	SW1/4 sec. 19, T. 28 N., R. 18 W.	F	Massive quartz vein appears to dip 30° SE., and is intimately associated with two mica monzogranite and pegmatite. Feldspar, muscovite, fluorite, and minor pyrite occur as thin seams less than 2.5 cm thick. The veins cut and are mutually cut by the monzogranite, suggesting a genetic relationship.
917	Unnamed site	NW1/4 sec. 19, T. 28 N., R. 18 W.	F	Quartz-pyrite-white mica-fluorite veinlets up to 5 cm thick cut a fine-grained facies of the two mica monzogranite.
920	Patsy (Neglected)	NW1/4 sec. 20, T. 28 N., R. 18 W.	Pb, Cu	Several prospect pits on a gently southwest dipping quartz-pyrite-galena-chalcopyrite vein, 0.9 to 1.2 m thick. Also present are cerussite, chrysocolla, pyrite voids and boxworks.
921	Unnamed prospect	SW1/4 sec. 17, T. 28 N., R. 18 W.	Pb, Ag	Considerable galena and cerussite exposed in a small pit. Country rock consists of quartzofeldspathic gneiss, amphibolite, and biotite sequences of the paragneiss unit.
923	Unnamed site	NW1/4 sec. 19, T. 28 N., R. 18 W.	F	An approximately east-west striking vertical vein cuts the two mica monzogranite and the adjoining gneiss. The vein includes quartz, pyrite, white mica, and fluorite. Some of the fluorite cubes reach 5 cm on a side. A potassium-argon age determination on white mica from this vein yielded an age of 68.8 m.y. (see text and table 3, this report).
927	Shelby mine (Harmonica)	NW1/4 sec. 17, T. 28 N., R. 18 W.	Au, Pb, Cu, V, Mo	Hilltop prospect pit exposes a pod of quartz-chalcopyrite-galena that is approximately 1.8 m thick. Examination of mineralogy on samples from dump revealed abundant gold approximately 1 mm diameter; galena, minor altered chalcopyrite, pyrite, wulfenite, vanadinite, chrysocolla, copper stain.
928	Unnamed adit	SE1/4 sec. 17, T. 28 N., R. 18 W.	Au, Pb, Cu	Lower adit is approximately 14 to 15 m long. Workings are along a quartz-galena-cerussite-gold-altered chalcopyrite (malachite) vein, approximately 0.9 m thick.
929	Gold Street (also titled (Climax group)	NE1/4 sec. 17, T. 28 N., R. 18 W.	Pb, Cu, V, Mo	Main shaft inaccessible but was approximately 9 m deep. A quartz-pyrite-iron carbonate-galena chalcopyrite-chlorite vein is poorly exposed. It appears to strike N. 25°-30° W. Some vanadinite, wulfenite, and copper stain were observed also.
931	Big Lease	NW1/4 sec. 8, T. 28 N., R. 18 W.	Trace Cu	Prospect pit is approximately 3 m deep on a zone of quartz-pyrite-chlorite-sparse chalcopyrite veins, 1.5 m thick. The veins are fractured, brecciated, and recemented somewhat similar to ore at the Cyclopic mine workings.
931a	Unnamed prospect	NW1/4 sec. 8, T. 28 N., R. 18 W.	Au	A small open cut, about 3 m deep and 12 m long lies in a zone of brecciated quartz lenses in a northwest-striking shear zone. Float suggests that this system of veining is the continuation of the zone of quartz veins extending through the Shelby mine (loc. 927). Vein includes quartz, pyrite, carbonate, chlorite, and gold.

Table 11.--Continued

Locality number (pl. 1)	Name	Approximate location (UTM 10,000-m grid, zone 11)	Commodities present	Comments
933	Unnamed prospect	NW1/4 sec. 5, T. 28 N., R. 18 W.	Trace Cu	Pit on quartz-pyrite-carbonate-chlorite vein, approximately 2.4 m thick. A trace of copper stain was observed on float. The vein strikes approximately east-west, and dips 35°N.
934	Star Extension no. 2	SW1/4 sec. 16, T. 28 N., R. 18 W.	Cu, Pb, Mo, Au?	Upper pit is on a quartz-pyrite-chalcopyrite-galena vein that ranges from 2.5 to 25 cm(?) thick. Minor chrysocolla and wulfenite present. No gold was observed. The vein strikes N. 25° E., and dips 75°SW. A mafic dike approximately 3 m thick is in the hanging wall of the vein, and the dike has a chilled margin against the vein.
935	Morning Star	SW1/4 sec. 16, T. 28 N., R. 18 W.	Au?	Morning Star is a shaft with a short connecting adit.
935a	Saint Charles	SE1/4 sec. 16, T. 28 N., R. 18 W.	Pb, trace Cu, Au?	Quartz-pyrite-galena-trace copper-bearing vein, 7 to 25 cm thick, strikes N. 10° E., and dips 35°E.
938	Round Top	NW1/4 sec. 22, T. 28 N., R. 18 W.	Pb, Cu, Au?	Quartz-pyrite-galena-chrysocolla vein occurs in a lens less than 0.9 m thick. Also present are cerussite and malachite. Vein and veinlets are concentrated in a shear zone. Country rock includes gneissic granodiorite below shear zone, and paragneiss above the shear zone.
938a	Unnamed adit	NW1/4 sec. 22, T. 28 N., R. 18 W.	Au, Pb, Cu	At this locality, a prospect pit in lower plate of gneissic granodiorite has been dug on rocks cut by numerous small quartz veinlets. This pit lies approximately 15.2 m below a N. 65° E.- 25°SE-dipping fault zone. The main quartz-pyrite-galena-chalcopyrite (cerussite-malachite)-gold vein near here, however, is less than 7.6 cm thick; and lies within the fault zone. Adit is 1.2 m in length.
940	Claude (Eastside)	NW1/4 sec. 22, T. 28 N., R. 18 W.	Au, Cu, Pb	Quartz-iron carbonate-pyrite-galena-chalcopyrite (minor)-gold vein is hosted by gneiss. Vein strikes N. 75° E., and dips 50°NW.
941	Lester no. 1 and 2	SW1/4 sec. 15, T. 28 N., R. 18 W.	Pb, Au	An approximately 8-m-long adit is driven along a southeast-dipping fault zone in gneiss. The quartz vein is fragmented and recemented; and overall is not notably mineralized except at the north end where galena, cerussite, pyrite, and trace gold were observed.
942	Ridge Lode (For Years)	SE1/4 sec. 16, T. 28 N., R. 18 W.	Pb, Cu, Au	A quartz-pyrite-galena-carbonate-chalcopyrite-gold-bearing vein is 0.3 m thick, here; it strikes approximately N. 45° E., and dips 40°SE.
947	Unnamed prospect	NW1/4 sec. 28, T. 28 N., R. 18 W.	Pb, Cu	Galena and copper stain noted in a small prospect pit dug on the ridgeline, approximately 30 m south of the contact between gneissic granodiorite and porphyritic monzogranite.
948	Grand View	SE1/4 sec. 10, T. 28 N., R. 18 W.	Au, Cu, Pb	Prospects and open cuts lie on group of en echelon veins striking N. 55°-75° W; dipping 55°-70°NE. Lower adit is approximately 7 m long and includes a 7-m open cut driven on a N. 45° W.-, 65°W.-dipping fracture zone containing irregular quartz, iron carbonate, and pyrite veinlets. The fracture zone is 5 cm wide in the gneissic granodiorite. A second adit uphill is about 13 m long and was driven along a quartz vein system ranging from 1 to 60 cm in thickness; it occupies a N. 55°W.-, 55°NE-fault in the gneissic granodiorite. The system consists mostly of a zone 8 cm to 0.6 m wide that is made up of branching quartz veinlets. A third prospect here explores a fracture-vein system which strikes N. 75° W. and includes individual quartz veinlets up to 8 cm wide. Sericitization of the gneissic granodiorite extends about 3 m out from the fracture-vein system. Free gold was noted in oxidized vein material on the dump. Individual veins may include variable amounts of galena, chalcopyrite, quartz, carbonate, pyrite, cerussite, and limonite.
949	Valley View no. 2	SW1/4 sec. 10, T. 28 N., R. 18 W.	Cu, Pb, Au?	Two prospect shafts approximately 5 to 6 m deep explore a 75-cm-wide vein of white quartz containing less than 1 percent overall pyrite, chalcopyrite, iron carbonate, and gold(?).

Table 11.--Continued

Locality number (pl. 1)	Name	Approximate location (UTM 10,000-m grid, zone 11)	Commodities present	Comments
952	Valley View	SW1/4 sec. 10, T. 28 N., R. 18 W.	Au?	There are two shafts near this locality. Southern shaft exposes 3-m-wide contorted gouge zone containing blocks of vein quartz up to 1 m long. The mineralogy of the veins includes quartz, carbonate, and pyrite.
957	Unnamed placer workings	SE1/4 sec. 28, T. 29 N., R. 18 W.	Au?	Gulches in this general area have been placered very heavily during several intervals of what appears to have been prolonged occupations.
964	Unnamed placer workings	NW1/4 sec. 29, T. 29 N., R. 18 W.	Au?	Gulches on both sides of the road in this general area were worked extensively for their placer gold content. Apparently the placer gold was concentrated on fractured but coherent, gneissic basement rocks.
967	Unnamed prospects	NE1/4 sec. 31, T. 29 N., R. 18 W.	Cu, Pb, Au?	Four shallow prospect pits, the deepest of which is about 4 m, explore a series of northeast-north-northeast-striking southeast-dipping milky quartz veins. The veins contain local concentrations of chalcopyrite, galena, and carbonate. The veins are lenticular and branch approximately parallel to foliation in the paragneiss country rock.
968	Unnamed drywasher site	NE1/4 sec. 32, T. 29 N., R. 18 W.	Au	Placer gold occurs in particles up to approximately 1 mm across. The gold is hosted widely by the slopewash debris, and the gold is associated with relatively sparse concentrations of magnetite.
971	Unnamed drywasher site	NW1/4 sec. 31, T. 29 N., R. 18 W.	Au	Several small colors, and one cerussite-encrusted pebble of galena were obtained from material collected from a small gulley cut in Quaternary-Tertiary gravel. False bedrock is not well-cemented by caliche, but instead consists of gravel cemented by a red clay-rich matrix.
972	Unnamed drywasher site	NW1/4 sec. 1, T. 29 N., R. 19 W.	Au	Some relatively coarse placer gold, some particles measuring more than 1 mm across, was obtained from a heavily worked gulch, approximately 200 m northeast of the cabin at Owens mine.
973	Owens mine	NW1/4 sec. 1, T. 28 N., R. 19 W.	Cu, Fe	Underground workings at the mine probably measured at least 100 m. Head frames and ladders have been removed. Considerable chrysocolla and malachite occur as staining along a narrow fault zone which parallels the gneissic layering in its hanging wall. There is a slight discordance of the fault plane with the attitude of the layering in the footwall gneisses. Amphibolite and biotite gneiss are the main rock types in the mine area, but at least one 0.6-m-thick bed of laminated iron-formation crops out at several points southwest and west of the main shaft. Calc-silicate rock is cut locally by quartzose veins or pegmatitic alaskite. The veins include fine-grained granular quartz, iron carbonate, specularite, pyrite, and secondary copper minerals. Sericitization is intense and widespread.
973a	Hope	NW1/4 sec. 1, T. 28 N., R. 19 W.	Cu	A shallow 3-m pit shows altered and copper-stained schistose cataclastic gneiss. Malalchite, cuprite(?), and chalcopyrite occur in veinlets, up to 2.5 cm wide. They parallel foliation and layering. Brecciated zones in the gneiss are cemented also by iron- and copper-oxide minerals.
974	Unnamed drywasher site	SE1/4 sec. 36, T. 29 N., R. 19 W.	Au	Relatively abundant, and moderately coarse fragments of detrital gold obtained entirely from Quaternary-Tertiary gravel. The bulk of the gold at this locality is concentrated on caliche-cemented false bedrock.
976	Unnamed drywasher site	NE1/4 sec. 12, T. 28 N., R. 19 W.	Au	Very few colors were obtained from this site. One fragment of gold measured 0.5 mm across. In addition, the overall abundance of magnetite in the sand at this site is relatively low.
980	Unnamed drywasher site	NW1/4 sec. 17, T. 28 N., R. 19 W.	Au	Relatively abundant concentrations of magnetite occur in the Quaternary-Tertiary gravel, but only one color was found.

Table 11.-Continued

Locality number (pl. 1)	Name	Approximate location (UTM 10,000-m grid, zone 11)	Commodities present	Comments
988	Excelsior mine	NW1/4 sec. 22, T. 28 N., R. 18 W.	Pb, Au?	Thin quartz-carbonate veinlets parallel foliation in a highly foliated zone that strikes N. 35°-40° E. The highly foliated shear zone shows silicification, sericitization, and flooding by carbonate, and the zone occurs between gneiss and porphyritic monzogranite. The bulk of the alteration and quartz veinlets are concentrated in a zone approximately 7 m wide. The veins include quartz-carbonate-chlorite-pyrite-galena (trace)-gold(?) assemblages.
990	O.D. no. 1	SW1/4 sec. 22, T. 28 N., R. 18 W.	Pb, Cu, Au?	Up to 0.6 m of well-mineralized quartz occupies a west-northwest-dipping fault zone--possibly the extension of the Excelsior vein system. Abundant cerussite after galena, local concentrations of malachite and chrysocolla staining, and iron oxide pseudomorphs after pyrite.
992	Unnamed prospect	SW1/4 sec. 22, T. 28 N., R. 18 W.	Pb	Shaft 15 m deep shows stoping to that depth along a 0.3- to 1.0-m-thick vertical quartz vein occupying a N. 10° E-striking sericitized shear zone. Two biotite lamprophyre dikes are visible in main shaft. One dike 15 cm thick, crosscuts the vein, and the other, which is 40 cm thick, lies 0.6 m east of the vein. Galena and weathered pyrite occur in the vein quartz.
1031	Unnamed drywasher site	SE1/4 sec. 7, T. 29 N., R. 17 W.	Au	Considerable coarse-grained and fine-grained fragments of gold are associated with a moderate amount of magnetite, some barite, and a considerable amount of cerussite-encrusted galena. The coarse fragments of gold are moderately rounded, whereas the fine fragments are angular.
1036	Unnamed prospects	SW1/4 sec. 8, T. 29 N., R. 17 W.	U?, W?	Radioactivity is up to seven times background locally in some hot spots. At this prospect a magnetite-bearing leucogranite pegmatite contains cataclastic margins characterized by fine-grained magnetite. The margins of the pegmatite have the highest counts in areas along the hanging wall. A block of skarn occurs in the wash at the prospect. Some calcite, quartz, garnet, pyrite, amphibole, and scheelite(?) were noted in the skarn.
1043	Unnamed prospect	UTM: 756,030 m E., 3,988,780 m N.	Cu	Prospect is east of Burro Springs, in the Iceberg Canyon quadrangle. A 1-m-wide quartz vein contains some knots of brown-weathering carbonate, rather abundant pyrite, and a trace of secondary copper staining. The vein occupies a narrow augen gneiss cataclastic zone in an otherwise fresh porphyritic coarse-grained monzogranite.
1071	Lone Jack placer	SW1/4 sec. 15, T. 29 N., R. 17 W.	Au	Yellow-gray distinctly foliated to laminated quartzofeldspathic gneiss (medium grained) is the dominant clast type. Subangular to subrounded boulders up to 0.6 m in diameter are common. Pyritic vein quartz is present, but uncommon, and some pyritic and feldspathic altered wallrock of quartzofeldspathic gneiss is present. Gold was found northward along with limonite pseudomorphs after pyrite. Heavily worked in the late 1950's, and it is reported that fragments of gold greater than 1 mm were very common.
1086	Unnamed prospect	SW1/4 sec. 1, T. 28 N., R. 19 W.	Pb, Cu, Ba?, Fe	A 0.3-m-thick quartz vein containing some iron carbonate, albite, and some minor seams of barite(?) crops out here. Considerable late galena and oxidation products of chalcopyrite also occur in the vein. The vein occupies a minor normal(?) fault in predominantly amphibolite paragneiss, which includes a lens of well-laminated iron formation, approximately 100 m north-northwest of the 2-m-deep pit at this site.
1087	Unnamed prospects	NW1/4 sec. 1, T. 28 N., R. 19 W.	Cu, Pb?	These workings include approximately 10 m of vertical and inclined shafts. There is considerable chrysocolla, but very little galena, if any. Iron oxides after pyrite are rather abundant.

Table 11.--Continued

Locality number (pl. 1)	Name	Approximate location (UTM 10,000-m grid, zone 11)	Commodities present	Comments
1095	Senator mine	NW1/4 sec. 14, T. 28 N., R. 19 W.	Cu, Au?	An approximately 100-m-long adit has been driven to crosscut an approximately 0.6-m-thick breccia zone along a shallow-dipping fault zone. The fault zone dips 5 to 10° east-northeast, and has a hanging wall of brecciated gneiss, and a footwall of two mica monzogranite. Only traces of secondary copper minerals were noted to occur in the fault zone, approximately 20 m from the portal. The fault zone in the adit also includes some vein quartz.
1096	Buena Vista	SE1/4 sec. 11, T. 28 N., R. 19 W.	Au?	Two quartz lenses up to 2 m thick and 25 m along strike appear to lie on either side of a shear zone exposed poorly in a small prospect pit at the north end of the lenses. Indications of mineralization are very sparse. Faulting along the shear zone may have repeated a single lens. There are a few barren-appearing quartz veins in this general area, but no other prospects were noted.
1097	Unnamed site	SE1/4 sec. 11, T. 28 N., R. 19 W.	Cu	Altered amphibolite here shows silicification and flooding by carbonate. In addition, a quartz-carbonate-hematite-pyrite vein crops out here, and includes some secondary copper mineral(s).
1100	Unnamed site	NE1/4 sec. 15, T. 28 N., R. 19 W.	Pb, Cu	Quartz-white mica-pyrite veins cutting two mica monzogranite locally include relatively abundant concentrations of galena and trace amounts of secondary copper minerals(?).
1105	Unnamed prospect	NW1/4 sec. 14, T. 28 N., R. 19 W.	Au?	Prospect exposing fanglomerate of the Muddy Creek Formation in fault contact with paragneiss. The deep-brick-red and red-brown gouge of the fault zone, however, is not well exposed. The rocks in the lower plate here sporadically include tectonic blocks of crushed and recemented vein quartz similar to the Cyclopic-type ore.
1106	Unnamed prospect	NW1/4 sec. 14, T. 28 N., R. 19 W.	Au?	Up to 15-cm-thick lens of crushed quartz crops out in a prospect here. The prospect exposes these veins as gently east dipping crosscutting bodies enclosed in crushed, brecciated, and intricately faulted Proterozoic gneiss. The brecciated ore is restricted entirely to a tectonic sliver of gneiss between two mica monzogranite and fanglomerate.
1107	Unnamed adit	NW1/4 sec. 14, T. 28 N., R. 19 W.	Au?	Horizontal adit penetrates a low-angle fault, which is in turn offset about 1 m by a high-angle normal fault. An upper prospect nearby is an open cut 15 m long, entirely in mangled gneiss, containing commonly isolated, blocks, and lenses of crushed quartz. A trace of pyrite was found on one vein fragment.
1127	Unnamed site	NW1/4 sec. 32, T. 28 N., R. 16 W.	F	A 10-cm-thick vein of quartz, epidote, calcite, and fluorite crops out in a sheared and brecciated zone within the granodioritic border facies of the porphyritic monzogranite. Fluorite ranges from colorless to purple, and it also occurs together with white, coarsely crystalline calcite in veinlets which cut the quartz- and epidote-bearing vein.
1225	Unnamed prospect	NE1/4 sec. 26, T. 28 N., R. 20 W.	Au	Gold-bearing quartz+pyrite+carbonate vein material occuring in a coarse, angular landslide breccia. Trace of gold visible.
1356	Unnamed prospect	NW1/4 sec. 9, T. 29 N., R. 17 W.	Cu	Two prospects occur at this locality. In the first prospect, hematitic gossan, apparently associated here with a 30-cm-wide quartz vein originally carrying abundant sulfides, including chalcopyrite. The vein dips 35° and parallels the dip of layering in the enclosing gneiss and leucogranite complex. In the second prospect, a trace of chrysocolla was noted associated with a 1-m-wide quartz vein occupying a minor fault in nearly flat lying amphibolite gneiss.

Table 11.--Continued

Locality number (pl. 1)	Name	Approximate location (UTM 10,000-m grid, zone 11)	Commodities present	Comments
1357	Copper Glance no. 2 (Copper Blowout)	NW1/4 sec. 9,. T. 29 W., R. 17 W.	Cu	Gentle inclined adit exposes a 2-25-cm-thick zone of massive goethite-hematite lying parallel to the rounding undulating foliation. Some malachite and chrysocolla on dump. Another shaft is vertical and about 10 m deep; it passes through a flat-lying hematite+goethite+malachite+chrysocolla gossan exposed at the surface by cuts. The country rock is gently dipping amphibole-quartzofeldspathic gneiss and alaskite. This area seems to be dominated by a series of gently dipping quartz+ sulfide lenses parallel to layering in interlayered amphibole-quartzofeldspathic gneiss. Mineralization in this general area is referred to as Copper Blowout ridge in Deaderick (1980) and Krish (1974). Geochemical studies of minor elements in rocks in this area suggested to Krish that if there is a porphyry copper system buried here, the exposed rocks are above the outermost propylitic fringes of the system
1359	White Beauty (High Voltage)	SW1/4 sec. 9, T. 29 N., R. 17 W.	Pb, Cu	A vein up to 25 cm contains abundant galena, cerussite, malachite, chrysocolla, and bornite (?)

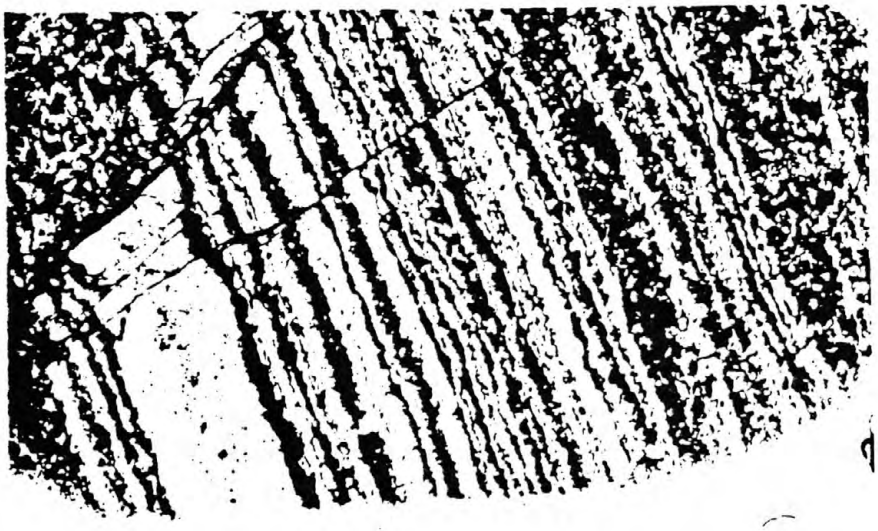

Figure 23.--Photomicrograph of oxide facies, banded iron formation. Plane polarized light. Photomicrograph is about 45 mm along its base. Sample number GM-303; NW1/4 sec. 16, T. 29 N., R. 17 W.

gossanlike stringers in brecciated quartz and highly altered granitoid pegmatite. The major minerals in these oxide facies iron formations are maghemite (magnetic hematite derived from magnetite) and quartz, which occur in alternating bands. Granoblastic quartz typically shows complexly sutured boundaries and may have long dimensions of about 4 mm in some quartz-rich hands that measure about 5 mm in thickness. However, such grains of quartz include swarms of extremely fine-grained, alined crystals of maghemite that parallel the trace of the maghemite-quartz bands. Therefore, recrystallization of these rocks must have involved a tremendous increase in grain size as has been reported in metamorphosed bedded iron formations elsewhere (see James, 1981). We infer these thinly banded maghemite-quartz rocks in the Gold Basin - Lost Basin districts to have initially been deposited as chemical precipitates related to sporadic volcanic activity during the largely epiclastic deposition of the protoliths of the surrounding metamorphic rocks. Indeed, some of the nearby enclosing rocks also include detrital magnetite (Deaderick, 1980, p. 16-19). Chemical analysis of a representative sample from the iron formation shows a content of about 43 weight percent total iron as FeO, and an SiO_2 content of 45.8 weight percent (analysis 3, table 10). However, the very high content of hematite in this sample is reflected in its high ratio of Fe_2O_3 to FeO, about nine to one (table 10).

Porphyritic to seriate, foliated metarhyolite also crops out in the general area of the iron formation at locality 303 (table 11). Phenocrysts and crystal fragments of albite-oligoclase (An_{10}) and quartz make up about 20 to 25 volume percent of the rock. These phenocrysts and crystal fragments range from 0.3 to 3.5 mm in size and probably average about 1.5 mm in their largest dimension. Some of the albite-oligoclase occurs in glomeroporphyritic aggregates, some of which include small, ovoid lithic clots of very fine grained granulose quartz plus chlorite. About one-third of the phenocrysts are quartz. Many of the quartz crystals are embayed, and several of them are obviously bipyramids. In addition, they are highly strained, showing a ribbon-type extinction under crossed nicols. Where the originally monocrystalline quartz phenocrysts have recrystallized, the newly grown crystals of quartz are associated with recrystallization of chlorite which is moderately abundant throughout the matrix. The matrix is poorly, but nonetheless distinctly foliated, a textural relation which is one of the most diagnostic

features of the rock. These laths of albite have poorly defined crystal boundaries with the surrounding matrix, and the laths are aggregated with quartz, chlorite, biotite, and additional granoblastic albite. Light- to medium-brown (Z) biotite is paragenetically earlier than chlorite. Minor accessories include apatite, zircon, and fine-grained granules of epidote. Chemical analysis of a grab sample from the metarhyolite shows an SiO_2 content of 71.4 weight percent, and an Na_2O plus K_2O content of 4.7 weight percent (analysis 4, table 10), which plots in the rhyolite field using the chemical classification of Middlemost (1980).

Marble, Calc-silicate, and Skarn

Generally less than 2-m-thick beds of marble, calc-silicate marble, and skarn crop out sporadically throughout much of the gneiss and feldspathic gneiss units figure 2. In detail, many individual beds of these carbonate or replaced carbonate beds are also associated spatially very closely with amphibolite. Most of the marble is impure and in places it occurs squeezed into the cores of very tightly appressed recumbent and overturned folds that measure perhaps 1 to 2 m across. Typically there are wide-ranging overall proportions of silicate minerals in these rocks both along individual beds and also among different nearby beds. The best replacement phenomena between carbonate and silicate minerals are recorded in some of the most calcite-rich, calc-silicate marble, as exemplified by sample number GM-290b (analysis 5, table 10). A relatively silica deficient, calc-silicate marble (17.8 weight percent SiO_2), this rock contains a composite actinolite, diopside-salite (trace), quartz, and sphene assemblage which shows excellent textural relations documenting multiple crystallization events. The earliest assemblage seems to have been calcite-diopside-salite. Then, medium-grained, approximately 2.0-mm-across crystals of calcite show incipient patchy replacement by early, pale-apple-green (Z) actinolite. Reaction fronts between unreplaced calcite and partially replaced calcite are exceptionally sharp, and they seem to be confined to select crystals of calcite scattered through the rock rather than defining planes cutting across the calcite's crystal boundaries. Further, alined fine-grained crystals of less strongly pleochroic actinolite (and thus probably more magnesian, see Deer, Howie, and Zussman, 1963) define foliae through the calc-silicate marble by their strong preferred dimensional orientation. Increased abundances of the fine-grained crystals of actinolite are concentrated mostly peripheral to lensoid clots of

finely crystalline quartz. In addition, there is some dimensional orientation of calcite in these domains. In some of the more heavily retrograded calc-silicate marbles, and also more siliceous than sample GM-290b, carbonate has been completely replaced by an assemblage of zoisite and clinozoisite, chlorite, white mica (possibly chloritoid), sphene, and quartz, and including relict plagioclase and various opaque minerals in trace amounts.

Some calc-silicate marble contains garnet as one of its diagnostic minerals. Isotropic garnet, probably rich in the grossular molecular end member, in these calc-silicate marbles typically includes medium-grained crystals of dioside-salite, a relation suggesting crystallization of diopside-salite preceded crystallization of garnet. Where foliated, the schistosity is confined primarily to the quartz and calcite-rich domains of the rock. Minor accessories include sphene and slightly rounded crystals of zircon.

Some pods of calc-silicate minerals in generally migmatitic gneiss sequences of rock show the development of zoned reaction rims with an adjoining pelitic schist. These reaction rims are millimeter sized, and they developed probably by a predominantly diffusion-dominant process (see Vidale, 1969; Hewitt, 1973; Vidale and Hewitt, 1973; for discussion of diffusion phenomena). Where the pelitic schist has not apparently reacted with the enclosed carbonate-rich pods, the pelitic schist contains a typical biotite-quartz-plagioclase (about An_{45})-apatite-opaque mineral assemblage (Zone I, fig. 24). However, within about 13 mm of the approximate original boundary between the pelitic schist and the carbonate-rich rock, the first mineralogical changes begin to occur. These changes are (1) the sporadic nucleation of newly crystallized clinozoisite that either envelopes an opaque mineral (probably magnetite) or occurs very close to an opaque mineral, (2) a marked decrease in the average maximum dimension of biotite from about 0.5 mm in Zone I to about 0.12 mm in Zone II; and (3) a progressive decrease in the grain size of biotite and a concomitant increase in the modal abundance of largely untwinned plagioclase (approximately An_{50}). The boundary of Zone II on the side of the calc-silicate pod is placed at the point of final disappearance of biotite. However, a bladed opaque mineral, which is most likely ilmenite, appears initially about two-thirds of the way into Zone II and continues through Zone III; the ilmenite disappears finally about one-quarter of the way through Zone IV (fig. 24). A weakly pleochroic amphibole in Zone III, probably tremolite-actinolite, occurs as stubby crystals that have an overall

Q, quartz; pl, plagioclase; bi, biotite; op, opaque mineral; ap, apatite; wm, white mica; zr, zircon; Tr, trace; cz, clinozoisite; trem-act, tremolite-actinolite; sph, sphene; cc, carbonate, mostly calcite; gr, garnet, completely isotropic; zo, zoisite; epi, epidote; ilm, opaque mineral, bladed habit, probably ilmenite

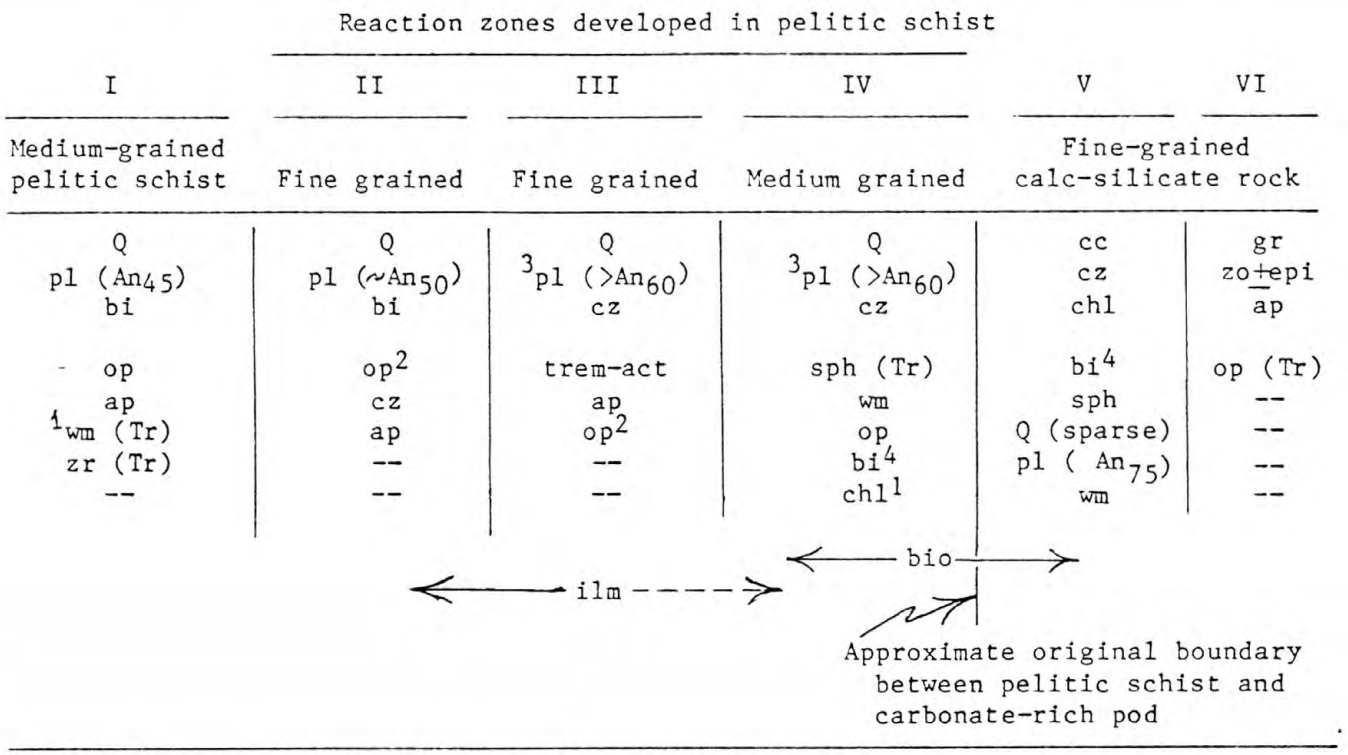

[1]Retrograde.
[2]Includes both bladed and equant varieties; probably ilmenite and mostly magnetite, respectively.
[3]Mostly untwinned plagioclase.
[4]Altered mostly to chlorite.

Figure 24. Schematic diagram of the sequence of mineral assemblages developed in zones near the contact between medium-grained biotite pelitic schist and fine-grained calc-silicate rock.

shredded aspect and make up about 10 to 15 volume percent of the zone. From the specific mineral assemblage and modal composition of Zone III, we infer it as having the lowest K_2O content of the three reaction zones (II-IV) developed in rock that formerly had the same overall bulk composition as the unreacted pelitic schist. Relative to Zones III and VI, there are increased abundances of the phyllosilicates biotite (now mostly retrograded to chlorite) and white mica in Zones IV and V, and this increase is confined mostly to a domain near the original approximate boundary between pelitic rock and carbonate-rich rock. The modal concentration of sphene is highest in Zone I, on the carbonate side of the original boundary between the carbonate and pelitic rocks. Thus all these relations above suggest that the following chemical changes, occurred across the pelitic-carbonate contact during metamorphism: (1) a depletion of potassium in the pelitic rocks immediately adjacent to the carbonate, (2) a concomitant flow of calcium from the carbonate out into the pelitic rock, (3) possibly a fixation of some of the potassium released from the pelitic rock into biotite and white mica along the original boundary between pelite and carbonate, and (4) a possible flow of titanium from the breakdown of biotite into the recrystallizing carbonate. Vidale (1969) documented experimentally the differential movement of potassium, calcium, and magnesium across juxtaposed pelite and carbonate assemblages. However, in her experiments potassium and calcium moved away from the carbonate. Thus, the nucleation of newly grown biotite and white mica in Zones IV and V (fig. 24) most likely refects circulation of a second pulse of fluids primarily along the former pelitic schist and calc-silicate contact.

Zone VI contains a relatively simple composite assemblage consisting of isotropic garnet, zoisite and (or) epidote, sparse apatite, and an opaque mineral in trace amounts (fig. 24). The garnet apparently replaced mostly the fine-grained intergrowths of clinozoisite, calcite, and chlorite of Zone V. Further, the crystallization of garnet appears to have overstepped that of zoisite because crystals of zoisite typically have been enveloped by a primarily grain-boundary-controlled growth of garnet. The garnet-zoisite assemblage in Zone VI is similar to assemblages in zoned calc-silicate rocks in kyanite grade regionally metamorphosed rocks described by Vidale (1969).

Small bodies of skarn, measuring several meters across, crop out sporadically in many of the Proterozoic metamorphic and igneous units of figure 2. Generally, the skarn consists of discontinuous layers of coarse

intergrowths of garnet, dark fibrous amphibole, and quartz; or garnet, epidote, and quartz with or without pyrite and calcite. Locally, some skarn has been prospected for scheelite (tungsten), and scheelite crystals as coarse as 2.5 cm in maximum dimension occur in podlike masses of skarn which are related probably to nearby, thin, pegmatite dikes (loc. no. 25, table 11).

Proterozoic Igneous and Meta-igneous Rocks

Proterozoic X igneous and meta-igneous rocks in the districts range widely in size and include leucogranite (Xl), gneissic granodiorite (Xgg), feldspathic gneiss (Xfg), biotite monzogranite (Xm), leucocratic quartz monzonite (Xlm), porphyritic monzogranite (Xpm), and granodiorite (Xgd) (fig. 2). In addition, varying proportions of igneous and metasedimentary rock combine to yield a variety of migmatitic rocks in the exposed basement of the districts. The most widely exposed migmatitic rocks are along the western lower flanks of Garnet Mountain. Furthermore, there is another igneous rock in the districts that we presume to be Proterozoic Y in age; this is scattered undeformed diabase as dikes, sills, and small intrusive masses. In addition to small bodies of all of these Proterozoic igneous rocks, the gneiss also includes locally some prominently exposed hornblende-biotite orthogneiss that has the composition of monzonite (fig. 25).

Leucogranite

Masses of gneissic leucogranite (unit al of Blacet, 1975) range in size from several-centimeter-wide stringers parallel to compositional layering in the gneiss to the 1-km-long sill that crops out about 3 km northeast of the Cyclopic mine. This sill strikes north-south and dips to the west, roughly conformable with foliation in the surrounding gneiss (Xl, fig. 2). On the south, the sill of leucogranite appears to be truncated by the large mass of gneissic granodiorite that crops out in the Gold Basin district. Throughout the gneiss, the fabrics of individual bodies of leucogranite texturally may grade from coarse-grained granitoid to pegmatitic, containing potassium feldspar phenocrysts up to 8 cm across. In addition, leucogranite ranges from relatively undeformed to intensely mylonitized rock. Although mylonitized coarse-grained leucogranite is generally conformable with its surrounding rocks, locally it cuts amphibolite and garnetiferous gneiss. Nonetheless, the two diagnostic overall features of the Proterozoic X leucogranite are (1) its sill-like concordant relation with the gneiss, and (2) its commonly gneissic to even intensely mylonitic fabric. In addition, many of these leucogranite

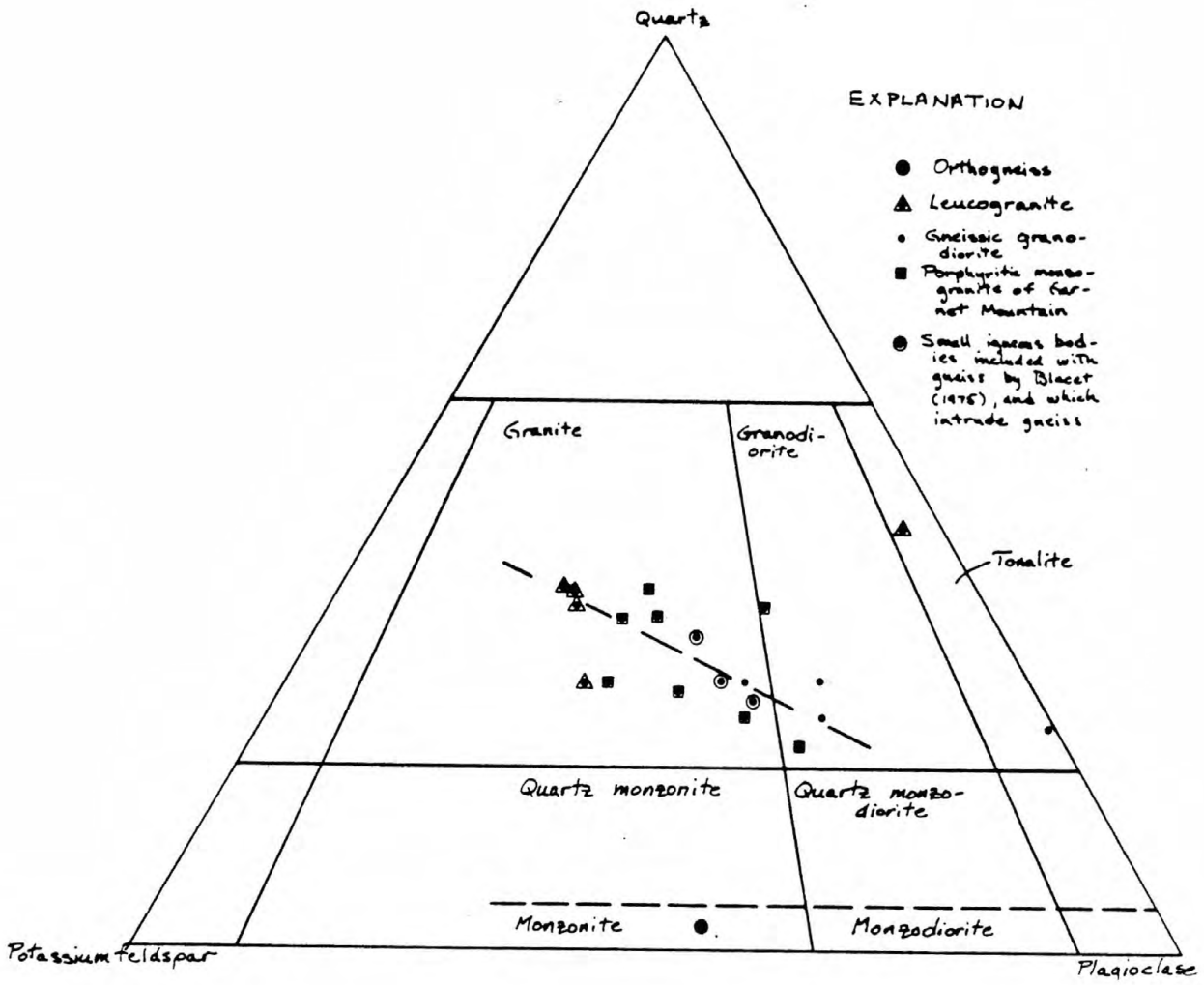

Figure 25.--Ternary diagram showing modes of Proterozoic igneous and metaigneous rocks from the Gold Basin-Lost Basin mining districts. Data from table 12. Compositional fields from Streckeisen and others (1973).

sills contain bluish-gray, highly vitreous quartz which occurs in wispy segregation lenses. Northeast of the Gold Hill mine, large sills of pegmatitic leucogranite increase in abundance, and eventually grade into complexes of highly deformed migmatitic leucogranite (unit mal of Blacet, 1975). These complexes include swarms of leucogranite, aplite, and pegmatite dikes, together with pegmatoid quartz veins, all cutting gneiss. All of the relations indicate that initial emplacement of leucogranite into gneiss occurred during the intense ductile deformation of the gneiss. Although we infer the mapped body of leucogranite to be older than all other Proterozoic igneous rocks, some leucogranite in the Proterozoic terrane probably was emplaced penecontemporaneous with all other Proterozoic X igneous rocks here. Garnetiferous gneissic leucogranite, which ranges widely in grain size, locally becomes very strongly foliated and mylonitic near some minor tungsten (scheelite) prospects. It appears that this tungsten mineralization may be Proterozoic in age. In addition, the pink garnet in some of the leucogranite is concentrated near the walls of the leucogranite, especially where the leucogranite is in contact with biotite- or garnet-rich gneiss. Plots of modal data (table 12) for five samples of leucogranite show that all samples but one fall within the compositional field of granite (fig. 25). That one sample plots within the compositional field for tonalite.

Gneissic Granodiorite

A N. 25° E.-trending, elongate body of Proterozoic X medium-grained gneissic granodiorite crops out across approximately 10 km^2 in the Gold Basin district (fig. 2; unit ggd of Blacet (1975). The southernmost exposures of the gneissic granodiorite body crop out about 2 km northeast of the Cyclopic mine. The gneissic granodiorite apparently intrudes gneiss and some leucogranite, and is in turn intruded by Proterozoic X porphyritic monzogranite of Garnet Mountain and Proterozoic Y diabase, and presumably even younger pegmatitic leucogranite and gold-bearing veins. Some samples of typical gneissic granodiorite contain approximately 25 to 30 volume percent quartz and plot in the compositional field for granodiorite (fig. 25). However, other samples show wide-ranging alkali feldspar to plagioclase proportions yielding modal compositions that fall in the granite and tonalite compositional fields. Mafic minerals, mostly biotite, make up about 20 volume percent of the rocks. Plagioclase (approximately An_{20}) generally is altered intensely to white mica$\pm$carbonate$\pm$clinozoisite assemblages, whereas the

Table 12. Modal data for Proterozoic igneous and meta-igneous rocks from the Gold Basin-Lost Basin mining districts

	Total points counted	Quartz (volume percent)	Potassium feldspar (volume percent)	Plagioclase (volume percent)	Mafic minerals (volume percent)	Comments	Location
Proterozoic igneous and meta-igneous rocks							
GM-98 --------	1,468.	37.3	38.4	22.7	1.6	Foliated leucogranite dike in mixed granodioritic complex	NE1/4 sec. 15, T. 28 N., R. 16 W.
GM-98a -------	1,609.	38.8	38.2	20.4	2.6	Porphyritic leucogranite inclusion in sample 98 showing 3 cm crystals of potassium feldspar	Do.
GM-126a ------	3,535.	19.6	22.2	34.5	23.6	Biotite-hornblende granite of unit (Xgn)	NW1/4 sec. 24, T. 28 N., R. 16 W.
GM-638z ------	1,798.	2.2	33.4	40.	24.4	Orthogneiss included in gneiss unit (Xgn) of Gold Hill mine, T. 29 N., R. 18 W.	Approximately 1.7 km west-northwest
GM-824 -------	1,479.	39.1	38.4	21.4	1.	Garnet-bearing pegmatoid leucogranite in gneiss unit (Xgn)	SW1/4 sec. 4, T. 27 N., R. 18 W.
GM-830 -------	1,344.	21.4	24.9	49.8	3.9	Aplite dike, shallow dipping, presumably cogenetic with Xpm unit	NW1/4 sec. 4, T. 27 N., R. 18 W.
GM-848 -------	1,726.	24.3	16.2	40.7	18.8	Biotite granodiorite, slightly porphyritic, locally gneissic, in gneiss (Xgn)	NW1/4 sec. 3, T. 27 N., R. 18 W.
GM-874 -------	1,790.	22.6	21.1	32.7	23.7	Gneissic granite in gneiss (Xgn); presumably correlative with gneissic granodiorite (Xgd)	NE1/4 sec 23, T. 30 N., R. 19 W.
GM-893 -------	1,338.	21.1	21.2	35.1	22.6	Granite in gneiss (Xgn)	NW1/4 sec. 29, T. 28 N., R. 18 W.
GM-894 -------	1,660.	28.9	41.6	28.2	1.3	Leucogranite dike, 10 m thick, cutting gneiss (Xgn)	SW1/4 sec. 29, T. 28 N., R. 18 W.
GM-927 -------	1,767.	28.6	28.5	39.2	3.8	Gneissic granite in gneiss unit (Xgn)	NE1/4 sec. 17, T. 28 N., R. 18 W.
GM-945a ------	1,850.	20.7	17.5	42.2	19.6	Gneissic granodiorite (Xgd)	SE1/4 sec. 21, T. 28 N., R. 18 W.
GM-1000 ------	1,427.	20.7	.4	61.9	17.	Gneissic tonalite variant of gneissic granodiorite unit (Xgd)	NE1/4 sec. 21, T. 28 N., R. 18 W.
GM-1027 ------	1,086.	32.7	28.5	27.8	11.	Porphyritic biotite granite of porphyritic monzogranite (Xpm)	NE1/4 sec. 16, T. 30 N., R. 18 W.
GM-1051 ------	1,425.	33.6	28.6	35.1	2.7	Granite in gneiss unit (Xgn)	SE1/4 sec. 15, T. 29 N., R. 19 W.
GM-1063 ------	1,398.	44.6	3.9	48.1	3.4	Undeformed garnet-bearing leucogranite dike cutting gneiss (Xgn)	NE1/4 sec. 3, T. 28 N., R. 16 W.
GM-1081 ------	1,602.	27.2	32.8	36.8	3.1	Porphyritic granite from migmatite terrane (unit Xm)	SW1/4 sec. 33, T. 29 N., R. 17 W.

potassium feldspar is remarkably fresh and includes both microcline and perthitic varieties. Accessory minerals are sphene, apatite, and opaque minerals. Gneissic granodiorite may be a mafic, less siliceous variety of igneous rock more or less isochronous with feldspathic gneiss (Xfg, fig. 2).

Numerous shallow prospect pits and mine workings occur scattered throughout the gneissic granodiorite. However, the eastern contact of the gneissic granodiorite with the surrounding gneiss appears to have acted as a very important conduit for the circulation of fluids associated with gold mineralization. Prospects and productive mines, including the Malco mine in the SE1/4 sec. 21, T. 28 N., R. 18 W., are especially concentrated along an approximately 2-km-strike-length of this contact.

Feldspathic Gneiss

Proterozoic X feldspathic gneiss crops out in an approximately 5-km-long and 0.8-km-wide sliver bounded by faults in the southern part of the Lost Basin range (fig. 2; unit fgn of Blacet, 1975). These faults include both deep-seated mylonitic structures and shallow-seated structures marked by gouge. Generally, the feldspathic gneiss is light gray to light pinkish gray, fine-to medium-grained, and it has a compositionally homogeneous, and strongly lineated fabric. The feldspathic gneiss contains few mafic schlieren and inclusions. Locally, foliation in the feldspathic gneiss is highly contorted, and near the northern margins of the sliver, the attitude of foliation gradually converges with the mylonitic rock that occurs along its contact with the surrounding gneiss. The gneiss, just west of the western boundary fault of the feldspathic gneiss, contains abundant slickensides and short discontinuous shear zones, as well as iron-oxide staining and increased abundances of chlorite.

The feldspathic gneiss is cut by quartz-feldspar veins, some of which are gold-bearing, and sparse occurrences of syenitic aplite. Prospect pits, and abandoned shafts and adits are especially abundant near the northern end of the feldspathic gneiss. Generally, these workings follow copper (chalcopyrite, chrysocolla, malachite), lead (galena), and native gold shows along quartz plus yellow-brown carbonate veins. In places, the veins are about 0.5 m thick, and they attenuate down dip to stringers of about 1 to 2 cm thick. No indications of copper, lead, or gold mineralization were found to be associated with the syenitic aplite (P. M. Blacet, unpub. data, 1967-1972), although the pits dug on some of the outcrops of syenitic aplite include

quartz and orange-brown carbonate vein material, and clear crystalline calcite.

Biotite Monzogranite

Three bodies of equigranular to sparsely porphyritic, Proterozoic X biotite monzogranite are mapped in the Garnet Mountain quadrangle: (1) an approximately 1 km^2 east-west-trending mass near Rattlesnake Spring, which is about 5 km southeast of Garnet Mountain; (2) an approximately 0.1 km^2 body, about 2 km southwest of Rattlesnake Spring; and (3) a north-south trending, dikelike mass which has been traced discontinuously for about 4.5 km in the southern part of the Gold Basin district (fig. 2; unit qm of Blacet (1975)). The biotite monzogranite is in contact mostly with porphyritic monzogranite of Garnet Mountain. Age relations between the biotite monzogranite and porphyritic monzogranite of Garnet Mountain cannot be established conclusively because their contact typically is not exposed and can be located only within about 10 m. Nonetheless, the porphyritic monzogranite of Garnet Mountain near the contact is altered more than the biotite monzogranite, and the porphyritic monzogranite of Garnet Moutain also contains narrow, discontinuous cataclastic or protoclastic zones. Near Rattlesnake Spring, however, the biotite monzogranite is associated spatially with moderately abundant rose quartz-bearing pegmatite and other pegmatite. Some similar pegmatites occur definitely as inclusions in the adjoining porphyritic monzogranite of Garnet Mountain (P. M. Blacet, unpub. data, 1967-1972), relations from which we infer the biotite monzogranite may be older than the porphyritic monzogranite of Garnet Mountain. In addition, the biotite monzogranite is intruded by small numbers of diabase dikes, some of which also include leucocratic differentiates.

The biotite monzogranite which crops out in the southern part of the Gold Basin district is a rather homogeneous light-gray body, and shows only minor variability in overall composition and in igneous fabric. The biotite monzogranite is mostly a fine-grained rock, ranging typically between 0.5 and 1.0 mm in average grain size. Regardless, some facies of this rock in places become medium grained and contain euhedral potassium-feldspar phenocrysts up to 8 cm in their long dimension, and sparse quartz phenocrysts up to 1.5 cm across. Other rocks are foliated. Thin sections of six representative samples of fine-grained biotite quartz monzonite show predominantly equigranular hypidiomorphic granular textures, and minor porphyritic, seriate,

and glomeroporphyritic textures. Modally, these rocks would plot in the compositional field of granite, using the classification of Streckeisen and others (1973). Some phenocrystic quartz, perhaps 1 to 2 percent by volume, is aggregated into approximately 2.5 mm wide clots. Primary biotite (dark brown, Z) makes up typically about 5 to 10 volume percent, and it has been altered sparingly to chlorite with or without epidote. Plagioclase (mostly An_{15-20}) shows varying degrees of replacement by white mica and epidote. The intensity of replacement is highest adjacent to Cretaceous(?) episyenitic rocks which largely developed from the biotite monzogranite. Potassium feldspar, mostly microcline but including also some untwinned but perthitic varieties, is generally quite fresh. Minor accessories include apatite, sphene, and opaque minerals. Locally pyrite is disseminated in the biotite monzogranite where it is intergrown with coarsely crystalline, anhedral fluorite.

The biotite monzogranite which crops out in the southern Gold Basin district hosts numerous fluorite-bearing, quartz-carbonate veins, some of which contain visible gold. In addition, this body of biotite monzogranite also is cut by several very small masses of Cretaceous(?) episyenite, one of which near the eastern edge of the biotite quartz monzonite contains fluorite and disseminated gold (Blacet, 1969; see below).

Chemical data on three representative samples of biotite monzogranite from the Gold Basin district are presented in table 13. The major-element analyses are generally similar to the "average" granite of LeMaitre (1976), also listed in table 13 for comparison. However, these three samples of biotite monzogranite are richer in K_2O than the "average" granite of LeMaitre (1976), and the samples are also lower in Na_2O. The average of total alkalis (sum of K_2O and Na_2O) in the three samples is 8.3 weight percent, and this value is close the 7.75 value for total alkalis in the "average" granite of LeMaitre (1976). Minor elements in the three samples of biotite monzogranite appear generally to be typical of those commonly associated with granitic rocks. However, there are some exceptions. The contents of fluorine in the biotite monzogranite appear to be atypically high, 0.07 to 0.45 weight percent (table 13). However, the bulk of the fluorine may have been introduced during the development of episyenite sometime during the Cretaceous (see below). The estimates by Vinogradov (1962) and Turekian and Wedepohl (1961) for the abundance of minor elements in granitic rocks suggest low calcium granites and felsic granites and granodiorites to contain 4.0 and 0.5 ppm cerium

Table 13. Analytical data of Proterozoic X biotite monzogranite

[Chemical analyses of 1 and 2 by rapid-rock methods; analysts, P. L. D. Elmore and S. Botts. Methods used are those described in Shapiro and Brannock (1962), supplemented by atomic absorption, and Shapiro (1967). Spectrographic analyses of 1 and 2 by Chris Heropoulos. Results are reported to the nearest number in the series 1., 0.7, 0.5, 0.3, 0.2, 0.15, 0.1, 0.07, etc., which represent approximate midpoints of interval data on a geometric scale. The precision of a reported value is approximately plus or minus one series interval at 68 percent confidence or two intervals at 95 percent confidence. Looked for but not found: Ag, As, Au, B, Bi, Cd, Mo, Ni, Pd, Pt, Sb, Sn, Te, U, W, Zn, Hf, In, Li, Re, Ta, Th, Tl, Pr, Sm, Eu. Chemical analysis of sample 3: major oxides by X-ray spectroscopy; J. S. Wahlberg, J. Taggart and J. Baker, analysis; partial chemical analyses by standard methods; P. R. Klock and J. Riviello, analysts. Spectrographic analyses of sample 3 by Judith Kent. Looked for but not found Ag, As, Au, Bi, Cd, Sb, Sc, W, Ge, In, Re, Tl, and Hg; —, not detected; n.d., not determined]

	1	2	3	4
Field number	GM-19	GM-19c	79GM12	
Chemical analyses (weight percent)				
SiO_2	72.9	70.7	72.9	71.3
Al_2O_3	14.	14.	13.4	14.32
Fe_2O_3	1.4	2.1	2.15	1.21
FeO	1.4	2.	1.05	1.64
MgO	.10	.40	.36	.71
CaO	1.2	2.4	.85	1.84
Na_2O	2.6	2.6	2.54	3.68
K_2O	5.6	5.5	6.08	4.07
H_2O^+	.68	.74	.64	.64
H_2O^-	.04	.08	.06	.13
TiO_2	.35	.51	.31	.31
P_2O_5	.07	.14	.06	.12
MnO	.06	.06	.04	.05
CO_2	<.05	.05	.06	.05
F	.15	.45	.07	n.d.
Cl			.004	
S			.17	
Subtotal	100.6	101.7	100.74	100.07
Less O = F	.06	.19	.03	n.d.
Total	100.54	101.51	100.71	n.d.
Semiquantitative spectrographic analyses (weight percent)				
B	—	—	0.0007	n.d.
Ba	0.07	0.15	.026	n.d.
Be	.0003	.0003	.0007	n.d.
Co	—	.0005	.0003	n.d.
Cr	.0003	.0007	.0002	n.d.
Cu	.0001	.0003	.0002	n.d.
La	.02	.02	.024	n.d.
Mo	—	—	.0003	n.d.
Nb	.003	.003	.0054	n.d.
Pb	.007	.007	.0058	n.d.
Sc	.0005	.001	—	n.d.
Sn	—	—	.0008	n.d.
Sr	.015	.03	.0013	n.d.
V	.001	.002	.0015	n.d.
Y	.003	.007	.0036	n.d.
Zr	.02	.03	.002	n.d.
Zn	—	—	.02	n.d.
Ce	.05	.05	.047	n.d.
Ga	.002	.002	.0019	n.d.
Yb	.0003	.0007	.0003	n.d.
Nd	.015	.015	—	n.d.
C.I.P.W. norms (weight percent)				
Q	33.7	29.7	32.8	29.06
c	2.	1.	1.5	.92
or	32.9	31.9	35.7	24.5
ab	21.9	21.6	21.4	31.13
an	4.4	7.4	3.0	8.04
en	.25	.98	.89	[1]3.37
fs	.94	1.2	—	n.d.
mt	2.	3.	2.	1.75
hm	—	—	.8	—
il	.66	.95	.59	.58
ap	.17	.33	.14	.28
fr	.29	.88	.13	n.d.
pr	—	—	.32	—
cc	—	.11	.14	.12
Total	99.2	99.	99.4	99.75
Salic	94.9	91.6	94.4	93.65
Femic	4.3	7.4	5.	6.1
D.I.	88.5	83.3	89.9	84.24

[1]Hypersthene.

1. Biotite monzogranite, fine grained, SE1/4 sec. 27, T. 28 N., R. 18 W.
2. Biotite monzogranite, medium grained, slightly porphyritic; SE1/4 sec. 27, T. 28 N., R. 18 W.
3. Biotite monzogranite, medium grained, SE 1/4 sec. 27, T. 28N., R. 18W
4. Granite, average of 2,485 analyses, from LeMaitre (1976).

respectively. The three samples of biotite monzogranite show cerium contents of 50 ppm (table 13). Thus, this body of biotite monzogranite may be more fractionated than the average granite.

Leucocratic Monzogranite

The bulk of the Proterozoic X leucocratic monzogranite (unit lqm of Blacet (1975)) crops out as discontinuous, lensoid masses across a 4-km-wide and 12-km-long belt that trends N. 20-25° W. along the western front of Garnet Mountain (fig. 2). Two other very small exposures of leucocratic monzogranite crop out near the intersection of Grapevine Wash with the Grand Wash Cliffs at the eastern edge of the Garnet Mountain quadrangle. The leucocratic monzogranite probably has a total outcrop area of about 5 to 6 km^2, and much of the leucocratic monzogranite occurs within the more widespread porphyritic monzogranite of the Garnet Mountain. Contacts between leucocratic monzogranite and the porphyritic monzogranite of Garnet Mountain locally are quite sharp and the transition between the two rock types can occur across 8 to 10 cm. Elsewhere, the contact is gradational across approximately 0.5 m. Further, there is an increased abundance of potassium feldspar phenocrysts in the leucocratic monzogranite nearest the porphyritic monzogranite. Although the actual contact between these two rocks may be highly irregular in detail at the scale of a single outcrop, the overall attitude of the contact maintains a generally northwest strike. In addition, the potassium-feldspar phenocrysts, which are concentrated on the leucocratic monzogranite side of the contact with porphyritic monzogranite of Garnet Mountain, also are commonly oriented with their long dimensions trending northwesterly. Locally, where the contact between these rocks is well exposed, offshooting dikes of porphyritic monzogranite of Garnet Mountain definitely cut leucocratic monzogranite, and in places both rocks are cut in turn by fine-grained dikes of granite. On the other hand, some exposures of the contact between leucocratic monzogranite and porphyritic monzogranite of Garnet Mountain show complexly mixed flowage structures involving both rocks. These relations suggest that initial emplacement of the leucocratic monzogranite to the levels currently exposed was followed very closely by intrusion of the porphyritic monzogranite of Garnet Mountain--so closely that the leucocratic monzogranite in places probably was only partially crystalline. We infer initial emplacement of the leucocratic monzogranite to predate somewhat the biotite monzogranite.

The leucocratic monzogranite in outcrop is typically a light-yellowish-gray rock which most commonly is medium-grained, hypidiomorphic granular in overall texture. Compositionally, these rocks are granite, and generally they are nonporphyritic although they can grade into slightly porphyritic, micropegmatitic varieties. Partly chloritized, dark-red-brown (Z) biotite makes up less than 5 volume percent of the equigranular varieties. In addition, very fine granules of opaque mineral(s) are concentrated in chlorite which replaces the earlier primary biotite, whereas primary opaque mineral(s) (probably magnetite mostly) are relatively sparse and somewhat coarser grained than the secondary, opaque mineral(s). Plagioclase (An_{15-25}) makes up 30 to 40 volume percent of the rocks, and it is moderately clouded by a dense intergrowth of clay mineral(s), white mica, and sparse epidote. Potassium feldspar is relatively fresh with patches of microcline twinning, which is concentrated usually in the cores of the potassium feldspar crystals. The potassium feldspar also includes irregularly developed bead perthite. Myrmekite is developed sparsely along potassium feldspar-plagioclase grain boundaries. Primary quartz makes up about 20 to 25 volume percent of the leucocratic monzogranite and in some samples the primary quartz hosts relatively abundant and prominent fluid inclusions. These fluid inclusions are concentrated along secondary and pseudosecondary annealed microfractures through the primary quartz. At room temperature, the fluid-inclusion population consists of a two-phase liquid-rich type, a three-phase type containing liquid carbon dioxide, and a third type which contains from one to three nonopaque daughter minerals. One of these daughter minerals is undoubtedly halite and another is probably sylvite. The third daughter mineral is highly birefringent and shows equant to rod-shaped habits. Heating and freezing tests were not performed on these samples from the leucocratic monzogranite (see below). However, the relative proportions of the daughter minerals in many of the inclusions suggests that highly saline, carbon dioxide-rich fluids containing up to approximately 60 weight percent NaCl equivalent at some time must have circulated through some of the leucocratic monzogranite.

The leucocratic monzogranite contains locally some narrow 1- to 2-m-wide zones of very well foliated gneissic rock of roughly the same composition as the nonfoliated, equigranular leucocratic monzogranite. These zones crop out near contacts between leucocratic monzogranite and porphyritic monzogranite of

Garnet Mountain, and the attitude of the zones parallels closely the attitude of the contact between the two rocks. The foliation is defined principally by (1) a preferred concentration of stubby crystals of dark-brown (Z) biotite into highly discontinuous, 0.2-mm-wide lepidoblastic domains, and by (2) a preferred dimensional orientation of highly strained, ribboned quartz. The fact that these zones are extremely fresh (the biotite is not chloritized, and the plagioclase is not clouded) suggests the zones may have been generated protoclastically.

Pegmatite in the leucocratic monzogranite previously has been prospected for sheet mica, as exemplified by the M.P. Mica mine, which occurs in the SE1/4 sec. 26, T. 28 N., R. 17 W. (see loc. nos. 138-139, table 11). At several places in the general area of the M.P. Mica mine, muscovite books occur in approximately N. 10° W.-striking, discontinuous pegmatite dikes and lenses. These dikes and lenses range from 2 to 5 m in width. The pegmatite shows well-developed quartz cores, and it includes some sparse concentrations of red-brown garnet near its margins with the leucocratic monzogranite.

Porphyritic monzogranite of Garnet Mountain

The porphyritic monzogranite of Garnet Mountain (unit pqm of Blacet, 1975), crops out in three main areas in the districts: (1) east of Hualapai Valley and east of Grapevine Mesa, near the Grand Wash Cliffs, (2) near the northwestern corner of the area, in the White Hills, and (3) in the southern White Hills near the southwestern corner of the area where it hosts several of the gold-bearing quartz veins (fig. 2). The largest exposed body of the porphyritic monzogranite crops out east of Hualapai Valley, roughly centered on Garnet Mountain itself. Here the porphyritic monzogranite is the principal rock unit exposed in an area of about 60 km^2. Several northwest-striking dikes and irregularly shaped small bodies of diabase intrude the porphyritic monzogranite in this general area. The porphyritic monzogranite is overlain unconformably by the Lower Cambrian Tapeats Sandstone about 4 km east of Garnet Mountain, and, at Iron Mountain, about 5 km northeast of Garnet Mountain, both the porphyritic monzogranite and the diabase are capped unconformably by flat-lying rocks including the Tapeats Sandstone, Tertiary gravel, and Tertiary basalt. From Garnet Mountain, the porphyritic monzogranite can be traced to the north in fairly continuous exposure where it crops out in progressively smaller areas east of Grapevine Mesa and in the low hills leading to the Grand Wash Cliffs. Near the northwestern corner of the

area, the porphyritic monzogranite crops out in three irregularly shaped bodies which total approximately 5 km^2 in area. Fanglomeratic sequences of the Tertiary Muddy Creek Formation, the Pliocene-Miocene Hualapai Limestone Member of the Muddy Creek Formation, Tertiary ancestral Colorado River deposits (not delineated separately on fig. 2), and various types of Quaternary unconsolidated deposits all rest unconformably on some part of these three bodies of porphyritic monzogranite. As mapped in the southern White Hills, the porphyritic monzogranite crops out in an approximately 10 km^2 area that is roughly triangular shaped. Its maximum inferred dimension at the surface is about 6 km in an approximately N. 40° E. direction.

The age of emplacement of the porphyritic monzogranite was established by Wasserburg and Lanphere (1965) to be about 1,660 m.y. using the potassium-argon method and rubidium-strontium techniques. Samples of porphyritic monzogranite and pegmatite were obtained by them from several localities in the SW1/4 sec. 27, T. 28 N., R. 16 W., near the Boyd Tenney Ranch in the Quartermaster Canyon SW 7-1/2-minute quadrangle. These localities are approximately 3.2 km, north-northeast of the southeast corner of the Garnet Mountain quadrangle, and from them, the porphyritic monzogranite can be traced continuously to Garnet Mountain itself. Hornblende from a sample of porphyritic monzogranite, described by Wasserburg and Lanphere (1965) as "coarse-grained biotite-hornblende monzogranite characterized by abundant microcline phenocrysts", yielded a potassium-argon age of 1,630 m.y. The initial Sr^{87}/Sr^{86} ratio for the porphyritic monzogranite is 0.702. Abundant dikes of pegmatite cut the porphyritic quartz monzonite and the metamorphic rocks, which include garnet-biotite-potassium feldspar gneiss and diopside-hornblende gneiss, at these localities. Comprehensive analytical results on various minerals from these pegmatites plot on a well-defined isochron of 1,660 m.y. showing an initial Sr^{87}/Sr^{86} ratio equal to 0.704 (Wasserburg and Lanphere, 1965). Apparently, plutonism here of about 1,660 m.y. forms part of a northeast-trending magmatic arc that ranges in age from 1,610 to 1,700 m.y. (Silver and others, 1977). Such plutonism in the districts occurred well within a broad Proterozoic province of 1.72- to 1.80-b.y. (billion-year) -old, apparently supracrustal rock, and this plutonism may reflect magmatism associated with the accretion of another 1.65- to 1.72-b.y.-old terrane outboard to the southeast (Condie, 1982).

The characteristic feature of the porphyritic monzogranite of Garnet Mountain is conspicuous, abundant, large potassium feldspar phenocrysts. The phenocrysts are typically pinkish gray to pale pinkish cream, and they are set in a light-pinkish-gray, coarse-grained hypidiomorphic granular groundmass. Many exposures of porphyritic monzogranite show tabular phenocrysts up to 10 cm long. Textures elsewhere in the porphyritic monzogranite are predominantly subporphyritic seriate and such rocks show an almost continual gradation in size of euhedral potassium feldspar phenocrysts from about 1.5 cm to 10 cm in their long dimension (fig. 26A). In addition, some of the potassium feldspar phenocrysts show evidence of partial rounding. Generally in the porphyritic monzogranite, near its contact with the leucocratic monzogranite, tablets of phenocrystic potassium feldspar show a well-developed preferred orientation. Where oriented, the phenocrysts are alined with their long axes parallel to the general strike of the contact. In addition, the phenocrysts are also parallel roughly to dimensionally oriented schlieren and inclusions of leucocratic monzogranite. However, the border zone of the porphyritic monzogranite is not everywhere typified by alined phenocrysts of potassium feldspar. Locally, in the Gold Basin district this border zone between porphyritic monzogranite and gneiss is marked by a prominent display of randomly oriented blocks of included biotite-rich and garnet-bearing schist and gneiss. Nonetheless, the contact between gneiss and porphyritic monzogranite is conformable generally with the trend of foliation in the gneiss as exemplified by relations in sec. 29, T. 28 N., R. 18 W. Yet on a scale of a large outcrop, the contact between porphyritic monzogranite and gneiss cuts the schistosity in the gneiss at a high angle and there is no evidence for shearing along the contact. In places, the contact can be located to within about 1 cm. Elsewhere in the Gold Basin district, the porphyritic monzogranite becomes very distinctly porphyritic as its contact with the surrounding schist and gneiss is approached. In such border areas, the porphyritic monzogranite includes both euhedral and ovoid phenocrysts that may or may not be mantled by plagioclase. However, such rapakivi textures are not restricted exclusively to widespread exposures of the porphyritic monzogranite. In the Gold Basin mining district (fig. 2), the porphyritic monzogranite also includes some irregularly shaped areas approximately 0.1 to 0.2 km^2 in size, too small to show on the map, which consist of mixtures of porphyritic monzogranite and gneiss. In some exposures within these areas,

Figure 26.--The porphyritic monzogranite of Garnet Mountain. A, Large microcline phenocrysts in somewhat seriate-textured, porphyritic monzogranite in the southern White Hills; NW1/4 sec. 34, T. 28 N., R. 18 W.; B, Microcline mantled by rims of myrmekite (note relations at head of arrow) in a rapakivi dikelike mass which cuts a pendant of mostly biotite gneiss within porphyritic monzogranite in the southern White Hills. The feldspars crystallized largely in a matrix of gneiss. (See fig. 27, A and B for larger scale view of microcline-myremekite relations.) Scale is 18 cm long; C, Pegmatite-cored pod occurring as an inclusion in porphyritic monzogranite in the SW1/4 sec. 20, T. 218 N., R. 16 W. Note rock hammer in center of photo for scale.

A

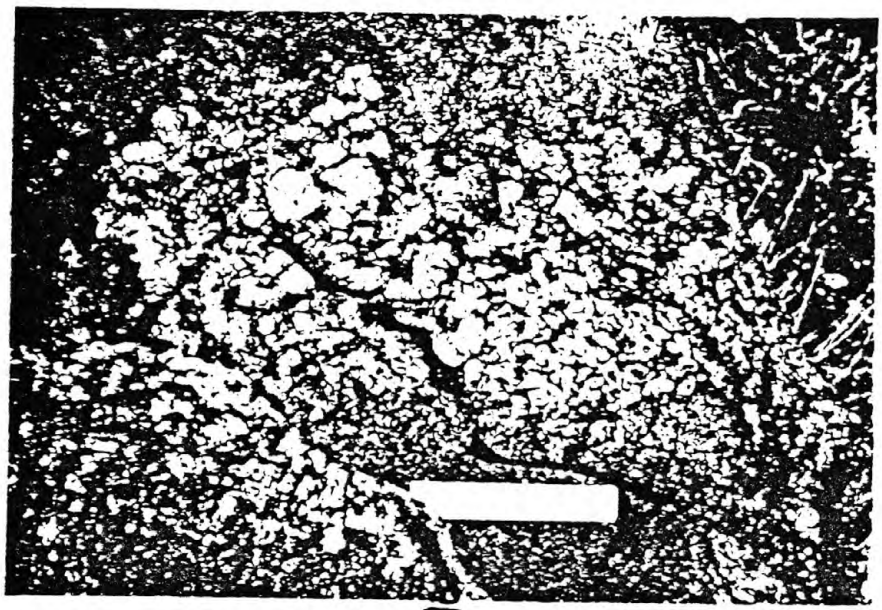

B

C

large crystals of apparently completely mantled microcline are very common (fig. 26, B), and they define irregularly bounded, dikelike masses of rock whose matrix is mostly biotite-epidote gneiss. In addition, these areas of mixed rock, which undoubtedly are very close to a local "roof" of the porphyritic monzogranite, also contain quartz-cored, graphic-granite pegmatite probably associated genetically with the porphyritic monzogranite. However, relatively deep seated portions of the porphyritic monzogranite in the general area of Garnet Mountain also contain pegmatite. Some of this pegmatite is earlier than porphyritic monzogranite owing to the pegmatite's occurrence as pods totally engulfed by subsequently crystallized porphyritic monzogranite (fig. 26C).

In thin section, the large porphyroblastic crystals of mantled potassium feldspar are seen to consist of twinned microcline, which is mantled by approximately 2.0- to 2.0-mm-wide rims of oligoclase-dominant myrmekite (fig. 27,A). The rims of these microcline porphyroblasts also host some crystals of albite. In places, optically continuous microcline extends through the rims and is in contact with the biotite-epidote gneiss. Further, such microcline also engulfs very small fragments of biotite-epidote gneiss, and shows no development of a rim of myrmekite between the fragment and the microcline. Although myrmekite and rapakivi textures are difficult to interpret (see Smith, 1974), textural relations in these samples (fig. 27A, B) suggest that the mantles are a postmicrocline phenomenon, and thus possibly reflect a simultaneous coupling of (1) calcium migration toward the microcline, and (2) subsolidus exsolution of sodium-rich plagioclase.

In thin section, the porphyritic monzogranite of Garnet Mountain shows an extremely varied fabric (fig. 27C-F). Although most of the groundmass of fresh porphyritic monzogranite is hypidiomorphic granular, even the least deformed hornblende-biotite porphyritic facies (C) and biotite equigranular facies (D) of this unit show minor amounts of postcrystalline strain exemplified by mildly bent biotite cleavage lamellae, and undulose quartz. Nonetheless, plagioclase, generally in the range An_{35} to An_{40}, in much of the porphyritic monzogranite is quite fresh, showing only slight alteration to white mica. Some plagioclase is zoned normally, and includes rims as sodic as oligoclase, An_{20-25}. In addition, hornblende (typically blue-green (Z)) and biotite locally are remarkably fresh, especially in the porphyritic monzogranite cropping out in the general area of Garnet Mountain. Although the

Figure 27.--Photomicrographs showing textural relations in gneiss immediately adjacent to porphyritic monzogranite, and in the porphyritic monzogranite itself. Crossed nicols. A, Microcline, mantled by myrmekite, showing porphyroblastic development in a matrix of biotite-epidote gneiss. From a pendant engulfed by porphyritic monzogranite in the southern White Hills. H, hole in thin section; M, mantle of myrmekite; B, Myrmekite microveining microcline across and along twin planes in the microcline. Sample same as A; C, Porphyritic monzogranite showing only slight evidence of deformation, including bent biotite crystals and a slight ribboning and undulosity of quartz (Q). Plagioclase (P) is andesine(An_{40}) and partly altered to white mica. Mafic minerals are clustered tightly into mostly hornblende-biotite aggregates (hb). Optically unzoned microcline phenocrysts (M) include flakes of biotite (B) and possibly titaniferous magnetite (mag). Sample number GM-50, same as analysis number 6, table 14; D, Equigranular biotite monzogranite facies of the porphyritic monzogranite. K, perthitic microcline; P, plagioclase (An_{35}). Includes accessory allanite, sphene, magnetite, apatite, zircon, and sparse secondary white mica. Sample number GM-70, same as analysis number 7, table 14; E, Porphyritic monzogranite deformed during the greenschist metamorphism of the area. Plagioclase (P) is partly altered to epidote and white mica. All primary biotite is replaced by chlorite (C). Perthitic potassium feldspar (K) is microveined by chlorite and epidote (C+E) and by other veins showing quartz-chlorite-white mica-epidote assemblages. Large crystals of sphene (S) are broken, veined, and altered partly to leucoxene. Accessory minerals in the rock include relatively large crystals of allanite (A). Sample GM-29 from approximately 1 km north of Iron Mountain; F, Intensely deformed porphyritic monzogranite. Crosshatch-twinned potassium feldspar (K) is veined by white mica, epidote, and quartz. Epidote-rich groundmass (G) also contains chlorite, white mica, and quartz. Fairly large crystals of sphene (S) are altered heavily to leucoxene and are veined by chlorite, quartz, epidote (Trace), and white mica. Sparse plagioclase (P) in rock partly is altered to white mica. Allanite (A) is accessory. Sample GM-29a, locality same as E.

A

B

C

D

E

F

most conspicuous potassium-feldspar in these rocks is perthitic microcline, the range in size of these crystals is quite wide. The size of perthitic microcline in the groundmass of much of the porphyritic monzogranite seems to decrease with decreasing abundance of microcline in the rock. Accessory minerals in the porphyritic monzogranite include zircon, apatite, allanite, sphene, and various opaque minerals. Very minor accessory minerals, found to occur sporadically in the porphyritic monzogranite, are pyrite and rutile.

Although the exposed levels of the porphyritic monzogranite of Garnet Mountain were not deformed syntectonically with the early upper-amphibolite facies metamorphism of the area, some of the porphyritic monzogranite has been deformed intensely during the retrograde greenschist event. Porphyritic monzogranite, for example, which crops out about 1 km north of Iron Mountain shows an intensely crushed and chlorite-rich metamorphic overprint (fig. 27E, F). The intense deformation of these greenish-gray rocks is indicated by their bent, kink-banded plagioclase (oligoclase-andesine, about An_{30}); and the replacement of all primary biotite by chlorite and secondary sphene. These foliae in turn show neocrystallization of even later, minute, undeformed porphyroblasts of greenish biotite, which have grown with their {001}-cleavage-lamella-traces at high angles to the foliation defined by chlorite. Large crystals of primary sphene in the rocks are also broken, veined, and altered to leucoxene. The large, up to 2 cm long, crystals of perthitic potassium-feldspar are brecciated, cut by microveinlets of quartz, epidote, chlorite, and white mica; and replaced by patches of deformation-related albite.

Petrographic studies reveal the unmetamorphosed porphyritic monzogranite has modal compositions which range from monzogranite to granodiorite (fig. 25). Most of these modally analyzed samples, however, plot in the compositional field of monzogranite; only two of the samples plot in the field of granodiorite, very close to the field of monzogranite. The color index of the porphyritic monzogranite ranges from about 5 to about 24 (tables 12 and 14).

Modal content of potassium feldspar in the samples of porphyritic monzogranite is among the highest of the Proterozoic X igneous rocks in the districts (fig. 25). This relation may be interpreted to be the result of differentiation. Projection of this trend line toward the quartz-plagioclase sideline suggests differentiation away from a region close to the plagioclase

Table 14. Analytical data from the Proterozoic X porphyritic monzogranite of Garnet Mountain.

[Chemical analyses by rapid-rock methods; analysts, P. L. D. Elmore and S. Botts. Methods used are those described in Shapiro and Brannock (1962), supplemented by atomic absorption; and Shapiro (1967). Spectrographic analyses by Chris Heropoulos. Results are reported to the nearest number in the series, 1., 0.7, 0.5, 0.3, 0.2, 0.15, 0.1, 0.7, and so on, which represent approximate midpoints of interval data on a geometric scale. The precision of a reported value is approximately plus or minus one series interval at 68 percent confidence or two intervals at 95 percent confidence. Looked for but not found: Ag, As, Au, B, Bi, Cd, Mo, Ni, Pd, Pt, Sb, Sn, Te, U, W, Zn, Hf, In, Li, Re, Ta, Th, Tl, Pr, Sm, Eu. —, not detected; n.d., not determined]

	1	2	3	4	5	6	7	8	9	10	11
Field number	GM-34	GM-553	GM-562	GM-566	GM-573	GM-50	GM-70	GM-120			
Chemical analyses (weight percent)											
SiO_2	71.6	71.9	69.8	69.4	70.8	64.4	70.4	67.7	69.5	71.30	72.2
Al_2O_3	14.1	14.3	13.8	14.2	13.8	15.4	14.6	14.3	14.3	14.32	13.8
Fe_2O_3	1.4	1.7	2.3	2.4	1.2	2.	1.6	2.1	1.8	1.21	1.9
FeO	2.2	1.2	2.1	2.4	2.3	4.7	3.3	3.5	2.7	1.64	1.5
MgO	.60	.40	.80	.80	.50	1.2	1.1	.80	.78	.71	.29
CaO	1.9	1.	2.2	2.6	1.5	4.	2.5	3.	2.3	1.84	1.5
Na_2O	2.5	2.5	2.8	2.8	2.9	2.6	2.5	2.8	2.7	3.68	2.6
K_2O	5.2	6.1	4.9	4.6	5.	4.	3.3	4.2	4.7	4.07	5.7
H_2O^+	.84	1.4	1.	1.	1.	.70	.77	.66	.92	.64	.69
H_2O^-	.06	.04	0.7	.02	.04	.03	.06	.04	.05	.13	.06
TiO_2	.60	.39	.62	.74	.52	1.3	.74	.95	.73	.31	.39
P_2O_5	.23	.17	.28	.30	.24	.50	.15	.36	.28	.12	.09
MnO	.00	.00	.09	.08	.03	.09	.00	.09	.05	.05	.05
CO_2	.08	.15	.11	<.05	<.05	.05	.06	.15	.10	.05	.06
F	.12	.06	.14	.13	.17	n.d.	n.d.	n.d.	.12	n.d.	.22
Subtotal	101.43	101.31	101.01	101.47	100.	100.97	101.08	100.65	101.03	100.07	101.05
Less O = F	.05	.03	.06	.05	.07	n.d.	n.d.	n.d.	.05	n.d.	.13
Total	101.38	101.28	100.95	101.42	99.93	100.97	101.08	100.65	100.98	100.07	100.92
Semiquantitative spectrographic analyses (weight percent)											
Ba	0.15	0.1	0.2	0.15	0.1	0.2	0.15	0.2	n.d.	n.d.	n.d.
Be	.00015	—	.0002	.0002	.0003	.0002	.00015	.0002	n.d.	n.d.	n.d.
Co	.0005	.0003	.0007	.0007	.0005	.001	.0007	.001	n.d.	n.d.	n.d.
Cr	.0007	.0005	.0007	.0007	.0005	.001	.003	.001	n.d.	n.d.	n.d.
Cu	.0003	.00015	.0007	.001	.0005	.001	.0015	.0015	n.d.	n.d.	n.d.
La	.015	.015	.005	.02	.015	.007	.02	.01	n.d.	n.d.	n.d.
Nb	.0015	.0015	.002	.003	.002	.003	.002	.002	n.d.	n.d.	n.d.
Ni	—	.0002	—	.0002	—	.0005	.001	.0003	n.d.	n.d.	n.d.
Pb	.003	.007	.002	.002	.005	.0015	.003	.002	n.d.	n.d.	n.d.
Sc	.001	.0005	.0015	.001	.001	.003	.0015	.002	n.d.	n.d.	n.d.
Sr	.05	.02	.03	.03	.02	.07	.03	.05	n.d.	n.d.	n.d.
V	.003	.002	.005	.005	.003	.005	.003	.005	n.d.	n.d.	n.d.
Y	.005	.003	.007	.015	.005	.007	.002	.007	n.d.	n.d.	n.d.
Zr	.02	.02	.05	.03	.03	.03	.03.	.03	n.d.	n.d.	n.d.
Ce	.03	.03	.015	.05	.03	.015	.03	.02	n.d.	n.d.	n.d.
Ga	.002	.003	.002	.002	.002	.003	.002	.002	n.d.	n.d.	n.d.
Yb	.0005	.0002	.0005	.0015	.0005	.001	.0001	.0007	n.d.	n.d.	n.d.
Nd	.01	.015	.01	.02	.015	.015	.015	.015	n.d.	n.d.	n.d.
C.I.P.W. norms (weight percent)											
Q	32.1	31.8	29.5	28.9	30.9	22.7	34.9	27.5	n.d.	29.06	n.d.
c	1.9	2.6	1.1	.87	1.9	.83	2.8	.90	n.d.	.92	n.d.
or	30.3	35.6	28.7	26.8	29.6	23.4	19.3	24.7	n.d.	24.5	n.d.
ab	20.9	20.9	23.5	23.4	24.5	21.8	20.9	23.5	n.d.	31.13	n.d.
an	6.6	2.5	7.5	10.	4.8	16.1	10.9	11.5	n.d.	8.04	n.d.
en	1.5	.98	2.	2.	1.2	3.	2.7	2.	n.d.	[1]3.37	n.d.
fs	1.9	.15	1.1	1.3	2.4	5.	3.4	3.3	n.d.	n.d.	n.d.
mt	2.	2.4	3.3	3.4	1.7	2.9	2.3	3.	n.d.	1.75	n.d.
il	1.1	.73	1.2	1.4	.99	2.4	1.4	1.8	n.d.	.58	n.d.
ap	.54	.40	.66	.70	.57	1.2	.35	.85	n.d.	.28	n.d.
fr	.20	.09	.23	.21	.31	--	--	--	n.d.	n.d.	n.d.
cc	.18	.34	.25	—	—	.11	.14	.34	n.d.	.12	n.d.
Total	99.1	98.5	98.9	98.9	98.9	99.3	99.2	99.3	n.d.	99.75	n.d.
Salic	91.7	93.4	90.3	89.9	91.6	84.8	88.9	88.1	n.d.	93.65	n.d.
Femic	7.4	5.1	8.6	9.	7.3	14.5	10.3	11.2	n.d.	6.1	n.d.
[2]D.I.	83.3	88.3	81.7	79.	85.	67.9	75.1	75.7	n.d.	84.24	n.d.
Modes (volume percent)											
Quartz	34.8	27.8	n.d.	n.d.	30.7	n.d.	n.d.	31.0	n.d.	n.d.	n.d.
Potassium feldspar	27.6	39.2	n.d.	n.d.	29.9	n.d.	n.d.	17.7	n.d.	n.d.	n.d.
Plagioclase	25.7	28.3	n.d.	n.d.	24.3	n.d.	n.d.	33.3	n.d.	n.d.	n.d.
Mafic minerals	12.	4.7	n.d.	n.d.	15.	n.d.	n.d.	18.	n.d.	n.d.	n.d.

[1]Hypersthene.

[2]Differentiation index of Thornton and Tuttle (1960), defined as the total of normative quartz plus normative orthoclase plus normative albite.

1. Porphyritic monzogranite; NW1/4 sec. 16, T. 28 N., R. 16 W.
2. Porphyritic monzogranite, fine-grained border facies.
3. Porphyritic monzogranite, biotite-rich mafic facies.
4. Medium-grained mafic pod in porphyritic monzogranite.
5. Porphyritic monzogranite.
6. Porphyritic monzogranite, hornblende bearing; SE1/4 sec. 12, T. 28 N., R. 17 W.
7. Porphyritic monzogranite; SE1/4 sec. 19, T. 28 N., R. 16 W.
8. Porphyritic monzogranite, in mixed granodioritic complex; NW1/4 sec. 26, T. 28 N., R. 17 W.
9. Average porphyritic monzogranite, from analyses 1-8 of this table, excluding detected values below limits of determination.
10. Granite, average of 2,485 analyses, from LeMaitre (1976).
11. Average biotite monzogranite (from table 13, this report).

corner of the ternary diagram. In addition, most of the samples of Proterozoic X leucogranite analyzed plot near the potassium feldspar-rich domain of the trend line, whereas samples of gneissic granodiorite plot near the plagioclase-rich portions of the trend line. However, a problem is that these modes may not be accurate because of the relatively large size of the potassium feldspar phenocrysts. Another problem is that many phenocrysts may have crystallized initially from a magma that was different from that represented by the matrix of the rocks (see Wilcox, 1979).

Chemical analyses of eight rock samples from the porphyritic monzogranite of Garnet Mountain suggest that the rocks are chemically quite uniform (table 14). These analyses include a sample from a medium-grained, mafic pod (analysis 4) hosted by the porphyritic monzogranite. Contents of SiO_2 in the eight samples range between 64.4 and 71.9 weight percent and they average 69.5 weight percent. The K_2O contents range from 3.3 to 6.1 weight percent, and the Na_2O contents are remarkably consistent, ranging from 2.5 to 2.9 weight percent. The ratio of K_2O to Na_2O ranges from 1.3 to 2.4; the content of K_2O is lowest (3.3 weight percent, analysis 6) in the sample containing the most CaO (4.0 weight percent). This sample (analysis 6) includes significant amounts of hornblende, and the analysis shows also the highest ferrous- to ferric-iron ratio determined, and the lowest content of SiO_2. Relatively mafic phases of the porphyritic monzogranite, exemplified by analysis 8 which is of a rock determined to have a color index of 18, only differ slightly from leucocratic phases (analysis 2, color index 4.7). These differences consist primarily of less SiO_2 and less K_2O, but more total Fe, CaO, and TiO_2. Much of the increased content of TiO_2 reflects probably an increase in the amount of sphene in the rock. Five of the samples of porphyritic monzogranite were analyzed for fluorine; the average content of fluorine is 0.12 weight percent (table 14), and there appears to be a slight correlation between the cerium contents of these samples and their differentiation indices (fig. 28). Generally the analyses of porphyritic monzogranite are very like the "average" granite of LeMaitre (1976), listed in table 14 as analysis 10 for comparison. Similarly, the analyses of porphyritic monzogranite are not much different from the analyses of biotite monzogranite (table 13), the average of which is also listed in table 14 (analysis 11). The "degree of alkalinity" of this suite of rocks from the porphyritic monzogranite and biotite

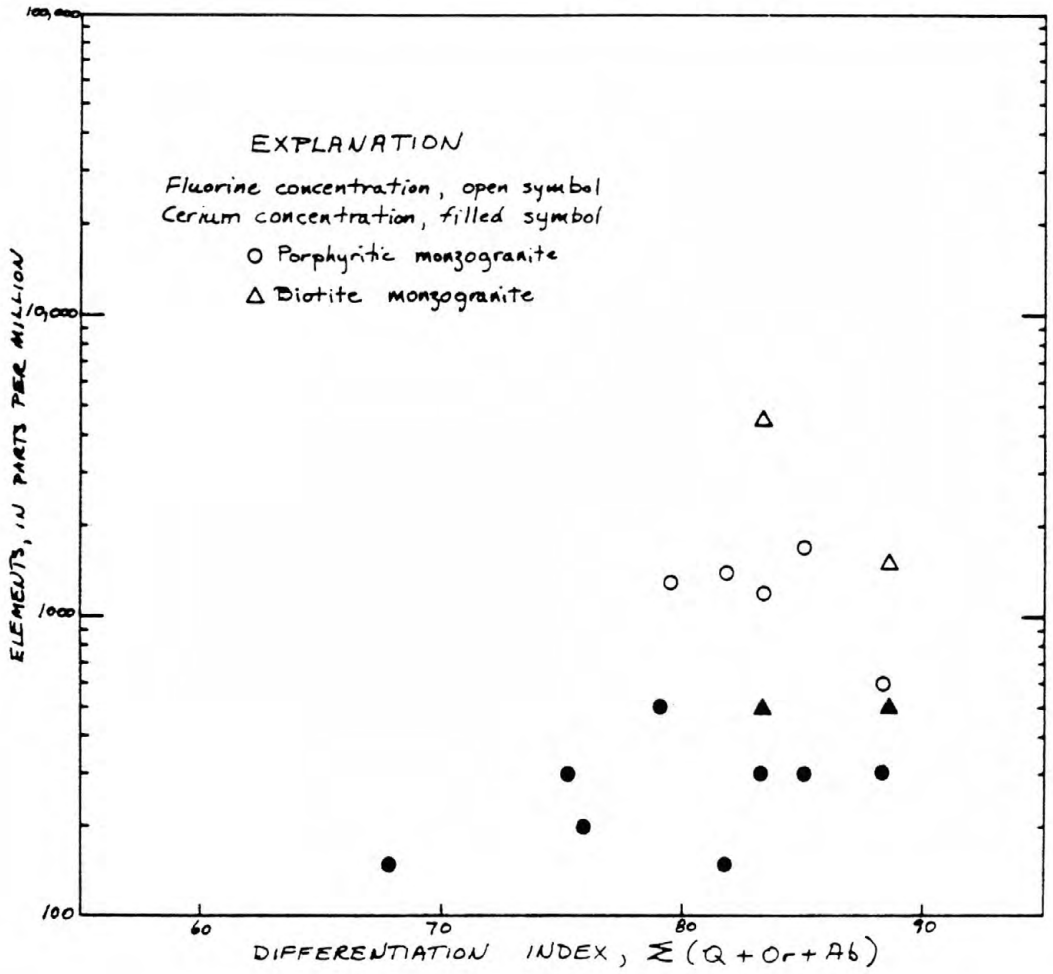

Figure 28.--Plot of fluorine and cerium contents (in ppm) versus the differentiation index, (Q+Or+Ab), of analyzed samples of Proterozoic X porphyritic monzogranite of Garnet Mountain and Proterozoic X biotite monzogranite.

monzogranite, as indicated using the alkali-lime index of Peacock (1931), is calc-alkalic (fig. 29).

The limited number of available analyses of the porphyritic monzogranite preclude our establishing well-documented variation trends. In the AlkFM diagram (fig. 30, A), the trend appears to be away from a region near the F corner to a point along the AlkF sideline, approximately one-third of the distance from the Alk corner. However, the two analyzed samples of biotite monzogranite, which apparently is older than the porphyritic monzogranite, plot near the terminus of such a variation trend. The ACF diagram (fig. 30, B) also shows a poorly developed variation trend projected toward the A corner of the diagram. The AKF diagram (fig. 30, C) shows more scatter than the two preceding diagrams, and suggests a variation trend projected away from the midpoint of the AK sideline. Last, figure 30, D shows normative proportions of Q, Or, and Ab in the analyzed samples from the porphyritic monzogranite and the biotite monzogranite. All these samples contain greater than 80 percent Ab+Or+An+Q; and all but one of the analyses (analysis 6, table 14; a hornblende-rich facies of the porphyritic monzogranite) contain greater than 75 percent Ab+Or+Q. The An contents of all analyzed samples of porphyritic monzogranite and biotite monzogranite, normalized to 100 percent Q+Or+Ab+An, range from 2.8 to 19.2 percent. However, if analysis 6 (table 14) is excluded, the range is 2.8 to 13.2 percent, and the average value of the normalized An contents is 8.2 percent. The normative proportions of Ab, Or, and Q in all but one of the analyzed rocks cluster tightly in an area showing either an increased K_2O/Na_2O relative to a trend line connecting the ternary minima at $P_{H_2O}=P_{total}=1$ kb for contents of An varying from 3 to 7.5, or decreased ratios of Q/(Ab+Or) relative to these minima (fig. 30D). However, this cluster of normative proportions of Ab, Or, and Q coincides with, and apparently is elongated along, the ternary minimum for $P_{H_2O}=P_{total}=2{,}000$ kg/cm^2 projected onto the anhydrous base of the Ab-Or-Q-H_2O tetrahedron determined by Tuttle and Bowen (1958). The plot of these data from the porphyritic monzogranite and biotite monzogranite thus suggests the rocks are highly differentiated, and that they may have crystallized from a magma at $P_{H_2O}=P_{total}=$ about 2 kb. Two assumptions are that (1) the samples analyzed reflect minimum melt compositions (see above, and Anderson and Cullers, 1978), and (2) the magma(s) were saturated with respect to H_2O (Steiner, Jahns, and Luth, 1975). The abundance of aplite dikes and pegmatites associated with the

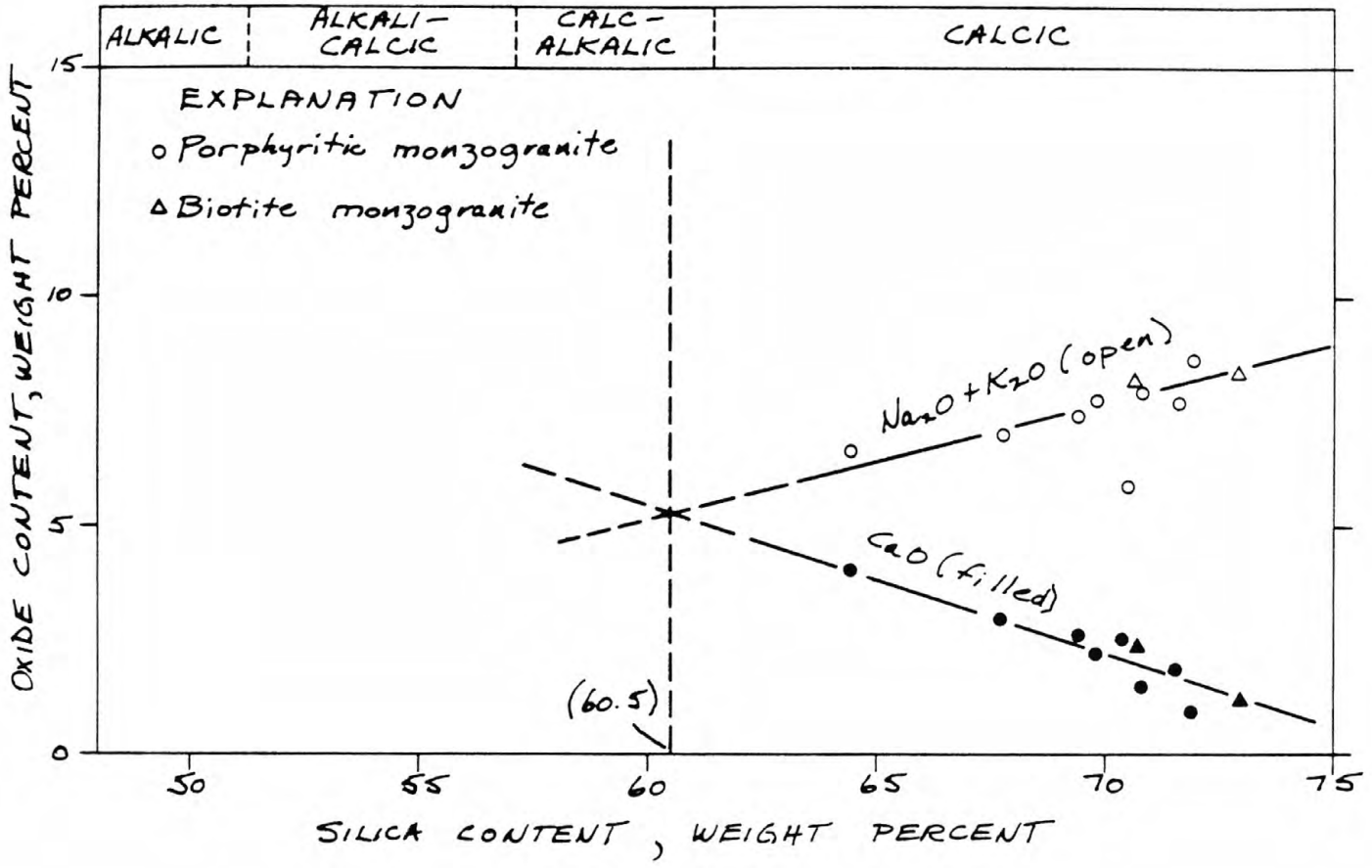

Figure 29.--Weight percent of the total alkalis (K_2O plus Na_2O) and CaO plotted against the weight percent of SiO_2 for analyzed samples of Proterozoic X porphyritic monzogranite and Proterozoic X biotite monzogranite in the general area of the Gold Basin-Lost Basin districts.

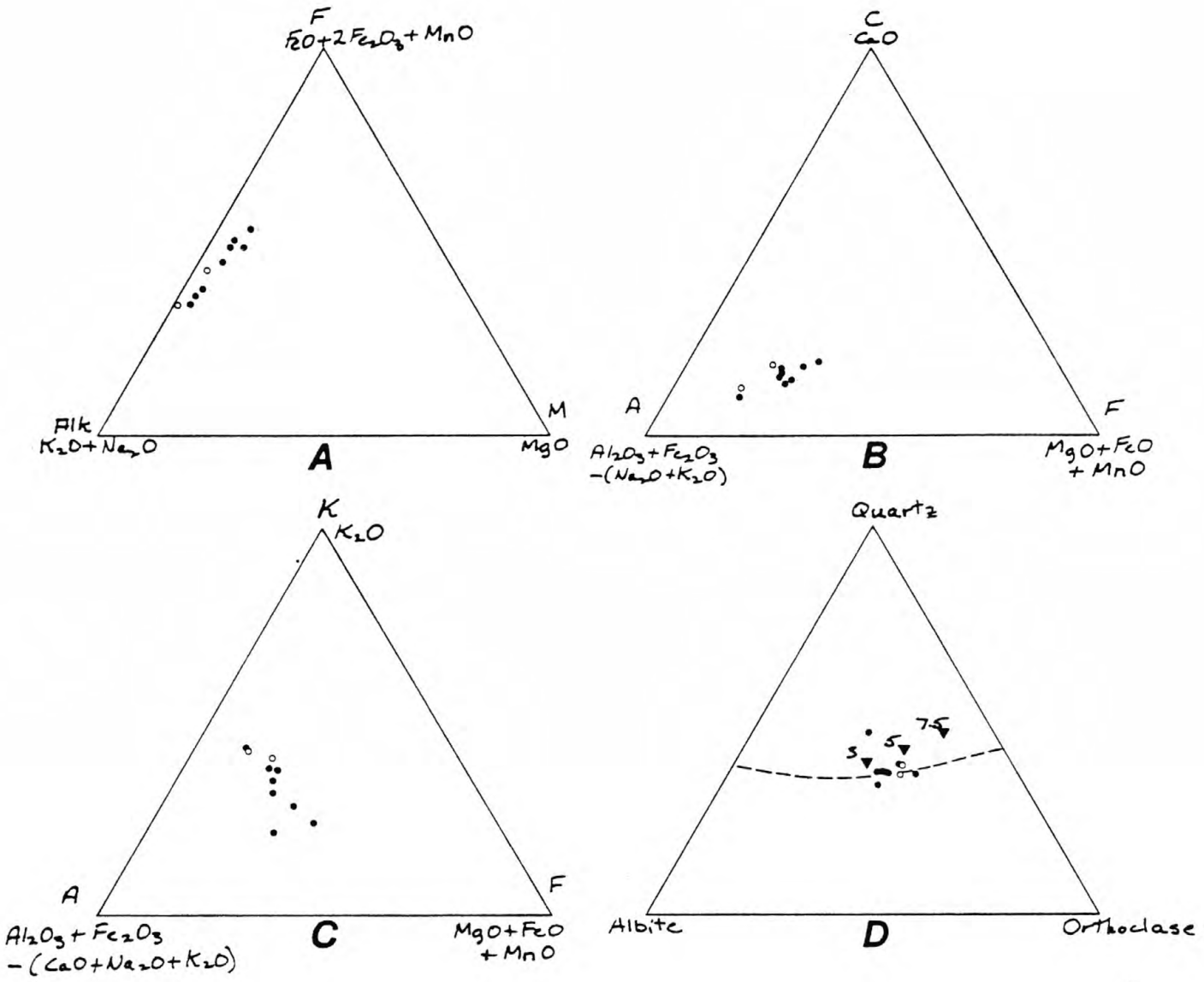

Figure 30.—Ternary chemical and normative diagrams of analyzed Proterozoic X porphyritic monzogranite and biotite monzogranite from the general area of the Gold Basin-Lost Basin mining districts. A, AlkFM diagram; B, ACF diagram; C, AKF diagram; D, Normative proportions of albite, orthoclase, and quartz. Data from tables 13 and 14. Dot, porphyritic monzogranite; open circle, biotite monzogranite. Filled triangles, ternary minimums from James and Hamilton (1969) at the designated weight percent An for $P_{total}=P_{H_2O}=1$ kb. Dashed line, locus of ternary minimum temperatures projected onto the anhydrous base of the Ab-Or-Q-H_2O tetrahedron for $P_{H_2O}=P_{total}=2{,}000$ kg/cm^2 from Tuttle and Bowen (1958).

porphyritic monzogranite and biotite monzogranite suggests their magma(s) were saturated with respect to H_2O (see Luth, 1969), at least during the final stages of their primary crystallization.

Analytical data based on the chemical composition of the Proterozoic X porphyritic monzogranite of Garnet Mountain and Proterozoic X biotite monzogranite in the districts appear to have the characteristics ascribed by Petro, Vogel, and Wilband (1979) to continental magmatic arcs generated at compressional plate boundaries. This relation is especially true when the data from the districts are compared to that for the central Sierra Nevada batholith. These data include from table 14 (1) a more or less unimodal distribution of differentiation indices (total range 67.9 to 88.3), (2) unimodal distributions of normative anorthite (average 28 weight percent), and (3) a calc/alkali index, which is defined as the value of SiO_2 for which $CaO/(Na_2O+K_2O)$ equals 1.00 (Christiansen and Lipman, 1972), greater than 60 (actually 60.5 from fig. 29). The alkali lime Peacock (1931) index for the central Sierra Nevada batholith is 60 (Kistler, 1974). Further, the high K_2O/Na_2O ratios and the high ratio of $(FeO + Fe_2O_3)/MgO$ in these rocks from the Gold Basin--Lost Basin districts suggest the rocks have continental rather than island arc affinities (see Jakes and White, 1972). If these analytical data were to be interpreted using the K-h (K_2O versus depth to the top of a seismic zone) techniques of Dickenson and Hatherton (1967), Hatherton and Dickinson (1969), and Dickinson (1975), a plot of percent K_2O at a projected 57.5 percent SiO_2 for these data would show that the depth inferred to the top of an inclined seismic zone would be anywhere from 160 to 270 km. Such values result from the data for continental margin arcs as modified from Dickinson (1975) by Keith (1978). However, the average dip of seismic zones or subducted slabs associated with compressional continental margins is perhaps 40° (Dickinson, 1975, p. 56). A significant unknown in the region is the position of the paleotrench approximately 1,660 m.y. ago (see Condie, 1982), coupled with the possibility of variably dipping seismic zones (Coney and Reynolds, 1977; Keith, 1978). Further, Wyllie (1981) notes that with increasing depths the composition of magma becomes depleted in SiO_2, and that high-SiO_2 granitic magmas cannot be generated by anatexis of crustal rocks at depths greater than about 30 km.

The porphyritic monzogranite of Garnet Mountain which crops out in the Gold Basin district, in the southern White Hills, hosts several gold-bearing quartz veins. The bulk of these veins strike north-northeast, and they parallel roughly the trend of the mapped bodies of gneissic granodiorite and the biotite monzogranite, which crop out north and east, respectively, of the main mass of porphyritic monzogranite (fig. 2). However, there are a few gold-bearing quartz veins in the porphyritic monzogranite that have northwesterly strikes. One of these veins crops out about 1.5 km south-southeast of the Malco Mine. Another consists of the swarm of veins that made up the deposit at the Cyclopic mine. At the Cyclopic mine, one of the earliest discoveries and the largest overall producer of lode gold in the districts (see above), a northwest-striking swarm of gold-bearing quartz veins was emplaced near a contact between porphyritic monzogranite and metamorphic rocks older than the porphyritic monzogranite (P. M. Blacet, unpub. data, 1967-1972). The dips of these veins are mostly to the northeast, and they range from shallow angles (15° to 25°) to steep (60° to 70°). The ore at the Cyclopic consisted of quartz-vein material, and not the unconsolidated gouge associated with the major Tertiary detachment fault which cuts the porphyritic monzogranite in the general area of the Cyclopic mine (see below). This Tertiary fault dips gently to the southwest. Crushed and brecciated porphyritic monzogranite crops out extensively near the Cyclopic mine, and locally the porphyritic monzogranite is stained highly by iron oxides. The porphyritic monzogranite near here is also sericitized and even strongly silicified in those areas where it is flooded by numerous veins and veinlets. The unconsolidated gouge, which reflects movements along the Tertiary fault, also includes locally several large blocks of vein quartz. In addition, striations and tectonic polish occur on many blocks of porphyritic monzogranite and vein quartz in the fault zone, thus documenting the age of mineralization at the Cyclopic mine as predating movement(s) along the Tertiary fault.

Granodiorite

Gray granodiorite (unit gd of Blacet (1975)) crops out along the western and southwestern flanks of Garnet Mountain as a mafic border facies of the porphyritic monzogranite of Garnet Mountain (fig. 2). The granodiorite occurs both as rather homogeneous, discrete bodies, and also in a unit termed a mixed granodioritic complex by Blacet (1975) which includes mostly granodiorite and

lesser amounts of porphyritic granodiorite and porphyritic monzogranite. All of these rocks are roughly coeval and comagmatic with one another. Contacts between granodiorite and porphyritic monzogranite are gradational. However, the mixed granodioritic complex also includes some of the leucocratic monzogranite, which is definitely older than the granodiorite as indicated by crosscutting relations. Locally, the granodiorite is coarse grained, and it is sparsely porphyritic, including perhaps 20 phenocrysts of potassium feldspar scattered across an exposure of about 0.1 m^2. Mostly, these phenocrysts are set in a coarse-grained hornblende-biotite hypidimorphic granular matrix that is very magnetite rich. Magnetite clots up to about 1.5 cm across are quite common in the granodiorite, and magnetite-rich sands are very characteristic of present-day arroyo bottoms that drain areas underlain by outcrops of granodiorite.

In thin section, samples of the granodiorite are seen to consist of somewhat variable proportions of biotite, hornblende, quartz, plagioclase, and potassium feldspar, and the minor accessory minerals magnetite, apatite, and zircon. Plagioclase is more abundant than potassium feldspar. The major overall texture of some of the medium-grained facies of this unit is hypidiomorphic granular, yet subporphyritic, seriate, and slightly gneissic fabrics are present locally. Figure 31A shows the fabric of a representative sample of medium-grained granodiorite. The color index of the granodiorite ranges from about 10 to about 25, and probably averages about 20. Plagioclase in the equigranular varieties of the granodiorite probably has an anorthite content of about 30 to 35, whereas early-crystallized plagioclase, which is included within some 2 to 3 cm across equant and euhedral phenocrysts of potassium feldspar, has anorthite contents of about 40. In addition, plagioclase in the granodiorite generally is altered sparsely to white mica. Nevertheless, parts of some crystals of plagioclase are almost completely replaced by sheathlike aggregates of white mica and clay mineral(s), with or without traces of clinozoisite and carbonate. Blue-green (Z) hornblende ranges from 0 to perhaps 15 volume percent of the granodiorite. In those facies of the granodiorite that include both hornblende and biotite, the biotite is red-brown (Z), whereas the hornblende-free facies show biotites that are dark brown (Z). Mafic minerals tend to cluster in the granodiorite, and these clusters in places contain very abundant concentrations of apatite (fig. 31B). Some samples of granodiorite show sparse concentrations of 4- to

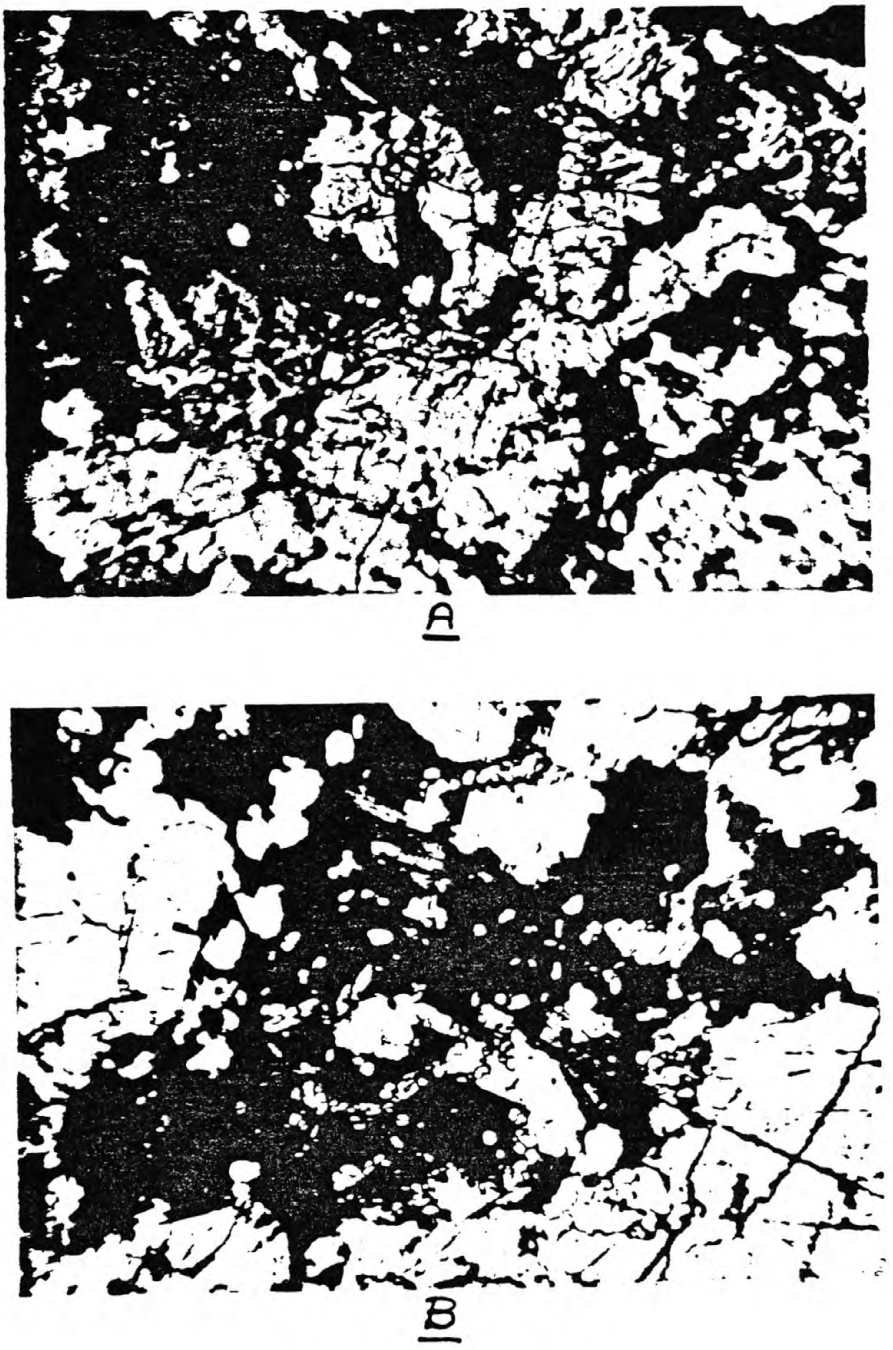

Figure 31.--Photomicrographs showing textural relations in Proterozoic X granodiorite border phase of the porphyritic monzogranite of Garnet Mountain. P, plagioclase; Q, quartz; K, potassium feldspar; B, biotite; H, hornblende. Sample GM-1131; SE1/4 sec. 25, T. 28 N., R. 17 W. A, Overall fabric of a representative sample of granodiorite. Crossed nicols; B, Textural relations among apatite- (A)-rich portions of mafic-mineral dominant domains of the granodiorite. M, magnetite; Z, zircon. Plane polarized light.

5-mm-across ovoid aggregates of polycrystalline, highly stained quartz, possibly reflecting incorporation of some material from the gneiss.

Fluid inclusions are abundant in some of the primary quartz crystals. Isolated, approximately 6 to 10 micron long fluid inclusions are concentrated in subhedral to ovoid crystals of quartz hosted by essentially unaltered phenocrysts of potassium feldspar. Some of these fluid inclusions are very carbon dioxide-rich because at room temperature they show the presence of three phases; the first phase is mostly liquid water, the second liquid carbon dioxide, and the third mostly carbon dioxide vapor. The proportion of liquid carbon dioxide to carbon dioxide vapor is very high, perhaps two or three to one, which suggests a high-trapping pressure at the time of the circulation of these carbon dioxide-rich fluids (see below). Such carbon dioxide-rich fluids are apparently not associated with any gold mineralization in the general area of Garnet Mountain. Nonetheless, we will document below that fluids related to gold mineralization, of both the disseminated and vein variety, contained appreciable amounts of carbon dioxide in the districts.

Diabase

Relatively small masses of fine-grained diabase (unit db of Blacet (1975)) crop out sporadically in the Proterozoic X metamorphic and igneous terranes (fig. 2). The most extensive exposures occur southeast of the Lost Basin district, about 2 km east of Garnet Mountain where an approximately 2- to 3- km-long, northwest-striking dike of diabase cuts porphyritic monzogranite of Garnet Mountain. The bulk of the diabase in and near the districts is undeformed and occurs in thin, planar dikes that crosscut both the igneous fabric of 1,660 m.y. rock, and all structural features in complexly folded metamorphic and migmatitic rocks. In addition, about 4 km north-northeast of the southeast corner of the Garnet Mountain quadrangle, an approximately 10 m thick diabase, dipping about 15° to the northwest, is truncated unconformably by Lower Cambrain Tapeats Sandstone (P. M. Blacet, unpub. data, 1967-1972). This diabase shows excellently developed chilled margins against porphyritic monzogranite. We presume all this undeformed diabase described above to be Proterozoic Y in age, correlative with the diabase of Sierra Ancha, Arizona first dated by Silver (1960) to have a minimum age of 1,075 $\pm$ 50 m.y. and a probable age of 1,200 m.y. or greater, and then further refined by Silver (1973) as having an original age of 1,150 $\pm$ 30 m.y. Nonetheless, there also appears to be some metadiabase in the

Proterozoic X terrane of the districts that is older than 1,150 m.y. Such metadiabase has a superposed metamorphic fabric, is cut sharply by narrow granitic pegmatite, and also very probably cut by coarse-grained, slightly porphyritic, rapakivi-textured granite.

In thin section, undeformed diabase shows typical diabasic textures. Subophitic texture is dominant in its chilled margins wherein normally zoned laths of labradorite (generally An_{55} to An_{60}) are about 0.3 to 0.35 mm in length and are set in a very fine grained matrix of granules of opaque mineral(s) and clinopyroxene. The lower chilled margins of some sills of undeformed diabase also contain rare, discontinuous, wispy, hairline micro-veinlets of blue-green (Z) hornblende and red-brown (Z) biotite. Ophitic texture is dominant in domains of the diabase interior to the chilled margins. Grain size increases to about 0.8 mm about 2 m from the chilled margins, plagioclase is somewhat more sodic, and sporadic crystals of red-brown (Z) biotite form part of the igneous fabric of the diabase. Nonpleocheroic, pale grayish-brown clinopyroxene crystals are coalesced into more or less equant plates enclosing the stout laths of plagioclase. Finally, about 6 m from the chilled margins, some of the freshest samples of undeformed diabase show concentrations of olivine perhaps reaching as much as 10 volume percent. Table 7 includes a chemical analysis of a sample of diabase collected from the main drift of the Golden Gate mine.

Cretaceous Crystalline Rocks

Two-mica Monzogranite

Cretaceous two-mica monzogranite, dated at 72.0 m.y. by the K-Ar method (see above), crops out north-northwest of the Cyclopic mine (fig. 2). This body of rock crops out mostly in the Senator Mountain quadrangle, where Blacet (unpub. data, 1967-1972) shows it to have a maximum inferred surface dimension of about 4.0 km across the trace of the lowermost strand of the low-angle detachment surface. As shown (fig. 2), the largest exposed body of two-mica monzogranite has been faulted against fanglomerate of the Muddy Creek Formation. Further, the two-mica monzogranite in the districts is part of a regionally extensive, inner Cordilleran belt of muscovite-bearing granitic rocks defined recently by Miller and Bradfish (1980) (fig. 32). However, in marked contrast to many of the two-mica granitic rocks along this belt, the two-mica monzogranite in the Gold Basin district does not exhibit pervasive cataclastic or mylonitic fabrics. The two-mica monzogranite, which is fine to

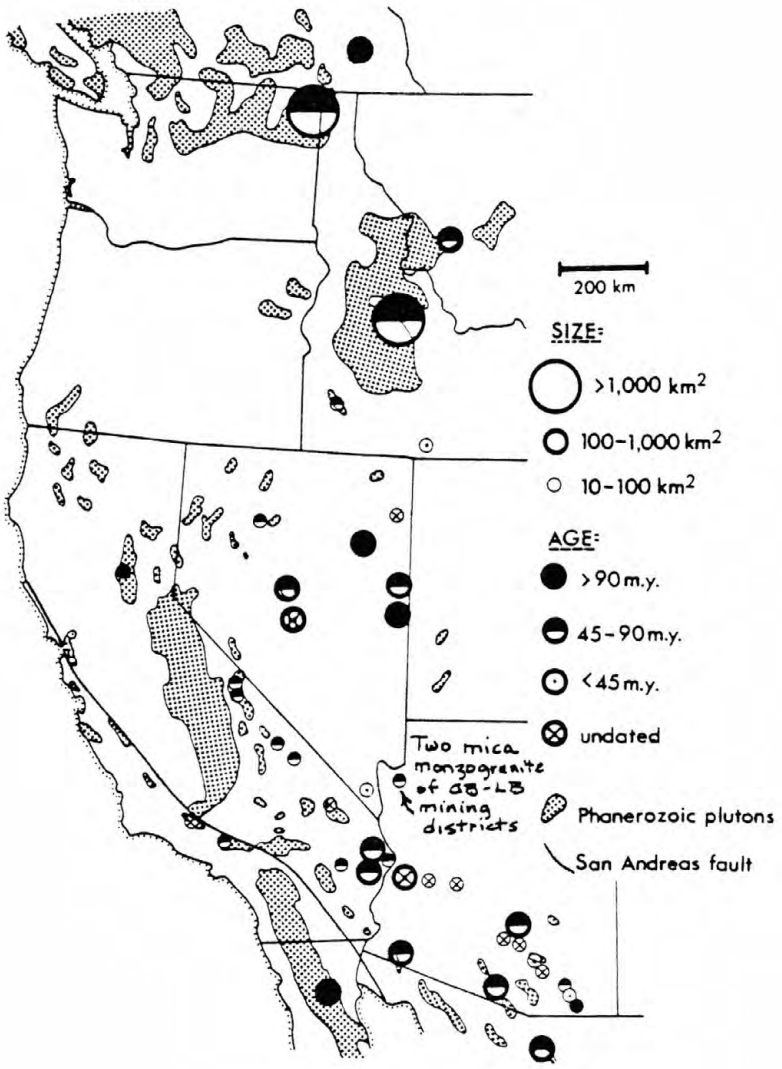

Figure 32.--Occurrences of Phanerozoic muscovite-bearing plutonic rocks in the western United States (modified from Miller and Bradfish, 1980).

medium grained, shows locally sharp contacts with surrounding amphibolitic gneisses. There is no progressive decrease in grain size of the two-mica monzogranite, no increase in the overall abundance of mafic minerals, and apparently no inclusions of wallrock in the vicinity of the contact. The two-mica monzogranite generally has an equigranular fabric, and overall its area of outcrop is remarkably homogeneous lithologically, showing a strong affinity to the compositionally restricted granite series of Pitcher (1979). In some localities, however, the two-mica monzogranite is porphyritic or slightly foliated. The prophyritic variants contain as much as 5 percent quartz phenocrysts that reach sizes of about 5 cm across. The foliated aspect is imparted by a very weakly defined primary layering of dimensionally oriented potassium feldspar and biotite, probably reflecting a flow fabric. Within the main body of the two-mica monzogranite, there are locally sharp contacts between a fine-grained, sparsely porphyritic biotite monzogranite facies and a muscovite biotite monzogranite facies. Close examination of these relations suggests that this muscovite-rich facies of the monzogranite is not a metasomatic replacement of biotite-rich monzogranite.

The two-mica monzogranite contains some syenitic zones. This syenitic rock probably reflects subsolidus episyenitization or fenitization judging from the associated enrichments in muscovite, fluorite, and potassium feldspar and depletion of primary quartz adjacent to local swarms of quartz-, pyrite-, and muscovite-bearing veins. Such veins in places also include some carbonate and fluorite and appear genetically related to the two-mica monzogranite, because the veins cut the two-mica monzogranite and are in places themselves cut by two-mica monzogranite also. Sparse concentrations of chalcopyrite and specular hematite also were noted by Blacet to be associated with some of the veins which cut the two mica monzogranite.

Veins and irregular quartz segregations also appear to be concentrated in gneiss in the general vicinity of the two-mica monzogranite. The irregular quartz segregations are associated spatially with aplite and muscovite-bearing pegmatite, an association giving the appearance that the quartz segregations are also related genetically to the two-mica monzogranite.

The two-mica monzogranite shows clear-cut contact relations with two other lithologies. The two-mica monzogranite is cut by some unmapped Tertiary dikes, one of which is shown in figure 33. Most such dikes are partly chloritized, porphyritic biotite dacite, probably related to the Mount Davis

Figure 33.--Photograph of a composite, partly chloritized, porphyritic biotite dacite Tertiary(?) dike containing a septum of the Cretaceous two-mica monzogranite. Note rock hammer in central part of photograph for scale.

Volcanics. On the southwest, the largest body of two-mica monzogranite is in fault contact with Tertiary(?) fanglomeratic rock of the Muddy Creek Formation. Crude striae are developed on the top most surfaces of unweathered two-mica monzogranite where it was excavated by Blacet (unpub. data, 1967-1972) along the trace of the fault. Further, immediately above the poorly striated pavement of two-mica monzogranite, there is a highly comminuted, 10- to 15-cm-thick zone of red, sandy clay gouge containing clasts less than 1 cm in diameter. Blacet traced this low-angle fault to the southeast where it crops out in the immediate area of the Cyclopic mine, and other nearby areas where it juxtaposes Tertiary(?) fanglomerate and Proterozoic X porphyritic monzogranite of Garnet Mountain (fig. 2).

In all, ten thin sections of the Cretaceous two-mica monzogranite were examined, which reveal a wide range in texture and composition. Modal compositions range from a biotite-free, felsic muscovite granodiorite to muscovite-biotite monzogranite (fig. 34). The samples of muscovite granodiorite are typified by approximately 2.0 mm grain sizes, and well-developed hypidiomorphic granular textures. The muscovite granodiorite includes up to about 47 percent by volume euhedral, tabular crystals of normally zoned plagioclase (oligoclase, An_{15-20}). The plagioclase typically is extremely fresh and shows only sparse dusting by minute crystals of white mica. Some samples, however, show crystallization of 0.2- to 0.4-mm-long books of white mica demonstrably subsequent to crystallization of plagioclase. Biotite in the more common two-mica monzogranite facies of this body of rock is generally a dark brown (Z), showing slight tints of green under the microscope, and the biotite occurs in very wide ranging proportions (from zero to about 10 percent by volume). Quartz is also highly varied in two-mica monzogranite, both texturally and modally. Rare quartz bipyramids were noted in some rocks, but more commonly the quartz occurs in 2-to 3-mm-wide ovoid aggregates of polycrystalline quartz. Such quartz generally is interstitial to plagioclase and potassium feldspar. Potassium feldspar, making up 25 to 35 volume percent of the rocks studied, is extremely fresh, and shows the well-developed cross hatch twinning of microcline. Some potassium feldspar crystals poikilitically include numerous oriented crystals of oligoclase (fig. 35A). Minor accessory minerals include zircon, opaque minerals (both equant and prismatic varieties), rutile (in places clustered in books of white mica, and elsewhere as needles in quartz) and rare garnet. Some extremely sparse,

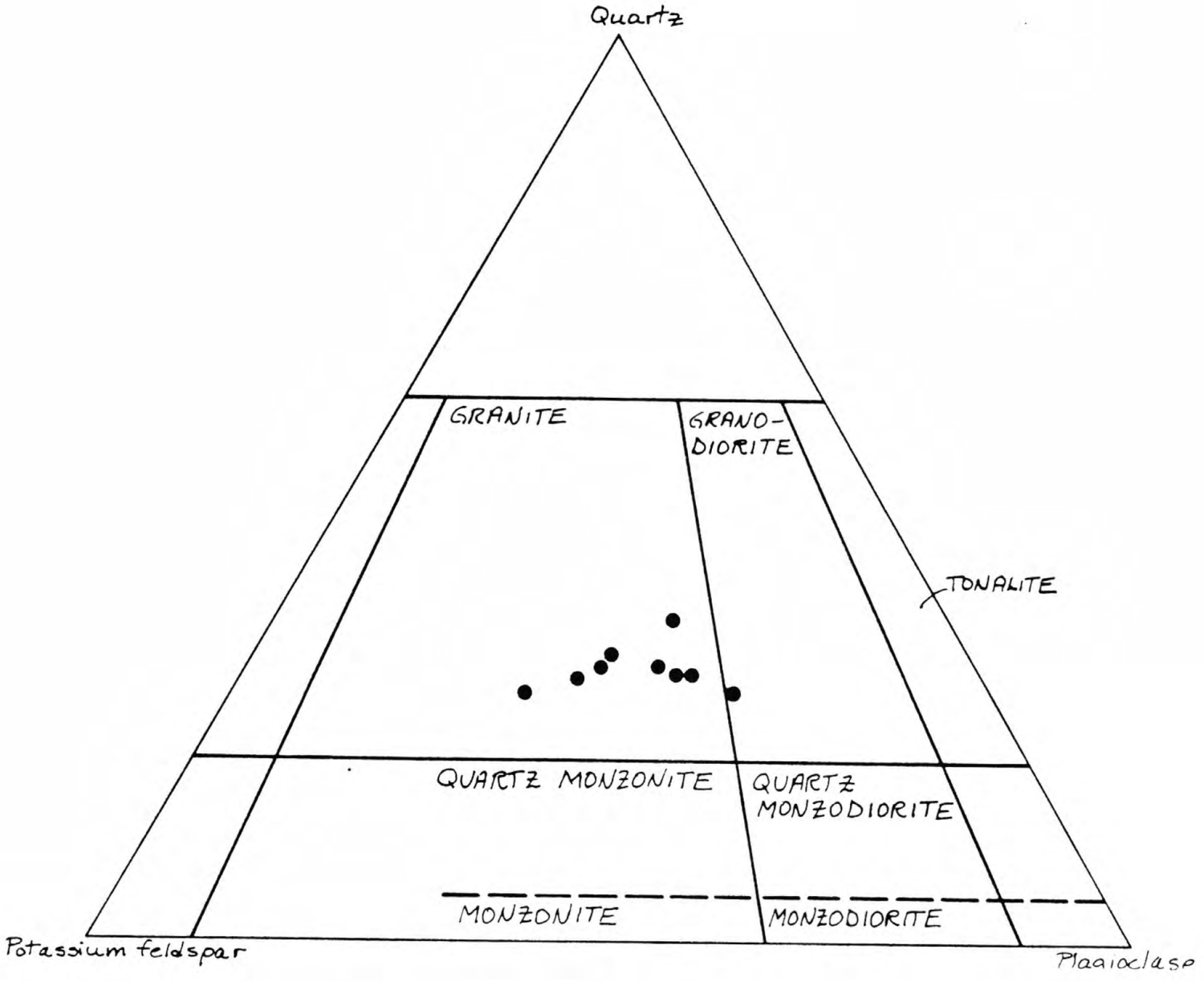

Figure 34.--Ternary diagram showing modes of Cretaceous two-mica monzogranite in the Gold Basin mining district. Compositional fields from Streckeisen and others (1973).

Figure 35. Textural relations in the Cretaceous two-mica monzogranite. A, Subhedral crystals of oscillatory zoned, perthitic potassium feldspar showing the inclusion of numerous small oriented, euhedral to subhedral crystals of partly seritically altered oliglclase (An_{15-20}). In addition, the crystal of included primary biotite (B) shows a marginal development of secondary white mica. Sample number GM-1090a. B, Coarsely crystalline white mica (M) filling interstices among a framework-supported network of euhedral plagioclase (P). Sample number GM-917c. C, Knife-edge contact between muscovite (M) and biotite (B) showing no alteration effects in either mineral. Sample number GM-1089. D, Biotite (B) cut by muscovite (M) which has in turn been cut by a subsequently crystallized, smoewhat finer grained generation of biotite. All biotites are greenish brown (Z). Sample number GM-1089.

A

B

C

D

relatively large crystals of apatite show euhedral, 0.8 mm-across basal sections containing euhedral laths of biotite.

Muscovite in the two-mica monzogranite occurs in a variety of textural associations with various light and dark minerals. In this report we use the term "muscovite" to describe relatively coarse white micas, generally subhedral to euhedral, that are terminated sharply and cleanly against primary biotite, primary plagioclase, and (or) primary potassium feldspar. Such muscovites show no secondary replacement textures relative to these three minerals that commonly are the same size as the muscovite. Most likely, however, the muscovite in the two-mica monzogranite is far from ideal, and it probably contains a significant celadonite ($K(Mg,Fe^{2+})_2Si_4O_{10}(OH)_2$) component (See Davis and others, 1979; Anderson and Rowley, 1981; C. F. Miller, E. F. Stoddard, L. J. Bradfish, and W. A. Dollase, unpub. data, 1981). Some coarse-grained white mica in the two-mica monzogranite obviously is post plagioclase in age, and it crystallized largely as an open-space filling of a mostly plagioclase supported network or framework (fig. 35B). In this association, {001} lamella traces commonly impinge the euhedral crystal boundaries of the earlier crystallized plagioclase at high angles. Further, there is no visible alteration of the plagioclase where it is in contact with the white mica. In another relation, stout books of white mica about 0.5 to 1.0 mm across show sharp, knife-edge contacts with dark greenish-brown (Z) biotite and again there is no bleaching visible at high magnifications of the biotite adjacent to the white mica (fig. 35C). Some coarse plates of white mica are engulfed totally by larger books of unaltered biotite measuring approximately 2.0 to 3.0 mm long, relations which are not diagnostic as to relative ages of crystallization between white mica and biotite. Some rocks, however, show obviously primary crystals of biotite to be cut by similarly sized crystals of white mica, and the white mica is in turn cut rarely by somewhat finer grained crystals of biotite (fig. 35D). Shredded, wormy intergrowths of very fine grained white mica preferentially concentrated at and along the edges of medium-grained plates of white mica must reflect crystallization during the circulation of post magmatic, hydrothermal fluids in the rocks. Such intergrowths of fine-grained white mica also replace some primary biotite locally in the two-mica monzogranite. Where this occurs, the adjoining biotite is bleached and altered partly to chlorite. Overall the two-mica

monzogranite, the coarse books of white mica appear to be the preferred nucleation site for the definitely secondary, hydrothermal-related white mica.

Chemical analyses of seven samples from the Cretaceous two-mica monzogranite are given in table 15. Five of the samples show a striking chemical homogeneity; the two exceptions (analysis nos. 5 and 7) are respectively of an episyenite zone within the two-mica monzogranite, and two-mica monzogranite partly altered by nearby quartz-fluorite-white mica veins. The five unaltered samples of the two-mica monzogranite show SiO_2 contents that range from 70.9 to 71.9 weight percent, Al_2O_3 contents that range from 14.9 to 15.5 weight percent, and total alkalis (K_2O plus Na_2O) that range from 8.03 to 8.96 weight percent. The mean ratio of Na_2O to K_2O in weight percent is 1.00 for the five samples. A plot showing the ratio of Al_2O_3: (K_2O + Na_2O + CaO) in molecular percent versus SiO_2 in weight percent for the analyzed samples of the two-mica monzogranite reveals the extent of alumina saturation in these rocks (fig. 36). For comparative purposes, we show also on this figure a field for selected Late Cretaceous to Eocene, two-mica granitoids from elsewhere within the cordillera, compiled by Keith and Reynolds (1980). The two samples of altered two-mica monzogranite (analysis nos. 5 and 7, fig. 36) plot significantly away from the field of two-mica granitoids, whereas the samples of unaltered two-mica monzogranite compare favorably with the field.

The two-mica monzogranite from the Gold Basin district is peraluminous. Five samples of unaltered monzogranite show values for Al_2O_3:(K_2O + Na_2O + CaO) in molecular percent that range from 1.09 to 1.21 (fig. 36). In addition, a plot of Na_2O+K_2O in molecular percent versus Al_2O_3 in molecular percent shows a strong clustering of the five samples of unaltered, two-mica monzogranite in the peraluminous field, approximately at 10 molecular percent Al_2O_3 (fig. 37). Such values of alumina saturation are similar to values reported for the Australian S-type granites by Chappel and White (1974) and Hine and others (1978). The two-mica monzogranite in the district shows CIPW normative corundum to be generally more than two weight percent (table 15; fig. 38), and in this regard corresponds with an S-type granite according to the criteria used by Chappel and White (1974). However, the two-mica monzogranite in the Gold Basin district shows some major element chemistry, significantly different from the Australian S-type granites. The alumina saturation in the two-mica monzogranite is largely a reflection of its

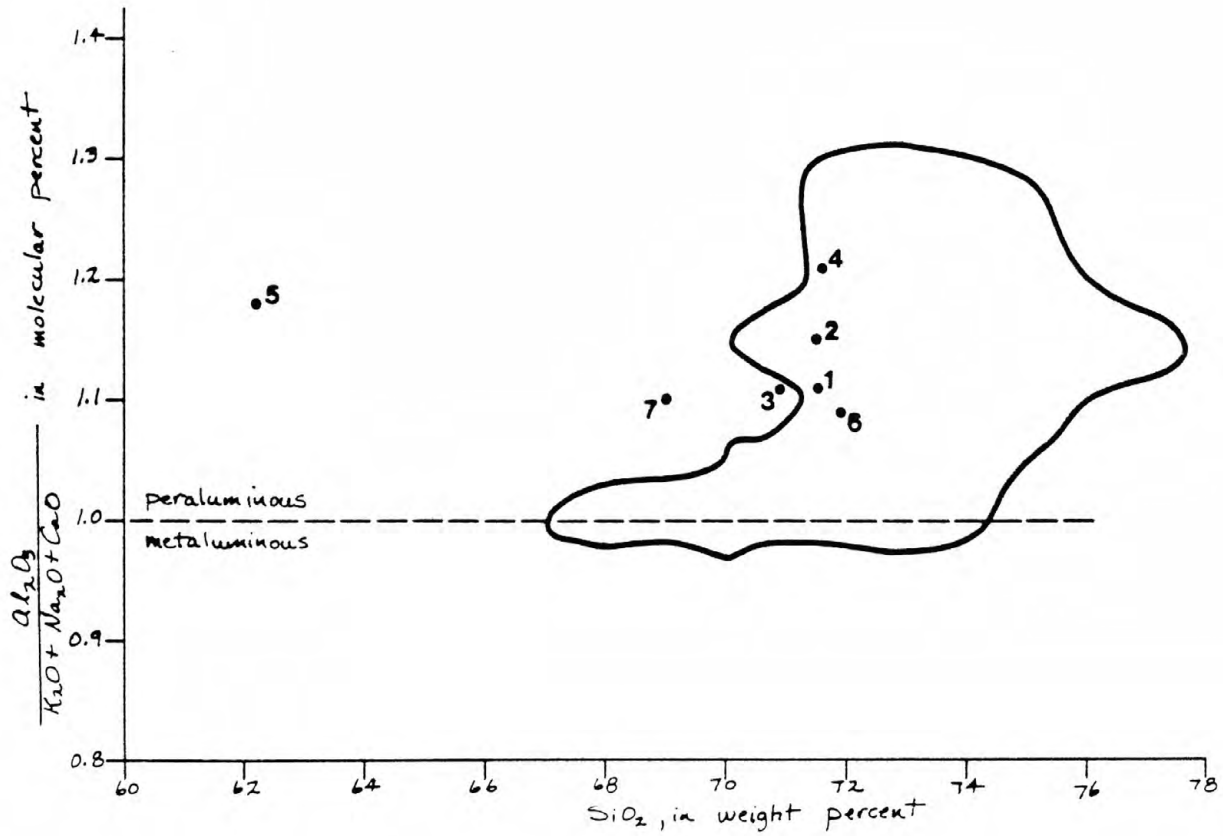

Figure 36.--Plot showing ratio of Al_2O_3: (K_2O + Na_2O + CaO) in molecular percent versus SiO_2 in weight percent from a Cretaceous two-mica monzogranite in the Gold Basin district. Analyses numbered same as table 15. Field for selected Late Cretaceous to Eocene peraluminous, two-mica granitoids from elsewhere in the cordillera also shown, modified from Keith and Reynolds (1980, fig. 5-1).

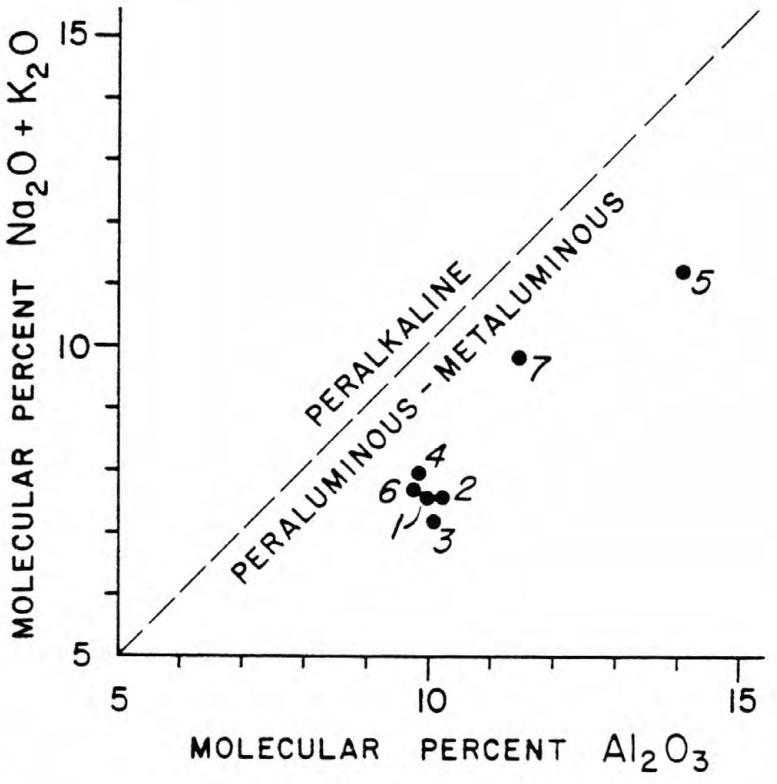

Figure 37.—Plot showing the sum of Na_2O plus K_2O in molecular percent versus Al_2O_3 in molecular percent from a Cretaceous two-mica monzogranite in the Gold Basin district. Analyses numbered same as table 15.

Table 15.--Analytical data from the Cretaceous two-mica monzogranite

[Chemical analyses: major oxides by X-ray spectroscopy, J. S. Wahlberg, J. Taggart, and J. Baker, analysts; partial chemical analyses by standard methods, D. Shepard and P. T. Klock, analysts; Au, Hg, W, and Zn, P. Briggs and J. Thomas, analysts. Spectrographic analyses by Chris Heroploulos. Results are reported to the nearest number in the series 1., 0.7, 0.5, 0.3, 0.2, 0.15, 0.1, 0.07, etc., which represent midpoints of interval data on a geometric scale. The precision of a reported value is approximately plus or minus one series interval at 68 percent confidence and two intervals at 95 percent confidence. Looked for but not found: Ag, As, Au, Bi, Cd, Pd, Pt, Sb, Te, U, and W. ——, not detected]

	1	2	3	4	5	6	7
Field number —	GM-1089a	GM-1089b	GM-880	GM-1088	GM-877	GM-1103	GM-923b
Sample number —	M-144485	M-144486	M-144476	M-144488	M-144489	M-144490	M-144491
Chemical analyses (weight percent)							
SiO_2	71.5	71.5	70.9	71.6	62.1	71.9	69.0
Al_2O_3	15.3	15.3	15.5	14.9	20.5	15.	17.3
Fe_2O_3	1.3	1.19	1.33	1.31	1.35	1.06	.4
FeO	.2	.21	.54	.15	.19	.28	.13
MgO	.23	.20	.36	.26	.32	.22	.11
CaO	1.09	.99	1.50	.26	.63	1.18	.56
Na_2O	4.3	4.21	4.43	3.72	5.69	4.33	5.69
K_2O	4.25	4.19	3.60	5.24	6.35	4.09	4.96
H_2O^+	.49	.46	.36	.64	.89	.43	.36
H_2O^-	.1	.1	.06	.04	.04	.04	——
TiO_2	.21	.2	.25	.17	.23	.16	——
P_2O_5	.06	.06	.09	.06	.1	——	.05
MnO	——	——	——	——	.03	——	.02
CO_2	.13	——	——	.12	.36	.19	.17
F	.07	.06	.06	.12	.3	.04	.07
Cl	——	——	——	——	——	——	——
S	.025	——	.018	.012	——	.026	.005
Subtotal	99.26	98.67	99.	98.6	99.08	98.95	98.83
Less O=F	.03	.03	.03	.05	.13	.02	.03
Total	99.23	98.64	98.97	98.55	98.95	98.93	98.8
Semiquantitative spectrographic analyses (weight percent)							
B	.0003	.0003	——	.0003	.0002	.0002	——
Ba	.1	.15	.15	.1	.15	.1	.015
Be	.0003	.0003	.0003	.0003	.0005	.0005	.0005
Co	.0002	.0002	.0003	.0002	.0002	.0002	——
Cr	.0002	.0002	.00015	.0002	.0002	.0002	.0002
Cu	.0005	.0005	.0005	.0005	.001	.0007	.0003
La	.005	.005	.01	.005	.007	.007	——
Mn	.015	.02	.015	.02	.03	.02	.02
Mo	——	——	——	——	.0005	——	——
Nb	.0007	.0007	.0007	.0007	.0015	.0007	.005
Ni	.0001	.0001	.00015	.0003	.0001	.00007	.0001
Pb	.003	.003	.003	.002	.005	.005	.005
Sc	.0003	.0003	.0002	——	.0003	.0003	——
Sn	.0007	——	——	——	——	——	——
Sr	.05	.07	.1	.02	.03	.07	.007
V	.002	.002	.003	.0015	.002	.0015	.0007
Y	.001	.0007	.0007	.0007	.001	.001	.0007
Zr	.01	.01	.015	.007	.007	.007	.0015
Ce	.007	.007	.015	.01	.015	.01	——
Ga	.003	.003	.003	.003	.005	.003	.007
Ge	——	——	——	——	——	——	.0007
Yb	.00007	.0001	.00007	——	.00007	.0001	——
Chemical analyses (parts per million)							
Au	——	——	——	.06	——	.05	——
Hg	.04	.01	.01	.01	.03	.04	——
W	2.	1.	——	3.	2.	——	——
Zn	53.	49.	67.	34.	72.	52.	23.
C.I.P.W. norms (weight percent)							
Q	28.5	29.3	28.3	30.1	4.7	29.2	16.6
C	2.3	2.4	2.	3.2	4.3	1.9	2.3
or	25.3	25.1	21.5	31.4	37.9	24.4	29.7
ab	36.7	36.2	37.9	32.	48.7	37.1	48.7
an	3.8	4.2	6.5	——	——	4.4	.9
en	.58	.51	.91	.41	.1	.55	.28
mt	——	.10	.95	——	.04	.33	.45
hm	1.3	1.1	.69	1.3	1.3	.84	.09
il	.36	.39	.48	.3	.44	.31	——
ru	.03	——	——	.02	——	——	——
ap	.14	.14	.22	.14	.24	——	.12
fr	.13	.11	.11	.24	.61	.08	.14
pr	.06	——	.04	.02	——	.06	.02
cc	.30	——	——	.02	.12	.44	.39
ag	——	——	——	.22	.59	——	——
Total	99.5	99.6	99.6	99.4	99.0	99.6	99.7
Salic	96.6	97.2	96.2	96.7	95.6	97.	98.2
Femic	2.9	2.4	3.4	2.7	3.4	2.6	1.5
D.I.	90.6	90.6	87.7	93.5	91.3	90.6	95.

1. Two-mica monzogranite.
2. Do.
3. Do.
4. Do.
5. Episyenite facies of two-mica monzogranite; NE1/4 sec. 24, T. 28 N., R. 19 W.
6. Two-mica monzogranite.
7. Two-mica monzogranite, partly altered by nearby quartz-fluorite-white mica veins; NW1/4 sec. 10, T. 28 N., T. 18 W.

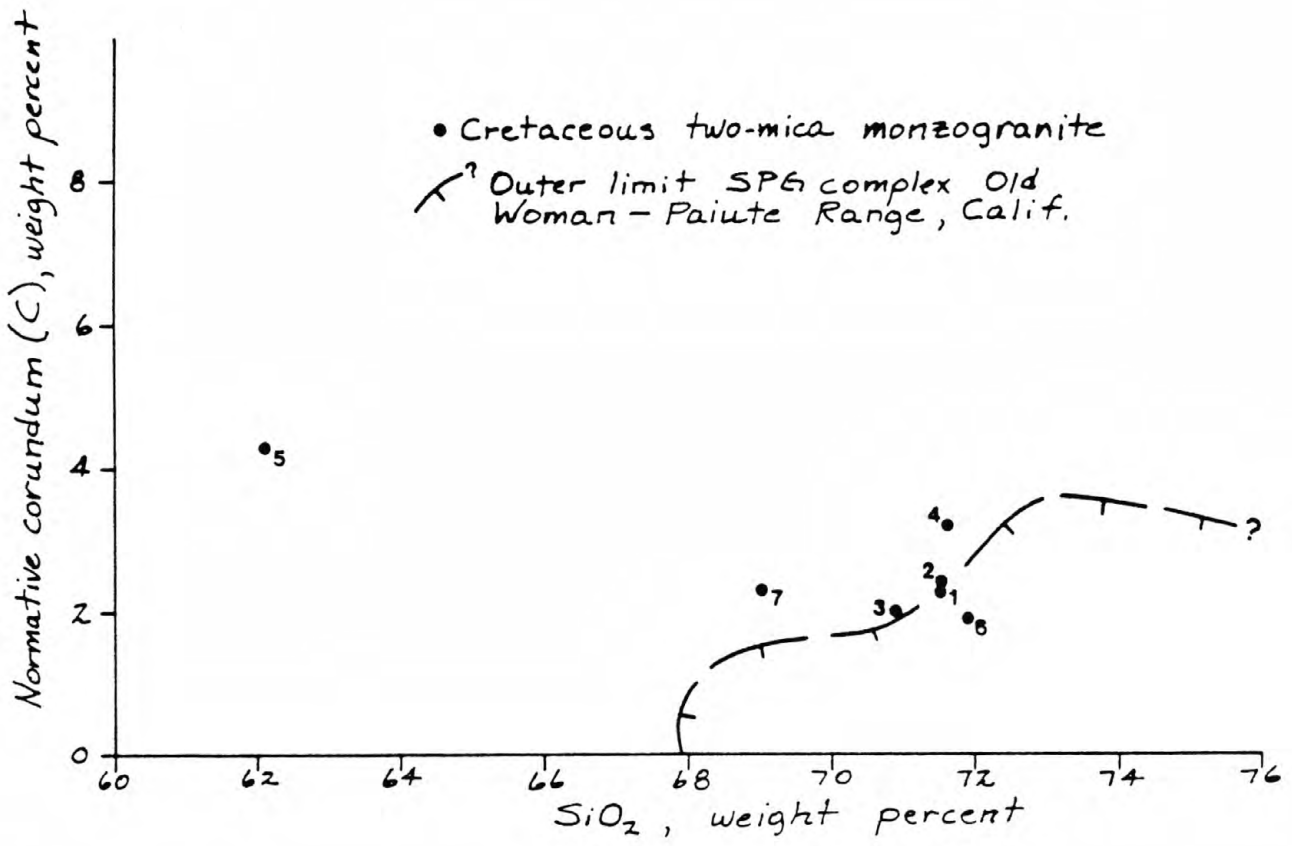

Figure 38.--Plot showing normative corundum (C), in weight percent, versus SiO_2 in weight percent, from a Cretaceous two-mica monzogranite in the Gold Basin district. Analyses numbered same as table 15. Outer limit of data points from the strongly peraluminous granitic complex in the Old Woman-Paiute Range, California slso shown (modified from Miller (1981)).

depletion in CaO. In this regard, the two-mica monzogranite differs from the Australian S-type granites because their alumina saturation results apparently from a depletion in Na_2O during weathering of the S-granites' source rocks (Chappel and White, 1974). The two-mica monzogranite is not depleted in Na_2O (table 15; see above), as are most other well-studied suites of two-mica granitoids in the southern cordillera (fig. 39; see also Keith and Reynolds (1980)). As shown on figure 39, the five samples of unaltered two-mica monzogranite from Gold Basin straddle the mutual boundary between the compositional fields defined by major element data obtained from the two-mica, Paleocene Pan Tak Granite of southern Arizona (see Wright and Haxel, 1981), and Late Cretaceous two-mica granitoids from the Whipple Mountains, California (Anderson and Rowley, 1981). All of these data from the Pan Tak Granite, from the Whipple Mountains, and from the two-mica monzogranite in the Gold Basin district plot on the albite-orthoclase side of the quartz-feldspar join at 500 km/cm^2, a relation which also clearly contrasts with that of the Austraian S-type granites (fig. 39). Further, in the Australian S-type granites, Na_2O is generally less than 3.2 weight percent for rocks showing K_2O contents of about 5 weight percent (Chappel and White, 1974), whereas the minimum content of Na_2O in the two-mica monzogranite from Gold Basin is 3.72 weight percent (table 15).

Fluorine occurs in the analyzed samples of the two-mica monzogranite from Gold Basin at concentrations in the range 0.04 to 0.12 weight percent (table 15). We do not have a significant number of analyses to document geochemical trends very well, but fluorine contents in these rocks appear to show some variation with other analytical data. The sample of unaltered two-mica monzogranite containing the highest concentration of fluorine (analysis no. 4, table 15) also is the most highly differentiated (93.5 D.I., table 15), and the most strongly peraluminous (fig. 36). The most weakly peraluminous sample (no. 6, table 15 and fig. 36), on the other hand, shows the lowest content of fluorine (0.04 weight percent). Fluorine contents of other suites of two-mica granitic rocks in the southern cordillera appear to be extremely low (S. J. Reynolds, oral commun., 1982). However, the fluorine contents of two-mica granites elsewhere compare favorably with the fluorine contents obtained from the two-mica monzogranite at Gold Basin. Two-mica-bearing granitic rocks from the southern part of Peninsular Thailand show fluorine contents in the range 0.09 to 0.25 weight percent (Ishihara and others, 1980). A two-mica granite

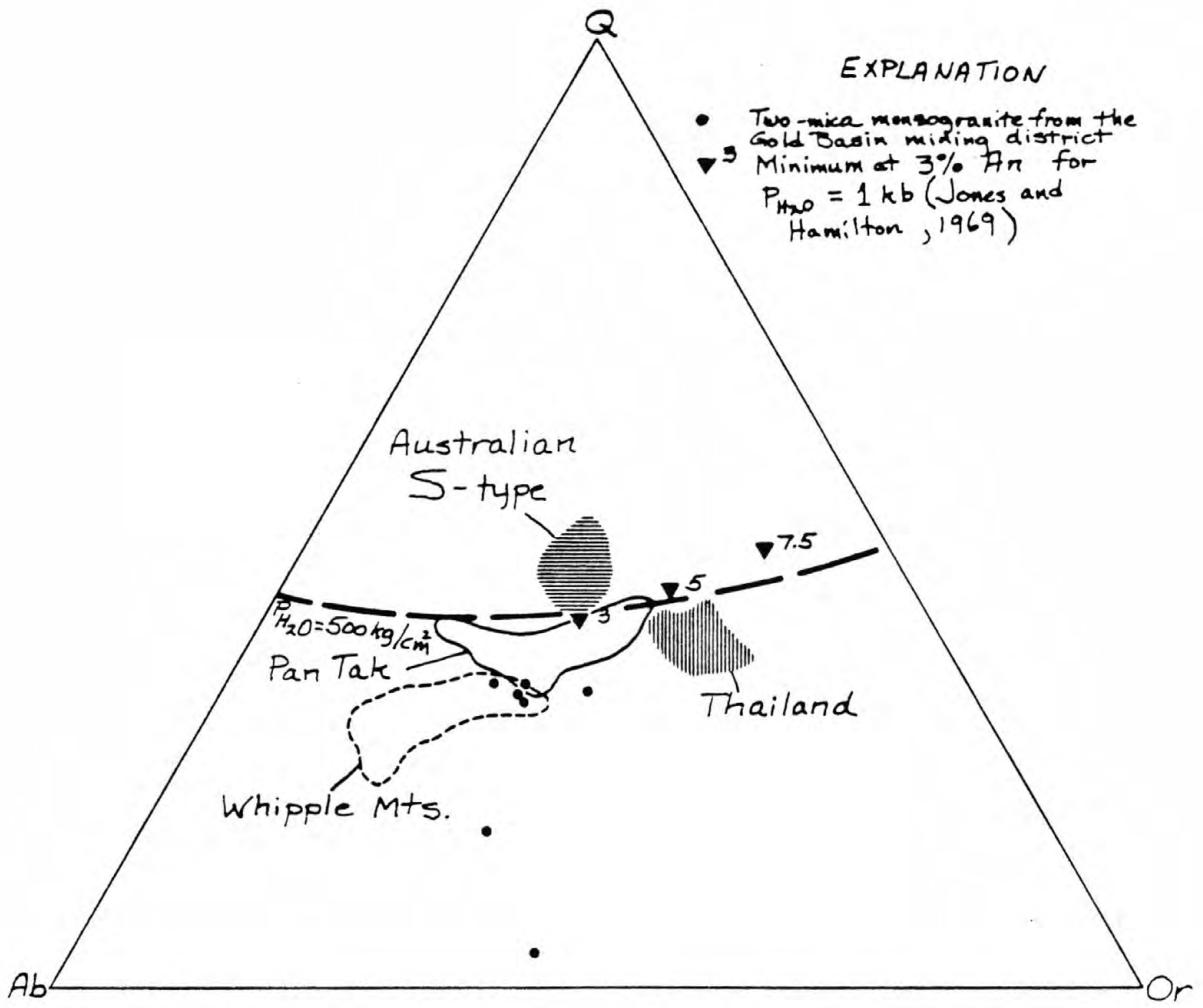

Figure 39.--Tertiary diagram showing normative proportion of albite, orthoclase, and quartz. Data points of Cretaceous two-mica monzogranite from table 15 shown as solid dots. Field of Australian S-type granites modified from White, Williams, and Chappel (1977). Field of granites showing a "predominantly S-type nature" from the southern part of Peninsular Thailand modified from Ishihara and others (1980). Field of the two-mica Pan Tak Granite, Coyote Mountains, Arizona (see Wright and Haxel, 1982) modified from Gordon Haxel (unpub. data, 1982). Field of Late Cretaceous, two-mica granitoids from the Whipple Mountains, California modified from Anderson and Rowley (1981). Filled triangles, ternary minimums from James and Hamilton (1969) at the designated weight percent An for $P_{total} = P_{H_2O}$ = 1kb. Dashed line, locus of ternary minimum temperatures projected onto the anhydrous base of the Ab-Or-Q-H_2O tetrahedron for $P_{H_2O} = P_{total}$ = 500 kg/cm^2 from Tuttle and Bowen (1958).

of the Marukh-Teberdin massif, Caucasus, USSR shows fluorine contents of 0.04 to 0.05 weight percent (Odikadze, 1971). Fluorine contents of muscovite-biotite granite in southwest England are reported by Bailey (1977, table VI) to be 0.16 weight percent. Muscovite-biotite granites in the Devonian Blue Tier batholith, Tasmania contain 0.06 to 1.02 weight percent fluorine (Groves and McCarthy, 1978).

Muscovite-bearing peraluminous granitic rocks contain world class deposits of tin in Malaysia and Thailand, significant deposits of uranium in France (Leroy, 1978), and significant concentrations of Li, Rb, Cs, Be, Nb, Ta, W, Mo, and F elsewhere (Tischendorf, 1974). However, gold is generally not associated with this type of igneous rock (see Boyle, 1979). In the Gold Basin-Lost Basin districts much of the known gold mineralization appears to be related temporally with emplacement of the Cretaceous two-mica monzogranite. As will be amplified fully below, one of the diagnostic features of the lode gold deposits in the Gold Basin-Lost Basin Districts is the high CO_2 content of the fluid inclusions in quartz and fluorite gangue. Such CO_2-rich fluid inclusions are also locally very abundant in primary quartz crystals in the two-mica monzogranite.

Episyenite

Several small bodies of episyenite were found by Blacet in the Gold Basin-Lost Basin mining districts. We herein apply the term episyenite according to the usage of Leroy (1978) to describe rocks that were desilicated and metasomatized hydrothermally under subsolidus conditions. These rocks now resemble syenite. All of these bodies crop out across very small areas and could not be shown on the geologic map. Nonetheless, because one of these bodies of episyenite contains disseminated, visible gold (Blacet, 1969), we have tabulated all occurrences of syenitic rock known to us in the districts (table 16). Indeed, because of the genetic and possibly economic importance of this occurrence, we include its petrographic details, and chemistry in the next section below describing Gold Deposits and Occurrences. Primarily because the upper Cretaceous two-mica monzogranite includes some episyenitic facies, we infer that episyenite distant from the upper Cretaceous two-mica monzogranite to be Cretaceous in age also.

Table 16. Occurrences of episyenitic and syenitic rocks known in the Gold Basin-Lost Basin mining districts
[Modified from P. M. Blacet, unpub. data, 1967-1972]

Description	Location	Commodities present	Comments
1. Series of four nearby coarse- and fine-grained fluorite-bearing potassium-feldspar episyenitic bodies. Locally abundant pyrite; some carbonate. Probably reflect alteration of Proterozoic rock during the Cretaceous	loc. 19, pl. 1	Au, F	Muscovite yields K-Ar ages of 128 and 129 m.y. (see above). The episyenite bodies are ovoid shaped, have maximum individual outcrop dimensions of about 10 m, and crop out for approximately 70 m along a N. 50° W. trend line
2. Medium- to coarse-grained episyenitic body. Contains fluffy-orange carbonate and some iron oxide	loc. 800, pl. 1	Au?	Episyenitic body measures approximately 55X20 m, and is elongated in a N. 60° E. direction. Ringed by an apparently genetically associated zone made up of stringers of quartz
3. Syenitic aplite dike. Abundant quartz and red-brown carbonate associated with this pyrite-bearing dike	loc. 297, pl. 1	Cu stain (trace)	A N. 35° E.-striking dike, approximately 8 to 10 m thick, poorly exposed
4. Episyenitic aplite. Some disseminated pyrite. Sparse carbonate	loc. 308, pl. 1	Au?	Exposed in area approximately 3 m long on south slope of small hill
5. Muscovite episyenite facies of upper Cretaceous two-mica monzogranite. Abundant quartz, muscovite, and colorless fluorite veins are associated spatially	loc. 877, pl. 1	F	Veins associated with episyenite range up to 8 cm in thickness. Sparse quartz fills cavities and selectively replaces potassium feldspar. Quartz encloses abundant fluid inclusions containing high proportions of liquid carbon dioxide

GOLD DEPOSITS AND OCCURRENCES

Lode and placer gold deposits and occurrences are widespread throughout the Gold Basin-Lost Basin mining districts (table 11). These reported lode deposits and occurrences include numerous veins, one occurrence of disseminated gold, and veins caught up along the Miocene detachment fault. The most productive placers occur along the east flank of the Lost Basin Range. Relatively minor placer deposits were worked along the west flank of the Lost Basin range, and south-southeast of the Golden Rule Peak in the Gold Basin district. In addition, relatively significant shows of secondary copper minerals occur in the general area of locality 1357 (table 11, pl. 1). This area was studied geochemically in detail by Krish (1974) who concluded that the geochemical associations in rock there most likely reflect those to be found very high in a buried porphyry copper system; beyond even the outermost extent of the dispersed propylitic halo. However, a careful review of available, evidence for and against the presence of a porphyry copper system at depth led Deaderick (1980) to conclude that its presence could not be substantiated.

The gold-bearing vein deposits and occurrences in the Gold Basin-Lost Basin mining districts appear to have been emplaced episodically over a very long time span that ranges from the Proterozoic X to the upper Cretaceous and (or) Paleocene. Indeed, Schrader (1909) recognized that the veins in the Gold Basin-Lost Basin districts contrasted sharply with those in the Black Mountain volcanic province (fig. 40). He grouped the veins in these districts with those of the Cerbat Mountains, about 50 km south of Gold basin, and noted that they appeared to be associated with "post-Cambrian intrusions of granite porphyry" (Schrader, 1909, p. 48). Schrader further noted that the fissure veins of the Black Mountains cut Tertiary volcanic rocks, and probably formed at depths shallower than those of the Cerbat Mountains. Blacet (1975, and unpub. data, 1967-1972) documented the occurrence of visible gold or the inferred presence of gold in more than 100 locations throughout the crystalline terranes of the Gold Basin-Lost Basin districts (table 11). Emplacement of these veins took place during at least three relatively restricted intervals of time. First, hydrothermal emplacement apparently occurred very rarely sometime during the Proterozoic X, most likely penecontemporaneous with the regional greenschist metamorphism. Some of the veins in the districts may have been emplaced penecontemporaneous with the

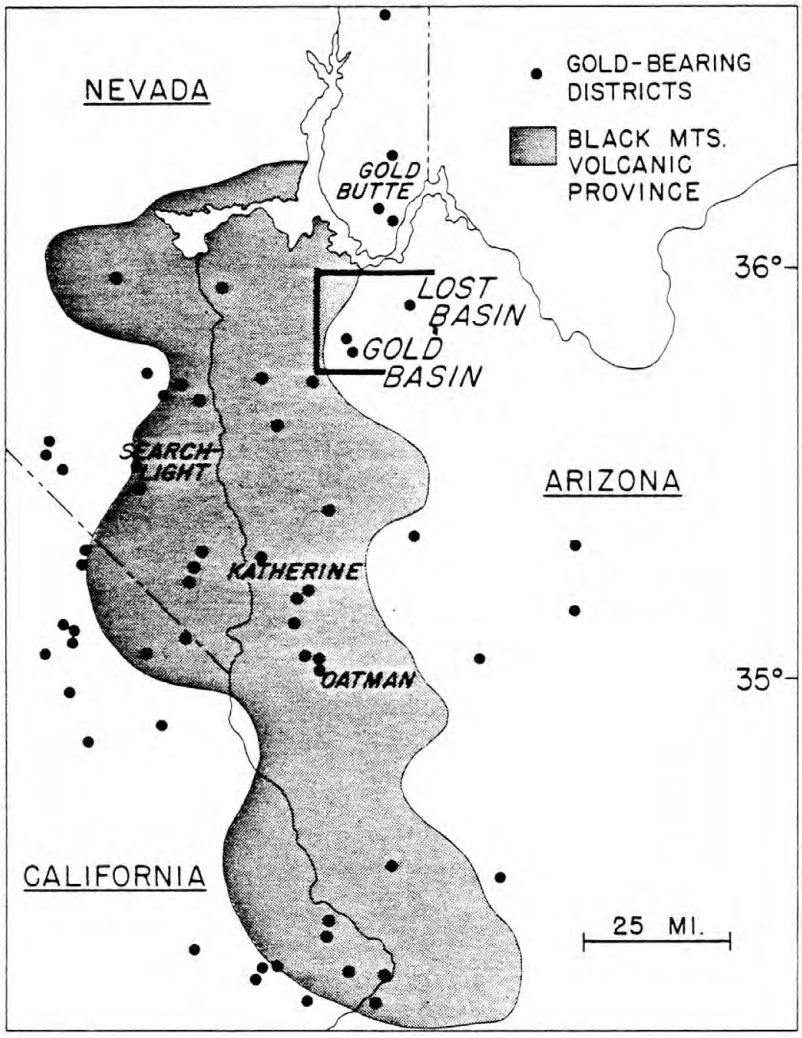

Figure 40.--Areas reported by Liggett and others (1974) to contain gold mineralization in the general area of the Black Mountains volcanic province of Liggett and Childs (1977).

apparently Proterozoic Y mineralization in the southern Virgin Mountains. In the southern Virgin Mountains, just north of Lake Mead, vein-type gold mineralization is related probably to the emplacement of the Proterozoic Y Gold Butte Granite of Longwell (1936) (Longwell and others, 1965). After a long gap in the mineralization record, the emplacement of gold-bearing veins then culminated most likely during the upper Cretaceous and lower Tertiary (Laramide). The most widespread introduction of gold-bearing veins occurred during this interval at which time many veins were localized along both high- and low-angle faults and fractures within the Proterozoic X metamorphic and igneous rocks. Finally, some of this vein-type mineralization also has been localized tectonically along the trace of the regionally extensive Miocene detachment fault where it crops out near the southwestern part of the Gold Basin district. The detachment fault in this part of the district produced low-angle gouge zones that locally contain fault blocks of gold-bearing quartz veins.

Gold mineralization in the Gold Basin-Lost Basin mining districts thus contrasts strongly with gold mineralization in much of the surrounding region. The bulk of the precious metal mineralization in the Black Mountains volcanic province of Ligget and Childs (1977) appears to be related with spatially associated Cenozoic volcanic centers, and this relation is probably best exemplified by mineralization in the Searchlight district, Nevada (Callaghan, 1939) and in the Oatman district, Arizona (Lausen, 1931; Clifton, Durning, and Buchanan, 1980). Gold mineralization in the Oatman district is probably younger than about ten m.y. (Thorson, 1971). Some other nearby areas outside the Black Mountains volcanic province also have been described recently as hosting significant gold mineralization older than the volcanism in the province. A gold-bearing breccia pipe in the Clark Mountain mining district, 72 km southwest of Las Vegas, Nev., has been dated at 100 m.y. (Sharp, 1980). In addition, the copper-nickel-cobalt-platinum ores associated with hornblendite intrustions at the Key West mine in the Bunkerville, Nevada mining district, northern Virgin Mountains, contained locally as much as 0.25 oz per ton gold (Beal, 1965, p. 69). Most early workers in the district (see Lindgren and Davy, 1924) believed the mineralization there to be Proterozoic in age. However, Beal (1965) suggested that hypogene copper there (chalcopyrite) may have been superposed on a nickel-cobalt-platinum metal association during late Cretaceous and (or) early Tertiary. The

unquestionably Proterozoic X massive sulfide deposits at Jerome, Arizona produced substantial amounts of copper ore containing byproduct gold and silver (Anderson, 1968). The United Verde deposit is reported to have produced 34 million tons of ore grading 5 percent copper, 1.7 ounces per ton silver, and 0.045 ounces per ton gold (Anderson and Guilbert, 1979, p. 42).

Proterozoic Veins

At least two occurrences of gold-bearing quartz veins are believed to be Proterozoic in age. One consists of irregular, centimeter-sized stringers of quartz together with much less abundant calcite, chlorite, galena, chalcopyrite, and pyrite, and trace amounts of gold visible along the associated iron-oxide-stained fractures through the quartz stringers. Secondary minerals along the veins include cerussite, wulfenite, and some green and blue secondary copper minerals. These veins are concentrated in a zone several meters across, and the veins unquestionably have been involved in the ductile deformation that has affected the enclosing mafic gneisses. In outcrop, individual veins appear to parallel approximately the local schistosity. However, close examination of vein-wallrock relations in thin section shows that some veins here locally crosscut the schistose fabric of their walls as they pinch and swell through the gneiss (fig. 41A). In addition, quartz in these veins has a recrystallized, granoblastic texture wherein the [0001]-axes of quartz appear to have a fabric similar to the fabric of quartz in the enclosing gneiss. Further, quartz in the veins is relatively free of fluid inclusions, and quartz-quartz crystal boundaries typically form 120° angles. The minor amounts of chlorite in the veins are concentrated along the medial portions of many individual veins, whereas biotite immediately adjacent to the veins has not been altered to chlorite. Calcite is a paragenetically late mineral in the veins, and it occurs interstitial to the tightly interlocking quartz crystals.

The second occurrence of gold-bearing quartz veins that may be Proterozoic in age is located in the general area of Salt Spring Wash, near the northeast corner of the Senator Mountain 15-minute quadrangle (loc. no. 735,, table 11 and plate 1). Gold mineralization here, however, is only provisionally assigned to the Proterozoic on the basis of two Proterozoic ages (712 and 822 m.y., see above) obtained from white mica separates from a vein at this locality. In contrast to the well-developed metamorphic fabric of the veins at the first locality of Proterozoic veins, these gold-bearing veins

Figure 41.--Photographs showing microscopic and megascopic relations in apparently Proterozoic veins. A, Vein deformed along with the biotite-dominant schistose fabric of its enclosing gneiss. The primary assemblage of the vein includes quartz-calcite-chlorite±galena± chalcopyrite±pyrite. Gold was found along iron-oxide-stained fractures. Secondary vein minerals include cerrusite and wulfenite. A, quartz; B, biotite. Plane polarized light. Sample number GM-911; B, Photograph of ferroan(?) gray-brown calcite (C) in the gold-bearing quartz (Q) at locality 735, table 11. Note coin at lower left corner of photograph for scale.

A

B

from the general area of Salt Springs Wash apparently have not been involved in the regional metamorphism of the area and may have been emplaced sometine during the Proterozoic Y, penecontemporaneous with the Gold Butte Granite (see above.) Altered amphibolite makes up the walls of the veins, and the rocks show some evidence of shearing and brecciation along both the footwall and the hanging wall of the most persistent of the veins. In fact, the veins at this locality appear to have been broken into a series of pods and segmented quartz veins along a steeply dipping shear zone which strikes about N. 10° W. (P. M. Blacet, unpub. data, 1967-1972). The primary assemblage in the veins at this locality includes milky white quartz, carbonate, galena, chalcopyrite, white mica(?), and gold. The carbonate is distributed sparsely and erratically through the quartz as grayish-brown irregularly shaped masses of ferroan(?) calcite (fig. 41B). Pyrite, some cubes reaching dimensions as much as 2.5 cm across, is typically replaced by coarsely to finely cellular boxworks that are very siliceous. The bulk of the gold appears to have been deposited very late during the overall paragenesis of the veins, and it occurs mostly as approximately 0.5-millimeter-sized flakes at the interface between milky-white quartz and very late clear quartz which lines some vugs and cavities together with drusy quartz. In addition, there is some evidence that the pyrite here is auriferous. Traces of very delicate, flowerlike clusters of gold occur in some of the siliceous boxworks that replace pyrite. Indeed, our collections from these veins, together with Blacet's earlier sampling, yielded a suite of samples showing generally nodular masses of paragenetically very late gold, some possibly even supergene, in various textural relations with earlier and subsequently crystallized quartz (fig. 42A-F).

Late Cretaceous-Early Tertiary Veins

The vast majority of the gold-bearing veins in the districts presumably are late Cretaceous to early Tertiary in age. The veins fill fissures and show sharply defined walls with the country rock. Further they are locally quite persistent, and in places have been traced for approximately 0.25 km by surface and underground workings (fig. 43A). The greatest concentrations of veins occur in the southern part of the Gold Basin district and in the central part of the Lost Basin Range (fig. 3). Generally, in both of these areas many veins crop out individually, and have northerly strikes, although a few have east-west strikes, their attitude controlled mostly by the attitudes of the surrounding and gneisses. Previously, Schrader (1917) suggested that the

Figure 42.--Scanning electron micrographs showing relations of gold in the apparently Proterozoic veins at locality number 735 (pl. 1) in the Senator Mountain 15-minute quadrangle. Au, gold; Q, quartz. Bar indicates scale in micrometers (1 μm = $1x10^{-6}$m). A, Blebby nodular gold deposited on euhedrally terminated quartz projecting into an open cavity. Sample number GM-735-1; B, Cluster of small nodules of gold perched on quartz crystals deposited along the walls of a cubic mold inferred to reflect a paragenetically earlier crystal of pyrite. Sample number GM-735-1c; C, Relatively large mass of nodular gold on and intergrown with quartz. Sample number GM-735-4; D, Closeup view of nodule of gold from rectangular area outlined in C showing repeated twinning on 111 and poorly preserved dodecahedral faces. Sample number GM-735-4; E, Paragenetically late, doubly terminated crystal of quartz on a surface of gold. Sample number GM-735-1b; F, Quartz crystal at head of arrow associated with nodules of gold, all of which rest on a matrix of gold. Sample number GM-735-1d.

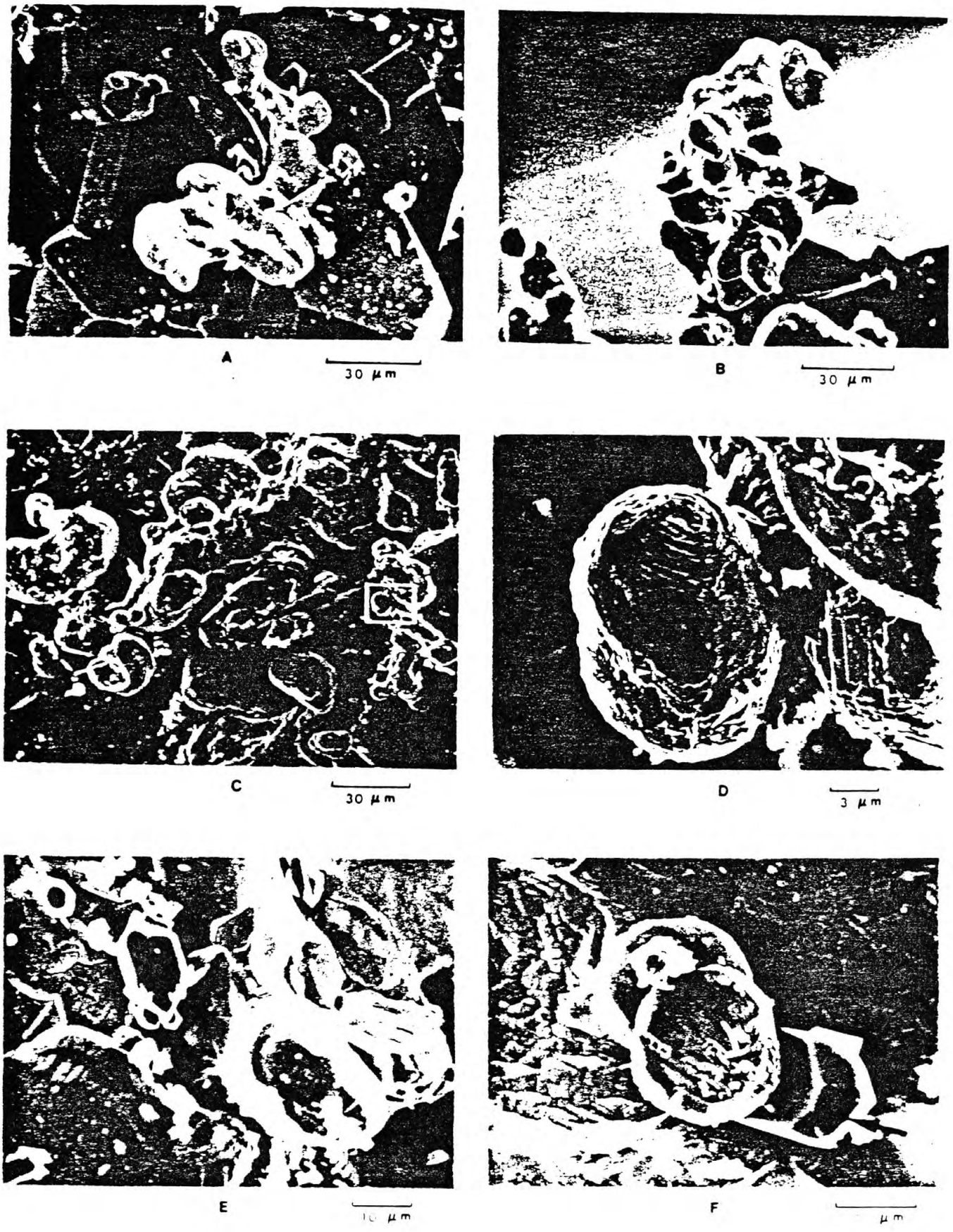
A
30 µm
B
30 µm
C
30 µm
D
3 µm
E
F
µm

Figure 43.--Photographs of selected mine workings, quartz veins, and quartz-cored pegmatite from the districts. A, View toward N. 10° W. showing surface workings along the north-south-striking quartz-carbonate-chalcopyrite-galena (trace)-gold vein at the Ford mine; B Quartz-albite-calcite-barite-pyrite-galena (trace) vein at locality 382 (table 11, pl. 1). Note pocket knife near lower right corner of picture for scale. Coarsely crystalline albite crystals, greater than 3 cm across, and cubes of limonite replacing pyrite are concentrated along the border zones of the vein. Dark-brown ferruginous calcite occurs in deeply corroded pits in the central parts of the vein. C, Vertical quartz-cored pegmatite including sericitically altered potassium feldspar in the general area of Salt Springs Wash. Note felt marker pen in the upper central part of the photograph for scale.

C

B

A

mostly gold-bearing veins in the Lost Basin range strike north-south, whereas the copper-bearing veins strike northwest-southeast. However, the preferred orientation of the strike of bulk of the veins measured in both districts is northeasterly. Figure 44 shows in projection the orientation of 325 veins in the Gold Basin-Lost Basin districts. Poles to veins in this diagram show double maxima that plunge to approximately N25° and N65°W at concentrations greater than three and four percent per one percent area. The orientation of these maxima is compatible with the bulk of the veins in the districts having been emplaced into a regional stress field wherein crustal extension during the late Cretaceous and early Tertiary was oriented north-northwest to south-southeast. As such, crustal extension in the districts during the Late Cretaceous and early Tertiary appears to have been oriented similar to that prevailing across much of the Basin and Range province of Arizona (Rehrig and Heidrick, 1976). There are some notable exceptions, however. Late Cretaceous and early Tertiary veins in the Wallapai mining district, which includes the Mineral Park porphyry copper deposit approximately 16 km northwest of Kingman, Arizona, show strong preferred concentrations of their strikes in a northwest direction (Thomas, 1949).

The predominant association of gold in the quartz veins of the Gold Basin-Lost Basin districts is with ferroan calcite, pyrite, and lesser amounts of galena and chalcopyrite in varying proportions. Free gold also occurs in two of the fluorite-bearing veins which are concentrated especially in the Gold Basin district, and free gold was noted to occur elsewhere in the districts in veins that include minor amounts of chlorite, topaz, and albite. An association between gold and albite was reported by Gallagher (1940) for many other districts. However, the apparent diversity in mineralogy is largely a reflection of gradual transitions in mineralogy as the veins and their cogenetic pegmatites evolved. For example, many veins in the districts show concentrations of coarsely crystalline albite and pyrite along their walls, along with increased abundances of ferruginous calcite in their central portions (fig. 43B). However, the overwhelming bulk of these veins most likely reflects the final stages of a mineralization event initiated by the emplacement of late Cretaceous-early Tertiary pegmatites and two-mica monzogranite into the Proterozoic rocks. Pegmatites with quartz cores are relatively abundant throughout the districts (fig. 43C). Although the pegmatites may crosscut the metamorphic fabric of the Proterozoic rocks at

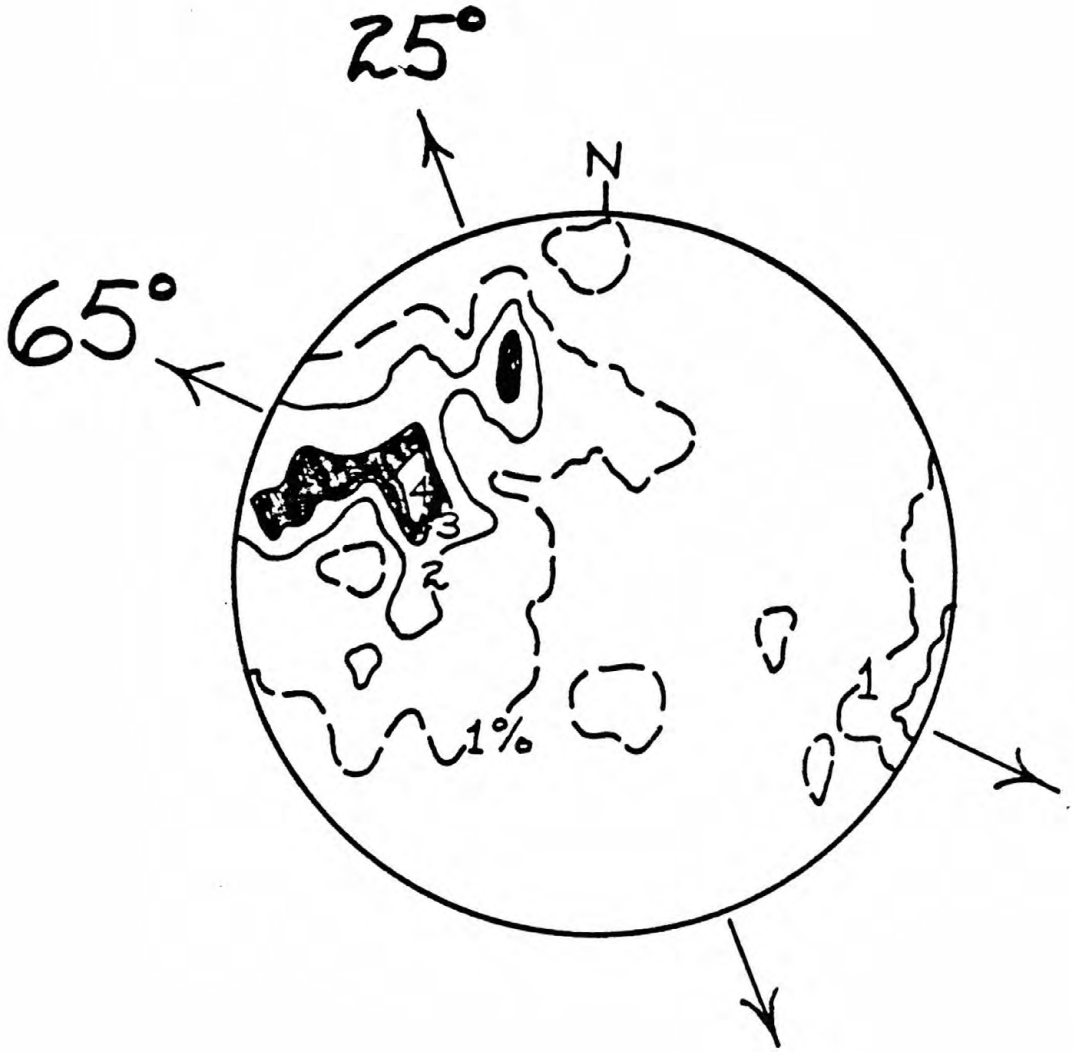

Figure 44.--Diagram showing orientation of poles to veins in the Gold Basin-Lost Basin districts. Lower hemisphere, equal area projection. Contours, 1, 2, 3, 4 percent per 1 percent area. Data modifed P. M. Blacet (unpub. data, 1967-1972).

high angles, the clusters of pegmatites appear locally to give way across a distance of about several hundred meters to quartz-dominant veins that closely parallel the schistosity in the surrounding metamorphic rocks. The overall dips of these veins vary widely in the districts from shallow to steep (fig. 45A-C).

The cogenetic relationship between the quartz-cored pegmatites and the gold-bearing quartz-ferroan calcite veins was established by Blacet at several localities where critical relations are well exposed and well developed (P. M. Blacet, unpub. data, 1967-1972). At these outcrops quartz-microcline-muscovite, 1- to 2-m-thick pegmatites give way internally to a well-defined central portion consisting of quartz, ferroan calcite, and some blades of white mica. However, locally in a few of these pegmatites small stringers of quartz plus orange-brown ferroan calcite project out from the pegmatite's quartz core, and into the surrounding Proterozoic gneiss. The quartz plus ferroan calcite stringers also pinch out away from the pegmatite, and these relations suggest quite strongly that the fluids associated with the quartz-ferroan calcite veins are related genetically to the quartz-cored pegmatites. Pyrite occurs not in these well-exposed pegmatites but rather in the quartz-ferroan calcite stringers where they cut the Proterozoic gneiss. Alteration to a chlorite-carbonate assemblage in the gneiss parallels both the pegmatite and the quartz-ferroan calcite stringers. Last, the alteration is confined tightly to rocks in the very immediate area of the pegmatite.

Elsewhere, however, the relations between quartz-cored pegmatites and quartz-ferroan calcite veins suggest a somewhat greater time gap between emplacement of pegmatites and the spatially separate veins. Pegmatites locally fill jointlike fractures in gneiss, and somewhat later quartz-ferroan calcite-pyrite-gold veins were emplaced along the same joint system. The veins locally crosscut the pegmatite, and visibly alter the earlier pegmatite and the enclosing granitic gneiss. Figure 46A-B shows relations between such quartz-ferroan calcite veins and sericitically altered granitic gneiss. Ferroan calcite, secondarily altered heavily to orange-brown limonite, here is one of the first minerals to be deposited and lines the walls of the larger veins and also occurs as gash-fillings in some of the more granoblastic portions of the gneiss. The veins cut the granitic gneiss at very high angles. Another series of prominent en echelon pods or veins, which crop out approximately 0.4 km east of the Golden Mile mine in the Lost Basin district,

Figure 45.--Photographs showing typical veins in the Gold Basin-Lost Basin mining districts. A, Unbrecciated shallow-dipping quartz-galena-pyrite-gold-chalcopyrite vein containing secondary malachite, chrysocolla, and wulfenite at the El Dorado mine workings. The vein occupies an intensely sheared zone wherein the hanging wall and footwall consist of genissic granodiorite. Note rock hammer in central part of picture for scale; B, Gently east dipping vein approximately 1.0 m thick exposed in one of the workings at the El Dorado mine; C, Steeply dipping vein in prospect in the northern part of the Gold Basin district.

A

B

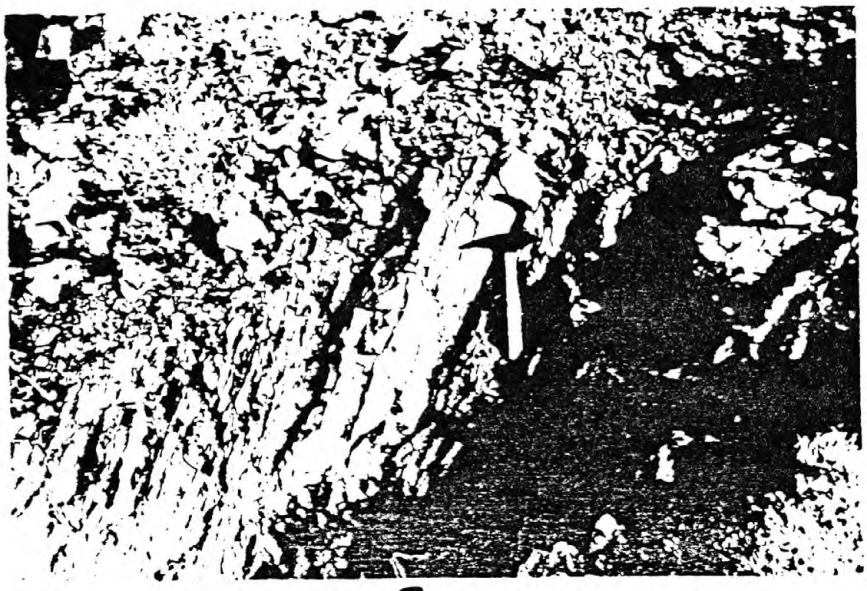

C

Figure 46.--Photomicrographs showing relations between quartz-ferroan calcite veins and sericitically altered, Proterozoic granitic gneiss. Q, quartz; li, limonite replacing ferroan calcite and pyrite (?); G, sericitically altered granitic gneiss. Sample number GM-637. A, General crosscutting relations between veins and gneiss. Note microstreaks of limonite concentrated in granoblastic domains of the gneiss away from the larger veins and roughly parallel with the veins. Plane polarized light. B, Closeup view showing textural relations within a quartz-ferroan calcite vein containing minor amounts of topaz (T). Not shown are minor amounts of albite that very locally also occur along the walls of this perpendicular vein. Crossed nicols.

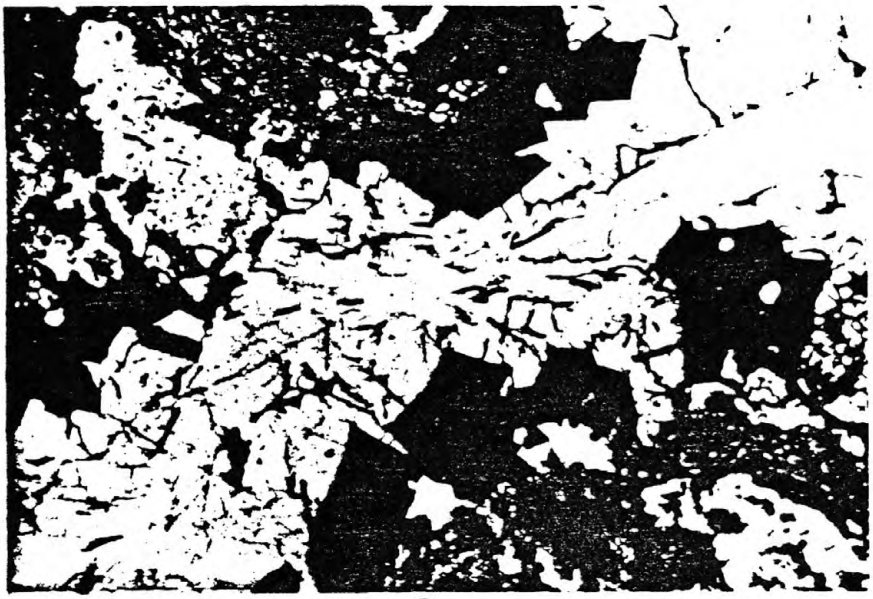

A

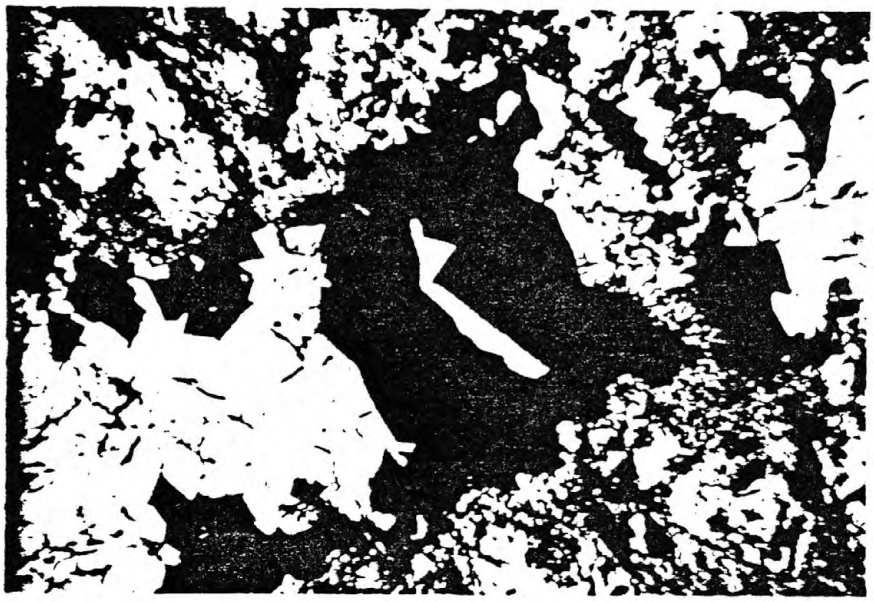

B

also document well the transition from feldspathic pegmatite to quartz vein. The veins at this locality have an approximately 20-cm-thick border zone containing coarsely crystalline albite, potassium feldspar, and smaller crystals of greenish-white mica. In places, single crystals of albite are as long as 18 cm. Milky-white quartz including some feldspar and irregular masses of ferroan calcite make up the cores of these veins. The cores pinch and swell along the outcrop of the veins and in places reach widths of about 1 m as the cores show relatively sharp transitions into the border zones.

In an attempt to document more fully the relations of gold to other minerals in these veins, detailed examination using the scanning electron microscope was made of a suite of gold-bearing samples from an approximately 1-m-thick vein at the Golden Gate mine, which is in the NW1/4 sec. 32, T. 30 N., R. 14 W. in the northern part of the Lost Basin district (loc. 11, table 11; plate 1). These studies revealed that the surface textures and forms of the free gold within even a single vein vary highly (fig. 47A-F). Filliform gold occurs draped across drusy quartz which is dominated by rhombohedron crystal terminations (fig. 47A). Such gold, however, has also been followed paragenetically by the crystallization of sparse amounts of extremely fine grained, doubly terminated crystals of quartz (fig. 47B). Some gold occurs also in a rather delicate dendritic form on prismatic crystals of quartz that line some cavities (fig. 47C), whereas other masses of gold show a nodular form containing moderately well developed dodecahedral faces (fig. 47D). Some irregularly shaped masses of gold occur in very close spatial association with equally sized, partially oxidized crystals of pyrite (fig. 47E). This relation suggests that at least some of the gold in the vein was not derived from the breakdown of earlier crystallized auriferous pyrite. The surface of the gold in this association shows a very irregular, almost pitted aspect. Although qualitative spot analysis of many of these particles of gold using the energy dispersive analyzer revealed they also contain silver and iron, the iron detected may in fact come from a thin partial dusting of nearby limonite on some of the gold. Such limonite may have been derived from pyrite which commonly is an important primary mineral. Finally, our SEM studies revealed the occurrence in the veins of small wedge-shaped stubby crystals containing significant amounts of vanadium, lead, and copper, and trace amounts of iron (fig. 47F). This unknown mineral may be a copper-rich mottramite, which, ideally has the formula $Pb(CuZn)VO_4OH$ (Roberts, Rapp, and

Figure 47.--Scanning electron micrographs of lode gold collected from the Golden Gate mine in the Garnet Mountain 15-minute quadrangle. Au, gold; Q, quartz. Bar indicates scale in micrometers (1 μm = $1x10^{-6}$m). A, Filliform gold in a cavity lined by drusy quartz terminated mostly by rhombohedrons. Sample number GM-11. B, An enlargement of the area enclosed by the rectangle in A. At the head of the arrow an extremely small, doubly terminated crystal of quartz rests on the surface of gold. The striations on the surface of gold probably reflect repeated twinning on {111}; C, Dendritic gold associated with prismatic crystals of quartz which line a cavity in vein quartz. Qualitative analysis of the gold using the energy dispersive X-ray microanalyzer indicates that the gold contains detectable amounts of silver and iron. Sample number GM-11h; D, Nodule of gold in a quartz cavity. The gold shows moderately well developed dodecahedral faces. Gold contains detectable amounts of silver and iron. Sample number GM-11d; E, Irregularly shaped, roughly textured particles of gold associated with partially oxidized cubes of pyrite (py). Sample number GM-11-1; F, Unknown mineral (U) showing a wedge-shaped habit and containing detectable amounts of vanadium, lead, copper, and iron (in trace amounts). The unknown mineral may be copper-rich mottramite, which ideally has the formula $Pb(Cu,Zn)VO_4$ OH (Roberts, Rapp, and Weber, 1974). Sample number GM-11-1a.

1 25KV 100UM 57.000

A

1 25KV 3UM 57.001

B

1 25KV 30UM 57.007

C

1 25KV 3UM 57.003

D

E

F

Weber, 1974). The mottramite(?) obviously crystallized subsequent to the bulk of the gold in the sample studied. SEM study of other gold-bearing samples showed that gold crystallized in them prior to the deposition of cerussite ($PbCO_3$), which was found by Blacet (unpub. data, 1967-1972) to be a fairly common secondary mineral throughout the districts.

Wulfenite ($PbMoO_4$), another secondary mineral, was found in 19 veins in the districts, and 9 of these veins also contain visible gold thereby emphasizing the strong association between lead, molybdenum, and gold here. Approximately two-thirds of the wulfenite occurrences are in the southern part of the Gold Basin district; the bulk of the remaining occurrences are clustered about 1.5 km east-northeast of the Golden Gate mine (table 11). On the other hand, none of the veins was noted to contain molybdenite (see also Deaderick, 1980, fig. 22), thus suggesting a supergene, cumulative derivation of molybdenum in the wulfenite from many relatively widespread and distant sources. Williams (1963) notes that wulfenite is abundant in many mining districts in the southwestern United States but, only rarely can it be related to hypogene sulfides. He further shows that molybdenum can be extracted fairly easily from wallrocks by oxidizing meteoric fluids. Further, Wilt (1980) and Wilt and Keith (1980) have shown that molybdenite in porphyry copper systems and wulfenite in Pb-Ag-Zn deposits are almost mutually exclusive.

The very strong association between lead (galena) and gold in the primary assemblages of 49 veins shown to contain visible gold in the districts is reflected in the following breakdown of specific, primary assemblages in these veins:

Group I	Group II	Group III
Quartz	Quartz	Quartz
galena	ferroan calcite	feldspar
gold	chalcopyrite	pyrite
± ferroan calcite	gold	gold
± chalcopyrite	± pyrite	± ferroan calcite
± pyrite		± topaz
± sphalerite (trace)		±chlorite (trace)
± chlorite		
± albite		
± fluorite		

Group I above includes roughly 85 percent of the veins that were shown to contain visible gold; group II contains about 14 percent; and group III about 1 percent. About one-third of the group I veins contain carbonate, mostly as an iron-rich or ferroan calcite. Although there is a very strong overall spatial association between fluorite-bearing veins and the distribution of occurrences of visible gold in the southern part of the Gold Basin district, only two veins there were found specifically to contain both visible gold and fluorite. This strong association between lead and gold in the Gold Basin-Lost Basin districts contrasts with the apparent strong accociation of gold with zinc, and silver with lead in the Cerbat Mountains (Hernon, 1938).

The preceding specific vein assemblages reflect mostly the final stages of a late Cretaceous and (or) event that began with the widespread introduction of pegmatite or granitic micropegmatite penecontemporaneous with the implacement of the two-mica monzogranite. The pegmatites include both potassium feldspar-rich and albite-rich types, and comprise a feldspar-dominant early stage in the evolution of these pegmatite and (or) vein systems. The feldspar-dominant portion of these systems is reflected primarily by the feldspar-rich border zones of the quartz-cored pegmatites. These border zones also include variable but generally minor amounts of quartz, carbonate (usually very iron rich), barite, apatite, pyrite, white mica, galena, and chalcopyrite. Barite locally is quite abundant in some of these pegmatite-veins, whereas galena and chalcopyrite occur sparsely in and near some feldspar-dominant border zones. This latter relation suggests thereby minor deposition of these minerals (together with traces of gold, as in the Group III gold-bearing assemblages listed above) early in the overall evolution of some of the pegmatite-vein systems. Quartz typically occurs in concentrations of about one-third to one-fourth of that of the feldspar (potassium feldspar and (or) albite) in the border zones. Further, as the pegmatite-vein systems evolved there appears to be a general decrease in the ratio pyrite:(galena+chalcopyrite) reflected primarily by a substantial increase in the amounts of galena and chalcopyrite late in the paragenesis. This change coincides with the increase in the amount of largely ferroan calcite deposited, and with a cessation in the crystallization of feldspar. As we discussed briefly above, fluorite locally is a very important accessory mineral during this predominantly quartz-sulfide-carbonate stage of the pegmatite-vein systems, especially in the southern part of the Gold Basin

district. Therefore, for descriptive purposes, we use a two-fold classification of the veins; that is, (1) a feldspar-dominant type (Group III, above), and (2) a mostly quartz-sulfide-carbonate type (Groups I and II), which includes the majority of the occurrences of visible gold known throughout the districts.

The intensity, type(s), and lateral extent of alteration related to the empacement of most veins are largely a function of the chemistry of the surrounding country rock and the chemistry of the fluids involved. A typical, approximately 0.5-m-thick vein, which includes a well-developed feldspar (albite) stage, will show alteration phenomena visible in outcrop for about 1 m away from its generally sharp walls. Alteration of amphibolite adjacent to one such well-studied vein clearly reveals the potassic character of some of the early fluids associated with vein emplacement (fig. 48). The effects of alteration were studied in a suite of samples of amphibolite collected 6 m, slightly over 1 m, 0.6 m, 8 cm, and 3 cm from the vein.

Amphibolite 6 m from the vein shows only crystallization and recrystallization effects related to the Proterozoic X metamorphic events. The amphibolite here contains a generally granoblastic fabric consisting of closely packed crystals of blue-green (Z) hornblende that show in small domains marginal recrystallization to epidote±carbonate, chlorite+quartz, and actinolite+chlorite assemblages. All of these latter, superposed assemblages presumably reflect the Proterozoic X retrograde metamorphic event.

Just beyond the alteration halo visible in outcrop, at a distance barely over 1 m from the vein's wall, thin section study of amphibolite reveals a marked increase in the abundance of chlorite, actinolite, epidote, and quartz, and the first appearance of sphene in the matrix. Here the hornblende takes on a ragged crystal outline and a generally rounded aspect when viewed in the microscope. We suggest that this increased growth of a chlorite-actinolite assemblage centralized in the pre-existing matrix reflects a narrow, subtle propylitic halo superposed on the earlier greenschist assemblages, and this halo thus marks the outer limit of alteration related to vein emplacement.

At a distance of about 0.6 m, the blue-green hornblende has been replaced almost totally by greenish-brown (Z) biotite in a rock showing a suite of superposed assemblages. Only the former crystal outlines of hornblende remain, well defined by granoblastic clusters of equant crystals of biotite, some of which show traces of their {001} cleavage planes following locally the

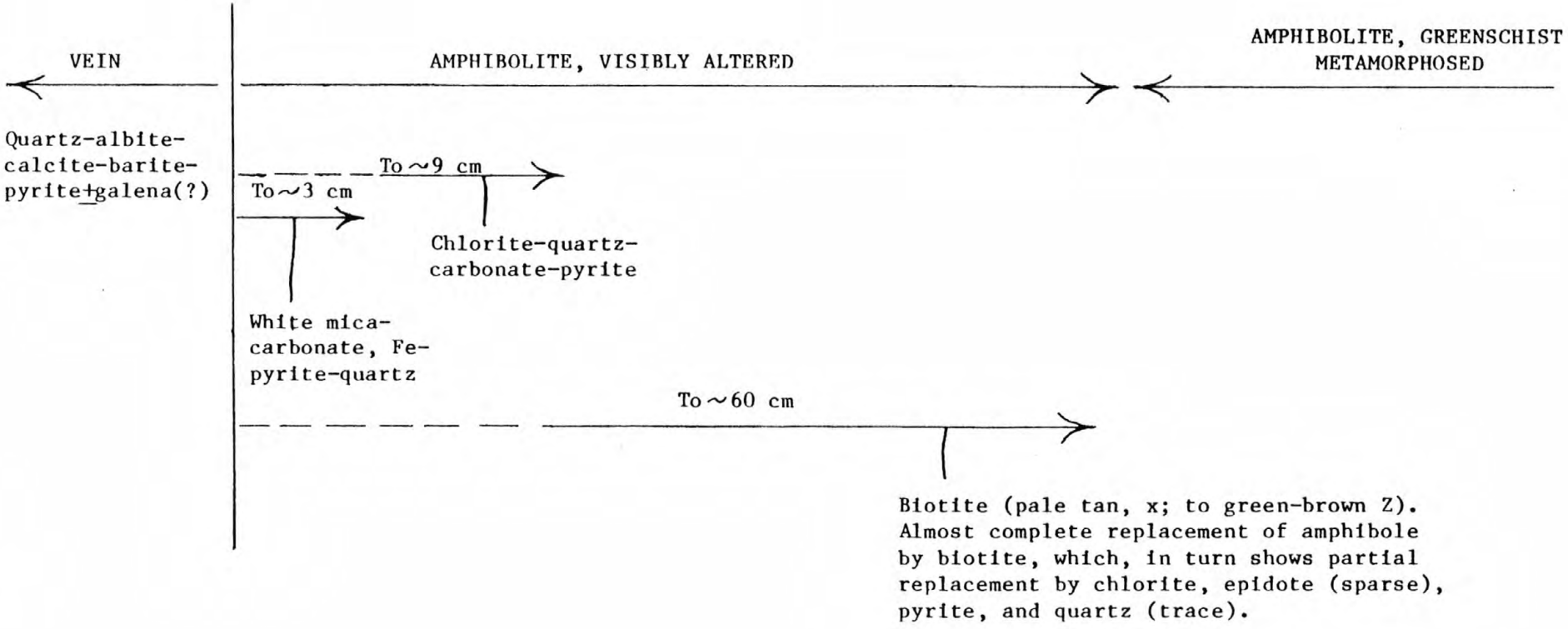

Figure 48. Diagrammatic summary of alteration surrounding a typical feldspar-stage vein including an albite-quartz-calcite-barite-pyrite-gold composite assemblage.

directions of {110} cleavage relict from the replaced hornblende. Biotite in very small domains of the rock appears to be compatible with carbonate (probably a very iron rich ankerite), opaque mineral (probably magnetite), quartz, and very minor amounts of apatite. The crystallization of biotite as a more or less complete replacement of earlier hornblende and its greenschist and propylitic assemblage breakdown products suggests a significant influx of potassium to yield the assemblage biotite-ankerite-magnetite (assemblage I, fig. 49). However, assemblage I is replaced partially in this rock by an epidote-chlorite-carbonate assemblage (II, fig. 49), and extremely small domains in the rock show incipient development of the apparently stable assemblage white mica-epidote-chlorite (III). Both of these latter two assemblages also include quartz. Very sparse occurrences of albite in the matrix of the rock may reflect incipient development of assemblage IV, which is the same as the early assemblage in the vein itself. Thus, the parageneses of these assemblages (I-IV, fig. 49) apprently reflect an initial potassium metasomatism, probably fissure controlled, that was in turn followed by a complex suite of assemblages related to final emplacement of the sodium-(albite)-rich vein. These relations imply that an early buildup in the ratio $(K^+)/(H^+)$ of the first fluids to circulate along the fissure was followed by a decrease in this ratio, an increase in $(Ca^{2+})/(2H^+)$, and then the actual emplacement of the vein was accompanied by fluids having a relatively high $(Na^+)/(H^+)$ ratio.

Amphibolite collected 8 cm from the vein shows a wispy, microfolded fabric defined by schistose domains of a relict greenish-brown (Z) biotite assemblage (I) heavily altered to a chlorite-ferroan carbonate-pyrite assemblage which includes some quartz. The rock shows an increased abundance of chlorite and disseminated ferroan carbonate relative to the previously described samples and also marks the first appearance of sulfide in the wallrock. Some plagioclase remains in the rock relict from the Proterozoic metamorphism(s). Furthermore, the amount of quartz in the rock is significantly greater than that in altered amphibolite farther out in the alteration envelope. This increase in the content of quartz and pyrite may result from a release of SiO_2 from biotite during sulfidation reaction(s) to yield a chlorite-dominant assemblage.

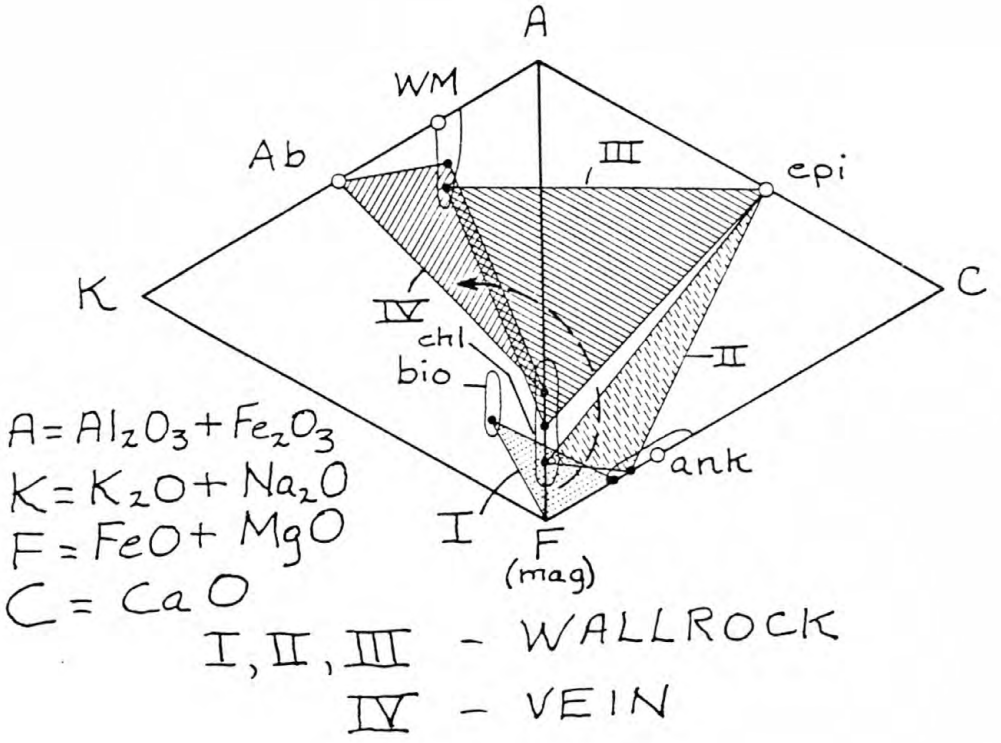

Figure 49.--Mineral assemblages in altered wallrock (assemblages I, II, and III) adjacent to a typical feldspar-bearing vein (assemblage IV). WM, white mica; Ab, albite; epi, epidote; chl, chlorite; bio, biotite; ank, ankerite; mag, magnetite. Quartz and apatite also commonly present. Compositional fields for white mica, biotite, and chlorite from Beane and Titley (1981). Compositional field for ankerite from Deer, Howie, and Zussman (1962, b). Dots, inferred compositions.

White mica is the dominant silicate gangue mineral approximately 3 cm from the vein. A white mica-ferroan calcite-quartz-pyrite assemblage is superposed here on a suite of minerals including chlorite, biotite (partly altered to chlorite), oligoclase, and opaque minerals--all relict from earlier recrystallization reactions related to passage of fluids associated with the emplacement of the vein. We envision the white mica assemblage adjacent to the vein to be the end product of a complex series of coupled reactions in the country rock controlled primarily by a concomitant decline toward the vein in at least two cation activity ratios of the associated fluid(s). A simultaneous decline in the $(Mg^{2+})/(2H^{+})$ and $(K^{+})/(H^{+})$ activity ratios of the fluid(s) may explain the relations observed among assemblages in this potassium- and magnesium-bearing alteration envelope (fig. 50; and see Beane and Tilley, 1981). The absence of talc from the biotite-bearing assemblage, which apparently was the earliest prograde assemblage to develop, suggests that initial values of $(Mg^{2+})/(2H^{+})$ in the fluid(s) were less than those required to form talc. Finally, the absence of potassium feldspar from any of the observed assemblages suggests that the cation activity ratios of $(Mg^{2+})/(2H^{+})$ and $(K^{+})/(H^{+})$ in the fluids remained outside the field of potassium feldspar.

Three samples of Proterozoic X quartzofeldspathic gneiss were collected approximately 1.1 m, 0.5 m, and 5 cm from the vein to compare their alteration assemblages with those in the adjacent amphibolite just described. The prograde regional metamorphic assemblage in the gneiss probably consisted of quartz, oligoclase (An_{15}), garnet, biotite, apatite, and opaque mineral(s). However, garnet and biotite are extremely rare in these samples because the rocks show moderate to heavy partial replacement by an assemblage of chlorite, epidote, white mica, carbonate, quartz, and opaque mineral. This chlorite- and epidote-rich assemblage is concentrated mostly in domains originally including abundant oligoclase. Indeed, as the vein is approached across this approximately 1 m distance, the quartzofeldspathic gneiss shows a progressive increase in the concentrations of white mica and epidote in the plagioclase. Very close to the vein, in the sample collected at a distance of 5 cm, there is a very well developed phyllonitic or ribboned texture in the quartz-rich domains suggesting some ductile flow in the country rock accompanied vein emplacement. This ductile flow may result from a hydrolytic weakening of quartz (see Griggs and Blacic, 1965). In addition, the country rock up to at

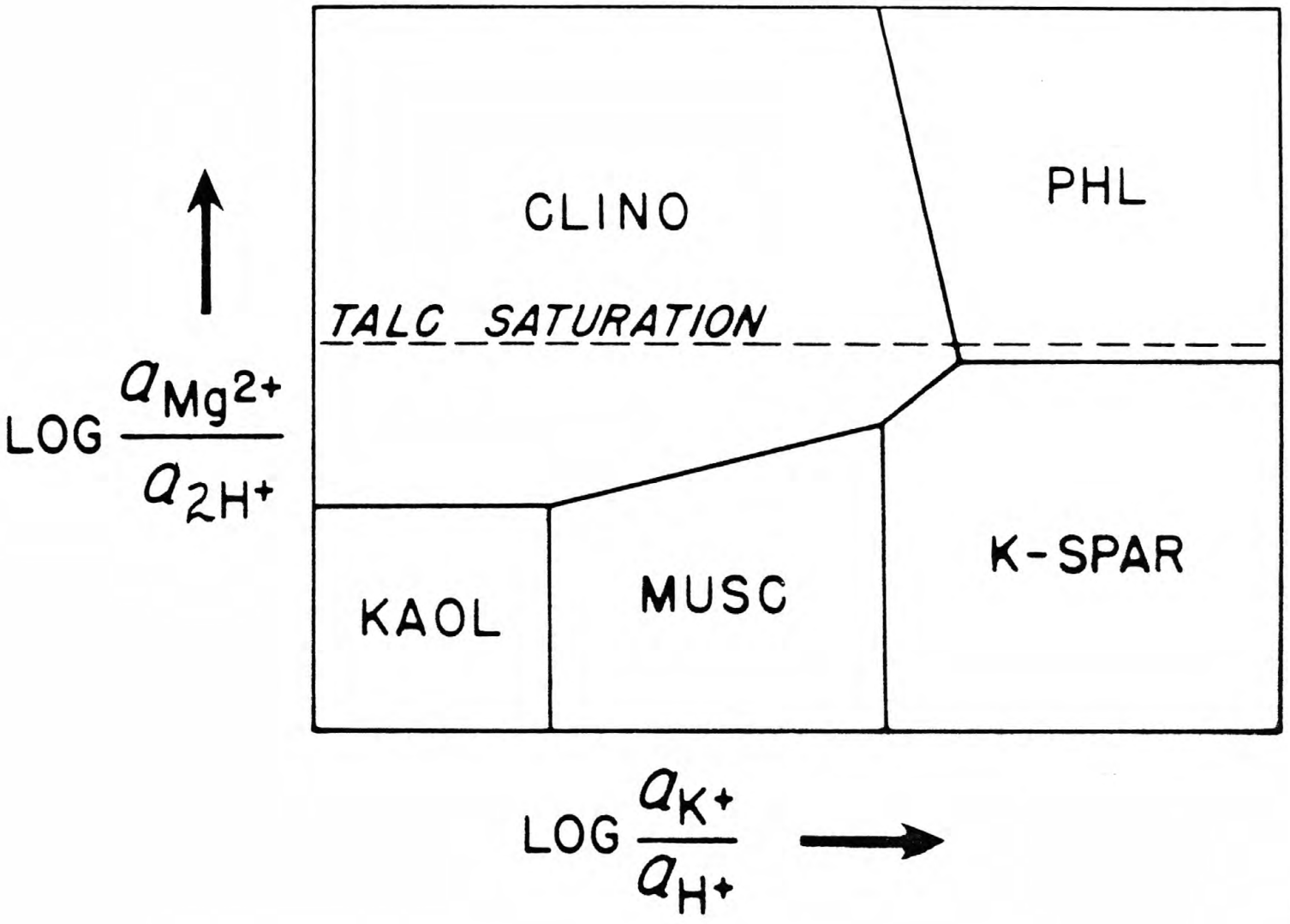

Figure 50.--Schematic stability relations among minerals as a function of $(Mg^{2+})/(2H^+)$ and $(K^+)/(H^+)$ cation activity ratios in the coexisting fluid (from Beane and Titley, 1981). Pressure 500 bars, temperature near 300°C. Excess quartz and H_2O. Clino, clinoclore; kaol, kaolinite; musc, muscovite; K-spar, potassium feldspar; phl, phlogopite.

least 5 cm from the vein shows (1) fresh albitic overgrowths on the white mica- and epidote-altered plagioclase, and (2) rutile as a common minor accessory. Thus, our petrologic studies of the quartzofeldspathic gneiss failed to document a strong, early potassic alteration stage comparable to that found in the amphibolite. However, the few shreds of biotite relict now in the white mica- and (or) chlorite-dominant rocks might be interpreted to reflect such a potassic stage during the process of alteration, although this does not seem probable. Instead, potassium feldspar is a more likely product in rocks of this overall chemistry as a result of an increase in the cationic activity ratio of $(K^+)/(H^+)$ of the associated fluids. It appears that for some reason such early K^+-enriched fluids did not circulate through the layer of quartzofeldspathic gneiss. However, the predominant type of alteration associated with the majority of veins throughout the districts appears to be propylitic.

Examination in the field (P. M. Blacet, unpub. data, 1967-1972) and in thin section shows that the propylitic alteration associated with these veins includes several specific assemblages together with wide-ranging intensities of development and depths of penetration into the surrounding country rock. Some quartz-albite veins measuring 0.5 to 1.0 m in thickness show visible pyrite-carbonate impregnations up to approximately 8 to 10 cm from the vein wall. As we described above, the ferroan carbonate together with some quartz in places fills tightly spaced, irregular microfractures at high angles to the foliation in the country rock. Generally, the ferroan carbonate-filled microfractures are discontinously confined mostly to the granoblastic portions of the gneisses. Other feldspathic veins about 15 cm thick show in outcrop an inner alteration zone of orange-brown carbonate as much as 10 cm thick in turn mantled by an outer 15-cm-thick zone of well-developed chloritization, which may include epidote and white mica with or without clinozoisite as specific assemblages. On the other hand, visible signs of ferroan carbonate plus pyrite alteration in outcrop can measure only several millimeters locally adjacent to some veins whereas elsewhere along the same vein the alteration may expand markedly into widespread zones of chloritization and flooding by ferroan carbonate. Feldspathic veins that include variable amounts of barite may also show some albite disseminated in the adjacent country rock. Quartz-fluorite veins including either feldspar, or muscovite, or sulfides and gold,

generally are characterized by white-mica dominant assemblages in their alteration envelopes.

The mineralogy of a small number of other veins in the districts appears to have been controlled significantly by the adjoining wallrocks. Where such veins cut quartzofeldspathic gneiss, the mineralogy of the vein consists of almost 100 percent quartz. However, where the same vein cuts hydrothermally altered amphibolite, the mineralogy of the vein includes abundant, irregularly shaped knots of ferroan calcite. The hydrothermal alteration in the amphibolite adjacent to such veins is predominantly propylitic and shows mostly a chlorite-carbonate assemblage.

The mineralized quartz veins in the districts mostly predate emplacement of thin, presumably Tertiary, biotite lamprophyre dikes which crop out sporadically throughout the crystalline terranes (P. M. Blacet, unpub. data, 1967-1972). In many prospect pits and several underground workings, such as those at the El Dorado mine (loc. 17, table 11), biotite lamprophyre is chilled consistently against the mineralized veins. In addition, at several other localities the biotite lamprophyre was found by Blacet actually to cut quartz-pyrite-muscovite veins. However, not all of the mafic dikes postdate the mineralized veins in the districts. Some mafic dikes clearly were intruded, contorted, and sheared during a postmetamorphic shear deformation (Laramide?) that involved local crumpling and shear folding of the Proterozoic X metamorphic rocks. Further, an at least 1-m-thick biotite lamprophyre at the L.P.M. mine (loc. 12, table 11) contains a ferroan calcite alteration assemblage possibly related to emplacement of the quartz-pyrite-gold vein there. This relation again suggests that the biotite lamprophyre at the L.P.M. mine may be prevein in age.

Disseminated Gold in Episyenite

An occurrence of visible gold, disseminated in several small alteration pipes, was recognized by Blacet during the initial stages of his regional mapping studies in the districts (loc. 19, table 11). Blacet (1969) described this occurrence as follows:

> ...The second type of lode deposit consists of small intrusive bodies of gold-bearing medium-grained, porphyritic leucosyenite containing several percent of interstitial fluorite. Miarolitic cavities in this

> leucosyenite contain small euhedral crystals of parisite [$(Ce,La)_2Ca(CO_3)_3F_2$]. Megascopically visible gold is disseminated throughout the leucosyenite and appears to be primary. The leucosyenite is tentatively considered to have crystallized in small pipelike conduits during late magmatic escape of highly potassic residual liquids that were enriched in H_2O, HF, CO_2, SO_2, Zr, Au, and rare earths...

The largest of the pipes measures at the surface about 8 m across in its longest dimension (fig. 51). On figure 51, only three pipes of episyenitic (see Leroy (1978)) rock are shown. However, another very small episyenitic body, approximately 3 m in longest dimension, crops out about 40 m southeast of section line A B, which is shown on figure 51. The alteration pipes consist of coarse-grained and fine-grained episyenitic rocks which cut across Proterozoic X fine-grained biotite monzogranite and a coarse-grained dike of Proterozoic X (?) monzogranite. Apparently, the coarse-grained monzogranite dike acted as a structural conduit to funnel fluids that produced the episyenitic rock. The episyenitic rock contains unevenly distributed concentrations of pyrite which is now oxidized to limonite and specular hematite. In places, the original pyrite content of the episyenitic rock probably was as high as 5 to 10 volume percent. Undoubtedly, the resulting color anomaly on the pipes first attracted prospectors to the site who explored the occurrence with two, shallow prospect pits. The prospect pits occur on the northernmost and the southernmost of the three pipes shown on figure 51.

In outcrop, the gold-bearing episyenitic rock in its coarse-grained facies shows locally a very quartz-poor, apparently igneous rock fabric, which contains well-developed potassium feldspar megacrysts, and which shows relatively sharp contact relations with its enclosing quartz-rich host (fig. 52). These relatively large megacrysts of potassium feldspar probably are relict from initial crystallization at magmatic conditions during Proterozoic X time. Significant removal of silica and potassium metasomatism accompanied by subsolidus crystallization and (or) re-equilibration of the megacrysts occurred during late Cretaceous and (or) early Tertiary. Late stage fluids

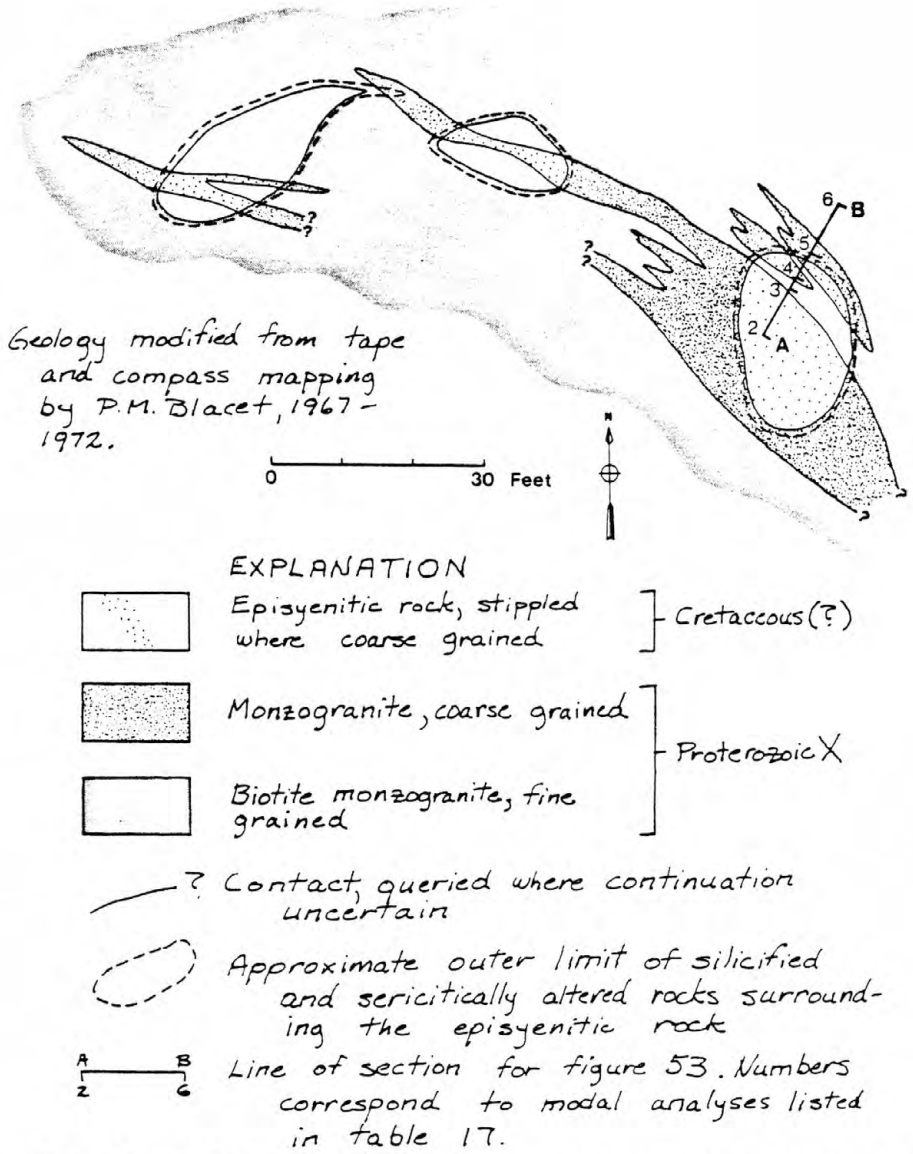

Figure 51.--Geologic sketch map of the area in the immediate vicinity of an occurrence of visible disseminated gold in episyenitic rock cropping out in the southeastern part of the Gold Basin mining district.

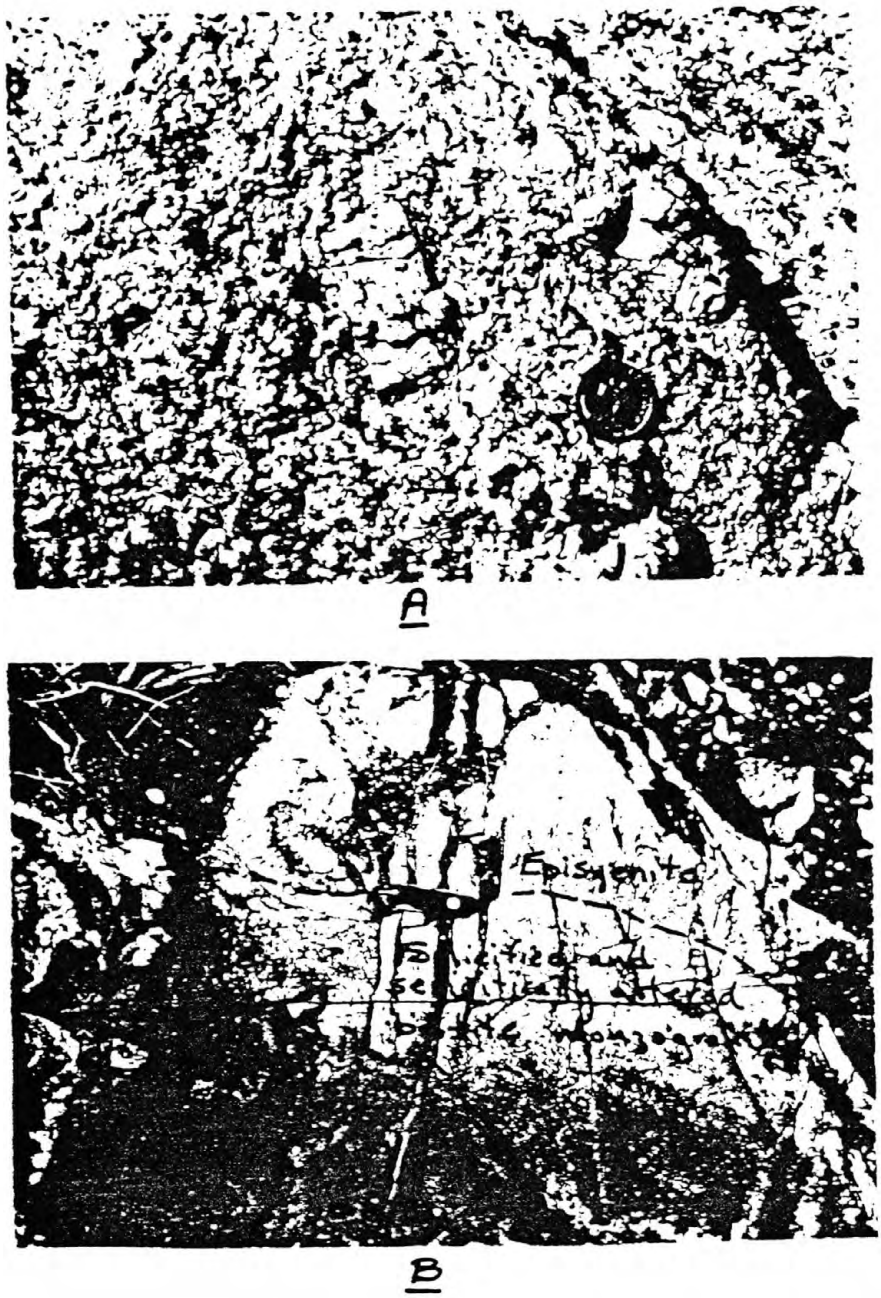

Figure 52.--Photographs from the area of an occurrence of visible, disseminated gold in episyenitic rock. A, Medium- to coarse-grained episyenitic rock containing probable mixed phenocrystic and porphyroblastic megacrysts of potassium feldspar; B, Contact relations between episyenitic rock and its mantle of silicified and sericitically altered Proterozoic X biotite monzogranite.

associated with this episyenitization finally deposited the gold. The interstitial matrix among the large potassium feldspar megacrysts is mostly potassium feldspar, but also includes very sparse secondary quartz, fluffy orange and red brown limonite and specular hematite (both replacing pyrite), purple fluorite, sparse carbonate, unevenly distributed flakes of free gold, and somewhat sporadic concentrations of white mica. As we described above, study of two white mica separates from the gold-bearing, episyenite pipes yielded ages of 127 and 130 m.y, undoubtedly reflecting the presence of excess radiogenic argon derived from the Proterozoic X host for the episyenite or minor contaminant of Proterozoic muscovite or Proterozoic feldspar in the mineral separate. These episyenite pipes also could be termed feldspathic fenite in the classification of Sutherland (1965b), or microclinite as used by Hanekom and others (1965).

Petrography

The episyenitic pipes include very sparse quartz and significant concentrations (generally more than 90 percent) of modal potassium feldspar, which decreases sharply through the approximately 1-m-wide contact zone surrounding the pipes. The variation in modal potassium feldspar and quartz across one of the pipes is shown in figure 53. Quartz in the central part of this studied episyenitic pipe makes up about 4 volume percent of the rock, but decreases to much less than 1 volume percent near the outer limit of the episyenitic rock (see table 17 for the complete modal analyses of these samples). In contrast, quartz occurs in concentrations of about 35 volume percent in a representative sample from the silicified and sericitically altered halo which surrounds the episyenitic rock. Potassium feldspar in the episyenitic rock ranges from about 84 to 92 volume percent, and it makes up about 42 volume percent of altered biotite monzogranite approximately 4 m from the episyenitic contact (analysis no. 6, fig. 53 and table 17).

Thin-sections from approximately 20 rocks were studied from the immediate area of the gold-bearing episyenitic alteration pipes. Fresh, complexly twinned potassium feldspar, which makes up typically 85 to 90 volume percent of the central parts of the episyenitic pipes, shows wide-ranging textures. The bulk of these rocks have seriate textures, and they contain many zoned potassium feldspar megacrysts whose margins are completely sutured. Some megacrysts of potassium feldspar consist of of nonturbid, crosshatch twinned potassium feldspar ovoid cores that are mantled by thin, approximately 0.4- to

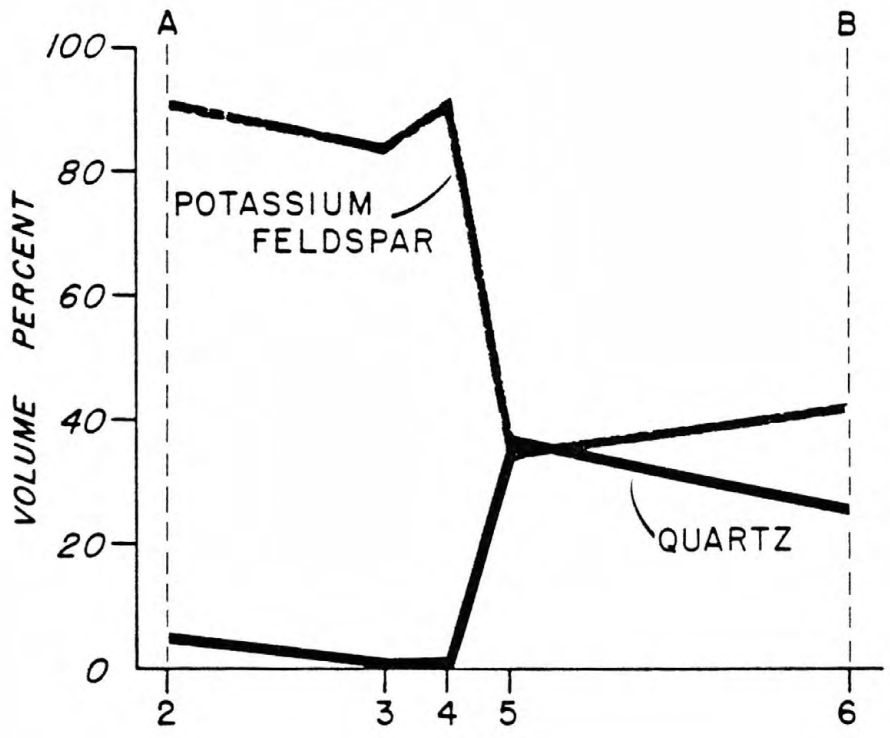

Figure 53.--Graph showing variation in modal potassium feldspar and quartz along section line AB of figure 51. Analyses numbers same as location numbers on figure 51.

Table 17. Modal analyses, in percent, of thin sections from rocks in the general area of the occurrence of visible, disseminated gold cropping out in the southeastern part of the Gold Basin mining district

[Analysis number same as location number on figure 51; --, not found]

	1	2	3	4	5	6
Field number	GM-1136d	GM-1134h	GM-1134k	GM-11341	GM-1134m	GM-1134q
Count total	600	600	600	600	600	600
Potassium feldspar	91.7	90.3	83.8	90.2	34.1	47.6
Quartz	1.	[1]4.2	.3	.2	35.9	[1]25.5
Plagioclase	--	--	--	--	--	15.3
Fluorite	.2	1.3	.2	1.	--	--
White mica	1.3	.3	3.7	.3	17.5	[2]11.3
Biotite	--	--	.2	--	--	1.8
Chlorite	--	--	--	--	--	[3]2.6
Opaque mineral(s)[4]	3.5	3.0	10.5	4.3	12.5	.4
Epidote	--	--	--	--	--	1.2
Carbonate	1.8	.3	.3	3.3	--	--
Apatite	.3	.5	.5	.3	--	.2
Zircon	.2	--	.5	.3	--	.2
Total	100.	99.9	100.	99.9	100.	100.1

[1]Quartz contains moderately abundant concentrations of rutile.
[2]Bulk of the white mica replaces plagioclase.
[3]Chlorite occurs as replacement of primary biotite.
[4]Mostly specular hematite and limonite after pyrite.

1. Episyenitic rock, coarse grained.
2. Episyenitic rock, coarse grained.
3. Episyenitic rock, fine grained.
4. Episyenitic rock, coarse grained.
5. Silicified and sericitically altered rock at margin of episyenitic rocks.
6. Biotite monzogranite, partly altered.

0.5-mm-wide borders of additional potassium feldspar. These borders comprise an inner zone of very complexly sutured potassium feldspar that appears to be developing at the expense of the crosshatch twinned core, and an outer zone of potassium feldspar that (1) is very turbid (largely because of the presence of numerous minute crystals of opaque mineral(s)) and that (2) forms a crustified lining for definitely paragenetically very late quartz- and (or) fluorite. We presume the borders of potassium feldspar grew in a predominantly hydrothermal, postmagmatic environment. However, such turbid versus nonturbid textural relations in the megacrysts do not persist throughout the episyenitic rocks. Other samples include microcline megacrysts showing ovoid turbid cores that are mantled by wide non-turbid borders. All of these specific textural relations impart an overall granoblastic fabric to the rocks. Other episyenitic rocks that formed from fine-grained Proterozoic X biotite monzogranite show, in places, wispy, irregularly shaped, comminuted domains of approximately 0.05 mm-sized, highly strained crystals of potassium feldspar. These fine-grained, discontinous domains are interstitial among fairly equant, 0.4-mm-sized crystals of potassium feldspar whose crystal boundaries initially were complexly sutured. In many of the episyenitic rocks studied, broken angular fragments of potassium feldspar, approximately 0.1 mm in their longest dimension, have been torn from some of the larger potassium feldspar megacrysts, and they are now included within secondary strain-free quartz which fills cavities. Elsewhere, rocks altered to episyenite are reported commonly as showing cataclastic phenomena (see Viladkar, 1980). In other samples at Gold Basin, some megacrysts of potassium feldspar occur as isolated crystals set in a fine-grained mesostasis of mostly potassium feldspar. Such megacrysts are largely strain free and they show evidence of interrupted crystal growth wherein euhedral outer growth zones mantle ovoid cores (fig. 54A). Hairline microveinlets of carbonate and white mica cut the megacryst, and open spaces at the edge of the megacryst are filled locally by iron-oxide that has replaced earlier pyrite. Examination of the edges of the megacrysts at high magnifications reveals that the edges of the megacrysts are in detail complexly intergrown with the groundmass. In addition, many megacrysts show no compelling, systematic textural relations with the groundmass from which their relative ages might be established confidently.

Figure 54.--Photomicrographs of relations in episyenitic rock. A, Megacryst of crosshatch twinned potassium feldspar (kfs) set in a fine-grained (avg 0.4 mm) mesosostasis (M) of mostly potassium feldspar, but including sparse amounts of carbonate, iron oxide(s), and white mica. The megacryst shows an ovoid core which is mantled by euhedral potassium feldspar. Partly crossed nicols. Sample number GM-280b (I); B Scanning electron micrograph showing a mat of rutile needles in residue remaining after decomposing episyenitic rocks in hydrofluoric acid. Sample number GM-280-51; C, Cavity in episyenitic rock filled by fluorite (F) and sparse amounts of white mica (wm). Potassium feldspar (kfs). Crossed nicols. Sample number GM-280b; D, Cathodoluminescent zonations in potassium feldspar (kfs) from the episyenitic rock. Crystal of potassium feldspar is mantled partly by specular hematite (hm) and other iron-oxide-stained potassium feldspar (fx). Note at the head of the arrow the zonation which crosscuts the regular growth zones in the potassium feldspar, and is scalloped toward the core of the potassium feldspar.

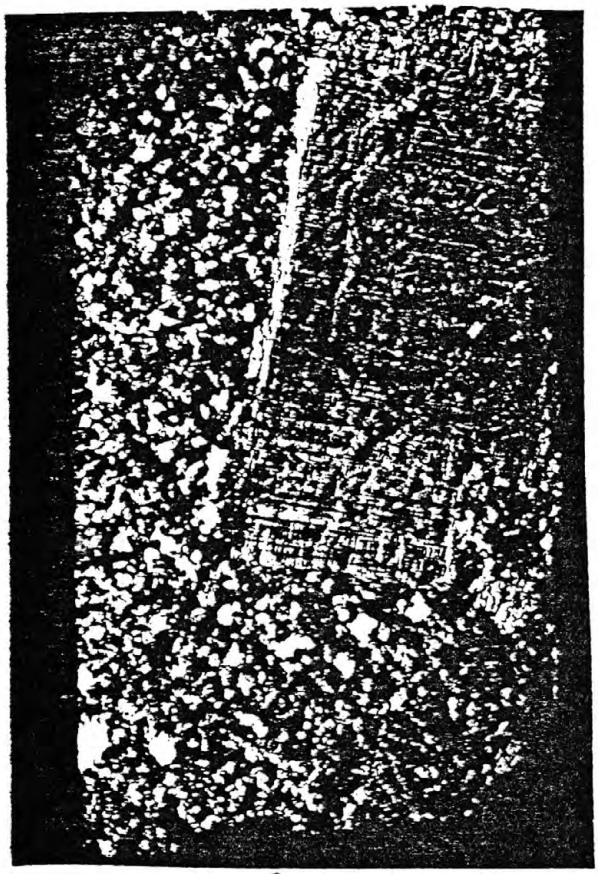

A

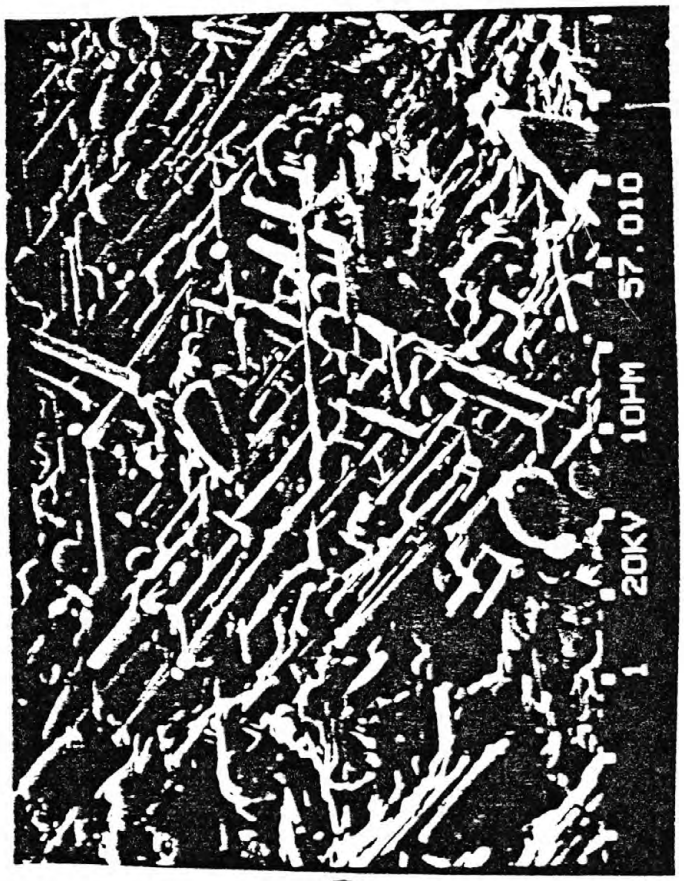

B

C

D

Two generations of quartz apparently occur in the episyenitic rocks. An early stage consists of very sparse, rounded, possibly resorbed inclusions of quartz that occur only in potassium feldspar crystals. The rounded quartz crystals generally are about 0.1 mm in their longest dimension, and they are set in equant potassium feldspar some of which measure approximately 0.7 to 0.9 mm across. In addition, some of the megacrysts of potassium feldspar larger than this include rounded quartz crystals together with other extremely small unidentifiable crystals all distributed unevenly around the periphery of former growth zones of the megacrysts. The most common textural relation between early stage quartz and potassium feldspar is for the potassium to host poikilitically clusters of rounded quartz in the central parts of the potassium feldspar. These clusters are relict from a much earlier, presumably Proterozoic X, weakly developed graphic texture in the biotite monzogranite. Further, relatively stout crystals of rutile are prominent in some of this early quartz. Relatively abundant rutile occurs in some of these early stage quartz crystals, and a mass of rutile crystals remains in residue of episyenitic rock digested in hydrofluoric acid (fig. 54B). Primary, medium-grained quartz in the biotite monzogranite which surrounds the episyenite also contains abundant rutile. The presence of rutile may be used thus to differentiate between primary and secondary quartz in the contact zone of the episyenite. The bulk of the quartz in the episyenite, however, is a late mineral which partly fills cavities among euhedrally terminated potassium feldspar crystals. Other minerals in the cavities and paragenetically about the same age as the late quartz, include white mica, apatite, fluorite, pyrite (now altered largely to limonite and (or) specular hematite), and native gold. Very typically in the episyenite, white mica and carbonate occur intergrown with each other interstitial to fresh potassium feldspar. Figure 54C shows a cavity filled mostly by fluorite. Under the optical microscope, many of the potassium feldspar crystals in direct contact with the minerals in the cavities, mostly quartz, show no visible signs of alteration. However, examination of such boundaries using cathodoluminescense on polished thick sections reveals that the typically regular and oscillatory growth zones in the potassium feldspar megacrysts marginally have been disrupted significantly by zones that luminesce (fig. 54D). These zonations are scalloped toward the cores of the potassium feldspar megacrysts, and the zonations are apparently related to adjacent areas of potassium feldspar which are stained heavily by

iron oxide and thus do not luminesce because of their high iron contents. The scalloped zonations may reflect domains of base leaching or base exchange (sodium for potassium) related chemically either to the final filling of the cavities, to the enrichment of Fe^{3+} in the late stage fluids and its substitution structurally in the potassium feldspar (Mariano, 1979), or to the subsequent alteration of these cavities in the zone of oxidation.

The approximately 1-m-thick zone of silicified and sericitically altered rocks which surrounds the episyenitic rocks shows significant variation in modal abundance and textures. In the silicified zone, which probably averages about 35 volume percent quartz in contrast to less than 5 volume percent in the episyenitic rock (table 17), subhedral almost tabular crystals of potassium feldspar about 6 to 8 mm in longest dimension show combined Carlsbad and cross-hatch twinning. These relatively large crystals appear to have grown porphyroblastically in a largely subsolidus environment, and to have been replaced partly by white mica concentrated in irregular patches. Such crystals also show inclusions of fine-grained, ovoid quartz crystals similar to the primary quartz in the potassium feldspar megacrysts of the episyenite. However, the overall size of individual quartz crystals ranges widely in these silicified rocks, and probably averages about 2.0 mm in the most quartz-rich domains. In these domains, textures are largely granoblastic, and quartz-quartz boundaries are highly sutured. Similar to the sparse primary quartz in the episyenitic rocks, quartz here in the silicified zone is also very strongly rutilated which relation suggests that primary quartz (rutile-bearing) was the site of nucleation for silica flooding marginal to the episyenite. Fluid inclusions are very abundant in the quartz, and they are mostly concentrated along annealed microfractures that cut the quartz grains. Many of these fluid inclusions contain liquid CO_2 at room temperature. In addition, the silicified and sericitically altered rocks contain fairly high concentrations of iron oxides that replace earlier crystallized pyrite. As shown in table 17, a typical sample from these altered rocks contains about 13 volume percent iron oxide(s). Paragenetically, the sulfide (probably pyrite) from which the iron oxide(s) have been derived is the same age as the white mica.

Minor sericitic alteration effects extend at least 4 m beyond the mapped outer limit of the silicified and sericitically altered halo. A sample of fine-grained Proterozoic X biotite monzogranite studied from this general area

(analysis no. 6, table 17 and fig. 53) shows a weakly developed gneissic fabric resulting from a dimensional orientation of primary quartz and biotite. The minimum content of plagioclase (sodic oligoclase, An_{10-15}) in these rocks is about 15 volume percent, but much of the white mica in the mode actually occurs with or without epidote as a partial but ubiquitous replacement of plagioclase. Some of the individual crystals of white mica that replace plagioclase are fairly large-sized, and they reach lengths of about 0.4 to 0.5 mm. Dark brown (Z) primary biotite is altered heavily to chlorite, also with or without epidote and opaque minerals, including possibly both magnetite and ilmenite. However, potassium feldspar in these rocks is quite fresh, and contains abundant cross-hatch twinning. Quartz, which here is obviously part of the igneous fabric of the rocks, contains conspicuous concentrations of needles of rutile. Minor accessories include apatite, zircon, and allanite. The presence of primary biotite, sericitically altered plagioclase, and abundant, primary quartz provide a substantial mineralogical contrast with the potassium feldspar-and fluffy orange carbonate-dominant mixed mineralogical assemblages in the episyenite.

Paragenetic Relations of Gold

Textural relations of gold in the episyenitic rock were studied using the SEM and standard optical methods. Examination of artificially broken surfaces of episyenitic rock revealed that small nodules of gold in places rest either on potassium feldspar or quartz in the episyenitic rock (fig. 55A, B). Many of these nodules of gold are featureless in the episyenitic rocks, whereas others (fig. 55C) show forms suggesting that they had been molded against a cubic mineral, most likely pyrite. Thus, at least some of the gold in the episyenite must have been introduced quite late paragenetically, post pyrite. Some of the pyrite in the episyenite pipes also contained gold because some of the cubic vugs are now fringed by limonite which includes sparse amounts of free gold. Qualitative analyses of many nodules of gold from the pipes using an energy dispersive X-ray microanalyzer on the SEM revealed that in places they contain some silver and apparently some unknown amounts of iron. The relatively late introduction of native gold into the episyenitic pipes is suggested also by the inclusion in these rocks of some gold in carbonate, probably ferroan calcite (fig. 56A, B). As can be seen in polished sections (fig. 56A-C), specular hematite is locally quite abundant. In addition, small pieces of episyenite, ranging anywhere in size from about 9 to 200 g, were

Figure 55.--Scanning electron microscope (SEM) micrographs of gold collected from the locality showing gold disseminated in episyenitic rock (loc. no. 19, table 11) in the Gold Basin mining district. Bar indicates scale in micrometers ($1\ \mu m = 1x10^{-6}m$). A, Small nodule of gold (Au) containing some Ag and Fe resting on potassium feldspar (k spar). The upper surface of the gold nodule apparently was abraded when the rock was fractured prior to mounting the sample in the SEM; B, Small mass of gold (Au) resting against a groundmass of secondary quartz (Q) which occurs locally in minor amounts in the episyenitic rock. The gold is featureless and shows no apparent crystal form; C, Small mass of gold (Au) obained from a heavy-mineral concentrate collected from the episyenite. The gold shows that it appears to been molded against a cubic mineral, most probably pyrite. Silver (Ag) was detected in the gold using the X-ray analyzer.

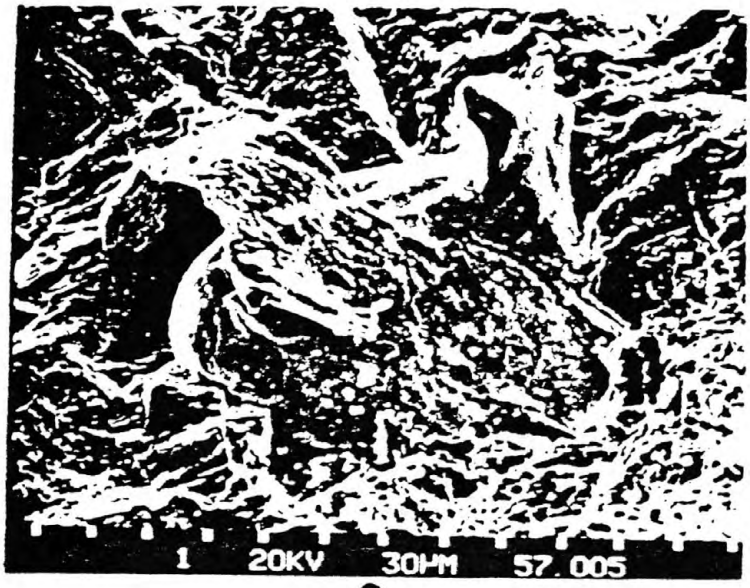

A

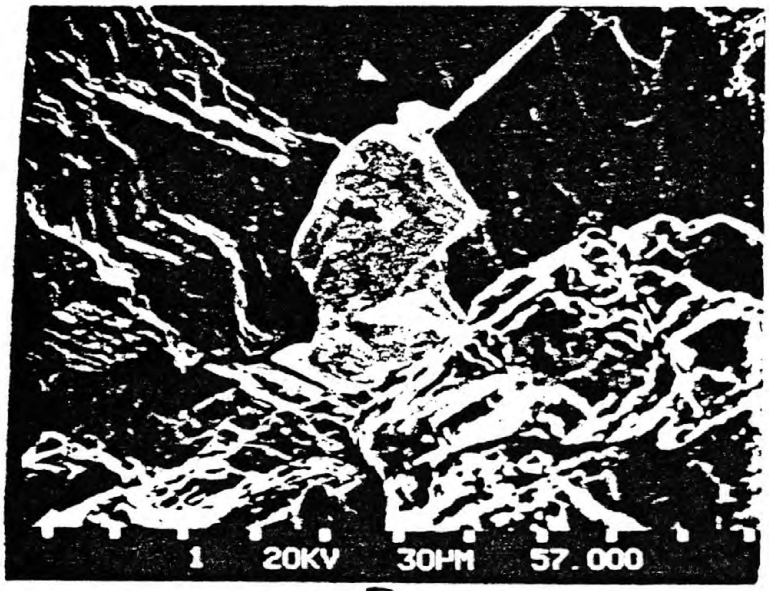

B

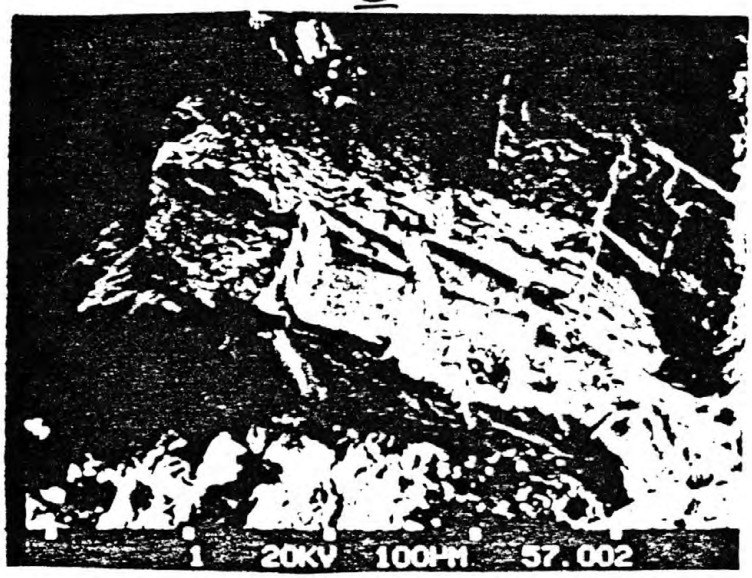

C

Figure 56.--Photomicrographs in plane-polarized reflected light of polished section of coarse-grained episyenite rock containing visible gold. Sample number GM-280b. Specular hematite (hm); limonite (li). A, Textural relations of gold (Au), carbonate (C), potassium feldspar (kf), specular hematite, and limonite; B, Closeup view showing details of relations among gold (Au), carbonate (C), specular hematite, and limonite in A; C, Slightly oxidized cube of pyrite (py), potassium feldspar (kf), specular hematite, and limonite.

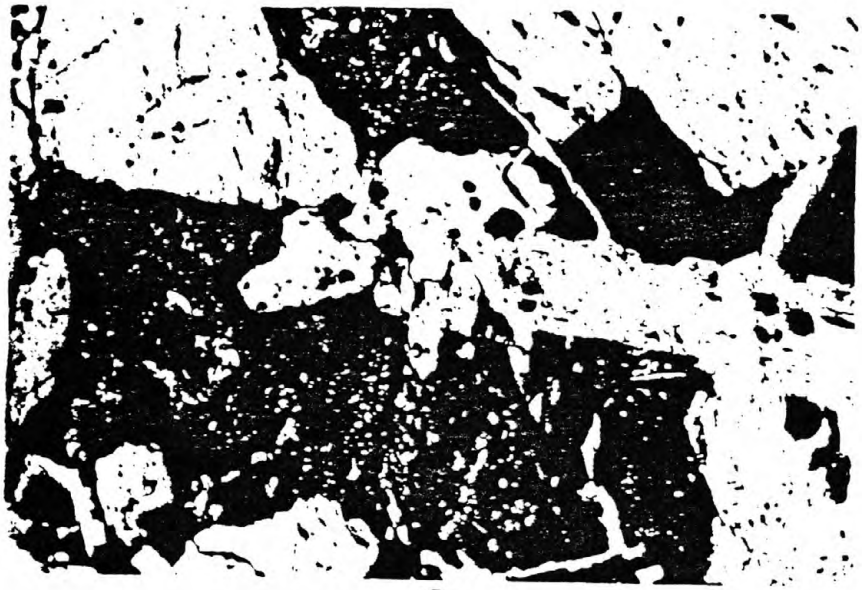

A

B

C

digested in hydrofluoric acid using the techniques of Neuerburg (1961, 1975). Residues from these procedures included some intergrown purple fluorite and gold (fig. 57), thus documenting their penecontemporaneous, late-stage emplacement in the episyenite. Fluorite in the episyenite mostly fills cavities most likely produced during the leaching of primary quartz and plagioclase from biotite monzogranite.

Chemistry

Chemical analyses are available for four fist-sized samples of episyenite (analysis nos. 1-4, table 18), three adjoining samples of the contact zone surrounding one of the pipes (nos. 5-7), and, as a comparison, a sample of fine-grained, Proterozoic X biotite monzogranite (no. 8) collected about 15 m southwest of the westernmost episyenite pipe shown on figure 51. One of the samples of episyenite (analysis no. 1, table 18) is from the westernmost pipe. The three remaining samples of episyenite (nos. 2-4), and the three samples analyzed from the contact zone are all from the episyenitic pipe on the east (fig. 51). Precise quantitative values of metasomatic additions and subtractions of all elements involved during the entire process of episyenitization are difficult to calculate because of the chemically dynamic and multi-stage nature of the event. However, the early stages of episyenitization involved (1) addition of potassium and probably barium, and removal of silica, sodium, magnesium and calcium; and (2) an overall increase of the porosity of the rock. The samples of episyenite contain more than 14 weight percent K_2O, and approximately 0.4 weight percent Na_2O. The content of normative potassium feldspar in the four samples of analyzed episyenite is in the range 83 to 91 weight percent; normative albite is in the range 1.7 to 4.3 weight percent (table 18). These values of normative potassium feldspar are quite similar to the modal contents of 84 to 92 volume percent found in the episyenite (table 17). Silica contents in the four analyzed samples of episyenite are in the range 56 to 65 weight percent, and these contents of silica contrast significantly with the 1-m-wide contact zone of silification and sericitization surrounding the episyenitic pipes, and with nearby Proterozoic X biotite monzogranite (table 18) that forms the protolith of much of the episyenite. Figure 58 shows a graphic comparison of normative potassium feldspar, normative albite, and normative quartz among episyenite, contact zone, and biotite monzogranite. Initially, episyenitization involved leaching of primary quartz, simultaneous breakdown and removal of many

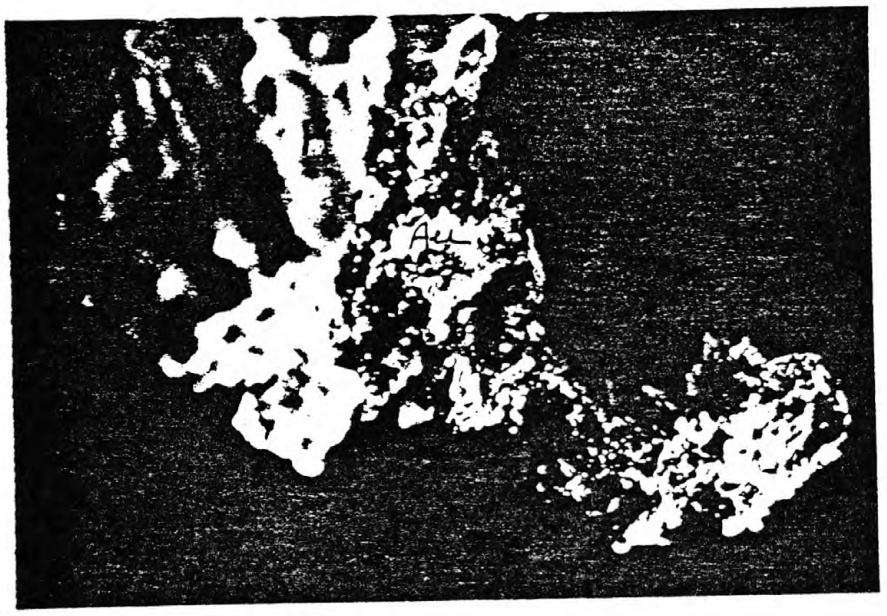

Figure 57.--Photomicrograph showing the morphology of intergrown fluorite (F) and gold (Au). Fluorite and gold are residues separated from a small (about 9 gm) sample of episyenite by decomposing the episyenite in hydrofluoric acid (see text).

Table 18.—Analytical data of late Cretaceous-early Tertiary episyenite, of the contact zone of the episyenite, and the adjoining host Proterozic X biotite monzogranite

[Chemical analyses: Numbers 1 and 2, P. L. D. Elmore and S. Botts, analysts. Methods used are those described in Shapiro and Brannock (1962), supplemented by atomic absorption; and Shapiro (1967). Numbers 3-8, major oxides by X-ray spectroscopy, J. S. Wahlberg, J. Taggart, and J. Baker, analysts; partial chemical analyses by standard methods, P. R. Klock and J. Riviello, analysts. Chemical analysis for gold (nos. 1 and 2) by a combined fire-assay-atomic absorption technique; Leung Mei, analyst. Au, Hg, and Zn (nos. 3-8, _____, analysts. Spectrographic analyses by Chris Heropoulos (nos. 1-2) and J. Kent (nos. 3-8). Results are reported to the nearest number in the series 1., 0.7, 0.5, 0.3, 0.2, 0.15, 0.1, 0.07, etc., which represent midpoints of interval data on a geometric scale. The precision of a reported value is approximately plus or minus one series interval at 68 percent confidence and two intervals at 95 percent confidence. Looked for but not found: As, Bi, Cd, Pd, Pt, Sb, Te (nos. 1-2), U (nos. 1-2), W (nos. 1-2), Ge (nos. 3-8), Hf, In, Li (nos. 1-2), Re, Ta (nos. 1-2), Th (nos. 1-2), Tl (nos. 1-2), Pr (nos. 1-2), Sm (nos. 1-2), Eu (nos. 1-2). ——, not detected; N.d., not determined]

	1	2	3	4	5	6	7	8
Field number	GM-280	GM-280b	GM-1134k	GM-11341	GM-1134m	GM-1134n	GM-1134o	79GM12
Chemical analyses (weight percent)								
SiO_2	62.2	64.4	56.1	60.8	75.2	76.9	76.0	72.9
Al_2O_3	17.7	18.4	16.7	17.6	10.9	10.1	9.94	13.4
Fe_2O_3	.90	1.	2.77	.97	2.31	1.78	2.63	2.15
FeO	.12	.44	.03	.03	.26	.17	.70	1.05
MgO	.00	.00	.20	<.10	.24	.17	.34	.36
CaO	1.8	.30	4.41	1.83	.35	.72	.49	.85
Na_2O	.50	.40	.21	.28	.28	<.15	<.15	2.54
K_2O	14.5	14.3	14.1	15.2	7.84	7.80	7.30	6.08
H_2O^+	.43	.54	.50	.18	.56	.38	.47	.64
H_2O^-	.00	.02	.04	.06	.08	.08	.12	.06
TiO_2	.44	.66	.57	.58	.34	.33	.54	.31
P_2O_5	.00	.12	.12	<.05	.09	.09	.13	.06
MnO	.02	.03	.05	<.02	<.02	<.02	<.02	.04
CO_2	.08	<.05	3.60	.84	.12	.46	.29	.06
F	1.1	.06	.15	.53	.21	.13	.16	.07
Cl	N.d.	N.d.	.010	.006	.004	.005	.004	.004
S	N.d.	N.d.	.001	<.001	.019	.028	.022	.17
Subtotal	99.79	100.67	99.56	98.91	98.80	99.14	99.14	100.74
Less O=F, Cl	.46	.03	.06	.22	.09	.05	.07	.03
	99.33	100.64	99.50	98.69	98.71	99.09	99.07	100.71
Semiquantitative spectrographic analysis (weight percent)								
Ag	<.00007	<.00007	——	——	——	——	——	——
B	——	——	.0006	——	.0012	.0006	.0007	.007
Ba	.3	.3	.1	.31	.095	.097	.13	.026
Be	——	——	——	——	——	——	.0003	.0007
Co	——	——	.0002	——	.0002	——	.0003	.0003
Cr	.0005	.001	.0019	.0009	.0005	.0007	.0008	.0002
Cu	.0002	.0015	.0024	.0016	.0007	.0067	.0037	.0002
La	.01	.03	.03	.032	.0097	.016	.023	.024
Mo	.0005	.001	.003	.0007	.0009	.0009	.0009	.0003
Nb	.0015	.005	.0076	.0059	.0038	.0038	.0069	.0054
Ni	——	——	.0003	——	.0003	.0002	.0003	——
Pb	.05	.003	.11	.034	.032	.0052	.0046	.0058
Sc	——	.0005	——	——	——	——	——	——
Sn	——	——	.0011	.0006	.0009	.0007	.0014	.0008
Sr	.02	.015	.01	.008	.0058	.0073	.0072	.0093
V	.0007	.001	.0023	.0042	.0036	.0018	.0033	.0015
Y	.002	.01	.0072	.0069	.0075	.013	.012	.0036
Zn	——	——	.018	.0022	.0014	.0022	.0031	.002
Zr	.02	.03	.055	.068	.011	.02	.051	.02
Ce	.02	.07	.065	.05	.011	.027	.047	.047
Ga	.002	.0015	.0016	.0012	.0017	.0012	.0016	.0019
Yb	.0002	.001	.0009	.0006	.0005	.0007	——	.0003
Nd	.007	.02	——	——	——	——	——	——
Chemical analyses (parts per million)								
Au	0.8, 1.1	1.6, 1.4						
Hg	n.d.	n.d.						
Zn	n.d.	n.d.						
C.I.P.W. Norms (weight percent)								
Q	3.7	7.3	0.98	1.1	43.9	46.5	47.4	32.8
C	1.1	2.2	1.1	.71	2.	1.4	1.8	1.5
or	86.3	83.9	83.8	91.	47.	46.5	43.5	35.7
ab	4.3	3.4	1.7	2.3	2.4	1.3	1.3	21.4
an	.37	.03	——	——	——	——	——	3.
hl	——	——	.02	.02	——	——	——	——
en	——	——	——	——	.33	.13	.37	.89
mt	——	——	——	——	——	——	.69	2.
hm	.91	.99	2.8	.98	2.3	1.8	2.2	.76
il	.3	.99	.17	.11	.55	.33	1.	.59
ru	.29	.14	.48	.53	.05	.16	——	——
ap	——	.28	.29	.12	.22	.22	.31	.14
fr	2.3	.10	.29	1.1	.33	.25	.31	.13
pr	——	——	——	——	.04	.06	.04	.32
cc	.18	.11	7.3	1.8	——	.76	.18	.14
mg	——	——	.42	.02	.23	.25	.41	——
Total	99.7	99.4	99.4	99.8	99.4	99.7	99.5	99.4
Salic	95.6	96.8	87.6	95.1	95.3	95.7	94.	94.4
Femic	4.1	2.6	11.8	4.7	4.1	4.	5.5	5.
D. I.	94.3	94.6	86.5	94.4	93.3	94.3	92.2	89.9

1. Episyenite, location number 19, table 11 and plate 1; obtained from the westernmost pipe shown on figure 51.
2. Episyenite, location number 19, table 11 and plate 1; obtained from the easternmost pipe shown on figure 51.
3. Episyenite, location number 19, table 11 and plate 1; obtained from the westernmost pipe shown on figure 51.
4. Episyenite, location number 19, table 11 and plate 1; obtained from the westernmost pipe shown on figure 51.
5. Contact zone surrounding easternmost episyenite pipe (see fig. 51).
6. Contact zone surrounding easternmost episyenite pipe (see fig. 51).
7. Contact zone surrounding easternmost episyenite pipe (see fig. 51).
8. Fine-grained Proterozoic X biotite monzogranite collected 15 m southwest of westernmost pipe on figure 51.

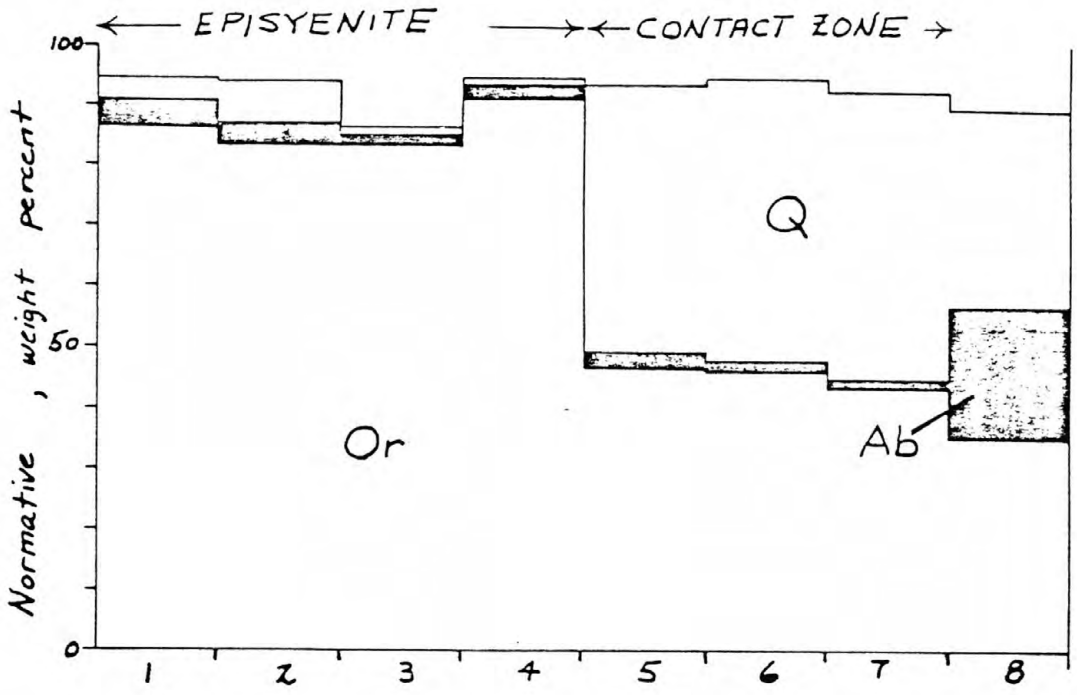

Figure 58.--Plot showing, in weight percent, normative potassium feldspar (Or), normative albite (ab), and normative quartz (Q) in analyzed samples of late Cretaceous-early Tertiary episyenite, contact zone of the episyenite, and a nearby sample of Proterozoic X biotite monzogranite. Data from table 18.

chemical constituents comprising plagioclase and biotite, and metasomatic addition of potassium. Total iron (as Fe_2O_3) makes up about 1 weight percent of the three samples of episyenite most deficient in CO_2 (analysis nos. 1, 2, and 4; table 18), whereas Fe_2O_3 makes up almost 2.8 weight percent of the sample (no. 2) of episyenite which has the highest content of CO_2 (3.6 weight percent). Most of the Fe_2O_3 in this particular sample must be in late stage ferroan carbonate which fills vugs. Some iron also may may have been fixed finally as limonite or specular hematite that replaced an early epigenetic stage of pyrite. Probably, more realistic estimates of the overall distribution of iron in the episyenitic pipes may be inferred from table 17 which shows modal opaque mineral(s) in episyenite to range from about 3 to 11 percent by volume.

There apparently has been no major metasomatic addition of alumina to the pipes during episyenitization. The analyzed sample (analysis no. 8, table 18) from the biotite monzogranite protolith is peraluminous, and shows a 1.09 value for Al_2O_3: (K_2O + Na_2O + CaO) in molecular percent. The sample is also corundum normative (1.5 weight percent C, table 18). This degree of alumina saturation may reflect removal of some calcium accompanying partial alteration of plagioclase during the Proterozoic greenschist metamorphic event. Such alumina saturation seemingly has been preserved during the late Cretaceous-early Tertiary emplacement of the episyenite pipes. The mean of those three analyzed samples of episyenite having minimal contents of CO_2 (analysis no. 1, table 19) shows that the episyenite is saturated similarly with respect to alumina. The value of Al_2O_3:(K_2O + Na_2O + CaO) in molecular percent for the average analysis of episyenite is 0.95. However, if the content of CaO is adjusted to account for the late stage fluorine and carbonate in the rock, then the average of the episyenite samples analyzed has a 1.04 value for Al_2O_3:(K_2O + Na_2O + CaO) in molecular percent.

Discussion

The mineral assemblages, chemistry, and genetically associated two-mica monzogranite of the episyenite pipes in the Gold Basin district resemble closely similar rocks elsewhere hosted by an assortment of geologic environments. Uranium-bearing episyenites and unmineralized episyenites occur in upper Paleozoic two-mica granites of the Central France Massif (Moreau and Ranchin, 1973). Emplacement of the mineralized episyenites there included (1) an almost total removal of primary plagioclase and primary quartz from the

Table 19. Chemical analysis of average episyenite from Gold Basin and chemical analyses of other syenitic and episyenitic rocks from elsewhere
[----, not detected; N.D. not determined or not listed]

	1	2	3	4	5	6
	Chemical analyses (weight percent)					
SiO_2	62.5	58.58	58.43	62.73	67.52	63.62
Al_2O_3	17.9	16.64	17.84	N.D.	13.58	18.27
Fe_2O_3	.96	3.04	5.09	N.D.	4.71	1.18
FeO	.20	3.13	--	N.D.	.20	.09
MgO	.--	1.87	.43	N.D.	1.03	.10
CaO	1.31	3.53	.80	N.D.	1.62	.80
Na_2O	.39	5.24	.38	.38	.40	.63
K_2O	14.7	4.95	13.9	14.97	10.	14.38
H_2O^+	.38	.99	1.05	N.D.	1.04	.18
H_2O^-	.03	.23	.11	N.D.	N.D.	N.D.
TiO_2	.56	.84	.34	N.D.	.09	.11
P_2O_5	.03	.29	.35	N.D.	.33	.12
MnO	.02	.13	.42	N.D.	N.D.	.02
CO_2	.31	.28	N.D.	N.D.	.20	.26
F	.56	N.D.	N.D.	N.D.	.30	N.D.
Subtotal	99.85	99.74	[1]99.32	N.D.	100.89	99.94
Less O=F	.24	N.D.			.13	
Total	99.61	99.74			100.76	

1. Episyenite (loc. 19, table 11). Average of analyses 1, 2, and 4 (table 18).
2. Syenite of LeMaitre (1976).
3. Potash trachyte, Toror Hills, Uganda (Sutherland, 1965, p. 370).
4. Partial analysis, fenitized granitic basement, Toror Hills, Uganda (Sutherland, 1965, p. 371).
5. Feldspar rock xenoliths in carbonatite, Amba Dongar, India (Deans and others, 1972, p. B5).
6. Microclinite, Palabora, South Africa (Hanekom and others, 1965).

two-mica granites, (2) conversion of primary biotite to chlorite, (3) subsolidus crystallization of additional white mica, and (4) an increased porosity of the rock. Viladkar (1980) also found a substantial reduction in silica during the development of the fenitized or episyenitized aureole around the Newmania carbonatite, Rajasthan, India. The final stages of mineralization in the episyenite pipes in the Central Franee Massif resulted in the partial filling of the leached cavities by carbonate(s), hematite, pitchblende, and some secondary quartz (Moreau and Ranchin, 1973). The chemistry of other episyenitic alteration zones or fenites associated with some carbonate complexes is very similar to the chemical make-up of the episyenites at Gold Basin. This relation is shown in the analyses of selected samples of potash trachyte and fenitized granitic rock from an area of carbonatites at Toror Hills, Uganda; feldspar rock xenoliths in carbonatite from Amba Dongar, India; and microclinite from the Palabora, South Africa carbonatite area listed in table 19 (compare analysis no. 1 to analyses nos. 4-7). These latter analyses show K_2O contents that range from about 10 to 15 weight percent, and extremely high K_2O to Na_2O ratios. The partial analysis for SiO_2, Na_2O, and K_2O of a sample of fenitized granitic basement (no. 4), and the "average" sample of episyenite analyzed from the Gold Basin District are similar. In addition, fluorite, apatite, and pyrite are common late-stage accessory minerals in many episyenites, or fenites, associated with carbonatite complexes (Smirnov, 1976), and fluorite even occurs in economically important tonnages and grades in some of them (Deans and others, 1972). Parisite, a mineral ideally having the composition $(Ce, La)_2 Ca(CO_3)_3 F_2$ (Roberts, Rapp, and Weber, 1974), also was reported by Blacet (1969) to occur rarely in these episyenitic rocks in the Gold Basin district. Parisite is considered by Smirnov (1976) to be one of the accessory minerals typically developed in carbonatite complexes, but important concentrations of gold are not generally known to be associated with such complexes (see Smirnov, 1976; Boyle, 1979). Some carbonatites, however, contain measurable amounts of gold. Copper concentrate from the Palabora, South Africa carbonatite is reported to contain 0.05 troy ounces gold and 24.5 troy ounces silver per ton (Hanekom and others, 1965, p. 158).

Our study of the gold-bearing episyenitic pipes suggests a protracted passage of potassium-charged and silica-deficient fluids initally occurred through a narrowly confined series of vents. This streaming of fluids

eventually culminated in the late-stage deposition of gold there. These episyenites are envisaged further as representing structurally deeper levels of mineralization than the veins in the districts. We infer that the early-stage fluids increased porosity and thereby enhanced permeability at the sites of the vents primarily by leaching primary quartz and primary placioclase from the rocks. This facilitated a continued circulation of late-stage fluid(s) associated with the introduction of gold, and its accompanying pyrite, fluorite, hematite, secondary quartz, carbonate, and white mica. Although two determinations of the age of white mica from the episyenite yielded anomalously old ages (130 and 127 m.y., see above), we nonetheless maintain that the process of episyenitization and the introduction of gold into the episyenites is related temporally and genetically to an upper Cretaceous, two-mica magmatic event. As discussed above, these anomalously old ages may reflect "contamination" of the evolving episyenite by radiogenic argon relict from the enclosing Proterozoic X rocks or contamination of the samples dated by Proterozoic mica and (or) feldspar. As will be shown below, the late-stage fluids in the fluorite-bearing and gold-bearing episyenitic rocks are the same chemically and approximately the same temperatures as those in a well-studied, fluorite-bearing vein which cuts the upper Cretaceous two-mica monzogranite, north of the Cyclopic mine as well as many other veins throughout the districts. This vein has been dated at 68 m.y. and white mica from the two-mica monzogranite yields an age of 72 m.y. (see above).

Veins Along Miocene Detachment Fault

Blocks of presumed late Cretaceous-early Tertiary age, mineralized quartz veins crop out along the Miocene detachment fault in the open-cut and underground workings at the Cyclopic mine (P. M. Blacet, unpub. data, 1967-1972). The workings at the Cyclopic mine, the deposit showing the largest production of lode gold from the districts to date, consist of a series of open cuts and shallow underground drifts along a strand of Miocene detachment fault that here has been shown to be post-Muddy Creek Formation in age (Blacet, 1975). Some displacements along the detachment fault may have been localized by shallow-dipping zones of weakness dating from upper Cretaceous or lower Tertiary time. The blocks of vein quartz comprise the ore in the deposit, and they occur sporadically in gouge of mostly the uppermost splay of the detachment zone. In the general area of the Cyclopic mine, the detachment zone in places consists of at least three stacked plates (Blacet, 1975).

Here, the detachment zone shows an approximately N. 50° W. strike, although individual splays along the zone show marked departures from the general trend. Further, some of the individual splays at the surface crop out across at least 40 m in some of the open cuts of the mine, and some can be traced at the surface up to 1.2 km as noted previously by Schrader (1909). However, the lowermost surface of some of these splays locally forms a very sharp, almost planar contact with the underlying metamorphic rocks (fig. 59A). In such well-exposed outcrops, the hard yellow-brown gouge zone resting immediately on the metamorphic rocks shows very faint striations that trend roughly parallel with the northwesterly trend of the trace of the detachment fault. Although dips within the detachment fault zone generally are quite gentle, some open cuts through individual splays reveal dips of approximately 50 to 55° in variably colored gouge zones which surround some of the large blocks of brecciated vein quartz caught up within the zone (fig. 59B). Some blocks of brecciated vein quartz are very resistant to weathering (fig. 59C), and together with the strong iron-oxide staining form excellent markers along the individual fault splays that make up the overall Miocene detachment zone. The mineralogy of these mineralized, tectonically bounded blocks of veins is the same as the late Cretaceous-early Tertiary veins described above. However, as pointed out by Schrader (1909, p. 125) the blocks of vein material at the Cyclopic apparently are not continuous to any great depth, nor do they * * *"have any definite fissure wall, but usually at a short distance below the surface [instead] give way to less firm material." Although the deposit at the Cyclopic is the only one known in the districts along the trace of the detachment fault, some dislocation surfaces elsewhere are reported to contain gold ore. Detachment surfaces associated with some cordilleran metamorphic core complexes in western Arizona and eastern California in places contain a chrysocolla-chalcopyrite-specular hematite-pyrite association, together with some barite and fluorite, that locally yielded values in gold (Reynolds, 1980; Wilkins and Heidrick, 1982).

Placer Gold Deposits

Placer gold deposits in the Gold Basin-Lost Basin mining districts are known to occur primarily in three areas. The most important deposits are in selected locations within a 10-km by 3-km area along the eastern flank of the Lost Basin range. Many reports refer to this area as the King Tut placer area. Some placer deposits were worked also in the northern part of the Gold

Figure 59.--Photographs showing relations along the Miocene detachment fault in the general area of the Cyclopic mine. A, South-dipping low-angle fault between Proterozoic metamorphic rocks on the north and gouge along the Miocene detachment surface; B, Discontinuous blocks of brecciated and unbrecciated blocks and fragments of mineralized vein quartz at extreme northwest end of large open cut; C, Large isolated block of brecciated vein quartz in flat-lying gouge zone between Proterozoic X porphyritic monzogranite in the hanging wall and mixed Proterozoic X metamoprhic rocks and upper Cretaceous two-mica monzogranite in the footwall.

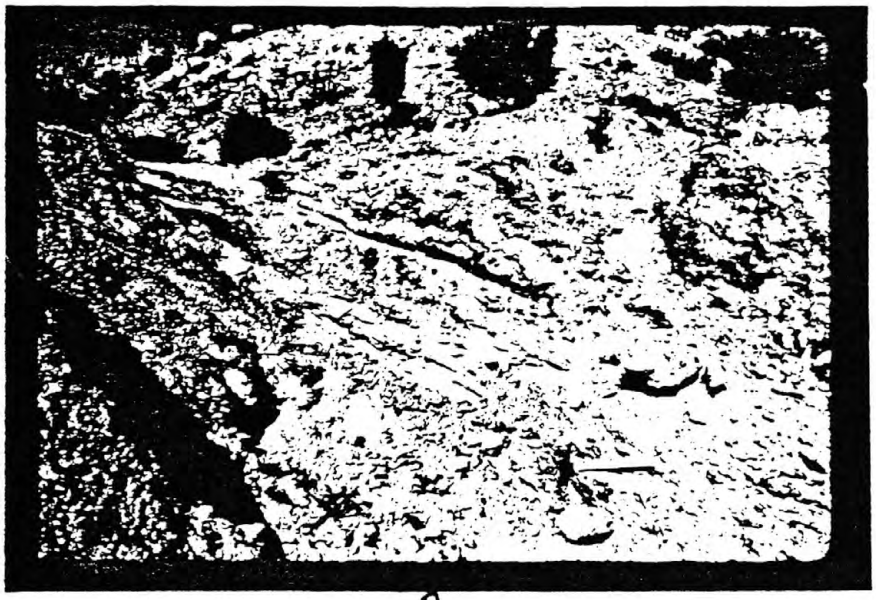

A

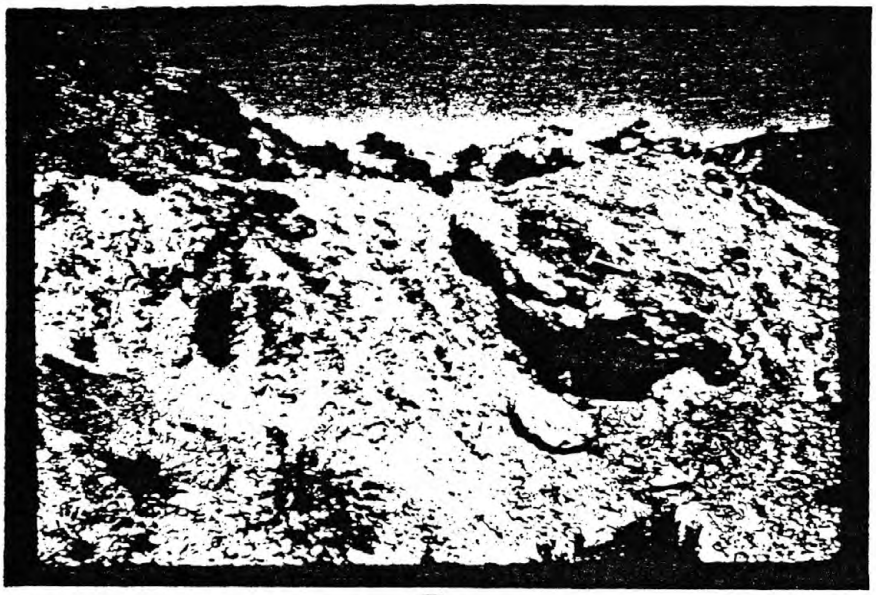

B

C

Basin district where they are clustered in an approximately 6-km^2 area, about 2 km south-southeast of Golden Rule Peak (Blacet, 1975). In the Gold Basin district, the placers are reported to have contained gold in erratically distributed channels (U.S. Geol. Survey, unpub. data, 1967). Finally, a few occurrences of placer gold were worked from the upper reaches of Quaternary gravel deposits along the western flank of the Lost Basin range. Although the overall areal extent of the deposits and occurrences along the west side of the Lost Basin range is about the same as that along the east side of the range, by far the largest production is credited to the King Tut placer area on the east side of the range. Koschmann and Bergendahl (1968, p. 40) estimate that total minimum gold production of the Gold Basin district was about 15,000 ounces. Most of this was from lode deposits as we described above. Johnson (1972, pl. 1) appraises the total production of placer gold at 1,000 ounces for each district, Gold Basin and Lost Basin.

The best concentrations of gold-bearing gravels were found in the placer deposits along the east flank of the Lost Basin range. The highest grade gold-bearing gravels there are generally less than 1 m thick, and these gravels are confined to present-day arroyo bottoms where they have been concentrated above caliche-cemented false bedrock after having been reworked primarily out of the Muddy Creek Formation (J. D. Love, written commun., 1966, 1967; P.M. Blacet, unpub. data, 1967-1972). The richest known concentrations of gold-bearing gravels apparently were abundant along the upper reaches of these arroyos (Blacet, 1975). Concentrations of placer gold nuggets obtained mostly from the King Tut placer area include coarse and angular nuggets, many showing sharp, ragged edges (Fig. 60A). These relations suggest that the nuggets have not traveled very far. In addition, some of the placer nuggets enclose rounded to angular granules of vein quartz (Frontispiece; fig. 60B) suggesting that some solution and reprecipitation of gold may have taken place in the environment of the placer gravels. Heavy minerals also are relatively abundant in the gold-bearing alluvial sand and gravel (fig. 60B). Deaderick (1980) also reports that an abundance of black sand is associated with the placer gold; this black sand consists largely of partially oxidized cubes of pyrite, magnetite, garnet, ilmenite, hematite, and limonite. In addition, he notes that placer operations in the late 1970's recovered gold nuggets containing a significant amount of attached chalcedonic matrix, partly as inclusions within some of the nuggets.

Figure 60.--Photographs of placer gold from the Lost Basin mining district (from J. David Love, written commun., 1966). A, Coarse angular nuggets of gold. Note pin for scale at bottom of photograph; B, Variably sized concentrations of placer gold; a, coarsest nuggets showing at head of arrow an approximately 1.2 cm across composite nugget with gold partly enclosing a rounded granule of quartz; b, medium-size nuggets; c, small nuggets; d, nonmagnetic heavy mineral concentrate in which all large fragments are gold.

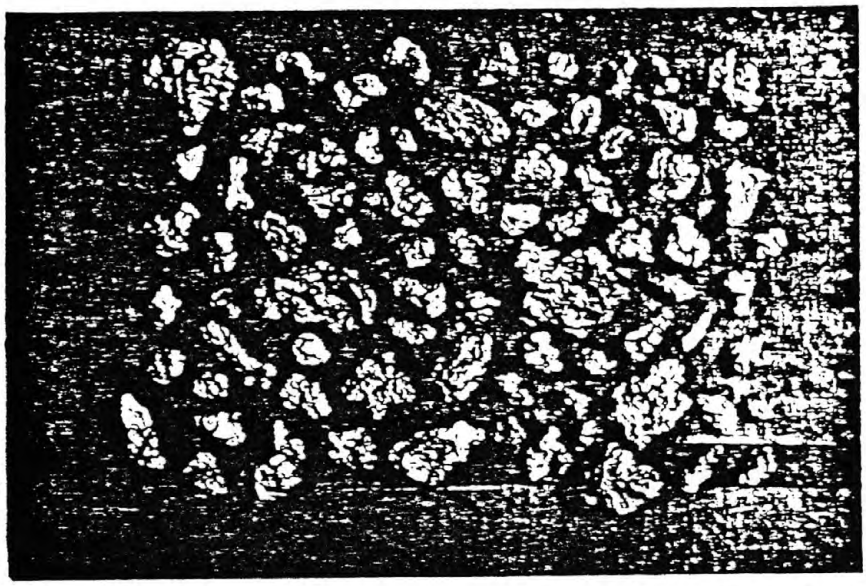

A

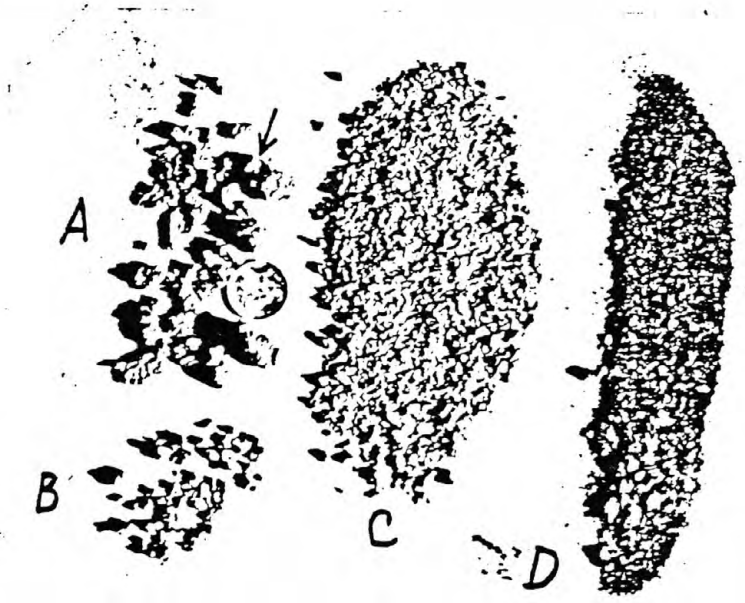

B

The surface morphology of selected placer nuggets, collected by a hand-operated dry washer (fig. 61) was examined using the SEM. A nugget from the King Tut placer area (fig. 62A) appears to be more worn than most from that general area, and this particular nugget shows, at very high magnifications, extremely well developed surface striae produced during transport (fig. 62B). Major transport of such a nugget, in contrast to the more ragged and angular other nuggets in the same general area, may have occurred during a period of flash flooding in an otherwise generally arid type erosion cycle, or it may have been transported farther than the more angular nuggets. Yeend (1975) showed experimentally that most physical changes in placer gold nuggets occur by exposure to a turbulent high-energy environment. He farther documented that most physical changes reflect the effects of cobbles rather than sand, and that gold is abraded faster by wet sand than by dry sand. Figure 62C shows the overall aspects of a "less worn appearing" nugget obtained from the northern Gold Basin mining district. Many of the nuggets examined by the SEM show that the gold typically contains numerous cubic molds indicating the former presence of pyrite or galena (fig. 62D), both of which are common minerals in the gold-bearing veins throughout the districts. Spot qualitative analyses of placer nuggets using the energy dispersive X-ray microanalyzer on the SEM revealed commonly detectable silver and iron. The iron probably is a local surface coating.

Some nuggets contain relicts indicating the former presence of carbonate in their hypogene assemblage. A large irregularly shaped, 11.9 g nugget obtained from placer workings in the NW1/4 sec. 3, T. 29 N., R. 17 W., approximately 2 km northeast of the main workings of the King Tut placers, shows extremely well developed rhombic molds (fig. 63). Measurement of the interfacial angles of these molds suggests that the carbonate may have been ankerite (Richard C. Erd, written commun., 1969), which is common together with siderite in the quartz-carbonate±base metals±gold stages of the vein-pegmatite systems throughout the districts.

Although the overall geometry and concentrations of placer nuggets reflect fluvial processes, some microscopic features, together with physical and chemical relations (see below), indicate some remobilization has taken place locally in the placer environment. Figure 64 shows a sequence of scanning electron micrographs, at successively larger scales, of textural relations found between native silver and gold in a small nugget collected

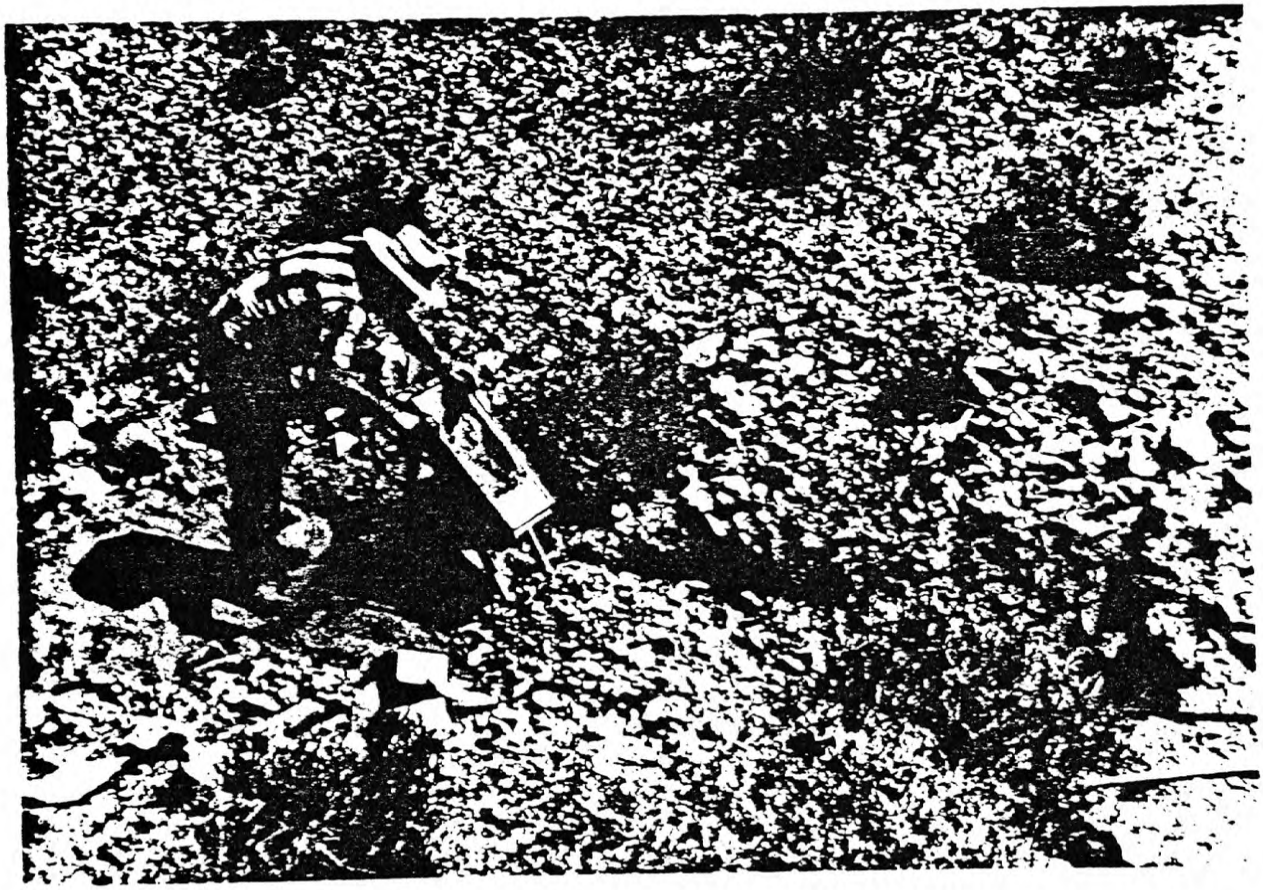

Figure 61.--Photograph showing small, hand-operated dry washer used to collect heavy mineral concentrates from unconsolidated sand and gravel in arroyo bottoms.

Figure 62.--Scanning electron micrographs of placer nuggets from the Gold Basin-Lost Basin mining districts. Bar indicates scale in micrometers (1 μm = $1x10^{-6}$m). A, Gold nugget from the King Tut placer workings, NE1/4 sec. 9, T. 29 N., R. 17 W. Weight, 15.3 mg. A small amount of iron was detected in the nugget using the energy-dispersive analyzer; B, Enlargment of area outlined in A showing surface striae produced during transport; C, Gold nugget from workings at the Old Placers area (informal name), SW1/4 sec. 10, T. 29 N., R. 18 W., approximately 1.5 km northeast of the Gold Hill mine; D, Gold nugget from a site at Twin Yucca gulch (informal name), SE1/4 sec. 9, T. 29 N., R. 18 W., approximately 1 km north of the Gold Hill mine. Weight, 38.9 mg. The nugget shows numerous cubic molds indicating the former presence of euhedral crystals of pyrite. A small amount of silver was detected in the nugget using the energy dispersive analyzer.

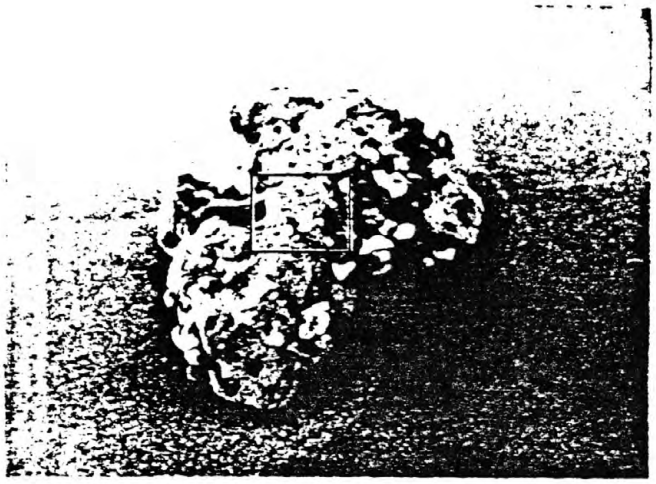

A 300 µm

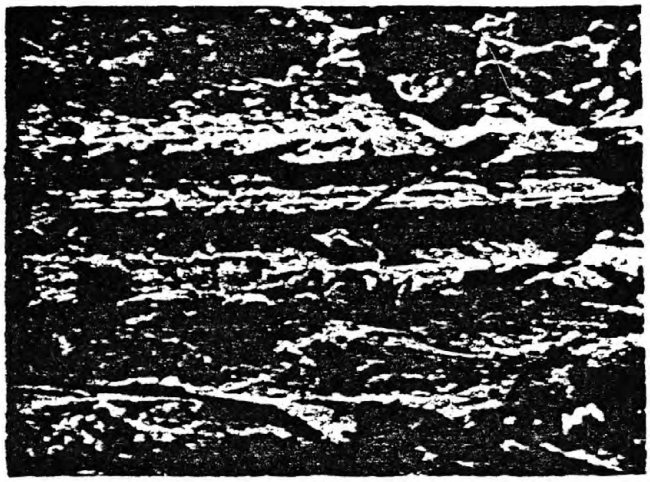

B 10 µm

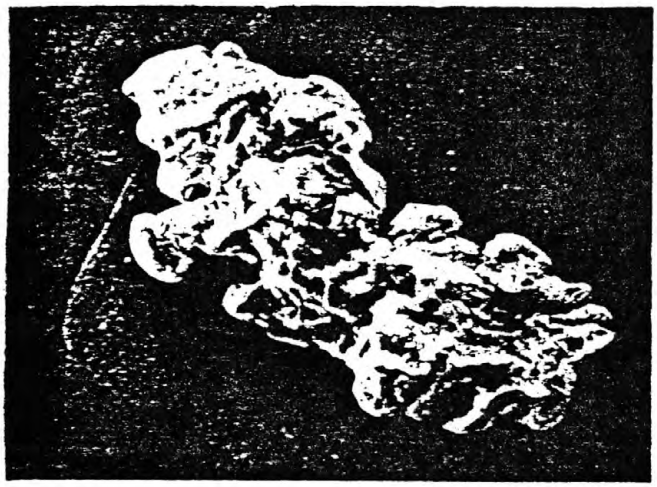

C 300 µm

D 900 µm

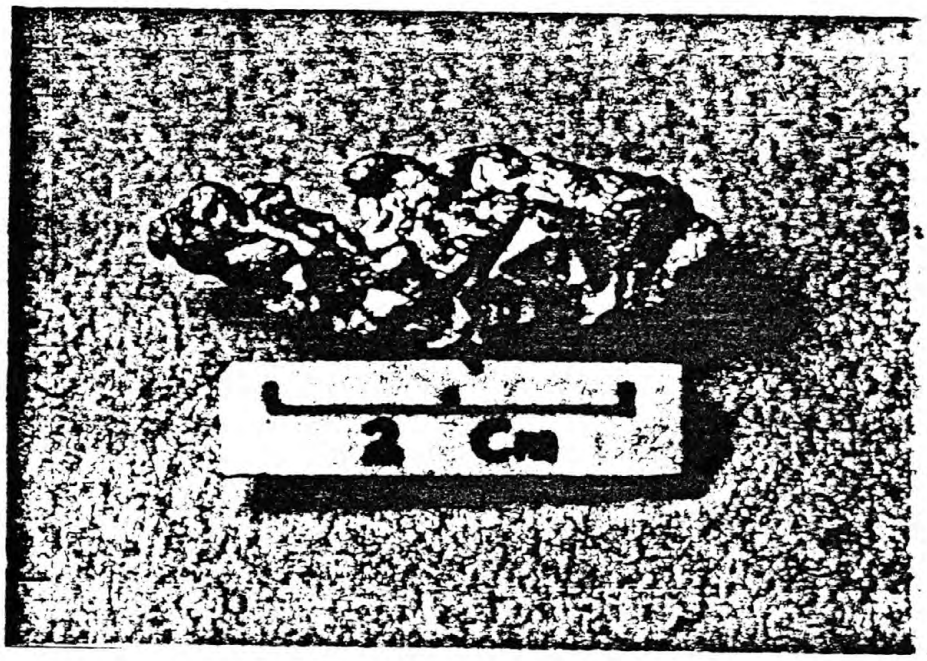

Figure 63.--Relatively large placer nugget from the Lost Basin mining district showing extremely well developed rhombic molds (see text).

Figure 64.--Scanning electron micrographs of silver-gold relations in a placer nugget obtained from the northern part of the Lost Basin mining district. Placer workings are near the Golden Gate mine, NW1/4 sec. 32, T. 30 N., R. 17 W. Bar indicates scale in micrometers (1 μm = $1x10^{-6}$m). A, Overall irregular shape of entire nugget showing area enlarged in B; B, Small oriented triangular facets of silver, approximately 5 m on a side but ranging down to much less than 1 m on a side, occurring on the surface of the gold nugget. The facets of silver are raised slightly relative to the surrounding surface of the gold nugget. Energy-dispersive analysis of the triangular facets of silver reveals no detectable gold, and analysis of the gold reveals no detectable silver. Outlined area is enlarged in C; C, Further enlargement of the triangular facets of silver showing their nested or stacking relations.

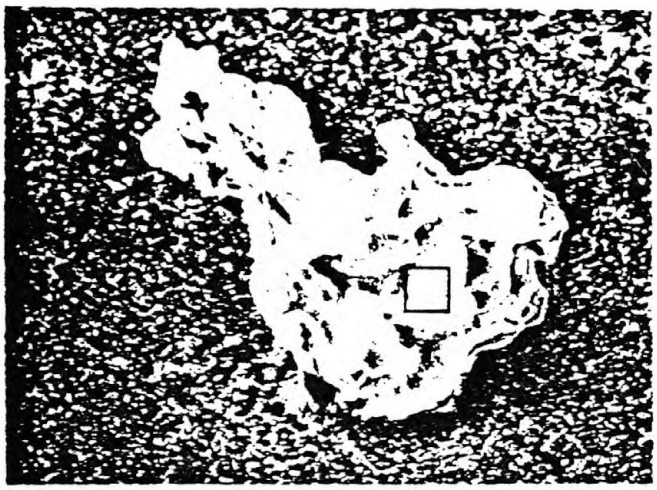

A

100 µm

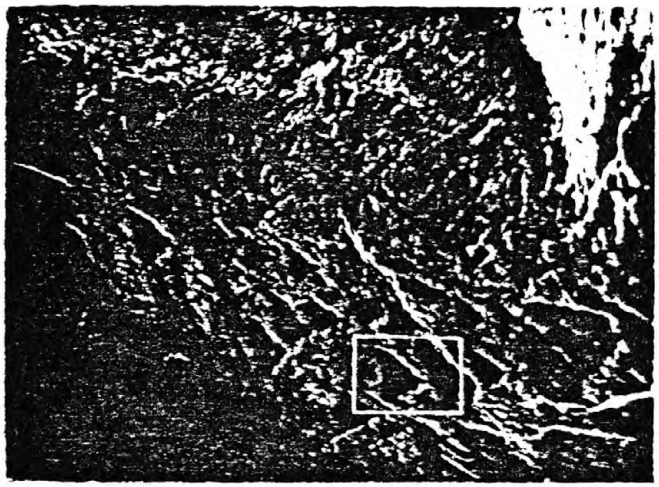

B

10 µm

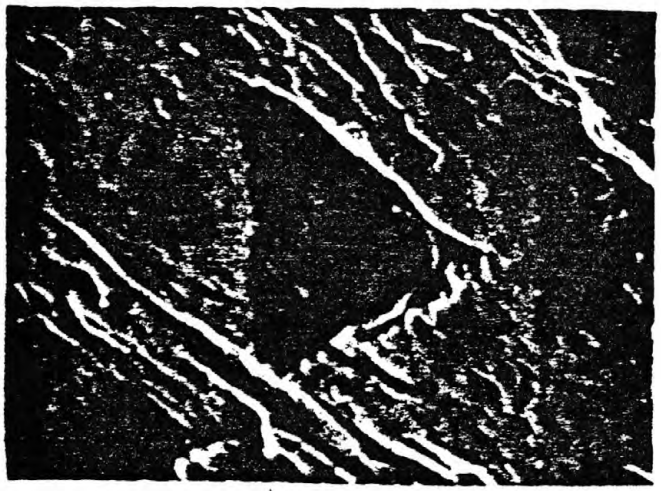

C

3 µm

near the Golden Gate mine. These relations between native silver and native gold were evaluated partly because Diman (1976) had determined previously that the association native silver-native gold is "forbidden" because of widely separate stability fields at elevated temperatures. The two metals can occur together under nonequilibrium conditions or at low temperature(s). Further, Desborough (1970) has shown that most placer gold grains include a relatively thin rim of low silver content Examination of this particular nugget at very high magnifications reveals that small oriented triangular facets of native silver, many approximately 5 μm on a side, occur on the surface of the gold nugget (fig. 64B). These facets of silver, identified using the energy-dispersive microanalyzer, are raised slightly relative to the surrounding gold, and the facets are all oriented similarly. Observation of these relations at an even greater magnification (fig. 64C) shows that some of the extremely small facets of silver are even nested on one another, but still retaining the same overall orientation of their outlines. Energy-dispersive analysis of the silver reveals no detectable gold, and analysis of the gold reveals no detectable silver. We suggest that the silver may reflect the following events in the placer environment: (1) sedimentation of the detrital nugget of gold in the Quaternary gravel; (2) dissolution of silver from a nearby source in the gravels, possibly galena or cerrusite, at a relatively elevated Eh and, only locally, a somewhat acidic pH (see stability relations of gold and silver in water at 25°C and 1 atm shown by Hallbauer and Utter (1977)); (3) final deposition of the silver on the surface of the gold, controlled largely by traces of {111} twin planes and primarily in response to a decline in the prevailing Eh of the overall system. There is some experimental work which suggests that such a succession of phenomena may have occurred. Salkarova, Batrakova, and Posukhova (1979) showed that at room temperature and atmospheric pressure dislocations and other surface defects can control the actual sites where native silver precipitates onto placer minerals from silver-charged acid or alkaline solutions. Even if such a sequence of physical and (or) chemical events contributed toward what appears to be a very local and very minor accretionary phenomenon, we do not believe that a similar chemical mechanism should be used to explain "growth" of the relatively large sized nuggets in the placers from "seeds" of relatively small sized masses of lode gold observed throughout the districts. In fact, such size contrasts are fairly common in many combined lode- and placer-gold

districts (see Antweiler, Doe, and Delevaux, 1972; Boyle, 1979; and many others). We suggest that the relatively large placer gold nuggets were derived mostly from the upper portions of the vein systems that have been removed by erosion. The source areas probable for the placer gold will be discussed below in this section.

Cursory geochemical studies were made of minor metals in seven heavy-mineral concentrates obtained from one lode site and several placer gold sites in the Gold Basin-Lost Basin mining districts (table 20). Spectrographic methods used are those by Grimes and Marranzino (1968). Included also in table 20 for comparison is an analysis (no. 1) of heavy minerals concentrated from the site of the gold-bearing episyenitic rock. We were not able to verify the site from which sample number 3 was collected by Blacet. However, the very high concentration of tungsten (greater than 2 weight percent) in sample number (table 20) in contrast to a maximum 0.3 weight percent tungsten in the six other samples of placer concentrates suggests that sample number 3 may be a scheelite concentrate handpicked from one of the seven others. The seven remaining samples analyzed include both magnetic and nonmagnetic fractions. Although the bulk of the samples analyzed consists of nonmagnetic portions, approximately one-tenth to one-third by volume of the concentrates include a magnetite-rich fraction that may be essentially separated magnetically using a 1-kg handheld magnet. In addition, all relatively large fragments of gold first were removed by handpicking the heavy-mineral concentrates before the concentrates were analyzed. Those eight samples, now consisting of composited fragments of gold, were analyzed separately for palladium, platinum, and ruthenium, together with nine other gold samples obtained similarly from various placer workings throughout the districts. No palladium, platinum, or ruthenium was detected in any of these 17 gold samples at limits of determination that range between 48 and 219 ppm (Joseph Haffty and A. W. Haubert, written commun., 1978).

The drainage basins contributing material to the placer sample sites from which we obtained and analyzed the heavy mineral concentrates are widespread, and they span the districts along their entire north-south length. As a consequence, the lode sources for these anomalous metal concentrations must also be widespread. We have not attempted to establish geochemical dispersion trains nor have we attempted to follow otherwise these metals back to their specific sources. Two analyzed samples show concentrations of 0.3 and 0.15

Table 20. Spectrographic analyses for minor metals in heavy mineral concentrates from a selected lode occurrence and previously worked placer deposits and occurrences in the Gold Basin-Lost Basin mining districts

[Spectrographic analyses by L. A. Bradley. Results are to be identified with geometric brackets whose boundaries are 1.2, 0.83, 0.56, 0.38, 0.26, 0.18, 0.12, etc., but are reported arbitrarily as mid-points of these brackets, 1., 0.7, 0.5, 0.3, 0.2, 0.15, 0.1, etc. The precision of a reported value is approximately plus or minus one bracket at 68 percent, or two brackets at 95 percent confidence. Symbols used are: G, greater than 10 percent or value shown; N.d., not detected; L, detected but below limit of determination; ----, not looked for. Looked for but not found, Pd, Pt, Sb, Te, Ge, In, Li, Re, Ta, Tl, Tb, Tm, Lu]

	1	2	3	4	5	6	7	8
Lab number	D194818	D194819	D194820	D194821	D194822	D194823	D194824	D194825
	Semiquantitative spectrographic analyses (weight percent)							
Mn	0.7	0.15	0.2	0.15	0.5	0.03	0.15	0.15
Ag	.0015	.03	N.d.	.0007	.0015	.15	.0003	.00015
As	N.d.	.15	N.d.	N.d.	N.d.	N.d.	N.d.	N.d.
Au	.01	.05	.003	N.d.	N.d.	N.d.	N.d.	N.d.
B	N.d.	N.d.	N.d.	L	N.d.	N.d.	L	L
Ba	.02	.005	.003	.02	.03	7.	.03	.03
Be	.0003	N.d.	N.d.	N.d.	N.d.	N.d.	L	L
Bi	N.d.	N.d.	N.d.	N.d.	N.d.	.3	N.d.	.003
Co	.007	.007	L	.01	.007	.005	.015	.015
Cr	.02	.015	.005	.015	.015	.003	.05	.03
Cu	.005	.002	.01	.03	.03	.03	.05	.05
La	1.5	.7	.007	1.	1.5	.015	.3	.3
Mo	.01	.0003	.03	.002	.003	1.5	.003	.002
Nb	.07	N.d.	.03	.007	N.d.	N.d.	.007	.007
Ni	.0015	.007	.001	.007	.002	.003	.01	.01
Pb	.15	.03	.007	.15	.15	G	.07	.07
Sc	----	.003	.001	.002	----	.0007	.002	.0015
Sn	.003	.003	.005	N.d.	N.d.	N.d.	.003	N.d.
Sr	.015	.003	.007	.015	.015	.15	.015	.01
U	N.d.	N.d.	N.d.	.3	----	.15	N.d.	N.d.
V	.02	.07	.015	.03	.015	.02	.05	.07
W	N.d.	.015	G2.	.3	L	N.d.	L	N.d.
Y	.15	.07	.007	.07	.07	.003	.05	.05
Zn	N.d.	.15	N.d.	N.d.	N.d.	N.d.	N.d.	N.d.
Zr	.15	.05	.01	.15	1.	.015	.07	.07
Ce	1.5	1.5	N.d.	2.	G2.	.07	.7	.7
Ga	----	.03	.005	----	----	----	----	----
Hf	N.d.	N.d.	N.d.	N.d.	.03	N.d.	N.d.	N.d.
Th	----	.5	N.d.	.5	.7	N.d.	.3	.2
Yb	.015	----	.0005	.005	.003	----	----	.0015
Pr	.3	.15	----	.3	.3	N.d.	.07	.07
Nd	1.	.7	----	1.	1.	.02	.3	.3
Sm	.15	.15	N.d.	.2	.2	N.d.	.07	.07
Eu	.01	.01	N.d.	L	L	N.d.	L	L
Gd	.05	----	----	.05	----	----	.03	.03
Dy	.03	L	N.d.	.03	.015	----	.005	.005
Ho	.01	.002	N.d.	.007	----	----	L	L
Er	.015	L	N.d.	.015	.015	----	.007	.005

1. Heavy mineral concentrate from gold-bearing episyenite (fig. 51); SE1/4 sec. 27, T. 28., R. 18 W.
2. Drywasher concentrate. Fine gold fragments visible; SW1/4 sec. 4, T. 27 N., R. 18 W.
3. Drywasher concentrate. Location uncertain.
4. Drywasher concentrate. SW1/4 sec. 10, T. 29 N., R. 18 W.
5. Drywasher concentrate, above caliche-cemented fanglomerate. Few fine gold fragments visible; NW1/4 sec. 31, T. 29n N., R. 17 W.
6. Drywasher concentrate, includes barite, magnetite, limonite after pyrite, cerussite, galena, and traces of gold; SW1/4 sec. 8, T. 29 N., R. 17 W.
7. Drywasher concentrate, SW1/4 sec. 31, T. 30 N., R. 17 W.
8. Drywasher concentrate, SW1/4 sec. 31, T. 30 N., R. 17 W.

weight percent uranium, and 0.5 and undetected amounts of thorium respectively. The Th:U ratio of about 1.7 in analysis number 4 (table 20) suggests a probable source in detrital grains of monazite, allanite, or euxenite derived from the Proterozoic X metamorphic and igneous rocks. The concentration of rare earth elements and the values of various rare-earth ratios suggest this relation also. Further, Reyner (1954) describes small pods of polycrase-, euxenite-, and monazite-bearing rock associated with pegmatite in SW1/4 sec. 10 and NE1/4 sec. 14, T. 28 N., R. 16 W., on the western lower flanks of Garnet Mountain. Analyses of four select samples from that locality range from 0.007 to 0.533 percent eU_3O_8.

The overall abundance of rare-earth elements and the values of various rare-earth ratios in the concentrates from five of the six placer samples are remarkably similar to the rare-earth signature of the heavy minerals concentrated from the apparently Cretaceous, gold-bearing episyenitic rock (table 20). The source areas of the placer samples are largely the Proterozoic X rocks. These relations suggest that the hydrothermal process of episyenitic rock development, may have occurred without a significant disruption of the rare earth geochemical signature of the Proterozoic protolith of the episyenite. These inferences do not preclude the possibility that there may have been some contamination of the heavy minerals obtained from the episyenitic rock during the current erosion cycle.

Gold in the King Tut placer area of the Lost Basin mining district apparently is being reworked out of the upper parts of the exposed sequences of the Muddy Creek Formation. However, these predominantly fanglomeratic deposits have been derived from several source areas as fans were coalescing and filling the Miocene trough along the Grand Wash fault zone. This trough is along present-day Grapevine Mesa (see Blacet, 1975). Detailed examination by P. M. Blacet (unpub. data, 1967-1972) of cobbles comprising the Muddy Creek Formation along the entire eastern flank of the Lost Basin range revealed that granitic cobbles and boulders from the rapakivi granite of Gold Butte, which crops out north of Lake Mead, occur in the Muddy Creek Formation only to approximately 3.5 km south of the northern boundary of figure 2. Just north of this boundary, granite of the Gold Butte area commonly occurs as 2 to 3 m across boulders throughout an at least 200-m-thick sequence of the exposed Muddy Creek Formation. In this general area west of the Meadview store in the southern part of the Iceberg Canyon 15-minute quadrangle, the Muddy Creek

Formation also includes abundant fresh cobbles and isolated boulders of light-pinkish-gray porphyritic monzogranite very much like the Proterozoic X porphyritic monzogranite cropping out in the southeastern White Hills, just east of the Cyclopic mine. In addition, subangular to moderately well rounded cobbles of medium- to coarse-grained metadiabase occur in the Muddy Creek Formation here, whereas the adjacent Lost Basin range includes extremely sparse abundances of this lithology generally north of the area of the Bluebird mine. These relations suggest that the bulk of the debris being shed into the depositional trough of the Muddy Creek Formation at the northern part of the Lost Basin district was being derived from a northerly source, but that some lesser amounts of fanglomeratic material were coming probably from the southwest also.

The lithology of clasts in the lowermost-exposed sequences of the Muddy Creek Formation at its southernmost exposures in the Lost Basin district, approximately 1.5 km west-southwest of the junction of the Pierce Ferry Road and the Diamond Bar Ranch Road, also suggest derivation from a source to the southwest (P. M. Blacet, unpub. data, 1967-1972). In this general area, the Muddy Creek Formation includes scattered cobbles and small boulders of basalt, unretrograded sparkling fresh garnet- and biotite-bearing schists, unretrograded amphibolite, pegmatoid alaskite, and aplite. The overall proportions of the lithologies of the Muddy Creek Formation suggest derivation from the southwest. Deaderick (1980, p. 96) analyzed the population of heavy minerals in concentrates from gravels along the eastern flank of the Lost Basin range, and concluded that the gold-bearing fanglomerates of the Muddy Creek Formation, out of which the gold placer are being reworked, must have been derived from some source to the west or southwest, more distant than the adjacent Lost Basin range. The Proterozoic X metamorphic complex which crops out beneath the lavas of the Table Mountain area, approximately 10 km south-southeast of the Cyclopic mine, includes lithologies in approximately the same proportions as the Proterozoic clasts in the Muddy Creek Formation at the south end of the Lost Basin range. The source area for the Muddy Creek Formation, which crops out at the south end of the Lost Basin range, could not have been from the Garnet Mountain tectonic block to the southeast. This block of Proterozoic X rock includes too much porphyritic monzogranite, and insufficient amounts of pegmatoid leucogranite and unretrograded metamorphic rock.

Progressively increasing abundances of lithologies derived from the Proterozoic X terrane of the Lost Basin range comprise the sequences of the Muddy Creek Formation north from about 3.5 km southeast of the Lone Jack placer mine (P. M. Blacet, unpub. data, 1967-1972). As pointed out by Deaderick (1980, p. 99), apparently it is only the Proterozoic X-metamorphic-clast facies of the Muddy Creek Formation that contains the gold here. Further, in this general area, the Muddy Creek Formation includes a considerable amount of 2.5 to 10.0 cm, rounded to subangular clasts of retrograded quartzofeldspathic gneiss. The clasts of quartzofeldspathic gneiss are yellowish-gray and they are well foliated to laminated. Sparse cobbles of pyrite-bearing vein quartz also occur here in the Muddy Creek Formation, as well as minor amounts of retrograded amphibolite. The dominant clast type is quartzofeldspathic gneiss in the Muddy Creek Formation from approximately 3.5 km southeast of the Lone Jack placer mine northward to several kilometers north of the main workings of the King Tut placer area. The relations suggest derivation of the bulk of the gold from sources to the west in the Lost Basin range, but possibly including some sources farther to the west in Hualapai Valley now covered by alluvial deposits younger than fanglomerate and tuff of the Muddy Creek Formation. Some placer gold may eventually have come also from the southwest. A probable sequence of depositional and structural events leading to the present-day geomorphologic relations was outlined above in figure 4.

Quaternary fanglomeratic deposits along the west flank of the Lost Basin range which host the placer deposits are clearly dissected and incised whereas those Quaternary deposits which were not worked previously for their placer gold are distinctly less disected (P. M. Blacet, unpub. data, 1967-1972; Blacet, 1975). In addition, there is a sharp geomorphic boundary between the placer-gold-producing Quaternary deposits and the nonproductive Quaternary deposits. This abrupt boundary occurs just south of the major canyon leading to the Bluebird mine. South of this boundary the alluvial fans are significantly less dissected and covered with conspicuously desert varnish-stained trains of boulders and reddish-brown soil. Displacement(s) along a buried fault that is largely post-Quaternary fanglomerate in age may explain these relations. However, the overall strike of such a fault is not readily apparent. On the one hand, an east-west-striking normal fault, south side down, may crosscut the bajada approximately at the geomorphic transition (P.

M. Blacet, unpub. data, 1967-1972). Movement(s) along this hypothetical fault may have increased alluvial gradients on the north thereby increasing both the dissection of the Quaternary deposits and the concentration of the placer gold. Alternatively, the geomorphic transition may reflect the approximate fulcrum-point of very late, predominantly scissors type movements along the approximately north-south striking fault bounding the Lost Basin range on the west (see Blacet, 1975).

Finally, analysis of the abundance of placer gold in various drywasher concentrates in the placers of the Gold Basin district suggested to Blacet (unpub. data, 1967-1972) that the placer gold there may not be locally derived. Apparently, the placer gold in this general area was concentrated by being reworked out of erosional thin gravel caps of older Quaternary gravels resting unconformably on the underlying Proterozoic X gneiss. Overall production of gold from these placer deposits in the Gold Basin district was quite small, and included 19 ounces of gold recovered in 1942 by several operators (Woodward and Luff, 1943, p. 251).

IMPLICATIONS OF THE COMPOSITIONS OF LODE AND PLACER GOLD

By

J. C. Antweiler and W. L. Campbell

Introduction

The purpose of this chapter is to report the results and our interpretations of about 250 compositional analyses on lode gold from 48 veins or mines in the Lost Basin mining district, and from 20 mines and prospects in the Gold Basin mining district, and of nearly 100 compositional analyses on placer gold from the Lost Basin district. Sample localities for the two districts are shown on figure 65. Many of the analyses on placer gold were on gold from the King Tut placer mines, but some were made on placer gold from other localities on the eastern side of the Lost Basin Range, and from seven localities on the western slopes of the Lost Basin Range.

The compositional data are discussed with regard to how they may be useful for (1) relating the placer gold deposits to bedrock sources, (2) implications as to ore depositional conditions for the veins, and (3) suggesting the possibility of relating some of the gold veins to a buried porphyry copper deposit. In previous papers (Antweiler and Sutton, 1970; Antweiler and Campbell, 1977, 1982), we suggested that compositional analyses

Figure 65.--Sample localities for compositional analyses of lode and placer gold obtained from the Gold Basin-Lost Basin districts. Locality numbers keyed to tables 21-26. (In pocket).

of gold provide information that can be applied to the search for undiscovered ore deposits or to studies of ore genesis, and the data presented here are examined for those possibilities.

The compositional analyses were mainly direct-current emission spectrographic analyses for quantitative determination of Ag and Cu in native gold (a natural alloy composed of Au, Ag, and Cu), together with semiquantitative determination of other elements. These analyses were made by E. L. Mosier on gold placed directly into graphite electrodes using a previously described procedure (Mosier, 1975). Supplementary analyses for Au, Ag, and Cu by electron microprobe were made by W. L. Campbell using methods described by Desborough (1970). The emission spectrographic data provide the basis for assigning signatures (Antweiler and Campbell, 1977) to gold from each locality. Signatures consist of alloy proportions of Au, Ag, and Cu together with one or more of the following elements: Pb, Bi, Sb, As, Zn, Te, Pt, Pd, Rh, Ni, Cr, Co, V, B, Ba, and Be. Elements of high crustal abundance (Fe, Mn, Ca, Mg, Si, Ti) that are found commonly in compositional analyses and elements such as Zr, La, and Y that may occur in mineral inclusions in gold grains are not known to be useful for prospecting or ore-genesis studies and are not included herein as part of the gold signature. Mercury was found in extremely variable amounts in all samples, but also is not included as part of the signature because it was found in all samples, and was highly variable from one analysis to another on replicate samples. Gold content was estimated by subtracting from 100 percent the sum of the percentages of Ag and other elements found in the analyses. Gold fineness (parts per thousand Au in native gold) was estimated by dividing the Au content by the sum of the Au and Ag content, and multiplying by 1,000.

We crushed and coarsely ground the lode samples from veins and mines, and recovered gold grains by panning and handpicking. We avoided use of chemical, amalgamation, or roasting procedures, because those recovery procedures alter the composition of the sample (Campbell, Mosier, and Antweiler, 1973). Gold from the placer deposits was recovered by dry placering or panning, and also was obtained without the use of procedures that might alter its composition.

Warren Mallory, president of the Apache Oro Company, Laramie, Wyo., which is reported to have mining claims in the districts, collected specimens with visible gold from many of the veins and generously donated them to us. He also gave us gold from the King Tut placer mines, and from many of the other

placer localities. Without his interest and generosity, this work would not have been possible.

Variations in Gold Composition

Many papers have been published on the composition of native gold (e.g., Warren and Thompson, 1944; Gay, 1963; Jones and Fleischer, 1969; Lantsev and others, 1971). Variations in composition occur even from point to point within the same grain (Desborough, 1970). Native gold in oxidized zones and in associated placers generally contains lesser amounts of Ag and other elements compared with the native gold in the corresponding primary deposits, and within some specific deposits single particles of native gold are relatively homogeneous, but in other deposits the native gold is heterogeneous (Boyle, 1979). Because variations in gold composition are natural rather than analytical, they are worthy of study, particularly if they can be understood. In spite of the variations, gold compositional data are useful in that they help characterize conditions of ore deposition and are commonly areally distinctive for mines, districts, or regions.

To lessen uncertainties in interpreting gold compositional data that are inherently subject to natural variations, replicate analyses of gold from the same sample locality should be made if possible. As a general guide, in a district in which no prior compositional information for gold is available, we believe that at least five spectrochemical analyses of 5 mg samples of gold are desirable for a single sample site to obtain a signature in which one can place confidence. However, in the context of many other analyses from the same district, a single analysis is of value. Fortunately, at many localities in both the Lost Basin and Gold Basin districts, sample quantities were available for several analyses. At some localities, however, limited quantities of sample precluded making more than one or two analyses.

The variations in composition of Lost Basin placer samples are shown in table 21, where it can be seen that in 46 emission spectrographic analyes of gold from the King Tut placer mines, Ag content ranges from ~2.1 to 15.0 percent and Cu content ranges from 0.0017 to 0.07 percent. Standard deviation for these analyses is nearly 50 percent of the mean for Ag (7.25=3.1 percent) and nearly 60 percent of the mean for Cu (0.0185=0.0114 percent). In individual analyses, Ag ranges from 2.1 to 20 percent (0.1 to 22.3 for electron microprobe analyses) and Cu from 0.001 and 0.097 percent.

Table 21.--Compilation of signatures of placer gold samples, Lost Basin District, Mohave County, Arizona

Sample locality	Number of analyses	Ag, percent			Cu, percent			Au					Characteristic trace elements in order of abundance
		Range	Mean	Standard deviation	Range	Mean	Standard deviation	Mean	Fineness $\frac{Au}{(Au+Ag)}$ X1000	Au/Ag	Au/Cu	Ag/Cu	
HuW-1	1		6.8			0.125		93.1	932	13.7	745	54	Pb,Zn
HuW-3	1		7.1			.023		92.9	929	13.1	4039	309	Pb,Mo
HuW-4	1		6.5			.250		93.4	935	14.4	374	26	Pb
HuW-5	1		12.2			.15		87.6	878	7.2	584	81	Pb,Mo
N33PC-7	4[1]	4.7- 8.1	5.7	1.6	0.048 -0.08	.062	0.0144	94.2	942	16.5	1519	92	Pb,Bi,Mo,Te
34PC-1	1		8.9				.0375	91.0	911	10.2	2426	237	None
LB-1	2	5.5-13.3	9.4	5.5	.018 - .06	.039	.03	90.5	910	9.6	3016	241	Pb,Bi
LB-2	3[1]	9.5-15.0	11.8	2.8	.014 - .027	.021	.0066	88.1	882	7.5	4195	562	Pb,Bi,Sb
LB-3	3[1]	18.9-19.8	19.3	.56	.038 - .055	.047	.012	80.6	806	4.2	1715	411	Pb,Te,Zn,Bi,Cd
King Tut (Analyses by microprobe)	45[2]	0.1-22.3	11.0	5.5	[2]/	[2]/	[2]/	89.0	890	8.1	[2]/	[2]/	
King Tut (Analyses by emission spectrograph)	46	2.1-15.0	7.25	3.1	.0010- .07	.0185	.0114	92.5	926	12.8	5000	392	Pb,Bi,Mo,Sb,Zn
10PC-4	10	4.0-20.0	11.6	5.7	.006 - .078	.029	.0216	88.5	886	7.6	3051	400	Pb,Bi
GAS	3		13.2			.01		86.7					Pb,Bi
10PC-3	1		2.3			.007		97.7	977	42.5	13957	329	None
10PC-1	1		10.7			.014		89.2	893	8.3	6371	764	Pb
LB-4	5	3.5- 6.5	4.9	2.4	.019 - .097	.053	.0325	95.0	951	19.4	1792	92	Bi,Pb,Pd,Te
15PC-4	1		4.3			.03		95.6	957	22.2	3187	143	Pb
14PC-2	1		2.0			.0125		98.0	980	49.0	7840	160	Pb
22PC-1	5	15.0-20.0	17.0	2.1	.022 - .03	.03	.0021	82.9	831	4.9	2763	567	None
26PC-1	4	7.5-12.5	10.0	2.0	.005 - .045	.022	.0168	89.9	900	9.0	4086	455	Pb

[1]All analyses on portions of the same nugget.

[2]45 individual grains were analyzed, each by 3-5 spot analyses which were then averaged for mean Au and Ag content. Copper was detected only occasionally.

At three localities (N33PC-7, LB-2, and LB-3), replicate emission spectrographic analyses were made on portions of the same nugget. Substantial variation is evident both in Ag and Cu content, although such variation is generally not so great as in analyses made on different grains.

The much smaller size of samples analyzed in electron microprobe work compared to emission spectrographic analyses (0.05-0.10 mg compared to 5 mg) resulted in greater standard deviation in Ag values (5.5 percent compared to 3.1 percent). Higher mean values for Ag content also resulted (11.0 percent compared to 7.25 percent). These higher mean values may indicate that the Ag content of grains analyzed by microprobe just happened to be higher than that of samples analyzed by spectrograph, but another explanation is that most of the microprobe analyses were made on polished interior surfaces of individual grains, whereas spectrographic analyses were made on several whole grains. Most of the grains that were analyzed by both methods were small. However, in spectrographic analyses of Lost Basin samples made earlier (Antweiler and Sutton, 1970), coarse gold (nuggets) averaged 10.4 percent Ag and 0.034 percent Cu, whereas finer gold (minus 60-mesh) averaged 5.6 percent Ag and 0.015 percent Cu. The lower Ag and Cu content in the smaller particle-size fraction was interpreted as having resulted from more surface exposure with attendant greater Ag and Cu loss through atmospheric and ground water leaching agents. Exterior surfaces of gold in placers commonly are deleted in Ag content (McConnell, 1907; Desborough, 1970). Electron microprobe analyses are ideal for determining such losses because the percentages of Au and Ag can be determined at any spot including exterior surfaces to which the microprobe beam is directed. A number of spot analyses were made on exterior surfaces of grains by microprobe; these analyses showed Ag content ranging from nil to 14 percent on exterior surfaces, and generally from 2 to 5 percent less Ag than in the interior of the grains. The zone of Ag depletion (and, Au enrichment) varied from grain to grain, but rarely penetrated into the interior of the grains more than a few microns. No attempt was made to compute the total percentage loss of Ag because the geometry ofthe grains varies considerably as does the Ag content. If the higher Ag content obtained in microprobe analyses is attributable to loss of Ag on grain surfaces, the Ag content obtained by microprobe should more nearly reflect the Ag content of the gold when it was in a vein, provided, of course, that no other compositional changes occurred.

The difficulty of identifying placer gold with a specific lode source is highlighted by the data in table 22, which shows the extent of variation in Ag and Cu content in lode gold from Lost Basin and Gold Basin. Only those samples are listed for which five or more spectrographic analyses are available. The Cu content of Lost Basin lode samples ranges from 0.017 percent to 0.7 percent, and the standard deviation at one locality, B-B1, is nearly 100 percent of the mean. Ag content ranges from 6.6 to 31.5 percent, but at most localities the standard deviation approximates 20 percent of the mean value--a generally smaller percentage than in the placer samples. The Gold Basin samples also show high standard deviations for Cu; samples from locality MAS, for example, have a Cu content ranging from 0.01 to 0.28 percent, resulting in a standard deviation of 0.14 percent Cu, which is 125 percent of the mean value. The standard deviation for most analyses for Ag in Gold Basin samples, like those in Lost Basin samples tends to be 20 to 25 percent of the mean value, although some are less than that and some are more.

Because gold in placers could have more than one source, and could have either a simple or a complex history in moving from a primary source to a placer site, wider variations in composition might occur than in lodes. Compositional variations in placers, however, are moderated to some extent by the natural refining that occurs during the transition from the environment of vein gold in bedrock to the environment of the placer gold. Although such natural refining may affect only the surface of gold grains, its net effect is an overall decrease in the content of Ag, Cu, and trace elements, with a higher percentage of Au content being the final product. If all the grains of gold in a placer deposit are uniform in composition, the chances appear favorable that all the grains came from one source area, which also would have gold of uniform composition. However, most of the lode gold in the Lost Basin and Gold Basin districts is rather heterogeneous in composition.

Comparison of Composition of Gold in Placers in Lost Basin with Possible Lode Sources

Most of the placer gold samples obtained in the Lost Basin district are not geographically relatable to a specific lode locality, but four of them are from drainages below veins from which gold was collected and analyzed (table 23). Even though this direct geographic relationship exists, gold in the placers on the eastern flank of the Lost Basin Range definitely was reworked out of the Muddy Creek Formation, which comprises locally the bedrock from

Table 22.--Variation of silver and copper content of lode gold samples from Lost Basin and Gold Basin as shown by replicate emission spectrographic analyses

Sample locality	Number of analyses	Ag, percent			Cu, percent		
		Range	Mean	Standard deviation	Range	Mean	Standard deviation
Lost Basin							
S	10	20.0-29.0	22.3	3.0	0.004 -0.014	0.0086	0.0033
HW	9	11.4-31.5	19.1	7.3	.03 - .5	.18	.1510
HET	5	15.9-23.9	20.7	3.8	.035 - .300	.15	.1110
GG	5	12.0-19.5	15.1	3.4	.04 - .13	.092	.0480
Climax	8	7.5-14.0	10.4	2.2	.015 - .025	.019	.0040
Golden Mile	6	6.6-12.5	10.7	2.5	.02 - .037	.035	.0149
B-J	10	9.7-18.0	14.4	3.0	.0175- .50	.092	.1465
B-B1	10	14.0-22.5	17.5	3.4	.03 - .39	.17	.1624
B-A	8	18.0 30.0	20.8	3.8	.014 - .06	.029	.0148
B-B1W	6	14.5-26.0	20.9	4.2	.02 - .70	.32	.2313
B-C	9	10.0-15.0	11.6	1.8	.028 - .10	.047	.0246
		6.6-31.5	16.7	3.5	.015 - .7	.1038	.0829
Gold Basin							
AWS-M	7	12.0-15.0	13.7	.94	.014 - .0455	.0215	.0114
GHM	8	14.0-25.0	19.3	3.1	.0075- .05	.0225	.0153
MAS	5	15.0-25.0	17.4	4.3	.0100- .28	.1120	.1400
ENW-2	7	25.0-31.0	29.0	2.2	.003 - .02	.008	.0056
MWS	5	10.0-35.0	18.0	9.8	.015 - .10	.0502	.0323
OLY	8	14.0-30.0	20.3	4.8	.036 - .07	.0495	.0140
		10.0-35.0	19.6	4.2	.003 - .28	.0440	.0364

Table 23.--Comparison of signatures of placer gold (P) and possible lode gold (L) sources

Sample locality	Number of analyses	Percent mean Au	Percent mean Ag	Percent mean Cu	Fineness Au	Au/Ag	Au/Cu	Au/Ag / Cu	Ag/Cu	Characteristic trace elements in order of abundance
GMG1 (P)	1	92.8	7.1	0.17	929	13.1	546	77	42	Pb
GMG1 (L)	6	89.2	10.7	.035	893	8.3	2549	237	306	Pb,Bi,Mo
LB4 (P)	5	95.0	4.9	.053	951	19.4	1792	366	92	Bi,Pb,Te
WSE2 (L)	2	84.4	15.5	.088	845	5.4	959	61	176	Bi,Pb,Te,W
N33PC7 (P)	4	94.2	5.7	.062	943	16.5	1519	266	92	Pb,Bi,Mo
Climax (L)	8	89.5	10.4	.019	896	8.6	4710	452	547	Pb,Bi,Mo
LB3 (P)	3	80.6	19.3	.047	807	4.2	1715	89	411	Pb,Bi,Sb,Zn,Cd
BL-1 (L)	2	76.7	23.0	.056	769	3.1	1351	55	411	Pb,Bi,Mo,Sb,Te

which the alluvial placers were derived. On the western flank of the Lost Basin Range, sample GM-G1 below the Golden Mile mine must certainly have come from the Golden Mile mine vein. The small volume of alluvium in the drainage where the placer sample was collected consists entirely of locally derived material from the nearby Proterozoic X rocks. Only enough placer gold was obtained for one analytical determination, which shows a Cu content of 0.17 percent, compared to a mean values for six analyses of the lode sample of 0.035 percent. Addition of Cu to native gold during the transition from vein to placer is unlikely; therefore, the high content of Cu in the placer sample probably reflects the presence of inclusions of chalcopyrite or other Cu-bearing minerals in the gold sample analyzed. Decrease of Ag content from 10.7 to 7.1 percent from lode to lacer gold is reasonable, as is the loss of Bi and Mo. On the eastern flank of the Lost Basin Range, lode-placer pair LB4-WSE2 (table 23) although geographically closely related, show the lack of a direct kinship. The placer sample has only 4.9 percent Ag compared to 15.5 percent Ag for the lode sample. If the placer sample came directly from the lode, its Ag content should have been at least 10 percent, and Te should not have been present in the placer if not in the lode. The lower Ag content could be explained as the addition of Au through chemical or physical accretion, but the appearance of Te in the placer poses a mystery. A likely possibility is that some or all of the placer gold had its immediate, though secondary, source in the Muddy Creek Formation, and had a more distant primary source. Alternatively, the placer sample could have come from a portion of the vein at WSE2 that is considerably different in composition from that which we analyzed.

A problem also exists with placer sample N33PC7 and the Climax vein sample. Although the Ag and trace-element content are compatible, the greater amount of Cu in the placer sample indicates the placer sample either came from a different lode, or from a portion or the Climax vein containing a much higher content of Cu than that found in the portion of the vein that we sampled.

Placer sample LB3 has a composition that is compatible with derivation from lode sample BL-1 except for the presence of Zn and Cd, which could be explained by assuming that inclusions of sphalerite containing Cd were present

in the particular placer gold analyzed. Absence of Mo and Te in the placer sample is readily explainable as the result of loss from oxidation or leaching in the transition from vein to placer.

All the lode samples from the Gold Basin and Lost Basin districts were examined in terms of their Ag content and fineness as possible sources for the Lost Basin placer deposits. Histograms showing the number of samples with a particular level of Ag concentration (fig. 66) and the fineness of Au in Lost Basin placer samples and Lost Basin and Gold Basin lode samples (fig. 67) show a lack of strong or convincing evidence to relate the lodes to the placers. For example, no lode sample was found that contained less than 6.0 percent Ag, but several placer localities had gold with less than 5 percent Ag, and in one the gold contained only 2 percent Ag. Also, the highest mean Ag content in any placer sample was 19.3 percent Ag, but the Ag content at some lodes was as high as 38 percent and at 20 localities the gold samples contained more than 20 percent Ag. If chemical accretion of dissolved Ag around detrital gold particles occurred, as indicated by examination of some of the nuggets (see frontispiece), the local veins presumably could have provided all the gold. It can be seen in figure 67 that nearly all the placer gold is of comparatively high fineness with respect to that of the lodes. Therefore, although some of the placer gold probably had its origin in Lost Basin veins (and possibly in Gold Basins as well), more than half of it must either have had a different lode source from any of those sampled, or have come from portions of veins no longer extant, or it represents gold that was at one time in solution, and was added to placer gold particles by chemical accretion or other processes. In any event, relating gold in the Lost Basin placer deposits to veins in either the Lost Basin or Gold Basin lodes appears extremely difficult, if not impossible.

Composition of Lode Gold from the Lost Basin district

Signatures for lode gold samples from Lost Basin are presented in table 24. They are arranged geographically from west to east and north to south (fig. 65) and grouped according to veins that may be related because of their proximity to one another. A crude zoning relationship was observed in the sulfides present in the veins. At both the southern and northern extremities of mineralization in the Lost Basin Range, galena and sphalerite were the abundant sulfides, and in some veins containing sphalerite and galena, it was not possible to obtain sufficient gold for analysis. In the central part of

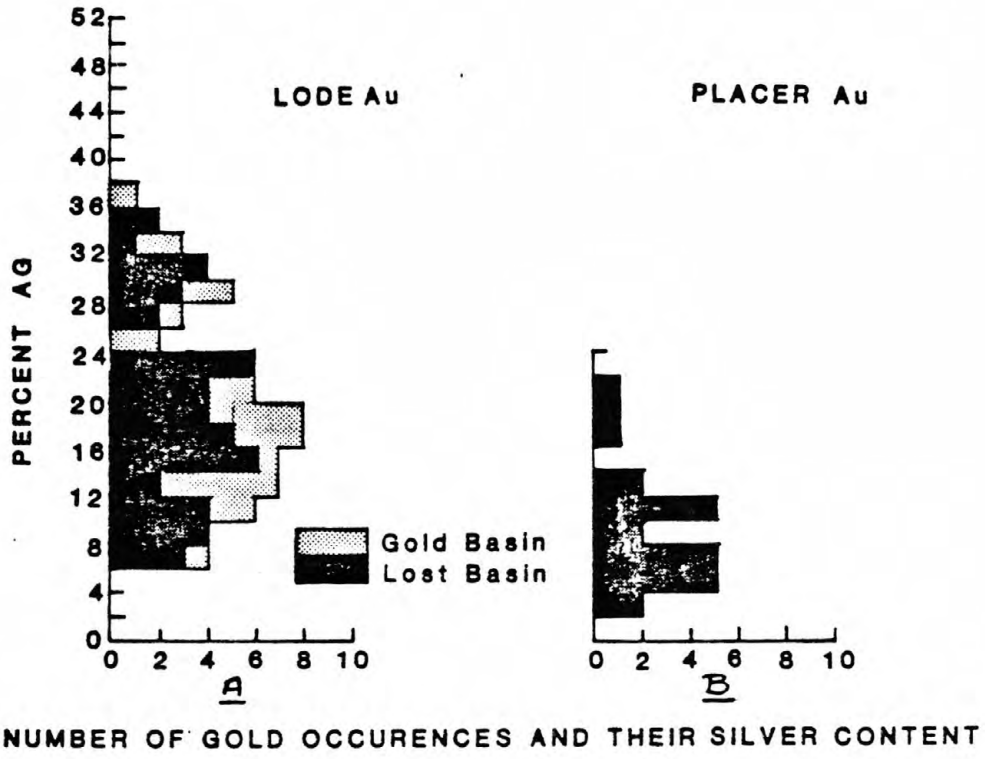

Figure 66.--Plots of percent silver versus number of gold occurrences for (A) lode gold from the Gold Basin and Lost Basin districts, and (B) placer gold from the Lost Basin district.

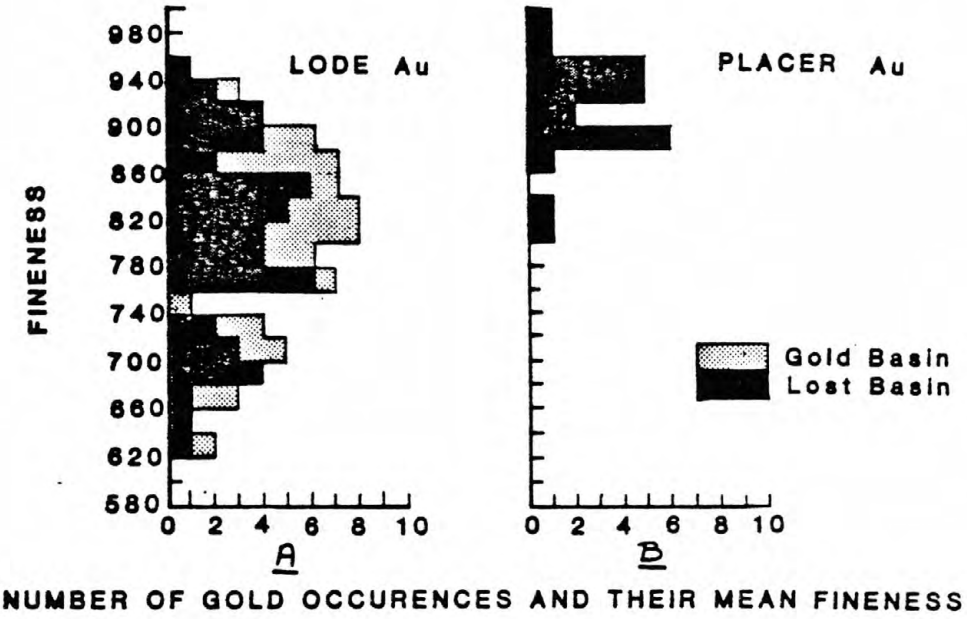

Figure 67.--Plots of mean fineness (see text) versus member of gold occurrences for (A) lode gold from the Gold Basin and Lost Basin districts, and (B) placer gold from the Lost Basin district.

Table 24.--Compilation of signatures of lode gold, Lost Basin District, Mohave, County, Arizona

Sample locality	Number of analyses	Ag, percent			Cu, percent			Au						Characteristic trace elements in order of abundance
		Range	Mean	Standard deviation	Range	Mean	Standard deviation	Percent	Fineness $\frac{Au}{(Au+Ag)}$ X1000	Au/Ag	Au/Cu	$\frac{Au/Ag}{Cu}$	Ag/Cu	
BDN1	2	27.9-35.6	31.8	5.4		0.075		67.8	681	2.1	900	28	425	Bi,Pb,Ba
BD	2	22.1-22.1	22.1		0.042 -0.085	.063	0.030	73.7	769	3.3	1170	52	351	Pb,Mo,Bi,Te,Co,Ni
BD summary	4	22.1-35.6	26.95		.042 - .085	.069		70.75	725	2.6	1025	38	391	Pb,Bi,Mo,Te,Ba,Co,Ni
S-NW	2	22.6-25.1	23.9	1.3	.025 - .047	.036	.016	76.0	761	3.2	2083	89	664	Pb,Bi
S	10	20.0-29.0	22.3	3.0	.004 - .014	.0086	.0033	77.6	777	3.5	9023	407	2593	Pb,Mo,Bi,Ba
S vein summary	12	20.0-29.0	22.6		.004 - .047	.013		77.3	774	3.4	5946	263	1738	Pb,Bi,Mo,Ba
WB-U	1		26.5			.019		69.7	725	2.6	3668	137	1394	Pb,Bi
WB-S	1		31.1			.070		63.9	694	2.1	913	30	444	Pb,Bi,Mo,Co,V,Ba
WB summary	2	26.5-31.1	28.8			.0445		66.8	710	2.4	2291	84	919	Pb,Bi,Mo,Co,V,Ba
Ford vein (F)	4	20.3-25.3	23.3	2.2	.01 - .07	.033	.026	75.8	764	3.3	2296	100	942	Pb,Bi
PB vein	1		29.8			.0125		70.2	703	2.4	5616	2384	192	Pb,Bi
GG (Golden Gate Mine)	5	12.0-19.5	15.1	3.4	.04 - .13	.092	.048	84.8	849	5.6	922	61	164	Pb,Bi,Sb,As,Zn,Pd,Cr, Ni
GGW-1	1		18.0			.125		81.9	820	4.6	654	37	144	Pb,Bi,As,Zn
Golden Gate summary	6	12.0-19.5	15.6		.04 - .13	.098		84.3	844	5.4	860	55	159	Pb,Bi,As,Zn,Sb,Pd,Cr, Ni
TP-1	2	5.9- 6.0	6.0	.07	.009 - .02	.0145	.078	93.9	940	15.7	6302	1082	4141	Bi,Pb,Pd,Mo
TP-2	5	3.6-16.8	6.1	5.0	.01 - .05	.0310	.0175	90.8	909	10.0	2929	322	294	Pb,Bi,Mo,Co,Ni,Cr
TP-3	5	5.0- 8.3	6.5	1.7	.0125- .03	.0190	.007	93.4	935	14.4	4916	758	342	Pb,Zn,Cd,Cr
TP-4	2	8.3-10.1	9.2	1.6	.005 - .0125	.0088	.005	90.7	908	9.9	10306	1120	1045	Pb,Bi,Zn,Cd,Cr
TP vein summary	14	3.6-16.8	6.7		.005 - .05	.021		92.2	923	13.8	4388	655	319	Pb,Bi,Cr,Mo,Zn,Cd,Mo, Pd,Co
HWW-G	2	30.2-31.2	30.7	.7		.03		69.1	692	2.3	2303	75	1023	Pb,Bi,Mo,Te
HWW	3	30.6-40.6	34.9	5.1	.2 - .4	.27	.11	61.4	638	1.8	227	6.7	129	Pb,Bi,Ba
HET	5	15.9-23.9	20.7	3.8	.035 - .3	.15	.11	79.2	793	3.8	528	26	138	Pb,Mo,Bi
HW	9	11.4-31.5	19.1	7.3	.03 - .5	.18	.15	80.8	809	4.2	449	23	106	Pb,Bi,Mo,W
HET-1	2	12.2-13.7	13.0	1.1	.025 - .028	.027	.015	86.6	869	6.7	3207	247	481	Pb,Mo,Bi
Harmon veins summary	21	11.4-40.6	22.3			.16		77.1	776	3.5	482	22	139	Pb,Bi,Mo,W,Te,Ba
Climax Mine	8	7.5-14.0	10.4	2.2	.015 - .025	.019	.004	89.5	896	8.6	4710	453	547	Pb,Bi,As,Mo,Zn
CBW-2	4	16.8-25.8	20.8	3.7	.016 - .025	.02	.003	79.0	792	3.8	3950	190	1040	Pb,Mo
CB-C	3	10.9-19.4	15.1	4.3	.015 - .03	.0225	.008	84.3	848	5.6	3750	249	671	Pb,Mo,Bi,As,Te
Climax Mine summary	15	7.5-25.8	14.1		.015 - .03	.02		85.7	859	6.1	4285	305	705	Pb,Mo,Bi,As,Zn,Te
BI-1	2	22.0-24.0	23.0	1.4	.05 - .065	.058	.011	76.7	769	3.3	1400	59	411	Pb,Mo,Bi,Sb,Zn,Cr,Ba
BI-8	3	19.0-39.0	29.0	10.0	.017 - .025	.022	.004	70.6	713	2.4	3200	109	1318	Pb,Mo,Bi,V,Ba,Sr
Blowout summary	5	19.0-39.0	26.6		.017 - .065	.036		73.0	733	2.7	2027	76	739	Pb,Mo,Bi,Sb,Zn,Ba,V, Cr

Table 24.--Compilation of signatures of lode gold, Lost Basin District, Mohave, County, Arizona--Continued

Sample locality	Number of analyses	Ag, percent			Cu, percent			Au						Characteristic trace elements in order of abundance
		Range	Mean	Standard deviation	Range	Mean	Standard deviation	Percent	Fineness Au/(Au+Ag) X1000	Au/Ag	Au/Cu	Au/Ag / Cu	Ag/Cu	
Golden Mile Mine Area														
GM	1		9.7			0.0375		90.1	903	9.3	2402	248	259	Pb,Bi,Ba,Cr
GMR	3	24.4-37.4	31.0	6.5	0.005 -0.010	.007	0.0026	68.8	689	2.2	9828	317	4428	Pb,Mo,Bi,Ba
GMG1	6	6.6-12.5	10.7	2.5	.02 - .037	.035	.0149	89.2	893	8.3	5986	238	718	Pb,Bi,Cr,Ba
Summary	10	6.6-37.4	16.7		.005 - .0375	.027		83.1	837	5.0	3078	185	618	Pb,Bi,Ba,Cr,Mo
Wall Street veins														
A. West veins														
WS-V	2	34.0-34.0	34.0		.0235- .0335	.029	.007	65.7	659	1.9	2270	67	1172	Pb,Bi
WS-W7	2	11.4-21.4	16.4	7.1	.15 - .30	.225	.106	83.0	835	5.1	370	23	73	Pb,Bi,Ba
WS-W	3	15.5-19.5	17.8	2.1	.02 - .036	.0277	.008	79.4	817	4.5	2890	160	647	Pb,Bi,Mo,Ni,V,Ba
WS-WG2	1		8.6			.0200		91.2	914	10.6	4560	530	430	Pb,Bi,Ba
WS-WG3	3	13.9-15.9	14.9	1.0	.018 - .028	.024	.007	84.9	851	5.7	3540	237	621	Pb,Bi,Te,Mo
WS-WG5	1		23.9			.010		76.0	761	3.2	7600	320	2390	Pb,Bi,Te,Mo,Cr,V,Ba
Summary West	12	8.6-34.0	19.3			.058		79.8	805	4.1	1376	71	333	Pb,Bi,Mo,Ba,Te,V,Cr, Ni
B. East veins														
WS-HVN	3	21.4-42.4	33.2	10.0	.0625- .0825	.0725	.010	64.7	661	1.9	890	27	458	Pb,Bi,Mo,Sn,V,Ba
WS-HV	3	26.6-28.6	27.9	7.2	.023 - .10	.0510	.043	71.7	720	2.6	1405	50	558	Pb,Bi,Mo,Sn,Zn,Cr,V
WS-E12	2	13.6-18.0	15.8	3.9	.0125- .25	.1300	.168	83.8	841	5.3	645	41	122	Pb,Bi,Te,V
WS-CL5	1		9.4			.0700		90.5	906	9.6	1290	138	134	Pb,Bi,Mo,Ba
WS-E1	2	17.3-21.1	19.2	2.7		.1500		79.6	806	4.1	530	28	128	Pb,Bi,As
Summary East	11	9.4-42.4	23.9		.0125- .25	.09		75.1	759	3.1	834	35	266	Pb,Bi,Mo,V,Ba,As,Zn, Cr,Ni
Summary West & East	23	8.6-42.4	21.5		.0125- .25	.07		77.6	783	3.6	1108	51	307	Pb,Bi,Mo,Ba,V,Te,As, Zn,Cr,Ni
Bluebird veins														
A. West of wash														
B-A	8	14.6-30.6	20.9	4.5	.014 - .06	.031	.015	78.7	790	3.8	2540	120	674	Pb,Bi,Ba
B-B1	10	13.4-23.4	18.4	3.1	.03 - .38	.17	.16	79.6	804	4.3	470	25	108	Pb,Bi,Sb,Zn,Ba
B-B1W	6	15.1-26.0	21.5	4.2	.02 - .7	.31	.26	77.9	782	3.6	250	12	69	Pb,Bi,Mo
B-C	9	10.3-15.3	11.9	1.8	.02 - .1	.046	.016	87.7	881	7.4	1900	160	259	Pb,Bi,As,Zn,Mo,Ba
BM-9	2	15.3-19.8	17.6	3.3	.006 - .018	.012	.008	81.7	823	4.6	6808	383	1467	Pb,Bi,Te,Cr,Ba
BM-8	1		29.2			.0075		71.5	716	2.4	9530	326	3893	Pb,Bi,Te,V,Ba
BM-3	2	8.7-14.2	11.5	3.9	.034 - .04	.037	.004	88.3	885	7.6	2390	208	311	Pb,Te
BM-3S	3	14.1-18.1	17.5	2.2	.032 - .0375	.035	.003	82.3	825	4.7	2400	134	500	Pb,Bi
BM-1S	2	8.8-15.8	12.3	4.9	.02 - .025	.0225	.004	87.3	877	7.1	3080	315	547	Pb,Bi
Summary	43	8.7-30.6	17.5		.02 - .31	.104		81.8	824	4.7	787	45	168	Pb,Bi,Te,Ba,Mo,Zn,Cr, V
B. East of wash														
B-J	10	9.9-18.2	14.6	2.9	.0175- .10	.0525	.032	85.2	854	5.8	1620	110	278	Pb,Bi
B-20L2	2	12.9-15.4	14.2	1.8	.019 - .026	.0225	.005	85.7	859	6.0	3800	268	631	Pb,Cr,V
B-JP	1		17.3			.0250		82.6	827	4.8	3300	190	692	Pb,V
Summary	13	12.9-18.2	14.7			.046		85.1	853	5.8	1850	126	320	Pb,V,Bi,Cr

the Lost Basin Range chalcopyrite was the dominant sulfide, and some veins contained molybdenite and arsenopyrite, with minor amounts of galena and sphalerite. The gold signatures reflect this zoning relationship only vaguely. The Climax vein samples, the samples in the vicinity of the "Blowout" (Bl-1, and Bl-8) and the samples designated "Wall Street East" appear to be near the center of the district. The trace elements in the gold signatures are dominated by Pb, Mo, and Bi, with analyses commonly showing the presence of As. Individual analyses could be singled ut to suggest that gold of high fineness occurs in some analyses, but the gold in nearly all the veins is extremely heterogeneous so that no convincing generalizations can be made. The vein with lowest Ag content, the TP vein is west of most of the veins where gold was found, but is about midway between the northern and southern boundaries of mineralization. The TP vein is more homogeneous than most of the other veins, and as the vein with the highest Ag fineness, may represent more nearly the center of the district than any of the other veins.

The abundance of veins in the Lost Basin district suggests the desirability of prospecting further, perhaps at depth, in the Lost Basin district.

Composition of Gold From Mines in Gold Basin

Signatures of lode gold from samples taken from the Gold Basin district are shown in table 25. These samples also are arranged from north to south (fig. 65). Northwest of the Gold Hill mine, a group of samles is designated with the prefix "AWS." Sample locality "AWS-M" in the center of this group showed in relicate samples, the least variation in Ag content of any of the lode samples in either the Gold Basin or Lost Basin districts. The Ag content of gold from this prospect was also somewhat less than most of the other prospects in the group, thus suggesting that AWS-M may have been a local center of mineralization. The other veins in this group vary widely in composition, however, and these veins like most others in the Gold Basin and Lost Basin districts are mixed sulfide veins and are generally small.

Platinum was found in gold from the Excelsior mine (sample loc. EXC) and Pd was found in gold from the Excelsior mine as well as from sample locality AWS-W. No apparent significance is attached to these occurrences. However, minor-element analyses of amphibolites from the general area of the Bluebird mine in the Lost Basin Range revealed the presence of detectable Pt and Pd (see above).

Table 25.--Compilation of lode gold signatures, Gold Basin District, Mohave County, Arizona

Sample locality	Number of analyses	Ag, percent			Cu, percent			Au						Characteristic trace elements in order of abundance
		Range	Mean	Standard deviation	Range	Mean	Standard deviation	Percent	Fineness $\frac{Au}{(Au+Ag)}$ X1000	Au/Ag	Au/Cu	$\frac{Au/Ag}{Cu}$	Ag/Cu	
SSM-W	1		11.3			0.0215		88.6	887	7.8	4100	390	526	Pb
Prospects northwest of Gold Hill Mine														
AWS-M	7	12.0-15.0	13.7	.94	0.014 -0.0455	.0215	0.0114	86.1	863	6.3	4004	293	637	Pb,Bi,Mo,Co,Cr,Ni,Ba
AWS-W	4	13.0-18.4	14.9	2.4	.008 - .026	.0155	.007	85.0	851	5.7	5484	368	961	Bi,Pb,Pd
AWS-E	1		17.0			.011		82.9	830	4.9	7536	445	1545	Pb,Bi,Ba
AWS-T	4	9.3-14.5	11.8	2.0	.02 - .05	.032	.015	88.0	882	7.5	2750	233	369	Pb,Mo,Bi,Ba
AWS-ES	1		7.5			.075		92.4	925	12.3	1232	164	2846	Pb,Mo,Ni
AWS-TS3	2	20.5-21.5	20.0	.7	.028 - .065	.05	.026	79.7	799	4.0	227	154	57	Pb,Bi,Cr
AWS-TS2	2	30.0-35.0	32.5	3.5	.2 - .5	.35	.21	67.4	675	2.1	193	6	93	Pb,Te,Mo,Bi,Co,Ni,Cr
Summary	21	9.3-35.0	15.8		.008 - .5	.058								
Gold Hill Mine	8	14.3-25.4	19.7	3.1	.0075- .05	.0225	.015	79.9	802	4.1	3551	227	875	Pb,Bi
Senator Mine	1		12.8			.0250		86.9	872	6.8	3480	271	512	Pb
MAS	5	15.6-25.6	18.0	4.3	.01 - .28	.112	.14	81.4	819	4.5	728	40	161	Pb,Bi,Sb,Zn,Cr,Sn,Mo
VVM	4	6.3-15.3	12.5	4.0	.014 - .0375	.0216	.0109	87.5	878	7.2	4050	333	578	Pb,Bi,Mo,Co
ENW-2	7	25.0-31.0	29.0	2.0	.003 - .02	.008	.0056	70.4	708	2.4	8850	300	3625	Pb,Sb,Bi,Co
ENW	3	14.4-18.4	16.7	2.1	.05 - .07	.058	.01	80.8	829	4.8	1403	83	288	Pb,Bi,As,Mo
EXC	3	28.3-42.5	36.1	7.2	.003 - .0375	.023	.018	62.9	635	1.7	2735	76	1570	Pb,Pt,Pd,Bi,Mo,Te
MAL-C	3	23.0-30.0	27.0	3.6	.007 - .014	.0117	.004	72.9	730	2.7	6230	230	2308	Pb
MWT	4	26.5-31.5	28.5	2.4	.003 - .0125	.0075	.004	71.3	714	2.5	9506	333	3800	Pb,Bi,Mo,W,Ba
MOK	3	46.2-54.2	49.5	4.2	.005 - .006	.0057	.0006	48.6	495	.98	8526	172	8684	Pb,Bi,Mo,Cr
MWS	5	10.5-35.5	18.5	9.8	.015 - .10	.05	.0287	81.2	814	4.4	1620	88	370	Pb,Bi,Mo,Cr,V,Pd
OLY	8	15.1-30.1	21.3	4.2	.036 - .118	.058	.0311	78.5	787	3.7	1570	64	367	Pb,Bi,Zn,Mo,V
OLY-SS	2	12.8-14.3	13.5	1.0	.0375- .0830	.06	.032	86.0	864	6.4	1430	107	225	Pb,Ba
FLU-SS	3	23.8-26.8	25.5	1.5	.008 - .012	.01	.002	69.0	730	2.7	6900	271	2550	Pb,Bi,Cr,Ni
CUR	1		12.5			.0375		87.4	875	7.0	2330	187	333	Pb,Mo,V,Ba
CYE	3	9.6-21.5	16.8	6.4	.005 - .03	.021	.0125	80.1	827	4.8	3815	227	800	Pb,As,Bi,Mo,Cr
CYC	1		24.0			.0125		74.7	757	3.1	5975	249	1920	Pb,Ba,Sr,Bi
CYC SW	1		18.1			.03		81.6	818	4.5	2720	150	603	Pb,Mo,Bi,Cr
MES4	1		32.4			.03		67.5	676	2.1	2250	69	1080	Pb,Cr

Gold of high silver content was found south of the Malco mine at sample locality MOK--the highest Ag content found in any of the samples from both Gold Basin and Lost Basin.

The average Ag content of lodes in the Gold Basin district is greater than that of lodes in the Lost Basin district although the Ag content varies widely in both districts. Cu content also varies widely in both districts, but is generally somewhat higher in the Lost Basin district. These observations suggest that perhaps in general, conditions of ore deposition were somewhat similar for both districts, but the temperature and pressure of ore deosition was probably somewhat greater in the Lost Basin district.

Similarity of Signatures of Gold From Some Sample Localities in the Districts to That of Gold From Some Porphyry Copper Deposits

In previous work, we have found that gold from some porphyry copper deposits has an Ag content of 25 to 30 percent, a Cu content of 0.04 to 0.15 percent, and a suite of trace elements that usually includes Pb, Bi, and Sb, and sometimes one or more other elements that might include Zn, As, Te, Sn, Cr, Ni, or W (Antweiler and Campbell, 1977, 1982). Probably the most important indicator in the gold signature is the quantity of Ag and Cu. Characteristically in hydrothermal deposits, native gold has maximum Cu and minimum Ag content at ore deositional conditions of high temperature and pressure, and minimum Cu and maximum Ag content at low temperature and pressure (Antweiler and Campbell, 1977). Gold from porphyry copper deposits, however, has an Ag content that is usually characteristic of epithermal or mesothermal deposits, but a Cu content more nearly like that of hypothermal deposits. Samples that contain or exceed 0.04 percent Cu content, and also contain at least 20 percent Ag should be considered in the context of their possible relationship to a porphyry copper deposit.

The Lost Basin and Gold Basin gold signatures were examined to determine whether any of the signatures were similar to those obtained on gold from porphyry copper deposits (Antweiler and Campbell, 1977, 1982). Samples with signatures that might qualify are shown in table 26 together with those from four porphyry copper deposits. The best candidates in the Lost Basin district are in a cluster northeast of the Golden Gate mine at sample localities BDN-1, BD, and S-HW; in a cluster at localities WB-S, HW, and HET; on the Bluebird vein at B-B1W, and B-B1; at the "Blowout"--samples locality BL-1; and on one of the "Wall Street" veins at locality WSE-1. The best locality in the Gold

Table 26--Signatures of gold from Lost Basin and Gold Basin that are somewhat similar to those of gold from porphyry copper deposits in other areas

Sample locality	Number of analyses	Ag, percent			Cu, percent			Au						Characteristic trace elements in order of abundance
		Range	Mean	Standard deviation	Range	Mean	Standard deviation	Percent	Fineness $\frac{Au}{(Au+Ag)}$ X1000	Au/Ag	Au/Cu	$\frac{Au/Ag}{Cu}$	Ag/Cu	
LOST BASIN														
BDN-1	2	27.9-35.6	31.8	5.4		0.075		67.8	681	2.1	900	28	425	Bi,Pb,Ba
BD	2	22.1-22.1	22.1		0.042-0.085	.063		73.7	769	3.3	1170	52	351	Pb,Mo,Bi,Te,Co,Ni
SHW	2	22.6-25.1	23.9	1.3	.025- .047	.0360	0.011	76.0	761	3.2	2083	89	664	Pb,Bi
WB-S	1		31.1			.07		63.9	694	2.1	913	30	444	Pb,Bi,Mo,Co,V,Ba
HW	9	11.4-31.5	19.1	7.3	.03 - .5	.18	.151	80.8	809	4.2	449	23	106	Pb,Bi,Mo,W
HET	5	15.9-23.9	20.7	3.8	.035- .3	.15	.111	79.2	793	3.8	528	26	138	Pb,Mo,Bi
B-BIW	6	15.1-20.0	21.5	4.2	.02 - .7	.31	.26	77.9	782	3.6	250	12	69	Pb,Bi,Mo
B-BI	10	13.4-23.4	18.4	3.1	.03 - .038	.17	.16	79.6	804	4.3	470	25	108	Pb,Bi,Sb,Zn,Ba
BL-1	2	22.0-24.0	23.0	1.4	.05 - .065	.058	.011	76.7	769	3.3	1400	59	411	Pb,Mo,Bi,Sb,Zn,Cr,Ba
WSE-1	2	17.3-21.1	19.2	2.7		.15		79.6	806	4.1	530	27	135	Pb,Bi,Cd
GOLD BASIN														
MAS	5	15.6-25.6	18.0	4.3	.01 - .28	.112	.14	81.4	819	4.5	728	40	161	Pb,Bi,Sb,Zn,Cr,Sn,Mo
ENW	3	14.4-18.4	16.7	2.1	.05 - .07	.058	.01	80.8	829	4.8	1403	83	288	Pb,Bi,As,Mo
NWS	5	10.5-35.5	18.5	9.8	.015- .10	.05	.0287	81.2	814	4.4	1620	88	370	Pb,Bi,Mo,Cr,V,Pd
MES-4	1		32.4			.03		67.5	676	2.1	2250	70	1080	Pb,Cr
OLY	8	15.1-30.1	21.3	4.2	.036- .118	.058	.0311	78.5	787	3.7	1353	64	367	Pb,Bi,Zn,Mo,V
GOLD FROM KNOWN COPPER PORPHYRY DEPOSITS														
Butte, MT	11[1]		25.9			.05		74.0	741	2.9	1500	58	518	Pb,Bi,Sb,Zn,Sn,Cr,Ni
Mineral Park, AZ	5[1]		29.6			.04		70.3	704	2.4	1800	60	740	Pb,Bi,Sb,Zn,As,Te
Cala Abajo, PR	1[1]		25.1			.15		74.8	749	3.0	500	20	167	Pb,Bi,Sb,Zn,As,Te
Stinkingwater, WY	1[2]		25.0			.15		75.0	750	3.0	500	20	167	Pb,W

[1]Antweiler and Campbell, 1977.

[2]Antweiler and Campbell, 1982.

Basin district is near the Malco mine at locality MAS, but some of the others may warrant examination. However, we should emphasize that no outcrops of Late Cretaceous-early Tertiary I-type granites are known to us in either of the districts.

FLUID INCLUSION STUDIES

Initial fluid inclusion studies of the precious- and base-metal vein deposits and occurrences, and the occurrence of disseminated gold in the districts were carried out in 1970-1972 by Nash in conjunction with the field investigations of Blacet. These studies included quantitative tests using heating and freezing techniques, visual estimates of approximate filling temperatures of about one-third of the studied samples, and the examination of fluid-inclusion relations in all available thin sections. Subsequently these investigations were supplemented by intensive heating and freezing tests by Theodore and T. F. Lawton of a few geologically critical samples to resolve some ambiguities remaining between mineralization and its associated fluids. About 60 doubly polished plates, approximately 0.5 to 1 mm thick, were prepared of rock and vein samples from about 40 different localities. Three different stages were used during the course of the investigations. The earlier studies by Nash used a custom fabricated heating stage probably having better than $\pm 5^{\circ}C$ accuracy and precision. Freezing tests were accomplished using cooling equipment that utilized approximately 7 liters of rapidly circulating acetone as the heat exchange medium (see Roedder, 1962). The later investigations by Theodore and Lawton used a comercially available Chaixmeca (use of brand names in this report is for descriptive purposes only and does not constitute endorsement by the U.S. Geological Survey) stage described by Poty, Leroy, and Jachimowicz (1976), and modified using insulation materials designed by Cunningham and Carollo (1980). The Chaixmeca stage uses dry nitrogen gas passed through a liquid nitrogen bath as the refrigerant. Repeated calibrations of this stage using natural and synthetic standards suggest temperature measurements are less than $\pm 0.1^{\circ}C$ in error in the range $-56^{\circ}C$ to $+200^{\circ}C$, and approximately $\pm$ $1.0^{\circ}C$ in the range 200 to $550^{\circ}C$. Carbon dioxide-rich inclusions were studied using the methods of Collins (1979). Daughter minerals were studied using the SEM, and an attached energy dispersive detector following the sample preparation techniques of Metzger and others (1977).

Types of Fluid Inclusions

Several types of well-developed and relatively large sized fluid inclusions occur in quartz and fluorite that are associated spatially and temporally with gold. The fluid inclusions may be classified as follows:

(a) Type I, moderate salinity type, consists of a liquid phase and a vapor phase (fig. 68A). The vapor phase of this very common inclusion type typically makes up about 15 volume percent of the inclusion at room temperature. Freezing tests show these inclusions to have salinities generally in the range 10 to 14 weight percent NaCl equivalent. Very rarely this type of fluid inclusion also contains an extremely small crystal of hematite. However, some sulfide minerals also have been trapped in these fluid inclusions during the growth of their host mineral, mostly quartz. These sulfides include chalcopyrite, galena, and pyrite (fig. 68B, C) and are believed to be captured minerals trapped during crystallization of the quartz; they apparently are not daughter minerals. Some type I inclusions also contain significant amounts of CO_2 because during freezing tests liquid CO_2 appears at temperatures slightly below room temperature as a thin meniscus around the vapor bubble. The moderately saline nature of the liquid in the type I fluid inclusions is reflected in the occurrence of extremely small, rounded crystals of NaCl, about 0.25μm across found near open fluid inclusions using the SEM, and indicate dessication from the evaporation of the released fluid-inclusion waters.

(b) Type II, a very low density, vapor rich type shows more than 50 volume percent vapor at room temperature. This type of inclusion is very rare in the Gold Basin-Lost Basin districts, and may reflect either local boiling or secondary necking down.

(c) Type III, a high salinity type, includes one, or more than one, nonopaque daughter minerals at room temperature. The most common daughter mineral is NaCl (fig. 68D, E). A highly birefringent mineral that has parallel extinction and is probably anhydrite, and very sparse occurrences of a carbonate mineral, probably calcite, also occur in some of this type of fluid inclusion. In addition, small crystals of opaque minerals may occur in this type of inclusion. Some type III inclusions also show relatively limited concentrations of liquid CO_2 at room temperature. Although we do not recognize optically the presence of sylvite (KCl) in these type III inclusions, some extremely small, rounded crystals of sylvite were found using

Figure 68.--Photomicrographs and electron micrographs of fluid inclusions in rocks from the Gold Basin-Lost Basin mining districts. Photomicrographs in plane polarized light. L, liquid; V, vapor; Q, quartz. A, Photomicrograph showing type I fluid inclusions consisting of mostly liquid H_2O and vapor hosted by vein quartz. Sample number GM-433; B, Electron micrograph showing chalcopyrite (cp) trapped in a fluid inclusion hosted by vein quartz from a quartz-carbonate-barite-albite-pyrite vein. Sample number GM-689; C, Electron micrograph showing pyrite (py), galena (gn), and calcite (C) trapped in a fluid inclusion hosted by vein quartz from a quartz-albite-calcite-barite-pyrite-galena vein. Sample number GM,-382; D, Electron micrograph showing a crystal of halite (NaCl) projecting from an irregularly shaped fluid inclusion in vein quartz from a quartz-carbonate-barite-albite-pyrite vein. Sample number GM-689; E, Electron micrograph showing a somewhat rounded crystal of halite (NaCl) in a fluid inclusion, about 3 μm in longest dimension. Also shown on the surface of artificially broken quartz is a cluster of rounded sylvite (KCl) crystals that individually measure about 1.0 μm across.

A

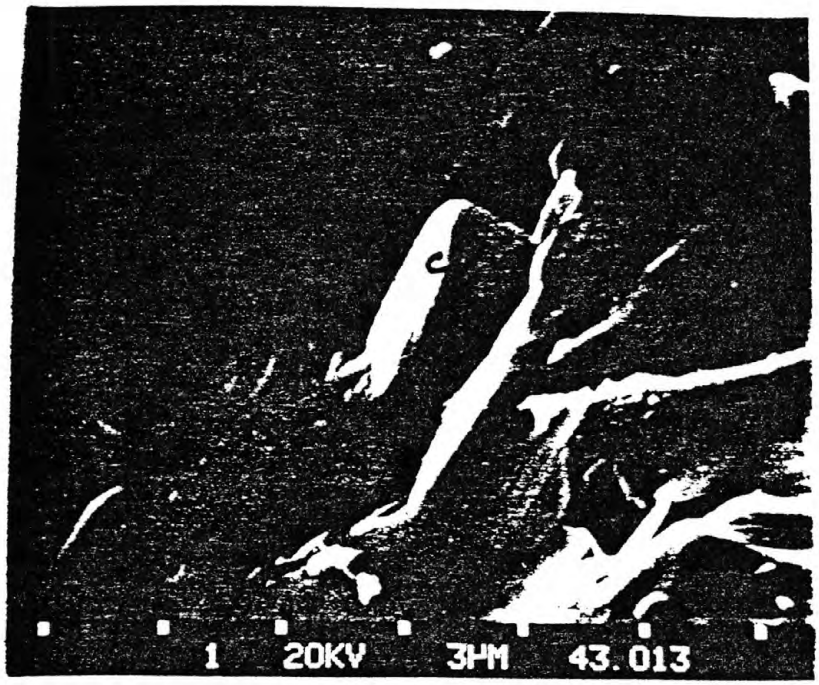

B

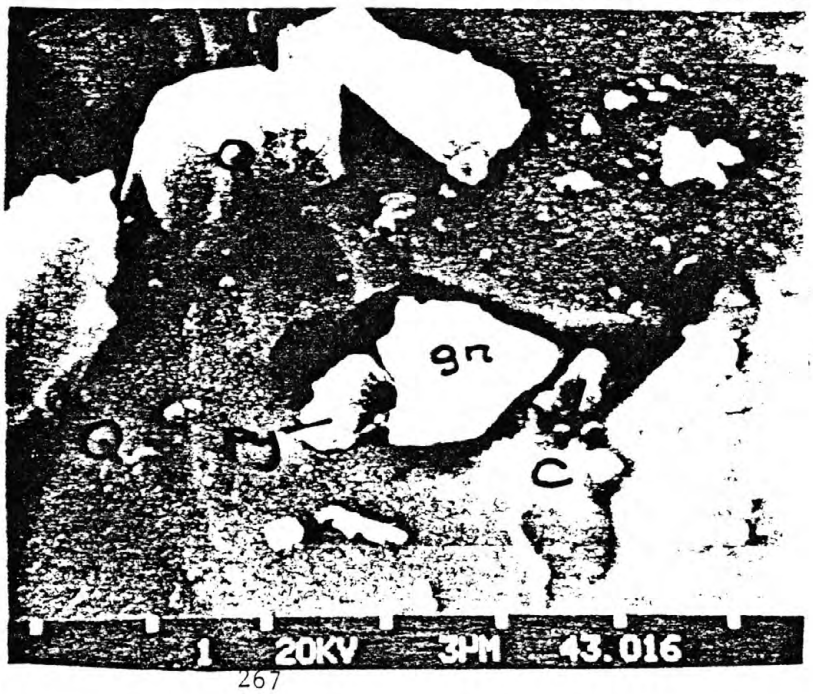

C

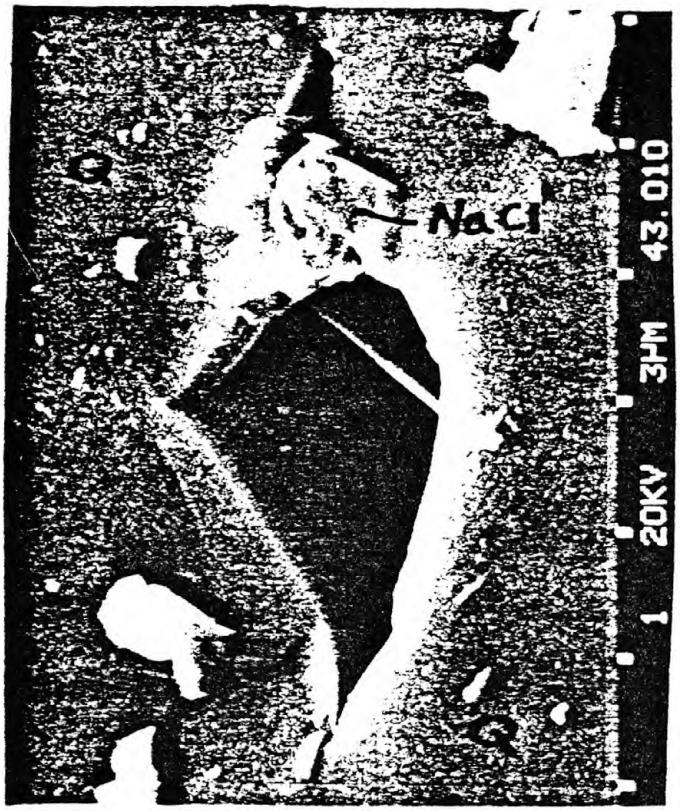

D

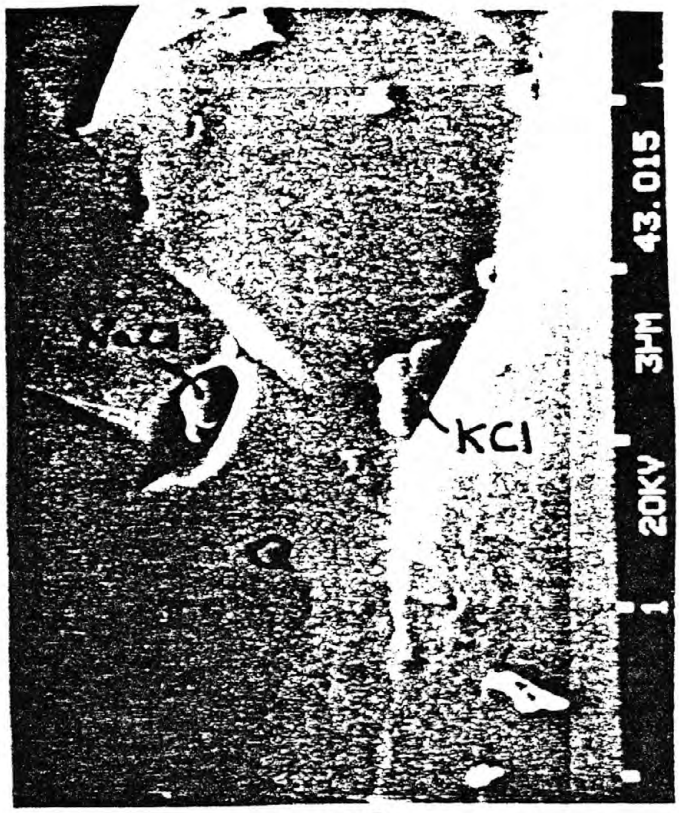

E

the SEM on broken surfaces of vein quartz (fig. 68E). These crystals probably formed during evaporation of liquid from the ruptured fluid inclusions. If so, these are not daughter minerals but attest to some minor amounts of potassium in the fluid. The proportion of vapor in the type III inclusions is about 15 volume percent. Type III inclusions are relatively rare in the examined deposits and occurrences, but they seem to be concentrated preferentially in quartz paragenetically associated with the feldspathic portions of the quartz-cored pegmatitic veins, or with narrow micropegmatitic veins that did not evolve a significant quartz-carbonate±base- and precious-metal stage.

(d) Type IV are three-phase inclusions which at room temperatures contain mostly liquid H_2O, relatively abundant of liquid CO_2, and CO_2-rich vapor. These CO_2-rich inclusions are the pre-eminent signature of the fluid inclusion populations associated with the gold-bearing veins and the gold-bearing episyenite (fig. 69A-E). About 70 percent of the samples studied contain the liquid carbon dioxide-bearing fluid inclusions. Typically, the combined liquid CO_2 plus vapor proportion of these inclusions is in the 15 to 20 volume percent range. Very sparse numbers of these inclusions also show extremely small opaque to partially translucent minerals. As will be shown below, the salinity of these type IV inclusions also is moderate (3 to 9 weight percent NaCl equivalent). In addition, primary quartz in the upper Cretaceous two-mica monzogranite contains abundant concentrations of type IV inclusions in clusters (fig. 69B, C), and in planar arrays along secondary, annealed microfractures (fig. 69D). Thus, the CO_2-rich fluids are probably younger than the initial crystallization of the two-mica monzogranite from a magma.

Artificially broken cleavage surfaces in galena also were examined using the SEM to study fluid inclusions. Generally, the fluid inclusions in galena are rounded and equant in the range 1.0 to 10.0 μm, although some elongate fluid inclusions are as long as 40 μm. The fluid inclusions are apparently free of daughter minerals, although this judgment is based on the examination of only a limited number of samples of galena. Some of the inclusions contain crystals of quartz, potassium feldspar, iron sulfide (possibly marcasite because of apparently orthohombic habit and comb structure), and an unknown silver telluride mineral. Many of these crystals are probably minerals captured during late crystallization stages of the host galena. Trace amounts

Figure 69.--Photomicrographs showing relations among liquid-carbon dioxide-bearing (type IV) fluid inclusions. Q, quartz; L_{H_2O}, mostly liquid H_2O; L_{CO_2}, mostly liquid carbon dioxide; V, mostly CO_2 vapor. Plane polarized light. A, Isolated, relatively large, pseudosecondary fluid inclusion containing abundant liquid carbon dioxide at room temperature. The inclusion is hosted by vein quartz from an approximately 0.6-m-thick quartz-chalcopyrite-galena vein emplaced along a shallow-dipping fault. Sample number GM-433; B, Typical concentration of type IV, apparently secondary fluid inclusions in primary quartz phenocrysts in the upper Cretaceous two-mica monzogranite. Sample number GM-1089; C, Closeup view showing relative proportions of mostly liquid H_2O, liquid carbon dioxide, and mostly carbon dioxide vapor occurring commonly in the fluid inclusions hosted by primary quartz in the upper Cretaceous two-mica monzogranite. Sample number GM-1103; D, Abundant, secondary type IV fluid inclusions along annealed microfractures in primary quartz in the upper Cretaceous two-mica monzogranite. Sample number GM-977.

A

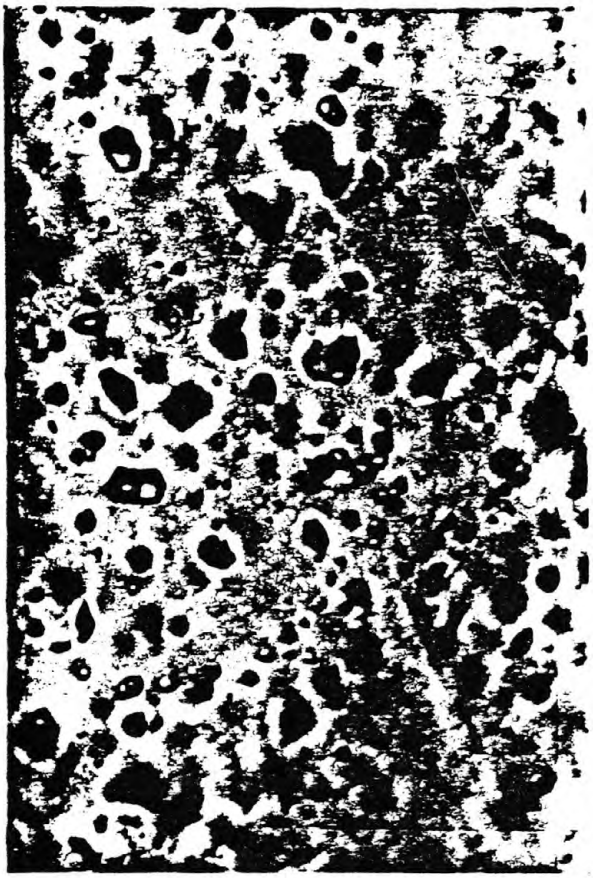

B

C

D

of silver also were detected locally in some crystals of galena by spot qualitative analyses using the energy dispersive analyzer.

Homogenization Temperatures and Salinities

Homogenization temperatures in the Gold Basin-Lost Basin districts are in the range 150 to about 300°C (table 27). However, most of the homogenization temperatures are approximately 200°C. Although the overwhelming bulk of the heating tests resulted in the fluid inclusions filling to liquid, some inclusions in two samples from the quartz+carbonate+sulfide(s) vein stage (B, table 27) homogenize to vapor. In addition, only one sample contains relatively abundant vapor-rich (type II) inclusions in late-stage clear quartz, a relation which suggests either that boiling occurred only locally during mineralization, and most likely during the final stages of the mineralization; or that these vapor-rich inclusions reflect secondary necking. There does not appear to be a significant difference in homogenization temperatures between the feldspar-dominant stage (mineralization stage A, table 27) and the quartz-carbonate-sulfide(s) stage (B) wherein the bulk of the gold finally was deposited. However, at most only six of the studied samples are from the feldspar-dominant stage of mineralization, and these samples probably include some quartz paragenetically later than the feldspar (mostly albite).

The salinities of the fluid inclusions determined from the districts range from about 35 to about 6 weight percent NaCl equivalent. The measured temperatures of first melting of ice in the fluid inclusions not containing a daughter mineral of NaCl are consistently near -24°C, a value which is very close to the -21.1°C expected eutectic temperature for the system NaCl-H_2O. From this relation we infer that the inclusion fluids contain sparse concentrations of calcium or magnesium, thereby supporting our referral of the data to the system NaCl-H_2O. The type I inclusions generally show salinities between 10 and 14 weight percent NaCl equivalent (table 27), and their abundance in the deposits, together with type IV inclusions, indicates the largely non-boiling nature of the mineralizing fluids. Only four of the samples studied contain NaCl daughter minerals, and the measured solution temperature of the NaCl in one of these samples (260°C) suggests that the salinities very locally were as high as 35 weight percent NaCl equivalent. However, within these overall salinity limits there is a wide range even within a single crystal of vein quartz or fluorite, suggesting the salinity of

Table 27. Homogenization temperatures and salinity data from fluid inclusion studies in the Gold Basin–Lost Basin mining districts
[N.D., not determined]

Sample number	Mineralization stage[1]	Mineral[2]	Homogenization temperature (°C)	Salinity[3]	Liquid CO_2[4]	Daughter minerals[5]	Comments
GM-14	B	F	250; >260	35.	x	NaCl	NaCl daughters dissolve 260°C
GM-14A	B	Q	180–255	14.1–14.4	x	——	Contains visible gold
GM-280	B	F	251–268	8.5–9.0	x	——	Fluorite-bearing episyenitic rock containing disseminated gold (see text)
GM-382	A	Q	195–205	10.3	x	——	Early-stage quartz
		Q	190±10	8.	——	——	Later quartz
		Q	193±5	15.8	——	——	Later quartz
GM-431	B	Q	N.D.	N.D.	x	Hm, Anh	Early-stage quartz
			175e	N.D.	——	Hm, Anh	Late-stage quartz
GM-433	B?	Q	250.±25	12–15.5	x	——	Early stage. Some inclusions fill to vapor
		Q	N.D.	N.D.	——	——	Late stage. Relatively abundant vapor-rich inclusions
GM-436b	B	Q	220±10	11–14	x	——	Early stage
		Q	N.D.	N.D.	——	——	Late stage
GM-437	B?	Q	210–230	15.4–22.	x	Anh	Early stage
		Q	205±5	12.–13.	——	Anh	Late stage
GM-447	B	Q	183±3	8.7–12.6	——	——	Early-stage milky quartz
		Q	167±3	8.–13.	——	——	Late-stage clear quartz
GM-456f	B	Q	225e	10.	x	——	
GM-466	B	Q	180–210	9.5–14.	——	——	
GM-467	B	Q	200e	N.D.	x	——	
GM-470a	B	Q	250e	14.	x	——	
			200±15	22.	——	——	
GM-479	B	Q	200±5	22.	——	Anh	
		Q	170	6.–12.	——	——	
GM-482	A or B	Q	N.D.	N.D.	x	Hem	
		Q	175	N.D.	——		
GM-489	B	Q	N.D.	N.D.	x	——	Early stage
		Q	190±10	7.–14.	——	——	Late stage
GM-513	B	Q	205±10	13.–16.	——	——	
GM-516A	B	Q	178–240	10.2–16.3	x	——	Contains visible gold in early-stage quartz
		Q	110–120	N.D.	——	——	Late-stage, secondary fluid inclusion
GM-567	B	Q	189	5.5	——	——	
GM-569	B	Q	186	17.–23.	——	——	
GM-576	B	Q	200e	N.D.	x	——	
GM-688	A	Q	250e	>30.	——	NaCl	
		Q	250e	N.D.	x	——	
		Q	200e	N.D.	——	——	
GM-689	A	Q	N.D.	N.D.	x		
		Q	250e	>30.	——	NaCl	
		Q	225–245	N.D.	——	Hm	
GM-690	A	Q	250e	N.D.	——	Hm, Anh(?)	Early stage. May have some NaCl daughter minerals
		Q	176–205	N.D.	——		Late stage
GM-735	B	Q	186–197	10.4	——	——	Contains visible gold
GM-735-1	B	Q	178–200	N.D.	——	——	Contains visible gold
GM-802A	B	Q	225e	N.D.	x	Anh(?)	
		Q	150	N.D.	——	——	Late secondary fluid inclusions
GM-802B	B	Q	225–230	>30	——	NaCl	
		Q	200e	N.D.	x	——	
		Q	200e	N.D.	——	Anh(?)	
GM-812	B	F	<200e	N.D.	——		
		Q	<200e	N.D.	——		
GM-837	B	Q	250e	N.D.	——		
		Q	250e	N.D.	x		
GM-878	A or B	Q	250e	N.D.	x	——	Some inclusions possibly contain Anh
GM-897	B	Q	200e	N.D.	——	——	
GM-913	B	Q	250e	N.D.	x	——	
GM-913v	B?	Q	200e	N.D.	——	——	Vein
GM-917e	B	Q	250±10	N.D.	x	——	Some fill to vapor
		Q	250–275e	N.D.	——	Hem	
GM-923	B	F	N.D.	N.D.	x	——	Secondary fluid inclusions
		Q	300	N.D.	x	——	Estimate 50 percent of inclusions contain CO_2
		F	250e	N.D.	x	——	
		Q	255	N.D.	x	——	Quartz very milky
		Q	167	N.D.	——	——	Late stage
GM-923a	B	Q	235–240	N.D.	x	——	
		Q	210±10	N.D.	——	——	
GM-927	B	Q	250	N.D.	——	Carb	
GM-1134h	B	Q	145–186	5.8–9.5	——	——	Fluorite-bearing syenitic rock containing disseminated gold (see text)

[1] A = Feldspar-dominant stage (quartz+albite±barite±sulfide(s)±white mica assemblage); B = quartz+carbonate+sulfide(s)±gold±fluorite stage.
[2] F, fluorite; Q, quartz.
[3] Equivalent weight percent NaCl using the freezing point depression method of Roedder (1962).
[4] x, liquid CO_2 present at room temperature; ——, liquid CO_2 not observed at magnifications of about 1,000X.
[5] NaCl, halite; Hm, hematite; Anh, anhydrite; Carb, carbonate; queried where identification uncertain; ——, daughter minerals not observed at magnifications of about 1,000X.

the fluids associated with gold mineralization varied widely. As shown on figure 70, the overall range in salinities of the fluids associated with gold mineralization largely bridges the interval in fluid compositions between many epithermal, precious-metal districts and porphyry copper deposits.

In an attempt to bracket closely the pressure-temperature-chemical environment(s) associated with upper Cretaceous-early Tertiary precious- and base-metal mineralization in the districts, fluid inclusion studies were focused especially on (1) samples from the episyenitic alteration pipes containing disseminated gold, and on (2) a quartz-fluorite-white mica vein that cuts the upper Cretaceous two-mica monzogranite.

Fluid Inclusions in the Episyenitic Alteration Pipes Containing Disseminated Gold

Abundant type I and type IV fluid inclusions occur in hydrothermal quartz and purple fluorite that fill cavities in the episyenitic alteration pipes which contain disseminated gold. Two samples (GM-280b and GM-1134h) were collected from coarse-grained episyenitic rock in the interior portions of two of the alteration pipes. However, the generally small size of the fluid inclusions in these rocks restricted our quantitative studies to fluid inclusions in fluorite from sample GM-280b, and to fluid inclusions in quartz from sample GM-1134h. All fluid inclusions are trapped in the fluorite along more or less planar arrays.

Type I fluid inclusions presumed to be primary, or having formed during initial crystal growth (Roedder, 1972), occur in diffuse planar arrays that commonly contain parallel linear trains of inclusions, the effect of which is to create a cubic network (fig. 71A). These networks are inferred to reflect the cubic habit and growth planes of the host fluorite, and suggest that the fluid inclusions were trapped on growth planes during early stages of the fluorite. The inclusions are equant in shape, generally rhomblike to circular, and range from less than 4 μm to 14 μm. They exhibit a consistent vapor fraction, which averages 20 volume percent at room temperatures. Although these early stage or primary type I fluid inclusions in fluorite show at magnifications of about 1,000X no liquid carbon dioxide at room temperature, they nonetheless may contain limited amounts of carbon dioxide. The solubility of carbon dioxide in H_2O at 25°C and at a pressure of 50 bars is approximately 2.1 mol. percent (Greenwood and Barnes, 1966), and the limit of detection optically is about 3 mol. percent (Ypma, 1963).

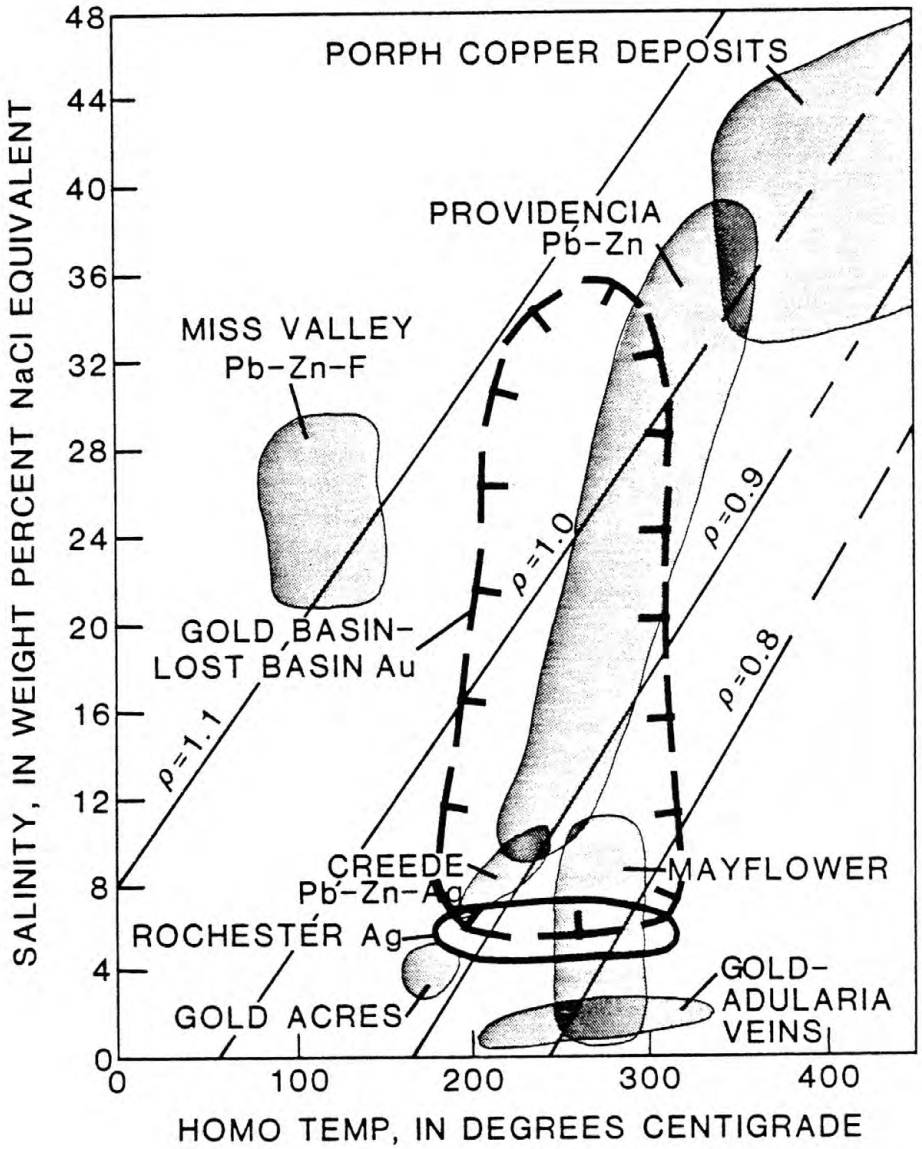

Figure 70.--Fluid-inclusion homogenization temperature and salinity data for various precious- and base-metal districts and deposits. Modified from Nash (1972). Data for the Rochester, Nev., silver district are from Vikre (1977, 1981) and have been corrected for inferred pressures of approximately 1 kb during mineralization. Data for the Gold Basin-Lost Basin districts are from this study.

Figure 71.--Photomicrographs of fluid inclusions in samples from the gold-bearing episyenitic rock. Plane polarized light. F, fluorite; Q, quartz; V, vapor; L_{CO_2}, liquid carbon dioxide; L_{H_2O}, mostly liquid H_2O. A, Extremely small, primary fluid inclusions defining a cubic network in fluorite. Also in the field of view, there are (1) discontinuous planar arrays of very small fluid inclusions, and (2) large type IV and rare type II fluid inclusions that are along discontinuous planes. Each of the latter two characteristics are inferred to reflect pseudosceondary relations. Sample number GM-280b; B, Relatively large pseudosecondary type IV fluid inclusion in fluorite. Sample number GM-280b.

A

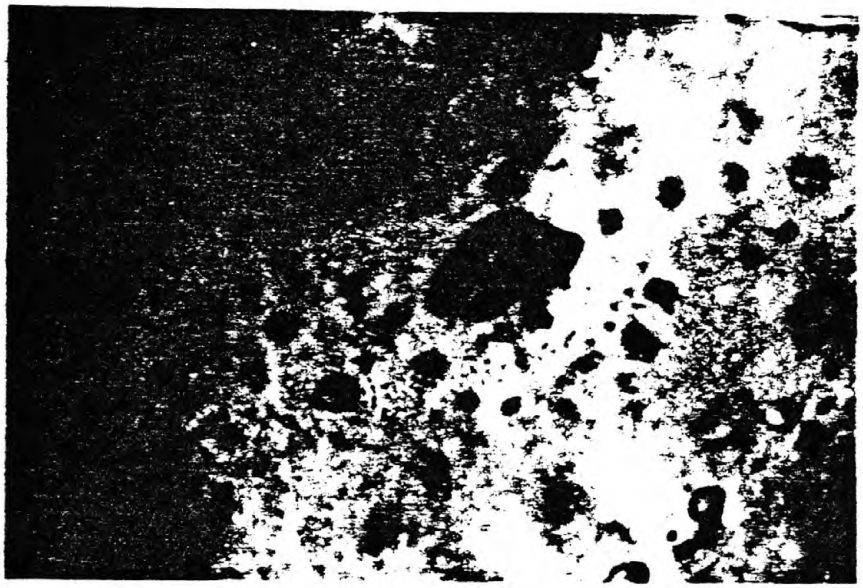

B

Type IV fluid inclusions in the fluorite are interpreted to be mostly pseudosecondary. This type of fluid inclusions is concentrated in discontinuous planar arrays that are confined to the interiors of the fluorite crystals, and trapped penecontemporaneous with the latter stages of growth of the fluorite. Crystallization of the fluorite must have continued after trapping of the fluids along these planar arrays. The type IV inclusions consist of saline fluid (mostly H_2O), vapor (mostly carbon dioxide), and about 15 to 18 volume percent liquid carbon dioxide. In fact, one of the diagnostic features of the pseudosecondary, type IV fluid inclusions in these gold-bearing episyenitic rocks is the high proportions of liquid carbon dioxide in them at room temperature (fig. 71B). The volume ratio of liquid carbon dioxide to vapor has a value of about nine, and liquid carbon dioxide plus vapor comprise typically about 20 volume percent of the inclusion. These type IV inclusions are somewhat larger than the primary type I fluid inclusions noted above, and the type IV fluid inclusions range in size from 16 to 35 μm. Their habits are equant to somewhat elongate. The type I and type IV fluid inclusions trapped together in the fluorite suggest that the fluids that circulated through the episyenitic rocks at various times during the crystallization of fluorite and thus during the introduction of gold there, included wide-ranging proportions of carbon dioxide.

Secondary fluid inclusions occur in fluorite along well-defined planes that converge, diverge, and intersect at various angles and which lack the generally orthogonal aspect of the primary inclusions. The planes commonly are broadly arcuate and cut crystal boundaries in the fluorite. Such secondary inclusions exhibit variable shapes, from smoothly elliptical to highly irregular, and variable sizes: inclusions from 10 to 48 μm in diameter were measured. The secondary inclusions are mostly a type I variety, and show a variable degree of vapor fill at room temperature with a range from 0 to 50 percent, although most frequently they contain between 2 to 10 volume percent vapor.

Salinities of the primary and pseudosecondary fluid inclusions in fluorite overlap significantly the salinities of the secondary fluid inclusions. Salinities of the primary type I fluid inclusions were determined using the depression of freezing point method (Roedder, 1962), and salinities of the pseudosecondary type IV were determined from the final melting temperature of clathrate, most likely $CO_2 \cdot 5\text{-}3/4\ H_2O$ (Roedder, 1963), formed

during the freezing runs (see Takenouchi and Kennedy, 1965; Bozzo and others, 1975; Collins, 1979). The overall range of salinities of the primary fluid inclusions is from approximately 3.0 to 9.0 weight percent NaCl equivalent (fig. 72A). Most salinity determinations are in the narrow range 8.5 to 9.0 weight percent NaCl, whereas the fluid inclusions containing liquid carbon dioxide at room temperature seem to show salinities at the lower end (3.0 to 8.0 weight percent NaCl equivalent) of the overall range. Salinities of obviously secondary fluid inclusions in fluorite mostly are approximately 6.5 to 7.0 weight percent NaCl equivalent (fig. 72B, C); they are approximately 2.0 weight percent NaCl less saline than the primary inclusions. However, the salinity of the secondary fluids ranges upwards to slightly more than 15 weight percent NaCl equivalent.

In all, 41 filling temperatures were measured from the primary, pseudosecondary, and secondary inclusions trapped in fluorite from the gold-bearing episyenitic rocks (fig. 73). The primary type I fluid inclusions show a very restricted range in filling temperatures between 251°C and 268°C (262°C mean). The pseudosecondary type IV fluid inclusions contain significant proportions of liquid carbon dioxide, as described above, and they have a lower or first homogenization wherein their vapor phase disappears between 26.9°C and 28.°C. The average temperature of vapor phase disappearance for these inclusions is 27.6°C. Continued heating of four of these inclusions results in their homogenization into a single liquid phase in the temperature range 280-282°C. The secondary fluid inclusions in fluorite all fill to liquid at temperatures in the 130 to 167°C range, which is significantly less than the filling temperatures of the primary and pseudosecondary fluid inclusions (fig. 73).

Limited freezing and heating tests also were performed on type I fluid inclusions hosted by irregular patches of secondary quartz that fills cavities (sample no. GM-1134h). The quartz which contains these fluid inclusions typically contains some needles of rutile that are concentrated near the margins of the quartz. The fluid inclusions range in size from less than 1 μm to 24 μm. Some have elliptical shapes, but many are irregular in outline and confined along planar, annealed microfractures, suggesting secondary origins. Eight freezing tests yield salinities in the range 5.8 to 9.5 weight percent NaCl equivalent; the mean is 7.8 weight percent NaCl equivalent. Heating tests show 17 fluid inclusions to fill to liquid in the range 144 to

Figure 72.--Histograms showing salinities in weight percent NaCl equivalent, of primary and pseudosecondary (A) and secondary (B and C) fluid inclusions in fluorite from the gold-bearing episyenitic rocks. Sample number GM-280b. Salinities of primary and pseudosecondary fluid inclusions (A) were determined using the depression of freezing point method for the type I, H_2O-rich fluid inclusions, and the final melting temperature of clathrate(s) for the type IV fluid inclusions (see text). Salinities of the secondary inclusions were determined using the depression of freezing point method (B), and the final melting temperature of clathrate(s) (C).

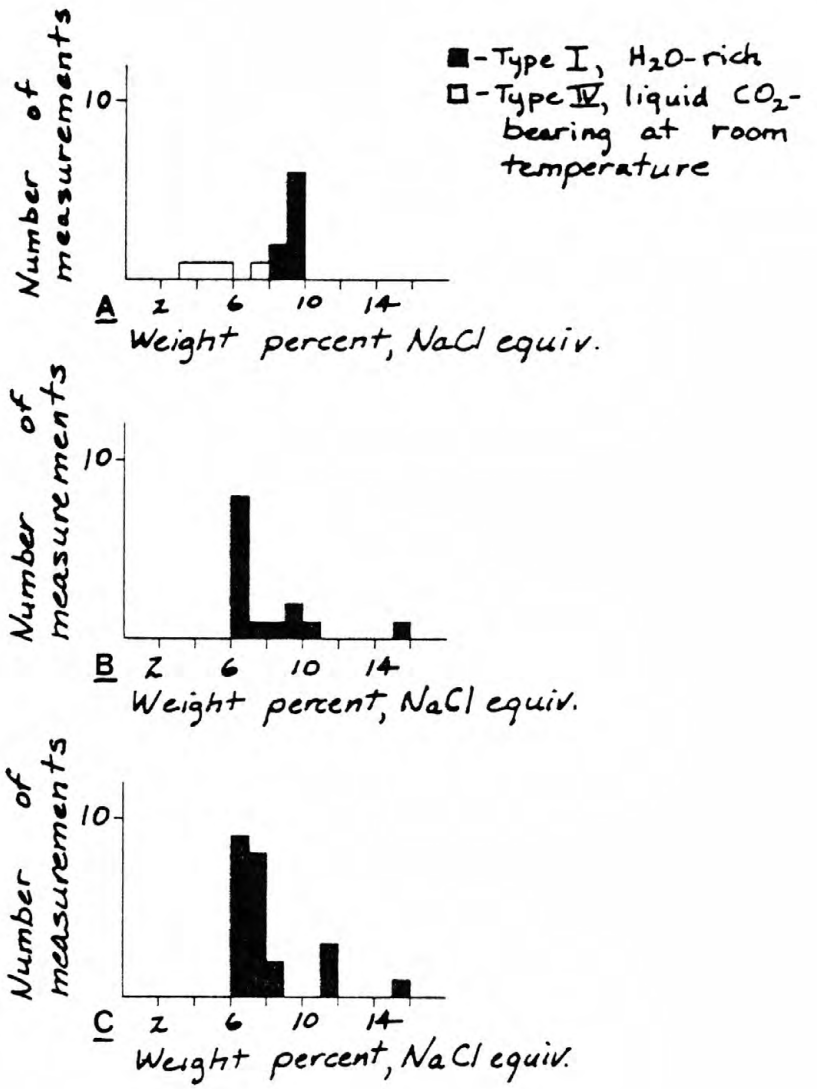
■-Type I, H2O-rich
□-Type IV, liquid CO2-bearing at room temperature
Number of measurements
10
A
2
6
10
14
Weight percent, NaCl equiv.
Number of measurements
10
B
2
6
10
14
Weight percent, NaCl equiv.
Number of measurements
10
C
2
6
10
14
Weight percent, NaCl equiv.

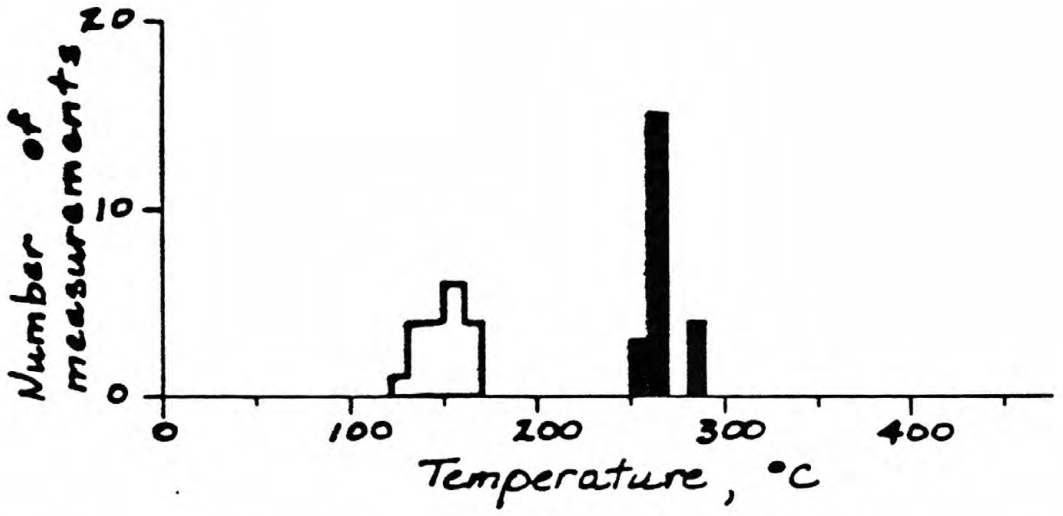

Figure 73.--Histogram showing filling temperatures in fluorite from the gold-bearing episyenitic rocks. Open pattern, secondary fluid inclusions; block pattern, primary and pseudosecondary fluid inclusions. Sample number GM-280b.

186°C. The filling temperatures for these fluid inclusions in quartz correspond quite well with the filling temperatures of the secondary fluid inclusions in fluorite; the mean filling temperature of the fluid inclusions in quartz is 159°C and the mean temperature of the secondary fluid inclusions in fluorite is 149°C. Thus, much of this paragenetically late quartz, sparsely distributed through the episyenitic rock, may have been introduced after the initial deposition of fluorite there.

Fluid Inclusions in a Selected Quartz-Fluorite-White Mica Vein THat Cuts the Upper Cretaceous Two-mica Monzogranite

Additional fluid inclusion studies were conducted on a sample of a carefully selected quartz-fluorite-white mica vein (sample no. GM-923) that unquestionably cuts the upper Cretaceous two-mica monzogranite, and that appears to be related genetically and temporally to it. The purposes of these detailed studies were to establish the pressure, temperature, and chemistry of fluids associated closely with the two-mica monzogranite, to compare and contrast such fluids with those in mineralized veins elsewhere in the district, and with the occurrence of gold-bearing episyenitic pipes. Sample GM-923 was obtained from a 25- to 45-cm-wide vein that cuts both the Proterozoic metamorphic gneisses and the two-mica monzogranite at its eastern margin. Elsewhere, at the nearby Jumbo prospect (P. M. Blacet, unpub. data, 1967-1972), similar veins are cut by two-mica monzogranite dikes. These complex crosscutting relations indicate that the vein is related genetically to the emplacement of the two-mica monzogranite. White mica from the vein yielded a K-Ar age of 68.8±1.8 m.y. (see above). The sample selected consists of massive milky white quartz which encloses colorless fluorite in anhedral crystals to 3 cm across; the sample also includes cubes up to 5 mm across of limonite and (or) hematite that has replaced pyrite, and muscovite flakes up to 2 mm wide.

Fluid inclusions in both quartz and fluorite consist essentially of two types: (1) liquid-rich two-phase, type I inclusions which are comprised of fluid plus vapor and (2) liquid-rich, type IV inclusions which consist of saline fluid plus vapor plus liquid carbon dioxide. However, in very small inclusions, carbon dioxide is commonly not visible, but its presence could be determined by behavior of the phases during heating and freezing tests, following procedures outlined by Collins (1979). When cooled, the inclusions show two freezing ponts, the development of clathrate and the second when the

saline liquid itself freezes. During warming, these small inclusions generally fail to show visible melting of ice at temperatures below 0°C because of the presence of clathrate. The first visible evidence of a phase change occurs when the clathrate melts somewhere in the temperature range between 0°C and 10°C. This melting is accompanied by rapid expansion of the vapor phase and sweeping of the vapor phase across the inclusion, commonly followed by the immediate reappearance of the third phase, liquid carbon dioxide. Fluid inclusions in quartz are slightly different from those in fluorite. Consequently, all inclusion types are described separately by host mineral.

Two-phase, type I fluid inclsions observed in fluorite occur in linear planar arrays. The inclusions have regular ovoid shapes that range in length from 2 to 22 μm. The percentage of vapor fill in the inclusions at 22°C is fairly consistent at 5 to 7 volume percent; salinities range from 6.3 to 10.1 weight percent NaCl equivalent (fig. 74A) with an average of 9.0 weight percent. Type I fluid inclusions homogenize by vapor disappearance between 149°C and 206°C, with an average of 177°C (fig. 74B). The narrow range of salinities and homogenization temperatures for these inclusions indicates that necking and resultant changes in vapor percentage and salinity were not significant following trapping of these inclusions. However, the occurrence of the type I inclusions along intersecting planar arrays contrasts with the mode of occurrence of the type IV fluid inclusions in the fluorite, and this relation suggests that the type I fluid inclusions studied are secondary.

Type IV, liquid carbon dioxide-bearing inclusions in the fluorite do not appear to be constrained to planar arrays. Instead, they occur in restricted clusters in which individual inclusions occur along wispy rays that radiate from a vague center. The type IV fluid inclusions are about the same size as the type I fluid inclusions and they also have consistently elliptical outlines. At 22°C, about 7 percent of the volume of a typical inclusion consists of vapor plus liquid carbon dioxide; of this 10 to 15 volume percent is vapor. The salinity of these fluid inclusions ranges from 5.5 to 6.0 weight percent NaCl equivalent, and is thus somewhat lower than many of the type I fluid inclusions (fig. 74A). The type IV fluid inclusions homogenize to the liquid, high density carbon dioxide phase by vapor disappearance between 28.1° to 29.1°C, with an average of 28.7° for 9 measurements. Further increases in temperature enhance the mutual solubilities of the phases, and

Figure 74.--Histograms showing salinity and filling temperature data obtained from a selected quartz-fluorite-white mica vein. Sample number GM-923. A, Salinities of fluid inclusions hosted by fluorite. Salinities of type IV, primary fluid inclusions determined using the final melting temperature of clathrate (see text), and salinities of the secondary, type I incluisons determined using the depression of freezing point method; B, Filling temperaures of fluid inclusions hosted by fluorite; C, Salinities of fluid inclusions hosted by quartz. Salinities determined as in A; D, Filling temperatures of fluid inclusions hosted by quartz.

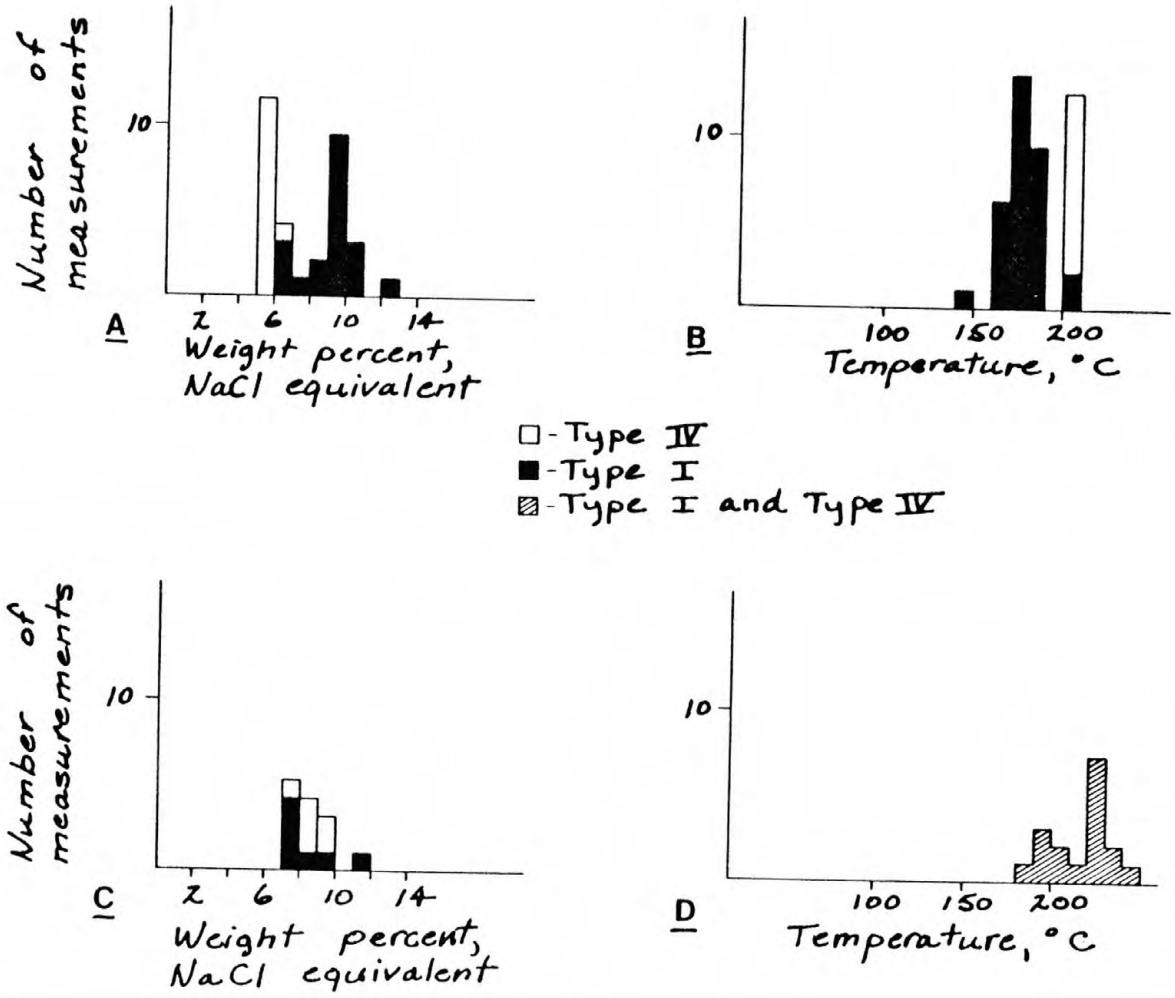
Number of measurements
10
A
2
6
10
14
Weight percent, NaCl equivalent
B
100
150
200
Temperature, °C
□ - Type IV
■ - Type I
▨ - Type I and Type IV
C
D

between 203° to 207°C, average 206°C, the type IV fluid inclusions homogenize to a single phase (fig. 74B). The chemistry, habit, and higher homogenization temperatures contrast the type IV fluid inclusions with secondary type I fluid inclusions in the vein fluorite and indicate that fluids circulating in the environment of the vein decreased in content of carbon dioxide and increased somewhat in salinity with time.

Both primary and pseudosecondary type I and type IV fluid inclusions in vein quartz occur dispersed randomly throughout the quartz and can be distinguished easily from planar trains of obviously secondary inclusions. The fluid inclusions tend to cluster by type, indicating that the silica-depositing fluid varied significantly in chemistry during the deposition of quartz. Type I fluid inclusions have 4 to 7 volume percent vapor at 22°C. They range from about 1 μm to 16 μm in size and have regular elliptical forms, and they show a very good correspondence of their salinities with the type IV fluid inclusions (fig. 74C). The full range of salinities determined for both types of fluid inclusions is between 7.0 and 11.0 weight percent NaCl equivalent, averaging about 8.2 weight percent NaCl equivalent. However, almost all of the type I inclusions studied contain some carbon dioxide because they develop clathrates during freezing tests. The clathrates persist to temperatures in the range 4.6 to 6.4°C. The type IV fluid inclusions in quartz range in size from less than 1 μm to 22 μm. The small size of the fluid inclusions commonly makes it difficult or impossible to resolve the liquid carbon dioxide meniscus even at magnifications of about 1,000X. For the larger of these type IV fluid inclusions, visual estimates suggest equal volumes of liquid carbon dioxide and vapor carbon dioxide at room temperatues. Typically, these fluid inclusions contain 80 to 90 volume percent saline liquid. The type IV fluid inclusions homogenize by vapor disappearances between 28.3° and 30.0°C, with an average of 29.4°C. This indicates that the carbon dioxide is somewhat less dense than in the fluorite inclusions, but still dense enough to homogenize to liquid carbon dioxide rather than vapor upon heating (see Kennedy, 1954; Koltun, 1965, fig. 5). Upon additional heating, the type I and type IV inclusions homogenize to a single phase in the range 188° to 240°C, averaging 218°C (fig. 74D). As such, these filling temperatures are slightly higher than those measured from the primary type IV fluid inclusions in fluorite (compare fig. 74B and D).

Comparison of Fluids in Veins and Gold-bearing Episyenitic Pipes

Similarities and differences in physical and chemical properties determined by fluid inclusion studies of veins and the gold-bearing episyenitic pipes provide an insight into the deposition of fluorite and quartz, and their accompanying gold mineralization in the districts.

Similarities include:

(1) Carbon dioxide densities of fluid inclusions from the episyenitic rock and the selected quartz-fluorite-white mica vein that is clearly related to the two-mica monzogranite have very similar low densities of about 0.61 to 0.66 g/cm^3. The fluids associated with the introduction of gold into the episyenitic pipes show a slightly greater density of carbon dioxide than fluids from the selected vein. Type IV fluid inclusions in fluorite from the episyenitic pipes homogenize by vapor disappearance in the range 26.9 to 28.5°C, which range corresponds to densities of carbon dioxide of about 0.64 to 0.66 g/cm^3. Type IV fluid inclusions in the well-studied quartz-fluorite-white mica vein (GM-923, above) homogenize by vapor disappearance in the range 28.1 to 30.4°C, which corresponds to densities of carbon dioxide of about 0.61 to 0.64 g/cm^3. Visual estimates of the proportion of liquid carbon dioxide present at room temperatures in many other veins throughout the districts suggest that their carbon dioxide contents are similar to the vein at locality GM-923.

(2) Carbon dioxide content of fluid inclusions of both the vein and the episyenitic pipes, calculated from visual volume estimates of the amount of carbon dioxide in the fluid inclusions at room temperatures, range from about 4 to about 8 mole percent. The proportions of carbon dioxide to saline water solution appear to be very consistent (see above), but precise determinations are difficult to make (Roedder and Bodnar, 1980).

(3) Salinities of fluids that deposited quartz and fluorite, and presumably gold, in the gold-bearing episyenitic pipes and the veins are in the same range. Fluid salinities range from 3 to 16 weight percent equivalent NaCl, and cluster especially in the interval from 6 to 10 weight percent NaCl equivalent, a range not common in many epithermal, gold-bearing hydrothermal systems.

(4) The mineral assemblages and parageneses in both the late gold-bearing stage of the episyenitic pipes and the veins are very similar. Hydrothermal

minerals in both include quartz, fluorite, pyrite, white mica, ferroan carbonate (ankerite), and gold. The relative amounts of quartz and fluorite, however, are variable in the two environments; quartz dominates in the veins and fluorite is more abundant than quartz in the gold-bearing syenitic rock, where together the two minerals occur as paragenetically late minerals filling cavities. Both the pipes and the veins show decreasing activity ratios of $[K^+]:[H^+]$ with time in their alteration envelopes, as the systems evolved from biotite stable (veins) and potassium feldspar stable (pipes) assemblages to white mica stable assemblages.

(5) Homogenization temperatures of the veins and the pipes are generally similar. Temperatures of final homogenization to a single fluid for both type I and type IV, primary and pseudosecondary fluid inclusions in fluorite from the gold-bearing syenitic rock are among the highest filling temperatures recorded throughout the mining districts. They range from 251° to 282°C (table 27). Nonetheless, many of the vein occurrences are estimated to have filling temperatures close to these values, and a few were measured correspondingly so (table 27). In contrast, fluid inclusions from veins probably emplaced near the final stages of the late Cretaceous-early Tertiary mineralization in the districts (exemplified by the vein at loc. GM-923 which cuts the two-mica monzogranite) show filling temperatures 45° to 60° less in quartz and 70° to 100°C less in fluorite (fig. 74) than those in the gold-bearing episyenitic rock.

Estimates of the Pressure-Temperature Environment of Mineralization

Fluid inclusion data and phase relations provide useful limiting estimates for the physical and chemical environment of mineralization. Consistent proportions of saline liquid, liquid carbon dioxide, and carbon dioxide-rich vapor for most early stage, type IV fluid inclusions in the gold-gearing episyenitic pipes suggest that they were trapped from a homogeneous fluid. Furthermore, the early-stage, CO_2-rich fluids (pseudosecondary type IV fluid inclusions in fluorite, see above) in the gold-bearing episyenitic pipes most likely include about 8 mole percent CO_2, and they are moderately saline, ranging from about 3 to 7 weight percent NaCl equivalent. These type IV fluid inclusions must also contain minimal amounts of calcium and magnesium as determined from the temperatues of first melting. Thus, we can model the behavior of the fluids by referring to the system $NaCl-H_2O-CO_2$. However, the

episyenitic pipes also show evidence (primary type I fluid inclusions) for the early-stage circulation there of CO_2-depleted fluids that range from 8 to 10 weight percent NaCl equivalent in salinity. The early-stage, relatively CO_2 rich fluid inclusions in the episyenitic pipes homogenize to a single fluid at temperatures of about 280° to 282°C. From this isotherm, and by assuming a fluid composition including 8 mole percent CO_2 and 6 weight percent NaCl, we interpret pressures at the times of trapping were above 500 bars. In making this interpretation for these fluids, we have assumed that the miscibility gap for the 280°C isotherm in the system H_2O-CO_2 initially determined by Todheide and Franck (1963), expanded an amount similar to that found experimentally by Takenouchi and Kennedy (1965). Takenouchi and Kennedy (1965) showed that addition of a limited amount of salt, about 6 weight percent NaCl, to the system H_2O-CO_2 significantly widens the miscibility gap. Furthermore, at a fluid composition of about 8 mole percent CO_2, isotherms converge tightly and they are extremely sensitive to slight differences in pressure (see discussion by Roedder and Bodnar, 1980).

An upper pressure estimate during the development of the episyenitic pipes may be inferred from the experimentally determined solubilities of quartz in the system SiO_2-H_2O (Kennedy, 1950; Fournier, 1977) and the fact that dissolution of primary quartz was an important process in the evolution of the episyenitic pipes. Kennedy (1950) showed a "solubility hump", or region of increasing solubility of silica for decreasing temperature at constant pressure, occurs in the system SiO_2-H_2O at pressures less than 750 bars. Subsequently, Fournier (1977) refined these experimental results and determined the apex of the "solubility hump" is at a pressure of 715 bars, and a corresponding temperature of 480°C.

This range of pressure (500 to 700 bars) estimated respectively from data derived from the type IV fluid inclusions in fluorite and the primary quartz solubility relations may be used to establish a +50 to + 70°C pressure correction for the primary type I fluid inclusions. Such a pressure estimate for the type I fluid inclusions appears to be geologically reasonable because of the very close temporal relations between the two related sets of fluid-inclusion types in the fluorite. The type I fluid inclusions were trapped from a homogeneous fluid at P-T conditions somewhere along an isochore, or line of equal volume, that originates at a temperature of 263°C on the two-phase or liquid-vapor curve for a solution approximately 9 weight percent NaCl

equivalent (fig. 72A). This temperature is the average temperature of filling to a liquid of 18 type I fluid inclusions (fig. 73). Then from the isochoric data for a 10 weight percent NaCl solution, as compiled by Roedder and Bodnar (1980, fig. 4), our best estimate is that the type I fluid inclusions in fluorite were trapped at temperatures of about 315 to 335°C.

Pressure corrections cannot be obtained successfully from inclusion data (fig. 74) of the quartz-fluorite-white mica vein that cuts the two-mica monzogranite because of lower carbon dioxide contents. But these data nonetheless indicate that pressures at the time of tapping were more than 100 bars to maintain the carbon dioxide content of the fluid, and to retard effervescing. Fluorite from this vein shows an average temperature of 206°C for the homogenization of its type IV fluid inclusions to a single phase. This value in a P-T diagram is then the temperature of the isotherm that marks the boundary between the two-phase and one-phase regions in the system H_2O-CO_2-NaCl (see Roedder and Bodnar, 1980, fig. 7). Yet, for a 9 weight percent NaCl equivalent solution containing approximately 4.5 mole percent CO_2 (values determined from the fluid inclusions), such an isotherm essentially would parallel the pressure axis, and the isotherm cannot be used to establish an effectual lower boundary for the pressure prevailing at the time of trapping of the fluid inclusions. At best, we only can estimate that pressures in the environment of this vein during its emplacement were greater than the pressure along the liquid-vapor curve at the point(s) of homogenization of its two-phase, type I fluid inclusions. These pressures are less than 100 bars. Therefore, we have not been able to determine well-defined limits of the pressures in the fluids associated with the final stages of precious-metal mineralization in the districts.

We judge the P-T conditions during the late-stage gold mineralization at the site of the episyenitic alteration pipes, namely more than 500 bars and 315 to 335°C, to be reasonable values for the physical conditions prevailing during the onset of upper Cretaceous-late Tertiary gold mineralization in the districts. A pressure estimate of 500 bars corresponds to a minimum depth of about 2 km under a lithostatic load, and a minimum depth of about 5 km under a hydrostatic load. Assumptions involved in the calculation of the hydrostatic load are (1) a nonstratified fluid column occurs above the site(s) of the gold-depositing fluids, and (2) the fluid column is open to and extends to the ground surface at the time of gold mineralization (see Roedder and Bodnar,

1980). A value somewhere between lithostatic and hydrostatic is most likely on geologic grounds, and the Paleozoic formations that must have overlain the districts total approximately 2.1 km in thickness (Peirce, 1976).

Discussion

Most of the fluid, mineral, and geologic relations of gold mineralization documented during our study compare well with observations in many other mesothermal (Jensen and Bateman, 1979) districts that show generally similar geology. For example, in the Hopewell and Bromide districts of New Mexico, gold-bearing fissure veins typically are associated with siderite, chlorite, pyrite, chalcopyrite, and galena (Graton, 1910). Gold vein deposits in the Grass Valley, California district yielded about $300 million (Clark, 1970). This district, about 30 km north of the northern terminus of the Mother Lode but considered generally not to be part of the Mother Lode (Albers, 1981), shows vein and wallrock assemblages containing quartz, iron and magnesium carbonates, white mica, chlorite, epidote, arsenopyrite, pyrite, galena, chalcopyrite and gold (Lindgren, 1896; Johnston, 1940). The wallrocks, which consist of Paleozoic and Mesozoic units intruded by a Mesozoic granodiorite (Johnson, 1940), are variably sericitized, carbonated, and chloritized. The bulk of the gold and galena in the veins was deposited during a quartz substage (Johnston, 1940). Further, liquid-vapor relations in fluid inclusions shown in Johnston (1940, pl. 22) suggest that the fluids associated with mineralization were trapped from homogeneous, non-boiling fluids. Wallrock alteration surrounding the gold quartz veins in the Alleghany, California district, about 30 km northeast of Grass Valley, include carbonates (mainly ankerite), albite, mariposite, and white mica (Ferguson and Gannett, 1932). The occurrence of late-stage gold, preceeded by a potassium-enriching and silica-depleting stage, as in the episyenitic pipes at Gold Basin, may be comparable more or less to gold-syenite associations reported elsewhere. Maclaren (1908, p. 100-101) mentions several occurrences of paragenetically late gold occuring in "acidic dyke rocks." Boyle (1979, p. 296) cites several reports of gold ore bodies that are hosted mostly by syenitic rock (Dyer, 1936; Derry, Hopper, and McGowan, 1948; North and Allen, 1948). At the Young-Davidson mine in the Matachewan district of Ontario, Canada, disseminated gold-bearing pyrite makes up about two volume percent of an early-phase syenite; minor associated minerals are chalcopyrite, galena, molybdenite, scheelite, and specularite. Subsequent fracture-controlled mineralization

there includes quartz-carbonate veins and free gold. However, the syenitic rocks in these districts may not be equivalent genetically to the episyenites we describe here. However, Comba, Gobson, and Lichtblau (1981) allude to a fenite (episyenite)-gold association at the Upper Canada gold mine at Dobie, Ontario.

Fluid-inclusion compositions and mineral assemblages in the veins and wallrocks provide fairly limiting constraints on the chemistry of the ore-depositing environment in the Gold Basin-Lost Basin districts, but most likely above a mass of Cretaceous two-mica monzogranite at depth. The exposed episyenitic pipes most likely reflect a mineralized level deeper than the bulk of the pegmatite-vein systems throughout the districts. At the episyenitic pipes, early stages of alteration initially must have involved a tightly confined flux of upward-streaming fluids whose $(K^+)/(Na^+)$ ratios eventually exceeded the buffering capabilities of potassium feldspar and plagioclase relict from the protolith (see discussion in Poty, Stalder, and Weisbrod (1974)). Such fluids also leached primary quartz from the Proterozoic X monzogranite protolith and increased the porosity at the sites. The potassium feldspar stage of episyenitization at Gold Basin may be comparable to the early alkaline, high temperature (450 to 600°C) stage of microcline crystallization associated with many greisens (Scherba, 1970). Further, some intragranitic veins associated with uranium mineralization show parageneses similar to the gold-episyenite relations at Gold Basin (see Nash and others, 1981). In the intragranitic Gunnar uranium deposit, Saskatchewan, Evoy (1961) has shown that albitization there preceded ore mineralization, and albitization produced a "syenite" by leaching primary quartz from the "syenite's" protolith. However, we have no fluid inclusion data documenting the character of the fluids at Gold Basin during the onset of flooding by potassium feldspar and dissolving of quartz. It is likely that these early stage fluids contained some fluorine and carbon dioxide, although partition of fluorine toward a vapor or aqueous phase in equilibrium with a granitic magma is low (Burnham, 1967; 1979; Koster van Groos and Wyllie, 1969; Carmichael, Turner, and Verkoogen 1974, p. 314-316). However, with progressive differentiation of granitic rocks, there is somewhat of a tendency for coexisting very late fluids to show a build-up in their fluorine contents (see Bailey (1977) for discussion of such relations). The overall HF content in these fluids must be subordinate to their HCl content because of the very

large partition coefficients of HCl in favor of the aqueous phase (Burnham, 1979). In such a supercritical, late-magmatic environment, fluorine probably combines into very soluble complexes, possibly including $(SiF_6)^{2-}$ (Scherba, 1970), which may be related to the early stages of development of the episyenitic pipes. Subsolidus consumption of primary quartz and replacement of plagioclase by potassium feldspar there may have occurred by a coupling of reaction (1) or reaction (2) to the alkali exchange reactions (3) and (4) proposed by Burnham (1979):

$$12HF + 6F^- + 3\ SiO_{2(s)} \longrightarrow 3(SiF_6)^{2-} + 6H_2O \quad (1)$$

$$2KF + H_2O + SiO_{2(s)} \longrightarrow KSiO_3 + 2HF \quad (2)$$

$$NaAlSi_3O_{8(s)} + KCl_{(v)} \longrightarrow KAlSi_3O_{8(s)} + NaCl_{(v)} \quad (3)$$

$$CaAl_2Si_2O_{8(s)} + KCl_{(v)} + SiO_{2(s)} \longrightarrow KAlSi_3O_{8(s)} + CaCl_{(v)} \quad (4)$$

Eventually, fluorite and gold were deposited in the pore spaces within the episyenitic pipes at temperatures as high as 315 to 335°C at pressures between 500 and 700 bars. As a comparison, the depths of such an environment appear to be similar to that of the more deeply-seated porphyry copper deposits (Nash, 1976). At these temperatures, deposition of fluorite may have occurred in response to a combination of interrelated factors (see Richardson and Holland, 1979; Holland and Malinin, 1979) including a common-ion effect with NaF(aq) as the system evolved, and possibly a decrease in salinity. However, the fluids associated with mineralization in the districts show no compelling evidence requiring a salinity decrease as an important component during deposition of the ores. Early and late stage fluids in quartz and fluorite of the pipes and veins both are correspondingly moderately saline in contrast to the early fluids at other fluorite deposits which are extremely saline (for example, see Nash and Cunningham (1973)). Further, such trapping temperatures (315 to 335°C) are quite common in mesothermal environments, which lead Barnes (1979) to suggest that cooling of post magmatic fluids is an important ore-depositing mechanism that must be considered also.

The prevailing high pressures in the mesothermal environment at the sites of the pipes and the veins during early and late stages of mineralization precluded boiling of the fluids with a concomitant loss of carbon dioxide. Loss of carbon dioxide can lead to a decrease in the solubility of carbonate (Ellis, 1963; Holland and Malinin, 1979). However, in the Gold Basin-Lost Basin districts fluid inclusion relations do not suggest significant boiling of fluids occurred during the quartz, carbonate (ferroan carbonate or

ankerite), white mica, fluorite, sulfide, and gold stage of mineralization. The fact that the fluids circulating at the pipes and in the veins typically were not boiling indicate a fairly widespread high fugacity of carbon dioxide favorable for the deposition of iron carbonate. In addition, the non-boiling of these fluids must have retarded the physical separation and removal of acid components (including mostly carbon dioxide) from the circulating fluids, and thereby enhanced the stability of white mica during the ore-depositing stage. This relation is in marked contrast to the preceding potassium feldspar-stable stage in the episyenitic pipes. The increased abundance of white mica both laterally toward the "pegmatitic"-vein systems and temporally as they and the episyenitic pipes evolved demonstrates a transition from high $(K^+)/(H^+)$ fluids to ones with lower $(K^+)/(H^+)$ (Hemley and Jones, 1964), and probably somewhat more acidic conditions. The association in the Gold Basin-Lost Basin districts of late Cretaceous-early Tertiary gold mineralization with fluids related to two-mica magmatism is apparently very rare in the southern cordillera. Most two-mica, peraluminous granites of Arizona and California are not associated with any significant ore deposits, although a few commercial tungsten deposits occur locally in wall rocks adjacent to some two-mica plutons (Reynolds, Keith, and DeWitt, 1982). Furthermore, Reynolds, Keith and DeWitt (1982) note that all two-mica peraluminous two-mica granitoids must incorporate significant crustal components because of their uniformly high Sr^{87}/Sr^{86} initial isotopic ratios. Therefore, we suggest that the gold and base metals, and possibly fluorine in the districts may also have a crustal source and may have been recycled from Proterozoic rocks. These crustal sources may include some near-surface Proterozoic rocks in the districts, possibly including some of the Proterozoic X metabasites described above (see Moiseenko and Fatyanov (1972)). However, the bulk of the gold in the late Cretaceous-early Tertiary occurrences most likely was incorporated in the magmatic stages of the two-mica monzogranite, and thus probably reflects anatexis of deep crustal rocks, whereas some gold may be remobilized from pre-late Cretaceous-early Tertiary sites.

The Proterozoic rocks in the districts and elsewhere in the region include some gold and fluorine that may be considered as potential sources for the late Cretaceous-early Tertiary occurrences and deposits. In this report, we have described above mineralized veins in Proterozoic rocks that have a fabric and mineral assemblage that seem to date from the Proterozoic

greenschist metamorphic event. In addition, some of the gold-bearing veins of the districts may have been emplaced penecentemporaneous with the copper, lead, and gold veining in the Gold Butte district that apparently is Proterozoic in age (Wasserburg and Lanphere, 1965). Proterozoic X gold occurs elsewhere in the southwest, as exemplified by an occurrence of stratiform gold in Proterozoic X rocks of Yavapai County, Arizona (Swan, Hansen, and Newell, 1981). Fluorine in the veins and episyenitic pipes in the Gold Basin-Lost Basin districts also may have been recycled from a Proterozoic protolith. Our analyses, for example, of the Proterozoic X porphyritic monzogranite of Garnet Mountain in the districts show contents of fluorine in the range of 0.06 to 0.17 weight percent (table 14). Remobilization of fluorite from Proterozoic igneous rocks into late Cretaceous and (or) early Tertiary veins has been postulated by Snyder (1978) at the Park Range, Colorado; and Antweiler, Doe, and Delevaux (1972) suggested somewhat similar relations for gold at Han's Peak, Colorado. Furthermore, Stephenson and Ehmann (1971) showed the depletion of gold from hydrothermally altered countryrock, and the apparent migration of gold into veins at the Rice Lake-Beresford Lake area, southeastern Manitoba. On the other hand, metal ratios in late Cretaceous-early Tertiary and Tertiary ore deposits in Yavapai County, Ariz., apparently do not reflect the metal ratios of the Proterozoic crust (DeWitt, 1982). Nonetheless, Boyle (1979, p. 65) maintains that transport and, by implication, remobilization of gold as gold-sulfide complexes by near-neutral to moderately alkaline, carbonate-depositing fluids must occur. On the other hand, the experimental studies of Henley (1973) reveal an inflection or solubility "hump" for gold that culminates in the range 300° to 350°C in three molar potassium chloride solution (approximately 18 weight percent KCl) at pressures less than 1 kb. Certainly the early-stage fluids at the episyenite pipes and at many of the veins in the Gold Basin-Lost Basin districts must have had high K/Na ratios because of their associated potassic alteration. We suggest that such fluids may have been primarily responsible for the remobilization and extraction of some gold from shallow Proterozoic sources, whereas the gulk of the gold was emplaced during the Cretaceous after having been incorporated into the magmas of the two-mica monzogranite. Experimental studies suggest that the gold-carrying capacity of the fluids associated with the final crystallization of the Cretaceous two-mica monzogranite would be more than adequate to account for all the known gold in the districts. Ten cubic

kilometers of such monzogranite (equivalent to the exposed two-mica monzogranite extending to a depth of about 0.5 km) would have the capacity to deposit or extract about 70 tons of gold, based on the experimental data of Ryabchikov (1981). Further, Korobeynikov (1976) reports a significant amount of gold to be soluble in the fluid-inclusion waters of minerals associated with skarn-and-vein-type gold deposits.

SUGGESTIONS FOR EXPLORATORY PROGRAMS

The known and inferred vilations of gold in its reported occurrences in the Gold Basin-Lost Basin districts suggest several geologic environments that should be evaluated carefully in exploratory programs. Certainly the most obvious would be any remaining high-grade ore shoots in the veins themselves. However, such occurrences most likely would not yield the relatively large tonnages of ore needed for a viable mining operation. Five environments that should be considered include (1) sequences of rock that might form favorable replacement zones adjacent to, or near any of the gold-bearing veins that crop out. Such sequences might include Proterozoic X carbonate, amphibolite, or any zones of porous rock that are premineral in age. Such favorable zones could include any rocks shattered tectonically prior to the major mineralizing event in the Late Cretaceous. (2) If the occurrence of disseminated free gold in the fluorite-bearing episyenitic alteration pipes in the Gold Basin district evolved generally as we described above, then such an environment must reflect a mineralized level geologically deeper than the bulk of the veins that crop out elsewhere in the districts. Thus, all quartz-fluorite-bearing veins should be evaluated as to whether or not they reflect the upper quartz-depositing portions of a system which at depth includes early quartz-dissolving- and late gold-depositing-parageneses. Similarly, the two mica monzogranite that crops out in the Gold Basin district might include some disseminated gold-bearing episyenitic facies at depth. (3) The entire trace of the low angle detachment surface or glide surface should be evaluated for the occurrence of Cyclopic-type deposits (see fig. 2). Much of the trace or inferred trace of this structure as mapped by Blacet along the western flank of the White Hills is poorly exposed, partly because it is locally covered by Quaternary sands and gravels. However, the occurrence of increased abundances of tectonically polished or striated vein quartz along some of the poorly exposed portions of its trace might be indicative of gold-bearing Cretaceous veins caught up tectonically along the

detachment surface. Further, detailed geologic mapping along the general trace of the detachment surface might reveal other fault strands that should be evaluated similarly. (4) The Proterozoic X metamorphic rocks in the districts should be considered as potential hosts for syngenetic, stratiform deposits. Certainly, as we described above, there are some indications in the rocks that boron-enriched fluids were important in the paragenesis of tourmaline-bearing schists. Such rocks might reflect emorations of boron-bearing fluids expelled from exhalative centers in the protolith of the metamorphic rocks. Tourmalinite makes up the major part of the ore in the gold deposit of Passagem de Mariana, Brazil, and this deposit yielded more than 60 tons of gold (Fleischer and Routhier, 1973). The exploration implications of tourmalinite horizons are exceptionally well described by Slack (1980, 1981a, and b) and Nicholson (1980). In fact, Nicholson (1980, fig. 1) shows a striking correlation between tourmalinite horizons and gold deposits. However, in the Proterozoic X metamorphic rocks of the Gold Basin-Lost Basin districts, some horizons of tourmalinite may be mistaken for amphibolite. Nonetheless, detailed, large-scale mapping of all tourmalinite horizons in the Proterozoic might yield some additional targets worthy of further exploratory efforts. Last, the oxide-facies iron formations known in the Proterozoic also should be considered as potential guides to sea-floor, volcanogenic-type gold deposits (see Hodgson, Chapman, and MacGeehan, 1982). We invision that such oxide-facies iron formations, if they prove to be anomalous in syngenetic gold, might be indicative of facies distal to disseminated gold either in an intermediate, pyritic facies of iron formation more or less along the same horizon, or in the immediate area of the vent. Finally (5), the minor-element signatures of native lode gold (mostly the content of silver and copper) from several localities in the Gold Basin and Lost Basin districts should be evaluated with respect to their potential relationship to a buried porphyry copper system (see the section above by Antweiler and Campbell).

LIST OF REFERENCES

Ackermand, D., and Morteani, G., 1977, The chemistry of the garnets, chlorite, biotite and tourmaline in the Steinkogel Schist (Salzburg, Austria; the geologic history of the central Alps): Neues Jahrbuch fur Geologie und Palaontologie Abhandlungen, v. 154, no. 3, p. 367-385.

Albers, J. P., 1981, A lithologic-tectonic framework for the metallogenic provinces of California: Economic Geology, v. 76, no. 4, p. 765-790

Allen, Percival; Sutton, John; and Watson, J. V., 1974, Torridonian tourmaline; quartz pebbles and the Precambrian crust northwest of Britain: Journal of the Geological Society of London, v. 130, no. 1, p. 85-91.

Anderson, C. A., 1968, Arizona and adjacent New Mexico, in Ridge, J. D., ed., Ore deposits of the United States, 1933-1967, The Graton-Sales Volume II: American Institute of Mining, Metallurgical, and Petroleum Engineers, p. 1163-1190.

Anderson, R. E., 1971, Thin skin distension in Tertiary rocks of southeastern Nevada: Geological Society of America Bulletin, v. 82, no. 1, p. 43-58.

Anderson, R. E., Longwell, C. R., Armstrong, R. L., and Marvin, R. F., 1972, Significance of K-Ar ages of Tertiary rocks from the Lake Mead region, Nevada-Arizona: Geological Society of America Bulletin, v. 83, no. 2, p. 273-288.

Anderson, J. L., and Cullers, R. L., 1978, Geochemistry and evolution of the Wolf River batholith, a late Precambrian rapakivi massif in North Wisconsin, U.S.A.: Precambrian Research, v. 7, p. 287-324.

Anderson, J. L., and Rowley, M. C., 1981, Synkinematic intrusion of peraluminous and associated metaluminous granitic magmas, Whipple Mountains, California: Canadian Mineralogist, v. 19, p. 83-101.

Anderson, P. M., and Guilbert, J. M., 1979, The Precambrian massive-sulfide deposits of Arizona--a distinct metallogenic epoch and province, in Ridge, J. D., ed., Papers on mineral deposits of western North America: The International Association on the Genesis of Ore Deposits, 5th Quadrennial Symposium, Proceedings, v. 2; Nevada Bureau of Mines and Geology Report 33, p. 39-48.

Anderson, R. E., and Laney, R. L., 1975, The influence of Late Cenozoic stratigraphy on distribution of impoundment-related seismicity at Lake Mead, Nevada-Arizona: U.S. Geological Survey Journal of Research, v. 3, no. 3, p. 337-343.

Antweiler, J. C., and Campbell, W. L., 1977, Application of gold compositional analyses to mineral exploration in the United States: Journal of Geochemical Exploration, v. 8, p. 17-29.

_____1982, Gold in exploration geochemistry, in Levison, A. A., ed., Precious metals in the northern Cordillera: Association of Exploration Geochemists, Calgary, p. 33-44.

Antweiler, J. C., Doe, B. R., and Delevaux, M. H., 1972, Lead isotope and other evidence on the bedrock source of placer gold at Hahns Peak, Colorado: Economic Geology, v. 67, no. 3, p. 302-314.

Antweiler, J. C., and Sutton, A. L., 1970, Spectrochemical analysis of native gold samples: U.S. Clearinghouse Federal Science Technical Information, P B Report 1970, no. 194809, 32 p.

Armbrustmacher, T. J., and Simons, F. S., 1977, Geochemistry of amphibolites from the central Beartooth Mountains, Montana-Wyoming: U.S. Geological Survey Journal of Research, v. 5, no. 1, p. 53-60.

Bailey, J. C., 1977, Fluorine in granitic rocks and melts: a review: Chemical Geology, v. 19, p. 1-42.

Barnes, H. L., 1979, Solubilities of ore minerals, in Barnes, H. L., ed., Geochemistry of hydrothermal ore deposits: New York, John Wiley and Sons, p. 404-460.

Bateman, P. C., 1961, Granitic formations in the east-central Sierra Nevada near Bishop, California: Geological Society of America Bulletin, v. 72, p. 1521-1537.

Beal, L. H., 1965, Geology and mineral deposits of the Bunkerville mining district, Clark County, Nevada: Nevada Bureau of Mines Bulletin 63, 96 p.

Beane, R. E., and Titley, S. R., 1981, Prophyry copper deposits, Part II. Hydrothermal alteration and mineralization, in Seventy-fifth anniversary volume, Economic Geology, 1905-1980, B. J. Skinner, ed., The Economic Geology Publishing Co., New Haven, CT., p. 235-269.

Binns, R. A., 1965a, Hornblendes from some basic hornfelses in the New England region, New South Wales: Mineralogical Magazine, v. 34, p. 52-65.

_____1965b, The mineralogy of metamorphosed basic rocks from the Willyama complex, Broken Hill district, New South Wales, Part 1: Mineralogical Magazine, v. 35, p. 306-326.

_____1965c, The mineralogy of metamorphosed basic rocks from the Willyama complex, Broken Hill district, New South Wales, Part 2: Mineralogical Magazine, v. 35, p. 561-587.

Blacet, P. M., 1968, Gold Basin-Lost Basin district, Arizona, in Geological Survey research 1968, Chapter A [abs.]: U.S. Geological Survey Professional Paper 600-A, p. A4.

_____1969, Gold placer and lode deposits, Gold Basin-Lost Basin, in Geological Survey research 1969, Chapter A [abs.]: U.S. Geological Survey Professional Paper 650-A, p. A1-A2.

_____1972, Late Cretaceous plutonism and metallization south of Lake Mead, in Geological Survey research 1972, Chapter A [abs.]: U.S. Geological Survey Professional Paper 800-A, p. A44.

_____1975, Preliminary geologic map of the Garnet Mountain quadrangle, Mojave County, Arizona: U.S. Geological Survey Open-File Map 75-93, scale 1:48,000.

Blair, W. N., 1978, Gulf of California in Lake Mead area of Arizona and Nevada during late Miocene time: American Association of Petroleum Geologists Bulletin, v. 62, no. 7, p. 1159-1170.

Blair, W. N., and Armstrong, A. K., 1979, Hualapai Limestone Member of the Muddy Creek Formation: The youngest deposit predating the Grand Canyon, southeastern Nevada and northwestern Arizona: U.S. Geological Survey Professional Paper 1111, 14 p.

Blair, W. N., McKee, E. H., and Armstrong, A. K., 1977, Age and environment of deposition--Hualapai Member of the Muddy Creek Formation [abs.]: Geological Society of America Abstracts with Programs, Cordilleran Section, v. 9, no. 4, p. 390-391.

Boyle, R. W., 1979, The geochemistry of gold and its deposits: Geological Survey of Canada Bulletin 280, 584 p.

Bozzo, A. T., Chen, H.-S., Kass, J. R., and Barduhn, A. J., 1975, The properties of the hydrates of chlorine and carbon dioxide: Desalination, v. 16, p. 303-320.

Brown, E. H., Babcock, R. S., Clark, M. D., Livingston, D. E., 1979, Geology of the older Precambrian rocks of the Grand Canyon, Part I. Petrology and structure of the Vishnu Complex: Precambrian Research, v. 8, p. 219-241.

Burchard, H. C., 1882, Report of the director of the mint upon the statistics of the production of the precious metals in the United States [1881]: U.S. Government Printing Office, Washington, D.C., 765 p.

_____1883, Report of the director of the mint upon the statistics of the production of the precious metals in the United States [1882]: U.S. Government Printing Office, Washington, D.C., 873 p.

Burchfiel, B. C., 1979, Geologic history of the central United States, in Ridge, J. D., ed., Papers on mineral deposits of western North America: The International Association on the Genesis of Ore Deposits, 5th Quadrennial Symposium, Proceedings, v. 2; Nevada Bureau of Mines and Geology Report 33, p. 1-12.

Burnham, C. W., 1967, Hydrothermal fluids at the magmatic stage, in Barnes, H. L., ed., Geochemistry of hydrothermal ore deposits: New York, Holt, Rinehart, and Winston, Inc., p. 34-76.

_____1979, Magmas and hydrothermal fluids, in Barnes, H. L., ed., Geochemistry of hydrothermal ore deposits, 2d Edition: New York, John Wiley and Sons, p. 71-136.

Busch, W., 1966, Petrographie und Abfolge der Granitisation im Schwarzwald V: Neues Jarbuch fur Mineralogie Abhandlungen, v. 104, p. 190-258.

Callaghan, Eugene, 1939, Geology of the Searchlight district, Clark County, Nevada: U.S. Geological Survey Bulletin 906-D, p. 135-188.

Campbell, W. L., Mosier, E. L., and Antweiler, J. C., 1973, Effects of laboratory treatments on silver and other elements in native gold: U.S. Geological Survey Journal of Research, v. 1, no. 2, p. 211-220.

Carmichael, D. M., 1969, On the mechanism of prograde metamophic reaction in quartz-bearing pelitic rocks: Contributions to Mineralogy and Petrology, v. 24, p. 275-292.

_____1978, Metamorphic bathozones and bathograds: a measure of the depth of post-metamorphic uplift and erosion on the regional scale: American Journal of Science, v. 278, p. 769-797.

Carmichael, I. S. E., Turner, F. J., and Verhoogen, John, 1974, Igneous petrology: New York, McGraw-Hill Book Company, 739 p.

Chappell, B. W., and White, A. J. R., 1974, Two contrasting granite types: Pacific Geology, v. 8, p. 173-174.

Christiansen, R. L., and Lipman, P. W., 1972, Cenozoic volcanism and plate tectonic evolution of the western United States. II. Late Cenozoic: Philosophical Transactions of the Royal Society of London, Series A, v. 271, p. 249-284.

Clark, M. D., 1979, Geology of the older Precambrian rocks of the Grand Canyon. Part III. Petrology of mafic schists and amphibolites: Precambrian Research, v. 8, p. 277-302.

Clark, W. B., 1970, Gold districts of California: California Division Mines and Geology, Bulletin 193, 186 p.

Clarke, F. W., 1924, Data of geochemistry: U.S. Geological Survey Bulletin 770, 841 p.

Clifton, C. G., Durning, P. W., and Buchanan, L. J., 1980, Controls of mineralization and exploration procedure in the Oatman mining district, Oatman, Arizona [abs.]: American Institute of Mining, Metallurgic, and Petroleum Engineers, Program with Abstracts, Annual Meeting, February 24-28, Las Vegas, Nev., p. 24.

Collins, P. F., 1979, Gas hydrates in CO_2-bearing fluid inclusions and the use of freezing data for estimation of salinity: Economic Geology, v. 74, p. 1435-1444.

Comba, C. D. A., Gibson, H. L., and Lichtblau, A., 1981, Four Corners fenite: Noranda, Quebec, Canada: Economic Geology, v. 76, no. 5, p. 1202-1205.

Condie, K. C., 1982, Plate-tectonics model for Proterozoic continetal accretion in the southwestern United States: Geology, v. 10, p. 37-42.

Coney, P. J., and Reynolds, S. J., 1977, Cordilleran Benioff zones: Nature, v. 270, p. 403-406.

Creasey, S. C., 1966, Hydrothermal alteration, in Titley, S. R., and Hicks, C. L., eds., Geology of the porphyry coper deposits, southwestern North America: Tucson, Ariz., Arizona University Press, p. 51-85.

Crittenden, M. D., Jr., Coney, P. H., and Davis, G. H., eds., 1980, Cordilleran metamorphic core complexes: Geological Society of America Memoir 153, 490 p.

Cunningham, C. G., and Carollo, Clyde, 1980, Modification of a fluid-inclusion heating/freezing stage: Economic Geology, v. 75, no. 2, p. 335-337.

Davis, G. A., Anderson, J. L., Frost, E. G., and Shackelford, T. J., 1979, Regional Miocene detachment faulting and early Tertiary(?) mylonitization, Whipple-Buckskin-Rawhide Mountains, southeastern California and western Arizona, in Abbott, P. L., ed., Geological excursions in the southern California area: Geological Society of America, November, 1979, 92d Annual Meeting, San Diego State University, p. 75-108.

Deaderick, A. J., 1980, Geologic investigation of the Apache Oro mining claims, Lost Basin range, Mohave County, Arizona: Unpublished report, New Mexico Institute of Mining and Technology, Socorrow, New Mexico, 273 p.

Deans, T., Sukheswala, R. N., Sethna, S. F., and Viladkar, S. G., 1972, Metasomatic feldspar rocks (potash fenites) associated with the fluorite deposits and carbonatites of Amba Dongar, Gujarat, India: Institution of Mining and Metallurgy, Transactions/Section B, v. 81, 1972, Bulletin no. 783, February, p. B1-B9.

Deer. W. A., Howie, R. A., and Zussman, J., 1962a, Rock-forming minerals. Volume 1. Ortho- and ring silicates: London, Longmans, Green, and Co. Ltd., 333 p.

_____1962b, Rock-forming minerals. Volume 3. Sheet silicates: London, Longmans, Green, and Co., Ltd., 270 p.

_____1962c, Rock-forming minerals. Volume 5. Non-silicates: London, Longmans, Green, and Co., 371 p.

_____1963, Rock-forming minerals. Volume 2. Chain silicates: London, Longmans, Green, and Co., 379 p.

Derry, D. R., Hopper, C. H., and McGowan, H. S., 1948, Matachewan Consolidated mine, in Structural geology of Canadian ore deposits: Canadian Institute of Mining and Metallurgy, v. 1, p. 638-643.

Desborough, G. A., 1970, Silver depletion indicated by microanalysis of gold from placer occurrences, Western United States: Economic Geology, v. 65, no. 3, p. 304-311.

DeWitt, Ed, 1982, The geochemistry of Precambrian crust and its effect on younger metallogenesis, Yavapai County, Arizona (abs.): Geological Society of America, Abstracts with Programs, v. 14, no. 4, p. 159.

Dickinson, W. R., 1975, Potash-depth (K-h) relations in continental margin and intra-oceanic magmatic arcs: Geology, v. 3, p. 53-56.

_____1980, Plate tectonic evolution of the southern cordillera, in Dickenson, W. R., and Payne, W. D., eds., Relations of tectonics to ore deposits in the southern cordillera, Arizona Geological Society Digest volume XIV, Tucson, Arizona, p. 113-136.

Dickinson, W. R., and Hatherton, T., 1967, Andesitic volcanism and seismicity around the Pacific: Science, v. 157, p. 801-803.

Diman, E. N., 1976, On the fineness of gold associated with pyrite: Geochemistry International 1976, p. 63-70; translated from 1976, Geokhimiya, no. 3, p. 404-412.

Donnelly, M. E., and Hahn, G. A., 1981, A review of the Precambrian volcanogenic massive sulfide deposits in central Arizona and the relationship to their depositional environment, in Dickinson, W. R., and Payne, W. D., eds., Relations of tectonics to ore deposits in the southern cordillera: Arizona Geological Society Digest, v. 14, Tucson, Ariz., p. 11-22.

Dyer, W. S., 1936, Geology and ore deposits of the Matachewan-Kenogami area: Ontario Department of Mines, v. 44, pt. 2, p. 1-55.

Ellis, A. J., 1963, The solubility of calcite in sodium chloride solutions at high temperature: American Journal of Science, v. 261, p. 259-267.

Engineering and Mining Journal, 1939, Arizona: v. 140, no. 13, p. 70.

Espenshade, G. H., 1969, Kyanite and related minerals, in Mineral and water resources of Arizona by U.S. Geological Survey and Arizona Bureau of Mines: Committee on Interior and Insular Affairs, 90th Congress, 2d session, p. 382-385.

Ethier, V. G., and Campbell, F. A., 1977, Tourmaline concentrations in Proterozoic sediments of the southern Cordillera of Canada and their economic significance: Canadian Journal of Earth Science, v. 14, p. 2348-2363.

Evans, B. W., and Leake, B. E., 1960, The composition and origin of the striped amphibolites of Connemara, Ireland: Journal of Petrology, v. 1, no. 3, p. 337-363.

Evoy, E. F., 1961, Geology of the Gunnar uranium deposit, Beaverlodge area, Saskatchewan: Madison, University of Wisconsin, Ph. D. thesis, 80 p.

Ferguson, H. G., and Gannett, R. W., 1932, Gold quartz veins of the Alleghany district, California: U. S. Geological Survey Professional Paper 172, 139 p.

Fleischer, Ronald, and Routhier, Pierre, 1973, The "Consanguineous" origin of a tourmaline-bearing gold deposit: Passagem de Mariana (Brazil): Economic Geology, v. 68, no. 1, p. 11-22.

Fournier, R. O., 1977, Constraints on the circulation of meteroic water in hydrothermal systems imposed by the solubility of quartz [abs.]: Geological Society of America Abstracts with Programs, v. 9, no. 7, p. 979.

Galbraith, F. W., and Brennan, W. J., 1970, Minerals of Arizona: Arizona Bureau of Mines Bulletin 181, 116 p.

Gallagher, David, 1940, Albite and gold: Economic Geology, v. 35, no. 6, p. 698-736.

Gay, N. C., 1963, A review of geochemical characteristics of gold in ore deposits: University of Witwatersrand, Economical Geological Research Unit, Information Circular 12, 70 p.

Gerry, C. N., and Miller, T. H., 1935, Gold, silver, copper, lead, and zinc in Arizona: U.S. Bureau of Mines Minerals Yearbook, 1934, p. 153-178.

Glen, R. A., 1979, Evidence for cyclic reactions between andalusite, "sericite", and sillimanite, Mount Franks area, Willyama Complex, New South Wales: Tectonophysics, v. 58, p. 97-112.

Goetz, A. F. H., Billingsley, F. C., Gillespie, A. R., Abrams, M. J., Squires, R. L., Shoemaker, E. M., Luchitta, Ivo, and Elston, D. P., 1975, Application of ERTS images and image processing to regional geologic problems and geologic mapping in northern Arizona: National Aeronautics and Space Administration Technical Report 32-1597, 188 p.

Graton, L. C., 1910, Rio Arriba County, in The ore deposits of New Mexico, by L. C. Graton and C. H. Gordon: U.S. Geological Survey Professional Paper 68, p. 124-133.

Greenwood, H. J., and Barnes, H. L., 1966, Binary mixture of volatile components, in Clark, S. P., Jr., ed., Handbook of physical constants: Geological Society of America Memoir 97, Revised edition, p. 385-400.

Gregnanin, Arrigo, and Piccirillo, E. M., 1969, Geology and petrography of the zone between Plan and Clava valleys, Alto Adige: Rendiconti della Societa Minerlogica Petrol. Italiana, v. 25, no. 2, p. 439-473.

Griggs, D. T., and Blacic, J. D., 1965, Quartz-anomalous weakness of synthetic crystals: Science, v. 147, no. 3655, p. 292-295.

Grimes, D. J., and Marranzino, A. P., 1968, Direct-current arc and alternating-current spark emission spectrographic field methods for the semiquantitative analysis of geologic materials: U.S. Geological Survey Circular 591, 6 p.

Groves, D. I., and McCarthy, T. S., 1978, Fractional crystallization and the origin of tin deposits in granitoids: Mineralium Deposita, v. 13, p. 11-26.

Haffty, Joseph, Hanbert, A. W., and Page, N. J., 1980, Determination of iridium and ruthenium in geological samples by fire assay and emission spectrography: U.S. Geological Survey Professional Paper 1129G, p. 61-64.

Haffty, Joseph, and Riley, L. B., 1968, Determination of palladium, platinum and rhodium in geologic materials by fire assay and emission spectrography: Talanta, v. 15, p. 111-117.

Hallbauer, D. K., and Utter, T., 1977, Geochemical and morphological characteristics of gold particles from Recent river deposits and the fossil placers of the Witwatersrand: Mineralium Deposita, v. 12, p. 293-306.

Hanekom, H. J., Staden, C. M. v. H. van, Smit, P. J., and Pike, D. R., 1965, The geology of the Palabora igneous complex: Geological Survey of South Africa Memoir 54, 185 p.

Hatherton, T. and Dickinson, W. R., 1969, The relationship between andesitic volcanism and seismicity in Indonesia, the Lesser Antilles, and other island arcs: Journal of Geophysical Research, v. 74, p. 5301-5310.

Helgeson, H. C., Delany, J. M., Nesbitt, H. W., and Bird, D. K., 1978, Summary and critique of the thermodynamic properties of rock-forming minerals: American Journal of Science, v. 278-A, 229 p.

Hemley, J. J., and Jones, W. R., 1964, Chemical aspects of hydrothermal alteration with emphasis on hydrogen metasomatism: Economic Geology, v. 59, p. 538-569.

Henley, R. W., 1973, Solubility of gold in hydrothermal chloride solutions: Chemcial Geology, v. 11, p. 73-87.

Hernon, R. M., 1938, Cerbat Mountains, in Butler, G. M., ed., Some Arizona ore deposits: Arizona Bureau of Mines Geological Series 12, [University of Arizona] Bulletin 145, p. 110-117.

Hess, P. C., 1969, The metamorphic paragenesis of cordierite in pelitic rocks: Contributions to Mineralogy and Petrology, v. 24, p. 191-207.

Hewett, D. R., Callaghan, Eugene, Moore, B. N., Nolan, T. B., Rubey, W. W., and Shaller, W. T., 1936, Mineral resources of the region around Boulder Dam: U.S. Geological Survey Bulletin 871, 197 p.

Hewitt, D. A., 1973, The metamorphism of micaceous limestones from south-central Connecticut: American Journal of Science, Cooper Volume 273-A, p. 444-469.

Hietanen, Anna, 1973, Geology of the Pulga and Bucks Lake quadrangles, Butte and Plumas Counties, California: U.S. Geological Survey Professional Paper 731, 66 p.

Hine, R., Williams, I. S., Chappel, B. W., and White, A. J. R., 1978, Contrasts between I- and S-type granitoids of the Kosciusko batholith: Journal of the Geological Society of Australia, v. 25, p. 4, p. 219-234.

Hodgson, C. J., Chapman, R. S. G., MacGeehan, P. J., 1982, Application of exploration criteria for gold deposits in the Superior Province of the Candian shield to gold exploration in the Cordillera, in Precious metals in the northern Cordillera, A. A. Levinson, ed., The Association of Exploration Geochemists, Proceeding of Symposium, April 13-15, 1981, Vancouver, British Columbia, p. 173-206.

Holdaway, M. J., 1971, Stability of andalusite and the aluminum silicate phase diagram: American Journal of Science, v. 271, p. 97-131.

Holdaway, M. J., and Lee, S. M., 1977, Fe-Mg cordierite stability in high-grade pelitic rocks based on experimental, theoretical, and natural observations: Contributions to Mineralogy and Petrology, v. 63, p. 175-198.

Holland, H. D., and Malinin, S. D., 1979, The solubility and occurrence of non-ore minerals, in H. L. Barnes, ed., Geochemistry of hydrothermal ore deposits, 2d edition: New York, John Wiley and Sons, p. 461-508.

Hoschek, G., 1969, The stability of staurolite and chloritoid and their significance in metamorphism of pelitic rocks: Contributions to Mineralogy and Petrology, v.22, p. 208-232.

Hotz, P. E., 1979, Regional metamorphism inthe Condrey Mountain quadrangle, north-central Klamath Mountains, California: U.S. Geological Survey Professional Paper 1086, 25 p.

Ishihara, Shunso; Sawata, Hideho; Shibata, Ken; Terashima, Shigeru; Arrukul, Surapon; and Sato, Kohei, 1980, Granites and Sn-W deposits of Peninsular Thiland, in Granitic magmatism and related mineralization, S. Ishihara and S. Takenouchi, eds., Mining Geology Special Issue, no. 8, p. 223-241.

Jakes, P., and White A. J. R., 1972, Major and trace element abundances in volcanic rocks of orogenic areas: Geological Society of America Bulletin, v. 83, no. 1, p. 29-40.

James, H. L., 1981, Bedded Precambrian iron deposits of the Tobacco Root Mountains, southwestern Montana: U.S. Geological Survey Professional Paper 1187, 16 p.

James, R. S., and Hamilton, D. L., 1969, Plase relations in the system $NaAlSi_3O_8$-$KAlSi_3O_8$-$CaAl_2Si_2O_8$-SiO_2 at 1 kilobar water vapour pressure: Contributions to Mineralogy and Petrology, v. 21, p. 111-141.

Jensen, M. L., and Bateman, A. M., 1979, Economic mineral deposits: New York, John Wiley and Sons, 593 p.

Johnson, M. G., 1972, Placer gold deposits of Arizona: U.S. Geological Survey Bulletin 1355, 103 p.

Johnston, W. D., Jr., 1940, The gold quartz veins of Grass Valley, California: U.S. Geological Survey Professional Paper 194, 101 p.

Jones, Bob, 1979, Tourmaline, its colors and its occurrences are truly legion: Rock and Gem, December 1979, p. 56-58, 61-62, 85-88.

Jones, R. S., and Fleischer, Michael, 1969, Gold in minerals and the composition of native gold: U.S. Geological Survey Circular 612, 17 p.

Keith, S. B., 1978, Paleosubduction geometries inferred from Cretaceous and Tertiary magmatic patterns in southwestern North America: Geology, v. 6, no. 9, p. 516-521.

Keith, S. B., and Reynolds, S. J., 1980, Geochemistry of cordilleran metamorphic core complexes, in Coney, P. J., and Reynolds, S. J., eds., Cordilleran metamorphic core complexes and their uranium favorability: U.S. Department of Energy Final report, Laboratory of Geotectonics, Department of Geosciences, University of Arizona, Tucson Arizona, Contract no. DE-AC13-76GJ01664 and Bendix subcontract no. 79-357, p. 247-321.

Kennedy, G. C., 1950, A portion of the system silica-water: Economic Geology, v. 45, p. 629-653.

_____1954, Pressure-temperature relations in CO_2 at elevated temperatures and pressures: American Journal of Science, v. 252, p. 225-241.

Kepezhinskas, K. B., and Khlestov, V. V., 1977, The petrogenetic grid and subfacies for middle-temperature metapelites: Journal of Petrology, v. 18, pt. 1, p. 114-143.

King, P. B., 1969, The tectonics of North America--A discussion to accompany the tectonic map of North America, scale 1:5,000,000: U.S. Geological Survey Professional Paper 628, 95 p.

Kistler, R. W., 1974, Phanerozoic batholiths in western North America, in Donath, F. A., Stehli, F. G., and Wetherill, G. W., eds., Annual review of Earth and Planetary Sciences, volume 2: Palo Alto, Calif., Annual Reviews, Inc., p. 403-418.

Koltun, L. I., 1965, Application of mineralothermometric analysis in studies of the origins of certain gold ore deposits in Ural, in Yermakov, N. P., ed., Research on the nature of mineral-forming solutions: New York, Pergamon Press, p. 426-457.

Korobeynikov, A. F., 1976, Gold in gas-liquid inclusions in minerals [abs.]: Abstracts of Fifth All-Union Conference in Thermobarogeochemistry, Ufa, USSR, 20-23 Sept., 1976: Ufa, Bashkir Section, Academy of Sciences of the USSR, Institute of Geology, p. 189-190 (in Russia).

Koschmann, A. H., and Bergendahl, M. H., 1968, Principal gold-producing districts of the United States: U.S. Geological Survey Professional Paper 610, 283 p.

Koster van Groos, A. F., and Wyllie, P. J., 1969, Melting relations in the system $NaAlSi_3O_8$-NaCl-H_2O at 1 kilobar pressure, with petrological applications: Journal of Geology, v. 77, no. 5, p. 581-605.

Krish, E. J., 1974, Relationship of trace element distribution to level of erosion in some porphyry copper deposits and prospects, southwestern U.S. and northwestern Mexico: Golden, Colorado School of Mines, M.S. thesis, 156 p.

Lantsev, I. P., Nikolaeva, L. A. Badalova, R. P., and Denisova, L. K., 1971, Distribution of trace elements in native gold from different deposits: Tr. Tsent. Nauch. Issled. Gornorazved. Inst., no. 96, pt. 1, p. 130-137; Chemical Abstracts, v. 77, 78005q.

Lausen, Carl, 1931, Geology and ore deposits of the Oatman and Katherine districts, Arizona: Arizona Bureau of Mines, Geological Series no. 6 [University of Arizona] Bulletin, 131, 126 p.

Leake, B. E., 1964, Chemical distinction of ortho- and para-amphibolites: Journal of Petrology, v. 5, p. 238-254.

Lebedev, M. M., Tarrain, I. A., and Lagovskaya, Ye. A., 1967, Metamorphic zones of Kamchatka as an example of the metamorphic assemblages of the inner part of the Pacific belt: Tectonophysics, v. 4, nos. 4-6, p. 445-461.

Lee, W. T., 1908, Geologic reconnaissance of a part of western Arizona: U.S. Geological Survey Bulletin 352, p. 9-80.

LeMaitre, R. W., 1976, The chemical variability of some common igneous rocks: Journal of Petrology, v. 17, p. 589-598.

Leroy, Jacques, 1978, The Margnac and Fanay uranium deposits of the La Crouzille district (western Massif Central, France): Geologic and fluid-inclusion studies: Economic Geology, v. 73, no. 8, p. 1611-1634.

Liggett, M. A., and Childs, J. F., 1977, An application of satellite imagery to mineral exploration, in Woll, P. W., and Fischer, W. A., eds., Proceedings of the first annual William T. Pecora memorial symposium, October 1975, Sioux Falls, South Dakota: U.S. Geological Survey Professional Paper 1015, p. 253-270.

Liggett, M. A., and others, 1974, A reconnaissance space sensing investigation of crustal structure for a strip from the eastern Sierra Nevada to the Colorado Plateau: National Aeronautics and Space Administration, Final Report of Investigation, Goddard Space Flight Center, Greenbelt, Maryland, NASA-CR-139434, E74-10705, 156 p.

Lindgren, Waldemar, 1896, The gold quartz veins of Nevada City and Grass Valley, California: U.S. Geological Survey 17th Annual Report, 262 p.

Lindgren, Waldemar, and Davy, W. M., 1924, Nickel ores from the Key West mine, Nevada: Economic Geology, v. 19, no. 4, p. 309-319.

Livingston, D. E., 1973, A plate tectonic hypothesis for the genesis of porphyry copper deposits of the southern Basin and Range province: Earth and Planetary Science Letters, v. 20, p. 171-179.

Longwell, C. R., 1936, Geology of the Boulder reservoir floor, Arizona-Nevada: Geological Society of America Bulletin, v. 47, no. 9, p. 1393-1476.

Longwell, C. R., Pampeyan, E.H., Bowyer, Ben, and Roberts, R. J., 1965, Geology and mineral deposits of Clark County, Nevada: Nevada Bureau of Mines Bulletin 62, 218 p.

Loomis, T. P., 1979, A natural example of metastable reactions involving garnet and sillimanite: Journal of Petrology, v. 20, pt. 2, p. 271-279.

Luchitta, Ivo, 1966, Cenozoic geology of the upper Lake Mead area adjacent to the Grand Wash Cliffs, Arizona: University Park, Pennsylvania State University, Ph. D. thesis, 218 p.

Luth, W. C., 1969, The systems $NaAlSi_3O_8$-SiO_2 and $KAlSi_3O_8$-SiO_2 to 20 kb and the relationship between H_2O content, P_{H_2O} and P_{total} in granitic magmas: American Journal of Science, v. 267-A (Schairer Volume), p. 325-341.

Maclaren, J. M., 1908, Gold: its geological occurrence and geographical distribution: The Mining Journal, London, 687 p.

Manson, Vincent, 1967, Geochemistry of basaltic rocks: major elements, in Hess, H. H., and Poldervaart, Arie, eds., Basalts--The Poldervaart treatise on rocks of basaltic composition: New York, John Wiley and Sons, Interscience Publishers, p. 215-269.

Mariano, A. N., 1979, Enhancement and classification of fenitization by cathodoluminescence [abs.]: Geological Association of Canada, Mineralogical Association of Canada, Annual Meeting, University Laval, Quebec, Program with Abstracts, v. 4, p. 65.

Mason, Roger, 1978, Petrology of the metamorphic rocks: London, George Allen and Unwin/Thomas Murby, 254 p.

McBride, E. F., 1963, A classification of common sandstones: Journal of Sedimentary Petrology, v.33, p. 664-669.

McConnell, R. G., 1907, Report on gold values in the Klondike high level gravels: Geological Survey of Canada Report 979, 34 p.

McCurry, Patricia, 1971, A pseudomorphic quartz-tourmaline relationship from northern Nigeria: American Mineralogist, v. 56, nos. 7-8, p. 1474-1476.

Mehnert, K. R., 1968, Migmatites and the origin of granitic rocks: Amsterdam, London, New York, Elsevier Publishing Co., 393 p.

Metzger, F. W., Kelly, W. C., Nesbitt, B. E., and Essene, E. J., 1977, Scanning electron microscopy of daughter minerals in fluid inclusions: Economic Geology, v. 72, no. 2, p.141-152.

Middlemost, E. A. K., 1980, A contribution to the nomenclature and classification of volcanic rocks: Geological Magazine, no. 1, v. 117, p. 51-57.

Middleton, G. V., 1960, Chemical composition of sandstones: Geological Society of America Bulletin, v. 71, no. 7, p. 1011-1026.

Miller, C. F., 1981, Cordilleran peraluminous granites: an ancient quartzofeldspathic source (abs.), in Howard, K. A., Carr, M. D., and Miller, D. M., eds., Tectonic framework of the Mojave and Sonoran Deserts, California and Arizona: U.S. Geological Survey open-file report 81-503, p. 70-72.

Miller, C. F., and Bradfish, L. J., 1980, An inner Cordilleran belt of muscovite-bearing plutons: Geology, v. 8, p. 412-416.

Mining Journal, 1929, Mining activities in the southwest: v. 12, no. 18, p. 25-26.

_____1933, Mill heads from western States: Sept. 30, 1933, v. 17, no. 9, p. 10.

_____1938, Concentrates from western states: v. 22, no. 14, p. 21.

Miyashiro, Akiho, 1958, Regional metamorphism of the Gosaisyo-Takanuki district in the central Abukuma Plateau: Tokyo University Faculty of Sciences Journal, sec. 2, v. 11, p. 219-272.

Moiseenko, V. G., and Fatyanov, 1972, Geochemistry of gold: 24th International Geological Congress, sec. 10, p. 159-165.

Moreau, Marcel, and Ranchin, Guy, 1973, Alterations hydrothermales et controles tectoniques dans les gites filoniens d'uranium intragranitiques du massif Central Francais, in Les roches plutoniques dans leurs rapports avec les gites mineraux, Phillippe Morin, ed., Masson and Co., Paris, p. 77-100.

_____1973, Metamorphism and metamorphic belts: London, George Allen and Unwin, 492 p.

Mosier, E. L., 1975, Use of emission spectroscopy for the semiquantitative analysis of trace elements and silver in native gold, in Ward, F. N., ed., New and refined methods of trace analysis useful in geochemical exploration: U.S. Geological Survey Bulletin 1408, p. 97-105.

Nash, J. T., 1972, Fluid-inclusion studies of some gold deposits in Nevada, in Geological Survey research, 1972: U.S. Geological Survey Professional Paper 800-C, p. C15-C19.

_____1976, Fluid-inclusion petrology--data from porphyry copper deposits and applications to exploration: U.S. Geological Survey Professional Paper 907-D, p. D1-D16.

Nash, J. T., and Cunningham, C. G., Jr., 1973, Fluid-inclusion studies of the fluorspar and gold deposits, Jamestown District, Colorado: Economic Geology, v. 68, no. 8, p. 1247-1262.

Nash, J. T., Granger, H. C., and Adams, S. S., 1981, Geology and concepts of genesis of important types of uranium deposits, in Seventy-fifth anniversary volume, Economic Geology, 1905-1980, B. J. Skinner, ed., The Economic Geology Publishing Company, New Haven, Conn., p. 235-269.

Neuerburg, G. J., 1961, A method of mineral separation using hydrofluoric acid: American Mineralogist, v. 46, p. 1498-1501.

_____1975, A procedure, using hydrofluoric acid, for quantitative mineral separations from silicate rocks: U.S. Geological Survey Journal of Research, v. 3, no. 3, p. 377-378.

Newton, R. C., 1966, Kyanite-andalusite equilibrium from 700° to 800°C: Science, v. 153, p. 170-172.

Nicholson, P. M., 1980, The geology and economic significance of the Golden Dyke Dome, northern Territory, in Ferguson, J., and Goleby, A. B., eds., Proceedings of the International Uranium Symposium on the Pine Creek Geosyncline, 1980: International Atomic Energy Agency, Vienna, Austria, p. 319-334.

Nitsch, K.-H., 1970, Experimentelle Bestimmung der oberen Stabilitatsgrenze von Stilpnomelan: Fortschritte der Mineralogie, v. 47, supplement 1, p. 48-49.

North, H. H., and Allen, C. C., 1948, Young-Davidson mine, in Structural geology of Canadian ore deposits: Canadian Institute of Mining and Metallurgy, v. 1, p. 839-845.

Odikadze, G. L., 1971, Distribution of fluorine in the granitoids of the Greater Caucasus and Dzirul′ massif: Geochemistry International, v. 8, p. 314-323.

Peacock, M. A., 1931, Classification of igneous rocks series: Journal of Geology, v. 39, p. 54-67.

Peirce, H. W., 1976, Elements of Paleozoic tectonics in Arizona: Arizona Geological Society Digest, v. 10, p. 37-58.

Petro, W. L., Vogel, T. A., and Wilband, J. T., 1979, Major-element chemistry of plutonic rock suites from compressional and extensional plate boundaries: Chemical Geology, v. 26, p. 217-235.

Pettijohn, F. J., 1949, Sedimentary rocks: New York, Harper and Brothers, 718 p.

_____1963, Chemical composition of sandstones, excluding carbonate and volcanic sands: U.S. Geological Survey Professional Paper 440-S, 21 p.

Pitcher, W. S., 1979, The nature, ascent and emplacement of granitic magmas: Journal of the Geological Society of London, v. 146, p. 627-662.

Plimer, I. R., 1980, Exhalative Sn and W deposits associated with mafic volcanism as precursors to Sn and W deposits associated with granites: Mineralium Deposita, v. 15, p. 275-289.

Poty, B. P., Stalder, H. A., and Weisbrod, A. M., 1974, Fluid inclusion studies in quartz from fissures of western and central Alps: Schweizerische Mineralogische und Petrographische Mitteilungen, v. 54, p. 717-752.

Poty, B. P.; Leroy, Jacques; and Jachimowicz, Leon, 1976, Un nouvel appareil pour la mesure des temperatures sous le microscope: l'installation de microthermometrie Chaixmeca: Societe Francaise Mineralogie et Cristallographie Bulletin, v. 99, p. 182-186.

Reinhardt, E. W., 1968, Phase relations in cordierite-bearing gneisses from the Gananoque area, Ontario: Canadian Journal of Earth Sciences, v. 5, no. 3, pt. 1, p. 455-482.

Rehrig, W. A., and Heidrick, T. L., 1976, Regional tectonic stress during the Laramide and late Tertiary intrusive periods, Basin and Range province, Arizona: Arizona Geological Society Digest, v. 10, p. 205-228.

Reyner, M. L., 1954, Preliminary reconnaissance report, page 43, in U.S. Atomic Energy Commission, 1970, Preliminary reconnaissance for uranium in Mohave County, Arizona, 1952 to 1956: RME-158, Grand Junction, Colo., 169 p.

Reynolds, R. C., Jr., 1965, Geochemical behavior of boron during the metamorphism of carbonate rocks: Geochimica et Cosmochimica Acta, v. 29, no. 9, p. 1101-1114.

Reynolds, S. J., 1980, A conceptual basis for the occurrence of uranium in cordilleran metamorphic core compleses, in Coney, P. J., and Reynolds, S. J., eds., Cordilleran metamorphic core complexes and their uranium favorability, U.S. Gepartment of Energy Final Report, Laboratory of Geotectonics, Department of Geosciences, University of Arizona, Tucson, Arizona, Contract no. DE-AC13-76GJo1644 and Bendix subcontract no. 79-357, p. 187-245.

Reynolds, S. J., Keith, S. B., and DeWitt, Ed, 1982, Late Cretaceous-early Tertiary peraluminous granitoids of Arizona-California and their related mineral deposits (abs.): Geological Society of America, Abstracts with Programs, v. 14, no. 4, p. 227.

Richardson, C. K., and Holland, H. D., 1979, Fluorite deposition in hydrothermal systems: Geochimica et Cosmochimica Acta, v. 43, p. 1327-1335.

Robbins, C. R., and Yoder, H. S., Jr., 1962, Stability relations of dravite, a tourmaline: Annual Report of the Director of the Geophysical Laboratory, Carnegie Institute of Washington Year Book 61, p. 106-107.

Roberts, W. L., Rapp, G. R., Jr., and Weber, Julius, 1974, Encyclopedia of minerals: New York, Van Nostrand Reinhold Co., 693 p.

Roedder, Edwin, 1962, Studies of fluid inclusions I: low-temperature application of a dual-purpose freezing and heating stage: Economic Geology, v. 57, no. 7, p. 1045-1061.

_____1963, Studies of fluid inclusions II: freezing data and their interpretation: Economic Geology, v. 58, no. 2, p. 167-211.

_____1972, Composition of fluid inclusions: U.S. Geological Survey Professional Paper 440-JJ, 164 p.

Roedder, Edwin, and Bodnar, R. J., 1980, Geologic pressure determinations from fluid inclusion studies, in Donath, F. A., Stehli, F. G., and Wetherill, G. W., eds., Annual review of Earth and Planetary Sciences: Palo Alto, Calif., Annual Reviews, Inc., v. 8, p. 263-301.

Rumble, Douglas, 3d, 1978, Mineralogy, petrology, and oxygen isotopic geochemistry of the Clough Formation, Black Mountain, western New Hampshire, U.S.A.: Journal of Petrology, v. 19, no. 2, p. 317-340.

Ryabchikov, I. D., 1981, Mobilization of ore metals by supercritical fluids from crystallizing magmas, in Chemistry and Geochemistry of solutions of at high temperatures and pressires. D. T. Rickard and F. E. Wickman, eds., Pergamon Press, Oxford, p. 529-535.

Sakharova, M. S., Batrakova, Y. A., and Posukhova, T. V., 1979, Causes of differentiation of gold and silver during their precipitation on natural minerals: Moscow University Geology Bulletin, v. 34, no. 4; translation, New York, Allerton Press Inc., p. 36-44.

Schrader, F. C., 1909, Mineral deposits of the Cerbat Range, Black Mountains, and Grand Wash Cliffs, Mohave County, Arizona: U.S. Geological Survey Bulletin 397, 226 p.

_____1917, Geology and ore deposits of Mohave County, Arizona: American Institute of Mining, Metallurgical, and Petroleum Engineers, Transactions, v. 56, p. 195-227.

Shapiro, Leonard, 1967, Rapid analysis of rocks and minerals by a single solution method, in Geological Survey research, 1967: U.S. Geological Survey Professional Paper 575-B, p. B187-B191.

Shapiro, Leonard, and Brannock, W. W., 1962, Rapid analysis of silicate, carbonate, and phosphate rocks: U.S. Geological Survey Bulletin 1144-A, p. A1-A44.

Sharp, J. E., 1980, Gold breccia pipe southwest of Las Vegas, Nevada [abs.]: American Institute of Mining, Metallurgic, and Petroleum Engineers, Annual Meeting, Program with Abstracts, February 24-28, Las Vegas, Nev., p. 24.

Shcherba, G. N., 1970, Greisens: International Geology Review, v. 12, p. 114-150; p. 239-255. Translated from Shcherba, G. N., 1968, Genesis of endogenic ore deposits (in Russian), Moscow, Nedra Press, 720 p.

Silver, L. T., 1960, Age determinations on Precambrian diabase differentiates in the Sierra Ancha, Gila County, Arizona [abs.]: Geological Society of America Bulletin, v. 71, no. 12, pt. 2, Abstracts of papers submitted for the meeting in Denver, Colo., October 31-November 2, 1960, p. 1973-1974.

_____1963, The uses of cogenetic uranium-lead isotope systems in zircons in geochronology, in Radioactive dating; proceedings of the Symposium on Radioactive Dating, Athens, 1962: Vienna, International Atomic Energy Agency, p. 279-287.

_____1966, U-Pb isotope relations and their historical implications in Precambrian zircons from Bagdad, Arizona [abs.]: Geological Society of America Special Paper 101, p. 420.

Silver, L. T., Bickford, M. E., Van Schmus, W. R., Anderson, J. L., Anderson, T. H., and Medaris, L. G., Jr., 1977, The 1.4-1.5 b.y. transcontinental anorogenic plutonic perforation of North America [abs.]: Geological Society of America Abstracts with Programs, v. 9, p. 1176-1177.

Skippen, G. B., 1971, Experimental data for reactions in siliceous marbles: Journal of Geology, v. 79, no. 4, p. 457-481.

Slack, J. F., 1980, Tourmaline--a prospecting guide for massive base-metal sulfide deposits in the Penobscot Bay area, Maine: Maine Geological Survey, Special Economic Studies Series no. 8, 25 p.

_____1981a, Prospecting with tourmaline for stratabound massive sulfide deposits: Examples from the Appalachian-Caledonide orogen [abs.]: IGCP-CCSS Symposium, May 1, 1981, Glasgow, Scotland, IMM Transactions, London (in press).

_____1981b, Tourmaline in Appalachian-Caledonian massive sulfide deposits and its exploration significance: Transactions of the Institution of Mining and Metallurby, sec. B (in press).

Slack, J. F., and Annis, M. P., 1981, Time-space relations of tourmaline-rich rocks at the Elizabeth mine and vicinity, Vermont Copper Belt [abs.]: Geological Society of America Abstracts with Programs, Northeastern Section Meeting, Bangor, Maine, April 9-11, 1981 (in press).

Smirnov, V. I., 1976, Geology of mineral deposits: Moscow, Mir Publishers, 520 p.

Smith, J. V., 1974, Feldspar minerals [vol.] 2, Chemical and textural properties: New York, Heidelberg, Berlin, Springer-Verlag, 690 p.

Snyder, G. L., 1978, Intrusive rocks northeast of Steamboat Springs, Park Range, Colorado, with a section on Geochronology by C. E. Hedge: U.S. Geological Survey Professional Paper 1041, 42 p.

Stanton, R. L., 1972, Ore petrology: New York, McGraw-Hill Book Co., 713 p.

Steiner, J. C., Jahns, R. H., and Luth, W. C., 1975, Crystallization of alkali feldspar and quartz in the Haplogranite system $NaAlSi_3O_8$-$KAlSi_3O_8$-SiO_2-H_2O at 4 kb: Geological Society of America Bulletin, v. 86, p. 83-98.

Stephenson, J. F., and Ehmann, W. D., 1971, Neutron activation analysis of gold in Archean igneous and metamorphic rocks of the Rice Lake-Beresford Lake area, southeastern Manitoba: Economic Geology, v.66, no. 6, p. 933-939.

Streckeisen, A. L., and others, 1973, Plutonic rocks; classification and nomenclature recommended by the IUGS subcommission on the systematics of igneous rocks: Geotimes, v. 18, no. 10, p. 26-30.

Suk, Milos, 1964, Material characteristics of the metamorphism and migmatization of Moldanubian paragneisses in central Bohemia: Krystalinikum Czechoslavak Academy of Sciences, Prague, v. 2, p. 71-105.

Sutherland, D. S., 1965a, Potash trachytes and ultra-potassic rocks associated with the carbonatite complex of the Toror Hills, Uganda: Mineralogical Magazine, v. 35, no. 270, p. 363-378.

_____1965b, Nomenclature of the potassic-feldspathic rocks associated with carbonatites: Geological Society of America Bulletin, v. 76, no. 12, p.1409-1412.

Swann, M. M., Hausen, D. M., and Newell, R. A., 1981, Lithological, structural, chemical, and mineralogical patterns in a Precambrian stratiform gold occurrence, Yavapai County, Arizona, in Hausen, D. M., and- Park, W. C., eds., Process mineralogy: Extractive metallurgy, mineral exploration, energy resources: TMS-AIME Process Mineralogy Committee, Symposium, 110th AIME Annual Meeting, Chicago, Ill., Feb. 22-26, 1981, Conference Proceedings, p. 143-157.

Takenouchi, Sukune, and Kennedy, G. C., 1965, Dissociation pressures of the phase CO_2 5-3/4$_2$0: Journal of Geology, v. 73, p. 383-390.

Thomas, B. E., 1949, Ore deposits of the Wallapai district, Arizona: Economic Geology, v. 44, no. 8, p. 663-705.

Thornton, C. P., and Tuttle, O. F., 1960, Chemistry of igneous rocks. Part 1. Differentiation index: American Journal of Science, v. 258, p. 664-684.

Thorson, J. P., 1971, Igneous petrology of the Oatman district, Mohave County, Arizona: Santa Barbara, University of California, Ph. D. thesis, 189 p.

Tischendorf, G., 1977, Geochemical and petrographic characteristics of silicic magmatic rocks associated with rare-element mineralization, in Stemprok, M., Burnol, L., and Tischendorf, G., eds., Metallization associated with acid magatism: International Geological Correlation Programme, Symposium on Metallization Associated with Acid Magmatism, Prague, Czechoslavakia, 1974, v. 2, p. 41-96.

Todheide, K., and Franck, E. U., 1963, Das Zweiphasengebiet und de kritische Kurve in System Kohlendioxid-Wasser bis zu Drucken von 3500 bar: Zeitschrift fur physikalische Chemie, v. 37, p. 388-401.

Turekian, K. K., and Wedepohl, K. H., 1961, Distribution of the elements in some major units of the earth's crust: Geological Society of America Bulletin, v. 72, p. 175-192.

Tuttle, O. F., and Bowen, N. L., 1958, Origin of granite in the light of experimental studies in the system $NaAlSi_3O_8$-$KAlSi_3O_8$-SiO_2-H_2O: Geological Society of America Memoir 74, 153 p.

van de Kamp, P. C., 1969, Origin of amphibolites in the Beartooth Mountains, Wyoming and Montana: New data and interpretation: Geological Society of America Bulletin, v. 80, no. 6, p. 1127-1136.

Vidale, R. J., 1969, Metasomatism in a chemical gradient and the formation of calc-silicate bands: American Journal of Science, v. 267, no. 8, p. 857-874.

Vidale, R. J., and Hewitt, D. A., 1973, "Mobile" components in the formatio of calc-silicate bands: American Mineralogist, v. 58, p. 991-997.

Vikre, P. G., 1977, Gold and silver mineralization of the Rochester district, Pershing County, Nevada: Stanford, Calif., Stanford University, Ph. D. thesis, 404 p.

_____1981, Silver mineralization in the Rochester district, Pershing County, Nevada: Economic Geology, v. 76, no. 3, p. 580-609.

Viladkar, S. G., 1980, The fenitized aureole of the Newania carbonatite, Rajasthan: Geological Magazine, v. 117, no. 3, p. 285-292.

Vinogradov, A. P., 1962, Average content of chemical elements in the principal types of igneous rocks of the earth's crust: Geochemistry, no. 7, p. 641-664.

Warren, H. V., and Thompson, R. M., 1944, Minor elements in gold: Economic Geology, v. 39, p. 457-471.

Wasserburg, G. J., and Lanphere, M. A., 1965, Age determinations in the Precambrian of Arizona and Nevada: Geological Society of America Bulletin, v. 76, no. 7, p. 735-758.

Wenk, Eduard, 1954, Berechnung von Stoffaustauschvorgangen: Schweizerische Mineralogische und Petrographische Mitteilungen, v. 34, p. 309-318.

White, A. J. R., Williams, I. S., and Chappel, B. W., 1977, Geology of the Berridale 1:100,000 sheet 8625: Geological Survey, N.S.W., 138 p.

Wilcox, R. E., 1979, The liquid line of descent and variation diagrams, in Yoder, H. S., Jr., ed., The evolution of the igneous rocks, fiftieth anniversary perspectives: Princeton University Press, Princeton, New Jersey, p. 205-232.

Wilkins, Joe, Jr., and Heidrick, T. L., Base and precious metal mineralization related to low-angle tectonic features in the Whipple Mountains, California and Buckskin Mountains, Arizona [abs.]: Geological Society of America, Abstracts with Programs, v. 14, no. 4, p. 245.

Williams, S. A., 1963, Oxidation of sulfide ores in the Mildren and Steppe mining districts, Pima County, Arizona: Economic Geology, v. 58, p. 1119-1125.

Willie, P. J., 1981, Magma sources in cordilleran settings, in W. R. Dickinson and W. D. Payne, eds., Relations of tectonics to ore deposits in the southern cordillera: Arizona Geological Society Digest XIV, Tucson, Arizona, p. 39-48.

Wilson, E. D., 1937, Pre-Cambrian Mazatzal revolution in central Arizona: Geological Society of America Bulletin, v. 50, p. 1113-1164.

_____1962, A resume of the geology of Arizona: Arizona Bureau of Mines Bulletin 171,140 p.

Wilson, E. D., Cunningham, J. B., and Butler, G. M., 1934, Arizona lode--gold mines and gold mining: Arizona Bureau of Mines Bulletin 137, Mining Technology series 37, 261 p.

Wilt, J. C., 1980, Arizona molybdenum minerals as keys to metallogenic types: Geological Society of America Abstracts with Programs, Rocky Mountain Section Meeting, Ogden, Utah, p. 309.

Wilt, J. C., and Keith, S. B., 1980, Molybdenum in Arizona: Fieldnotes, State of Arizona, Bureau of Geology and Mieneral Technology, v. 10, no. 3, p. 1-3, 7-9, 12.

Winkler, H. G. F., 1974, Petrogenesis of metamorphic rocks: New York, Springer-Verlag, 320 p.

Woodward, G. E., and Luff, Paul, 1943, Gold, silver, copper, lead, and zinc in Arizona, in Needham, C. E., ed., Minerals yearbook 1942: U.S. Bureau of Mines, U.S. Government of Printing Office, Washington D.C., p. 231-259.

Wright, J. E., and Haxel, Gordon, 1982, A garnet-two-mica granite, Coyote Mountains, southern Arizona: Geologic setting , uranium-lead isotopic systematics of zircon, and nature of the granite source region: Geological Society of America Bulletin (in press).

Yeend, Warren, 1975, Experimental abrasion of detrital gold: U.S. Geological Survey Journal of Research, v. 3, no. 2, p. 203-212.

Ypma, P. J. M., 1963, Rejuvenation of ore deposits as exemplified by the Belledonne metaliferous province: University of Leiden Thesis, 212 p.

4

PIECES